KTH Industrial Engineering
and Management

Solar-Driven Refrigeration Systems with Focus on the Ejector Cycle

Doctoral Thesis

By

Wimolsiri Pridasawas

Stockholm, October 2006

Division of Applied Thermodynamics and Refrigeration

Department of Energy Technology

School of Industrial Engineering and Management

Royal Institute of Technology, KTH

Solar-Driven Refrigeration Systems with Focus on the Ejector Cycle

Wimolsiri Pridasawas

TRITA REFR Report No 06/55
ISSN 1102-0245
ISRN KTH/REFR/ R06/55
ISBN 91-7178-449-7

Doctoral Thesis by Wimolsiri Pridasawas
Division of Applied Thermodynamics and Refrigeration
Department of Energy Technology
School of Industrial Engineering and Management
Royal Institute of Technology, KTH

Abstract

Interest in utilizing solar-driven refrigeration systems for air-conditioning or refrigeration purposes has grown continuously. Solar cooling is comprised of many attractive features and is one path towards a more sustainable energy system. Compared to solar heating, the cooling load, particularly for air-conditioning applications, is generally in phase with solar radiation.

The objective of this thesis is to establish a fundamental basis for further research and development within the field of solar cooling. In this thesis, an overview of possible systems for solar powered refrigeration and air-conditioning systems will be presented. The concept of the 'Solar Cooling Path' is introduced, including a discussion of the energy source to the collector, and choice of cooling cycle to match cooling load. Brief information and comparisons of different refrigeration cycles are also presented.

The performance of solar cooling systems is strongly dependent on local conditions. The performance of a solar divan air-conditioning system in different locations will therefore be compared in this thesis. Solar cooling systems can be efficiently operated in locations where sufficient solar radiation and good heat sink are available.

A solar-driven ejector refrigeration system has been selected as a case study for a further detailed investigation. A low temperature heat source can be used to drive the ejector refrigeration cycle, making the system suitable for integration with the solar thermal collector. Analysis of the solar driven ejector system is initiated by steady state analysis. System performance depends on the choice of working fluid (refrigerant), operating conditions and ejector geometry. Results show that various kinds of refrigerants can be used. Also, thermodynamic characteristics of the refrigerant strongly influence the performance of the cycle. An ejector refrigeration cycle using natural working fluids generates good performance and lower environmental impact, since traditional working fluids, CFC's and HFC's are strong climate gases. Further on, exergy analysis is used as a tool in identifying optimum operating conditions and investigating losses in the system. Exergy analysis illustrates that the distribu-

tion of the irrervsibilities in the cycle between components depends strongly on the working temperatures. The most significant losses in the system are in the solar collector and ejector. Losses in the ejector predominate over total losses within the system.

In practice, the cooling load characteristic and solar radiation are not constant. Therefore, a dynamic analysis is useful for determining the characteristics of the system during the entire year, and dimensioning the important components of the solar collector subsystem, such as storage tanks.

The final section of the thesis will deal with the ejector, the key component of the ejector refrigeration cycle. Characteristics of the actual ejector are shown to be quite complicated and its performance difficult to determine solely through theoretical analysis. Suggested design procedures and empirical equations for an ejector are offered in this thesis. Preliminary test results for one fixed ejector dimension using R134a as the refrigerant are also included.

Keywords: Solar Cooling; Solar-Driven Refrigeration System; Ejector; Ejector Refrigeration Cycle; Exergy Analysis; Dynamic Analysis

Acknowledgements

People have often inquired about my decision to stay and continue my studies in Sweden. Any attempt to justify the reason why I chose to come to a country, where the climate and environment are so extremely different from my own native country would be very difficult. Perhaps it can be explained by a burning desire for adventure, destiny, or a combination of both. Nevertheless, I would like to thank whatever forces that have brought me here, but in particular the *Energy Conservation and Renewable Energy Fund*, for providing me with a scholarship during my doctoral studies here in Sweden.

I would also like to take this opportunity to thank my supervisor, *Professor Per Lundqvist*. During my time here in Sweden, he has been extremely supportive of my ideas, and has provided an invaluable input to the project. You are a special person with a boundless capacity for ideas and a great inspiration for me. Thanks also for the brief lecture on classical music while sitting in an exclusive seat at the *Konserthuset* during a concert by Valerij Gergiev., as well as the sailing trip in to St. Nassa with your wonderful family, Anne, Felix and Max, which was both breathtaking and exciting.

Many thanks to the staff at the Division of Applied Thermodynamics and Refrigeration, *Professor Björn Palm, Professor Eric Granryd, Benny Sjöberg, Benny Andersson, Anders Johansson, Cecilia Hägg, Bo Johansson, Leif Nilsson (IIP), Bernt Jansson (HPT), Jaime Arias, Åke Melinder, Hans Johansson, Claudi Martín, Dimitra Sakellari, Samer Sawalha, Emilio Navarro, Jan-Erik Nowacki, Getachew Bekele, Joachim Claesson, Shota Nozadze, Peter Hill, Wahib Owhaib, Oxana Samoteeva, Raul Anton, Branko Simanic, Teclemariam Nemariam, Anita Elksne, Nabil Kasem, Birger Söderström, Tony Chapman and Chunhong Sheng*, gracious people who have all provided very useful help and advice during my stay here at the lab. A special thanks to *Inga Du Rietz*, the most considerate, kind-hearted and helpful secretary I have ever had the pleasure of encountering. Thanks also for the very enjoyable lunch dates and discussions we had in our lunch group consisting of *Susy Mathew, Primal Fernando, Rahmatollah Khodabandeh, Yang Chen, Richard and Dorothy Furberg*. Big thanks to *Anita Elksne* and *Damon Lane*, for the language corrections and valuable comments in the thesis.

I am forever grateful to my family and relatives in Thailand: my parents *Chamsri* and *Wirach*, my brother *Thanaphon* and my grandmother *Praphai*. I would like to extend a special gratitude to the 'Hägg' Family*, Gunvor, Lennart, Göran, Hans, Catharina, Anneli, Cecilia, Louise, and Wilhelm*, who welcomed me as a family member, and taught me Swedish culture. Christmas Eve celebrations in Brålanda, summers spent together in Sonnebo, and many other occasions were so memorable, that I will cherish them forever.

One of the places that most impressed me in Sweden was the Stockholm International Library (*Internationella Bilioteket*). The books and services here are truly remarkable. This library made the long and dark Stockholm winters more pleasurable.

This section would not be complete if I didn't mention all of my Thai friends here in Sweden who provided me with delicious food (either new inventions or traditional Thai dishes), endless smiles, laughs, crazy activities and creations. Thanks *P'Jom, Mats and Emilie Näslund, P'Aoy and Folke Andersons, P'Nid, Win, P'Tee, Thep, Nong, Nok, Nam, O+, Toey, Tum, Care, Mam, Lor,* and *Miles*. A special thanks to *P'Tee, Yang, Samer, Claudi, P'Nom, Sittisak, Manustai and Susy* who supported and took good care of me after my knee surgery, and during the following recuperation period.

Wimolsiri Pholasaeva

Stockholm, August 2006

Publications

Journal Papers:

Published:

Pridasawas, W. and Lundqvist, P. (2004): An Exergy Analysis of a Solar-driven Ejector Refrigeration System, Solar Energy, vol. 76, pp. 369-379.

In Review:

Pridasawas, W. and Lundqvist, P. (2006): A Dynamic Simulation of a Solar-driven Ejector Refrigeration System.

In review process for the International Journal of Refrigeration

Conference Papers (Peer Reviewed):

Pridasawas, W. and Lundqvist, P. (2002): Working Fluid Selection for an Ejector Refrigeration Cycle, Zero Leakage – Minimum Charge Conference, Joint meeting of the International Institute of Refrigeration Sections B and E, August 26-28, Stockholm, Sweden.

Pridasawas, W. and Lundqvist, P. (2003): Natural Working Fluids for a Solar-driven Ejector Refrigeration System, Eurotherm Seminar No. 72, Thermodynamics, Heat and Mass Transfer of Refrigeration Machines and Heat Pumps, March 31 – April 2, Valencia, Spain.

Pridasawas, W. and Lundqvist, P. (2003): Feasibility and Efficiency of Solar-driven Refrigeration Systems, 21st IIR International Congress of Refrigeration, August 17-22, Washington D.C., USA.

Pridasawas, W. and Lundqvist, P. (2004): Butane as a refrigerant for a solar-driven ejector refrigeration system, Proceedings of the 6th IIR Gustav Lorentzen Natural Working Fluids Conference, August 29th – September 1st, 2004, Glasgow, UK.

Conference Papers (Others):

Pridasawas, W. and Lundqvist, P. (2003): Technical Options for a Solar-driven Cooling System, ISES Solar World Congress 2003, June 14-19, Göteborg, Sweden.

Pridasawas, W. and Lundqvist, P. (2003): A Year-round Simulation of a Solar-Driven Ejector Refrigeration System, Proceedings of the International Conference on Fluid and Thermal Energy Conversion 2003, December 7-11, Bali, Indonesia.

Pridasawas, W. and Lundqvist, P. (2004): Optimization of a small-scale solar-driven ejector refrigeration system, Proceedings of the 14th international Sonnenforum, EuroSun2004, June 20-23, Freiburg, Germany.

Table of Contents

List of Figures

List of Tables

1 Introduction

1.1 Background

Energy supply to refrigeration and air-conditioning systems constitutes a significant role in the world. The International Institute of Refrigeration (IIR) has estimated that approximately 15% of all electricity produced worldwide is used for refrigeration and air-conditioning processes of various kinds (Lucas, 1988). According to the statistics survey by JARN[1] and JRAIA[2], the demand for air conditioners worldwide has the fundamental tendency of steady increase (IIR, 2006). The global growth rate is about 17%.

The cooling load is generally high when solar radiation is high. Together with existing technologies, solar energy can be converted to both electricity and heat; either of which can be used to power refrigeration systems.

The idea is not new, a solar-driven refrigerator was first recorded in Paris in 1872 by Albel Pifre (Thévenot, 1979). A solar boiler was used to supply heat to a crude absorption machine, producing a small amount of ice. Later, solar powered refrigeration systems have been installed worldwide in many countries e.g. Australia, Spain, and the USA. Most are thermally driven absorption systems, designed for air-conditioning purposes.

Being provided with a good electricity grid worldwide, people are, however, more likely to choose a vapour compression air-conditioning system. Before the energy crisis in the 1970s, research and development on solar thermal driven refrigeration systems was notably reduced. Subsequently, electricity-driven vapour compression systems have played a significant role on the market. At that time, photovoltaic (PV) technol-

[1] Japan Air Conditioning, Heating & Refrigeration News

[2] Japan Refrigeration and Air Conditioning Industry Association

ogy was expensive, had low efficiency and was not as widely available as today.

Due to energy shortage in some regions, especially after the energy crisis of the 1970's, solar energy as a renewable energy source has once again become a popular energy source. Research and development in the solar energy field has grown rapidly, along with research in solar cooling.

With the invention of the DC-motor, photovoltaic technology was first used for pumping water. Later the pump motor was modified to drive the vapour compression system. PV-driven water pumps and refrigerators have since become a relatively large business. Subsequently, researchers have integrated so -called Peltier coolers with PV-panels to simple, yet inefficient solar coolers. These systems are used in the cold chain projects of the World Health Organization (WHO). WHO initiated the development of solar refrigeration by photovoltaic panels in 1979, following the world conference on environment in Rio de Janeiro. The first specification of a solar refrigerator for medical use was published by the 'Expanded Programme of Immunization' (EPI). WHO and the United Nations International Children's Emergency Fund (UNICEF) adopted a certifying procedure to ensure that refrigerators from different companies had the same standard. In 1993, WHO reported that solar-driven refrigerators could improve the storage and transportation of vaccines in the EPI, which was better than the kerosene refrigerator (kerosene-driven diffusion absorption refrigerator, Electrolux type), and vaccines could consequently be distributed more efficiently. In 1996, WHO concluded that solar-refrigerators had significant benefits fulfilling immunization activities. Furthermore, the photovoltaic power system could be coordinated with other applications in a medical centre. However, WHO decided on refraining from an implementation programme that focused exclusively on solar vaccine refrigerators, contending that it could not compete with gas-powered units in terms of investment and recurring costs (WHO, 1996).

The International Energy Agency (IEA) inaugurated the 'Solar Heating and Cooling' program in 1976. This program is still on-going. Solar cooling is focused under task 25, "Solar Assisted Air Conditioning of Buildings" which was initiated on June 1, 1999 and ended on May 31, 2004. A new task (No.38) entitled 'Solar Air-Conditioning and Refrigeration' will be inaugurated in October 2006.

Solar cooling has been the main theme at several conferences e.g. IIR 1982 ('Solar Energy for Refrigeration and Air-Conditioning', Jerusalem), ISES 1997 ('Solar Mean Business', Taejon), ISES 2003 (Göteborg, Swe-

den), EUROSUN 2004 (Freiburg, Germany). An international session on 'Solar Heating and Cooling' was arranged during the National ATI Congress in Perugia, Italy, 2006. This session is supported by IIR.

The number of solar refrigerators has been increasing annually. Fléchon, Lazzarin et al., 1999, reported that a180 kilowatt peak (kWp) of solar-driven refrigeration capacity had been installed by 1985, 740 kWp by 1993 and 1600 kWp by 1997. Almost half of the systems are installed and operating in Africa for vaccine storage. There are a few commercial systems currently available, e.g. a vapor-compression/PV and an absorption/thermal collector. Solar air-conditioning systems have also been regularly in operation. Commercial absorption cooling machines e.g. Yazaki (Japanese) are available. According to Hans-Martin Henning (Fraunhofer Institute Ise, Germany), about 70 solar air-conditioning systems driven by the solar energy are in operation in Europe, with a total cooling capacity of 6.3 MW, corresponding to 17 500 m^2 of installed solar thermal collector area (Meyer, 2005).

1.2 Structure and scope of the Thesis

This thesis is comprised of two dimensions;: one broad, with the aim of providing a general picture of options for solar cooling, and one narrow, with the aim of investigating one particular cycle in detail. The choice of cycle for investigation is not arbitrary; previous work at the Department of Energy Technology, KTH has indicated that the ejector cycle has some interesting features such as simplicity, a low number of moving parts and the ability to operate with relatively low temperature heat sources; a feature that could potentially counterbalance the relatively low COP that could be expected. The development of new working fluids, as well as the re-discovery of old, produced to meet environmental challenges in the field of refrigeration is additional evidence that the available working fluids today are quite different compared to only a few years ago. Another interesting development influencing the scope of the thesis is the simulation techniques for dynamic analysis of energy systems and the possible coupling to software for detailed thermodynamic cycle analysis through so-called co-solving. Solar driven ejector refrigeration system has been modeled and yearly simulations have been performed in this way.

A broad overview of possible technologies for solar powered refrigeration and air-conditioning systems is presented in Chapter 2. The concept of the 'Solar Cooling Path' is introduced in order to organize and group

potential refrigeration cycles possible in solar cooling systems, dependant on solar conversion methodology, and required temperature level for cooling.

The importance of the local factors, with a few examples, is presented in Chapter 3. It is undeniably difficult to design a 'one-size-fits-all' refrigeration or air-conditioning system, which can be applicable world-wide. The effects of the widely varying local conditions must also be taken into consideration.

An in-depth study is started in Chapter 4, where a detailed model of the solar-driven ejector refrigeration system is presented. The following chapter, Chapter 5, deals with the selection of a proper working fluid for the ejector refrigeration subsystem to comply with performance as well as environmental requirements. Several different working media are compared.

A steady state simulation of the solar-driven ejector refrigeration system is presented in Chapter 6. The simulations in Chapter 6, as well as the exergy analysis in Chapter 7 are implemented by models developed in the Engineering Equation Solver Program, EES (Klein, 2004). Exergy analysis is used as a tool to analyse and quantify losses within the system – something that is impossible to do by an energy balance – based on the first law of thermodynamics. Exergetic efficiency and optimum operation conditions are described and analysed in Chapter 7.

The main energy supply to the solar-driven ejector refrigeration system is not constant and also strongly dependant on annual climate conditions. From a design point of view, a steady-state analysis cannot provide a proper design. The dynamic simulation can present the system characteristic during the whole year much clearer than a steady-state analysis. The dynamic simulation in Chapter 8 is performed by the TRaNsient System Simulation program, TRNSYS, (Klein, Beckman et al., 2004b) coupled to EES through so-called co-solving.

The ejector is the key component of the ejector refrigeration system. The design procedure and the typical ejector characteristics are thus discussed in Chapter 9. The theoretical dimensions of some parts of the ejector can be roughly calculated from the normal isentropic equations of an ideal gas. Suggested design procedures and empirical equations for steam ejectors can be found in literature, but data of this kind is rarely found for other working media than water. The actual result is, in fact, quite different from the result of the theoretical analysis. Only experiments can thus

illustrate the actual performance of each ejector. In this chapter, the test results for one specific ejector using R134a as the refrigerant is also included.

This is not a thesis where new models for solar collectors or buildings are developed, refined and evaluated although these components are modelled as an integral part of the work. Much more work can undoubtedly be performed in this area. This is a thesis within the field of applied thermodynamics and refrigeration with focus on the ejector cycle used in solar cooling applications.

The following section presents a short review of publications by the author

Paper 1:

Pridasawas, W. and Lundqvist, P. (2003): Feasibility and Efficiency of Solar-driven Refrigeration Systems, 21st IIR International Congress of Refrigeration, August 17-22, Washington D.C., USA.

In this paper, the history of solar cooling is presented. The possibilities for solar cooling in various climates and the dependency of local conditions are clarified by selecting a suitable and sustainable technology. The study adapts a systems perspective including the analysis of demand, local conditions, local possibilities, and various technical solutions rather than a specific technology. Currently, solar thermal-driven air-conditioning systems are appealing in many regions due to the increase of cooling demand which is generally in phase with the insolation. The sorption systems are primarily installed for this purpose. Furthermore, PV-driven refrigerators are commercially available for a mobile unit such as a cooling box. The cost of the solar cooling system is currently dependent on photovoltaic panels and solar collectors. The economical advantages of this system are still obscure due to high installation costs.

Paper 2:

Pridasawas, W. and Lundqvist, P. (2003): Technical Options for a Solar-driven Cooling System, ISES Solar World Congress 2003, June 14-19, Göteborg, Sweden.

Utilization of solar energy is one way of meeting the increasing demand for refrigeration and air-conditioning applications. New refrigeration technology based on solar energy has not fundamentally attracted much of the commercial refrigeration and air-conditioning industry thus far. This is an indication that the development and production of such equipment is a future business endeavour. This paper attempts to adapt a system perspective including the analysis of demand, local conditions and possibilities, as well as various technical solutions rather than a specific technology. An overview of a state of the art solar cooling technology towards sustainability is introduced. The technical consequences of a solar-cooling technology from energy source to service, for both solar thermal-driven systems and photovoltaic-driven systems are presented. The importance of both local conditions and demand is introduced as a guideline for choosing a suitable solar cooling system. The principle of cooling technique is briefly explained including the advantages and disadvantages of each system.

Paper 3 :

Pridasawas, W. and Lundqvist, P. (2002): Working Fluid Selection for an Ejector Refrigeration Cycle, Zero Leakage – Minimum Charge Conference, Joint meeting of the International Institute of Refrigeration Sections B and E, August 26-28, Stockholm, Sweden.

The paper presents a comparison of a single-stage ejector refrigeration cycle, operating with different refrigerants. This model is developed in Engineering Equation Solver (EES). The performance of the ejector refrigeration system is strongly dependent on the operating temperatures as well as the geometry. Thermodynamically possible refrigerants for the ejector refrigeration cycle and performances of some working fluids, such as R113, R114, R134a, R141b, R143a, R600, R600a, ammonia and water are presented and compared in detail with respect to the coefficient of performance (COP), fluid characteristics and environmental impact. Water, an environmentally friendly working fluid, generates a high COP, however a drawback is that a high vapour volume per refrigeration

capacity makes its dimension undesirable. Since the ejector cooling system can be operated at a low generating temperature low-graded heat, waste heat (e.g. from a truck engine) or solar energy with low efficiency conversion apparatus (e.g. flat plate solar collector) can be used. Guidelines for working fluid selection are given at various operating conditions.

Paper 4:

Pridasawas, W. and Lundqvist, P. (2003): Natural Working Fluids for a Solar-driven Ejector Refrigeration System, Eurotherm Seminar No. 72, Thermodynamics, Heat and Mass Transfer of Refrigeration Machines and Heat Pumps, March 31 – April 2, Valencia, Spain.

A solar-driven ejector refrigeration system with six natural working fluids: water, ammonia, methanol, butane, iso-butane and propane are simulated, and the results are compared. The coefficient of performance (COP), the system thermal ratio (STR), and the entrainment ratio and safety issues of each refrigerant are compared. Operating conditions (generating, condensing and evaporating temperatures), and characteristics of the refrigerant influence the system performance. The coefficient of performance (COP_{ejc}) of the refrigeration cycle is influenced by the operating temperatures whereas the STR is influenced by both the generating temperature and the solar collector efficiency. The STR increases at the low generating temperature but decreases at the high generating temperature due to the decrease of the solar collector efficiency. It is in proportion with the evaporating temperature, but in contrast with the condensing temperature. According to the results, water yields the highest performance, following by methanol, ammonia and hydrocarbon refrigerants (butane, iso-butane and propane).

Paper 5:

Pridasawas, W. and Lundqvist, P. (2004): An Exergy Analysis of a Solar-driven Ejector Refrigeration System, Solar Energy, vol. 76, pp. 369-379.

Exergy analysis is used as a tool for analyzing the performance of an ejector refrigeration cycle driven by solar energy. The analysis is based on the following conditions: a solar radiation of 700 W m^{-2}, an evaporator temperature of 10°C, a cooling capacity of 5 kW, butane as the refrigerant in the refrigeration cycle and ambient temperature of 30°C as the reference temperature. Irreversibilities occur among components and depend on the operating temperatures. The most significant losses in the system are in the solar collector and the ejector. The latter decreases inversely proportionally to the evaporation temperature and dominates the total losses within the system. The optimum generating temperature for a specific evaporation temperature is obtained when the total losses in the system are minimized. For the above operating conditions, the optimum generating temperature is about 80°C.

Paper 6:

Pridasawas, W. and Lundqvist, P. (2003): A Year-round Simulation of a Solar-Driven Ejector Refrigeration System, Proceedings of the International Conference on Fluid and Thermal Energy Conversion 2003, December 7-11, Bali, Indonesia.

In this study the TRNSYS-EES simulation tool is used to simulate the characteristic of the solar-driven ejector refrigeration system with a flat-plate, double-glazed solar collector. Butane is used as a refrigerant in the cooling subsystem and water is used as a heating medium in a solar-collector subsystem. The performance of the system is shown in terms of coefficient of performance (COP) for the refrigeration subsystem and system thermal ratio (STR) for the whole system. The simulation results show the characteristic of the system for the whole year. The system performance depends on the incident solar radiation and the operating temperatures in the refrigeration subsystem. The highest STR is generally achieved during midday and it is around 0.2 at a COP around 0.55.

Paper 7:

Pridasawas, W. and Lundqvist, P. (2004): Optimization of a small-scale solar-driven ejector refrigeration system, Proceedings of the

14th international Sonnenforum, EuroSun2004, June 20-23, Freiburg, Germany.

The TRNSYS-EES simulation tool is used to simulate the characteristic of the solar-driven ejector refrigeration system with a flat-plate, double-glazed solar collector. Butane is used as a refrigerant in the cooling subsystem and water is used as a heating medium in a solar-collector subsystem. The performance of the system is shown in terms of the COP for the refrigeration subsystem and the STR for the whole system. The simulation results illustrate the performance of the system, the annual electricity usage by the pumps and the auxiliary heater at different solar collector areas, storage tank volumes and water flow rates. The system performance depends on the solar radiation and the operating temperatures in the refrigeration subsystem. The STR is high conjointly when the solar radiation is high. The maximum STR that can be obtained is about 0.25 at a COP of 0.55. The optimum solar collector area for the average cooling load 4 kW is about 50 m^2. The system operates only during daytime; consequently, the volume of the well-mixed storage tank does not significantly affect the performance or the extra electricity usage of the system.

Paper 8 :

Pridasawas, W. and Lundqvist, P. (2004): Butane as a refrigerant for a solar-driven ejector refrigeration system, Proceedings of the 6th IIR Gustav Lorentzen Natural Working Fluids Conference, August 29th – September 1st, 2004, Glasgow, UK.

In this paper, the effect of the operating conditions in a solar-driven ejector refrigeration system with n-butane and iso-butane is studied. The properties, thermodynamics characteristics and safety issues of n-butane and iso-butane are discussed. In practice, it is difficult to achieve steady-state operating conditions due to constant solar radiation and cooling load change. The TRNSYS-EES simulation tool is used to model and analyse the performance of a solar-driven ejector refrigeration system. The entire system is modelled by using the TRNSYS program; however, the model of the ejector refrigeration sub-system is developed in the engineering equations solver (EES) program. The solar collector subsystem and load are modelled by use of TRNSYS. Performance of the system is presented in the form of system thermal ratio (STR), depending on both COP of the ejector refrigeration subsystem and solar collector efficiency.

The simulation results illustrate that the system using normal butane has a slightly better performance than the system using iso-butane. The cost of normal-butane is, however, much higher than iso-butane, therefore it is more beneficial to use iso-butane instead of normal-butane for this application.

Paper 9:

Pridasawas, W. and Lundqvist, P. (2004): A Dynamic Simulation of a Solar-driven Ejector Refrigeration System.

On the reviewing process of the International Journal of Refrigeration

In this paper, the performance of the solar-driven ejector refrigeration system with iso-butane (R600a) as the refrigerant is studied. The effects both the operating conditions and solar collector types have on the system's performance are also examined by dynamic simulation. TRNSYS and EES simulation tools are used to model and analyze the performance of a solar-driven ejector refrigeration system. The entire system is modelled under the TRNSYS environment; however, the model of the ejector refrigeration sub-system is developed in the Engineering Equations Solver (EES) program. The COP of the ejector refrigeration subsystem increases in proportion to the evaporator temperature. A solar fraction of 75% is obtained when using the evacuated tube solar collector. In a very hot environment, the system requires a relatively high generator temperature, thus a flat plate solar collector is not economically beneficial due to the high amount of auxiliary heat needed to boost the generator temperature. The results from the simulation indicate that an efficient ejector system can only work in a region with decent solar radiation, where a sufficiently low condenser temperature can be sustained. The maximum cooling capacity is about 3.5 kW.The average yearly system thermal ratio (STR) is about 0.22, the COP of the cooling subsystem is about 0.48, the solar collector efficiency is about 0.47 at T_e 15°C, T_c 5°C above the ambient temperature, evacuated collector area of 50 m^2 and hot storage tank volume of 2 m^3.

PART I:
System Definitions and Literature Survey

This part consists of:

Chapter 2 Solar Cooling Options and Technologies

2.1 Solar Cooling Paths

2.2 Definitions and Thermodynamic Limitation

2.3 Solar Driven Refrigeration Systems in Brief

Chapter 3 Effects on Local Conditions

3.1 Climate

3.2 Solar Cooling in Different Locations

3.3 Conclusions

2 Solar Cooling Options and Technologies

In this chapter, the concept of 'solar cooling path' from the energy source to the cooling service, is introduced. Before going into detail for each solar-driven refrigeration system, definitions, suitable efficiency terms, and thermodynamic limitations of solar cooling are described. Subsequently, an overview of possible solar-driven refrigeration and air-conditioning options are presented, including all possible and existing cooling cycles. The advantages and disadvantages of each solar cooling system are compared at the end of the chapter.

2.1 Solar Cooling Paths

The solar cooling system is generally comprised of three sub-sustems: the solar energy conversion system, refrigeration system, and the the cooling load. The appropriate cycle in each application depends on cooling demand, power, and the temperature levels of the refrigerated object, as well as the environment. A number of possible "paths" from solar energy to "cooling services" are shown in Figure 2-1.

Starting from the inflow of solar energy there are obviously two significant paths to follow; solar thermal collectors to heat or PV cells to electricity. For solar thermal collectors, different collector types produce different temperature levels. This indicates that the temperature level can be matched to various cycle demands. For example, the Rankine cycle (duplex type, explained later in this thesis), requires a rather high driving temperature whereas the desiccant cycle manages at a lower temperature level of heat supply.

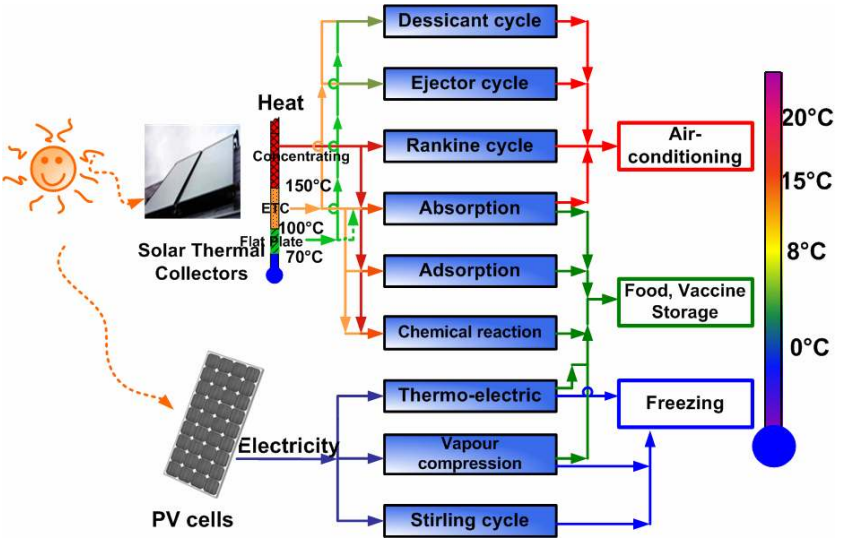

Figure 2-1 Solar Cooling Paths

The same type of temperature matching is important for the cold side of the solar cooling path, i.e in the cold object. Since several cycles typically operates with water as a working fluid, it is impossible to achive tempertures below 0°C for some cycles. The solar thermal-driven air-conditioning cycles can be based on absorption cycles, adsorption cycles, duplex rankine, desiccant cooling cycles, or ejector refrigeration cycles.

When using low temperature applications for food storage at 0 to -8°C, various cycles can be applied, i.e. the vapour compression cycle, thermoelectric cycle (Peltier), absorption cycle‡, adsorption§ cycle or a chemical reaction cycle. Applications requiring temperatures below 0°C generally require small storage volumes e.g., freezing boxes. A suitable cycle for this application has proved to be the PV-driven vapour compression cycle, or a PV-driven Stirling cycle. The double effect absorption cycle, adsorption cycle and chemical reaction cycle can also be used, especially for larger storage volumes, i.e. ice production.

‡ With ammonia as a working fluid

§ With ammonia as a working fluid

Typically for the cycles in Figure 2-1 is that, the efficiency of the electricity-driven refrigeration cycles are quite high but they require photovoltaic panels and batteries, which are expensive. Heat driven cycles on the other hand, are less efficient, but the thermal solar collectors may reach much higher conversion efficiencies than the PV's, even though the output is heat, not electricity. Therefore, the question is: which path provides the highest overall efficiency? One example:

System 1, a heat driven cycle with a cycle COP of 0.7 receives its heat from a solar collector with 80% efficiency. *System 2*, a vapour compression refrigeration cycle with a COP of 4 receives its electricity from a PV array with an efficiency of 15%. Which one give the highest overall efficiency? In this thesis, efficiency is denoted STR, System Thermal Ratio (defined in Equation 2.21)?

The calculation is simple and straightforward, whereas the result is more difficult to interpret. Apparently, there are at least two paths to the same overall efficiency. There is also a necessity to better define the various efficiencies needed for the analysis.

$$STR_1 = \eta_{collector} \cdot COP_{cycle} = 0.7 \cdot 0.8 = 0.56$$
$$STR_2 = \eta_{pv} \cdot COP_{cycle} = 0.15 \cdot 4 = 0.6$$

The calculation is simple and straightforward, whereas the result is more difficult to interpret. Apparently, there are at least two paths to the same overall efficiency. There is also a necessity to better define the various efficiencies needed for the analysis.

2.2 Definitions and Thermodynamic Limitations

Two groups of solar-driven refrigeration systems can be classified, depending on the type of energy converters, e.g. PV-electricity-driven and solar-thermal-driven. In this case, the term *refrigeration cycle* describes the thermodynamic cycle in which heat is absorbed at one temperature level and lifted it to a higher level where it is rejected.

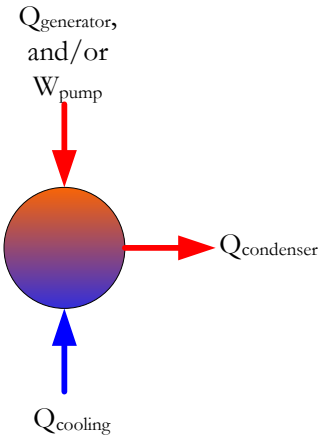

Figure 2-2 Heat Balance for a Refrigeration Cycle

The term "*system*" is frequently used in this thesis and here it typically refers to the combination of refrigeration cycles, a solar energy converter subsystem and cooling load subsystem in the same way that can be used for any other energy conversion system that can be enclosed by a system boundary.

2.2.1 Cycle Efficiencies

The performance of a refrigeration cycles is generally presented in terms of a coefficient of performance, COP, illustrating how much energy that-heat can be removed from a cold space (Q_e) for each unit of energy expended (W or Q_g). The COP can be written differently, depending on the type of drive energy. The frequently used definitions for COP of an electricity/work-driven system and thermally driven system are shown in equation 2-1 and 2-2, respectively.

$$COP_{el} = \frac{Q_e}{W} \qquad \textit{Eq. 2-1}$$

$$COP_{thermal} = \frac{Q_e}{Q_g} \qquad \textit{Eq. 2-2}$$

These definitions are frequently used in parallel. A system with very low use of electrify may thus be characterized by equation 2-1 and a COP of 15 to 20 has for example been suggested for sea water based district cooling (free cooling). This can be quite confusing and great care should be taken when reviewing commercial literature.

2.2.2 Solar Collector Efficiencies

The major energy gains in the absorber in a solar collector are from the direct absorption of visible light from the sun and, additionally, the absorption of infrared radiation from the warm glass. Important energy losses are infrared radiation emission, convective heat due to natural convection between the absorber and glass, as well as conduction of heat through the rear and sides of the collector. Therefore, the efficiency of the solar collector depends on all of these factors. The efficiency of the solar collector sub-system can be defined as the ratio of useful heat output to the total incident solar radiation (insolation).

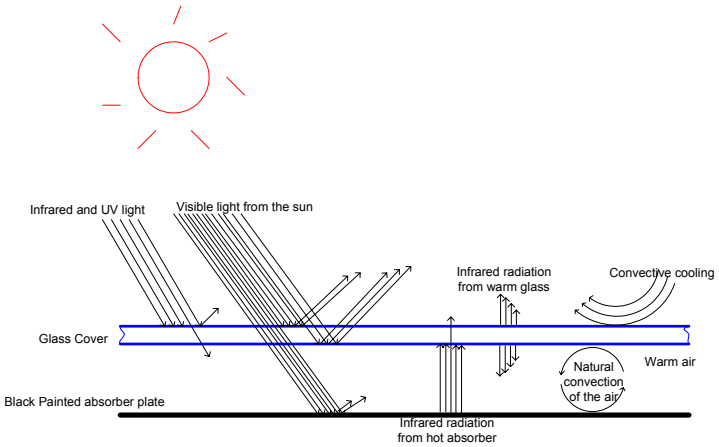

Figure 2-3 Energy Flows in a Single-Glazed Collector

In the following efficiency definition, it is assumed that radiation is in the hemispherical region, all rays reach the absorber, and the multiple reflections** between the cover and absorber are neglected. The solar collector efficiency can be written as,

$$\eta = F_m\left(\eta_{opt} - \frac{U_L(T_{abs,avg} - T_{a)}}{I}\right) \qquad \textit{Eq. 2-3}$$

F_m is called the collector efficiency factor or a heat transfer factor. The value of F_m depends on the type of the collector and operating conditions. Typical values of F_m is in the range of 0.8-0.9 for non-evacuated air collectors, 0.9-0.95 for non-evacuated liquid collectors, and 0.95-1 for evacuated collectors (Rabl, 1985).

In essence, it is easier to measure the temperature of the heat transfer fluid than to measure the temperature of the absorber surface temperature. Therefore, the solar collector efficiency is often written in terms of the temperature of the inlet (T_i) and outlet (T_o) temperature of the heat transfer fluid. The average temperature of the absorber surface can be assumed to be:

$$T_{abs,avg} = \frac{T_i + T_o}{2} \qquad \textit{Eq. 2-4}$$

The efficiency of the solar collector can be defined as

$$\eta = F_R\left(\eta_{opt} - \frac{U_L(T_i - T_{a)}}{I}\right) \qquad \textit{Eq. 2-5}$$

Or

$$\eta = F_R(\tau\alpha)_e - F_R U_L \frac{(T_i - T_a)}{I} \qquad \textit{Eq. 2-6}$$

F_R is the collector heat removal factor. The later equation is based on the 'Hottel-Whillier-Bliss' Equation. The value of factors $F_R(\tau\alpha)_e$ and $F_R U_L$ depend on the type of the collectors, layer of the cover glass and selective material. Typical values of these factors are shown in Table 2-1.

** Rays reflected back from the absorber to the glass are not accounted for

The efficiency of the solar collector (η) and the value of $(T_i-T_a)\ I^{-1}$ can be plotted in a graph, as shown below.

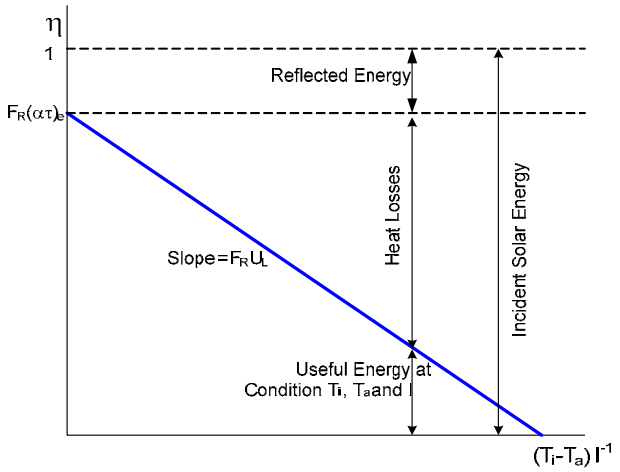

Figure 2-4 Characteristic Curve of a Solar Collector

Occasionally, the efficiency of a solar collector is written in quadratic form as shown in equation 2-7. This equation is commonly used in simulation to the solar collectors.

$$\eta = k(\Theta)\cdot c_0 - c_1\frac{(T_{abs,avg}-T_a)}{I} - c_2\frac{(T_{abs,avg}-T_a)^2}{I} \quad \textit{Eq. 2-7}$$

Where

$k(\Theta)$= incident angle modifier, which accounts for the influence of non-perpendicular incident radiation at the incident angle, Θ, in relation to the normal incidence radiation of $\Theta=0$

c_0 = optical efficiency

c_1 = linear heat loss coefficient

c_2 = quadratic heat loss coefficient

There are three major types of a thermal solar collector: Flat Plate Solar Collector, Evacuated Solar Collector and a Concentrating (Optical) Solar Collector. A flat plate solar collector allows both direct and diffuse solar radiation.

Table 2-1 The Value of $F_R(\tau\alpha)_e$ and $F_R U_L$ for Some Type of Solar Collector

Solar Collector Type	$F_R(\tau\alpha)_e$	$F_R U_L$ (W m^{-2} K^{-1})
Flat-Plate, Selective-Surface, Single-Glass Cover	0.80[a]	5.00[a]
Flat-Plate, Selective-Surface, Double-Glass Cover	0.80[b]	3.50[b]
Evacuated Tubular Collectors	0.80[a]	Range 1-2[a]
Parabolic-Through Concentrating solar collector (PTC)	0.70[c]	2.5[c]

Remark: (a) from Fléchon, Lazzarin et al., 1999
(b) from Huang, Chang et al., 1998
(c) average data from Table 4.1 in Henning, 2004

Flat Plate Solar Collectors

A flat plate solar collector is, often the most economical choice for low temperature applications such as solar water heating systems. Absorbers can be made of a plastic or a metallic plate such as copper. A tracking system is not necessary for this type of collector. The maintenance routines and structure are simpler than other types of solar collectors.

The optical efficiency of a flat plate solar collector can be written as a product of the transmissivity (τ) of the glass cover and absorptivity (α) of the absorber,

$$\eta_{opt} \cong \tau\alpha \qquad \textit{Eq. 2-8}$$

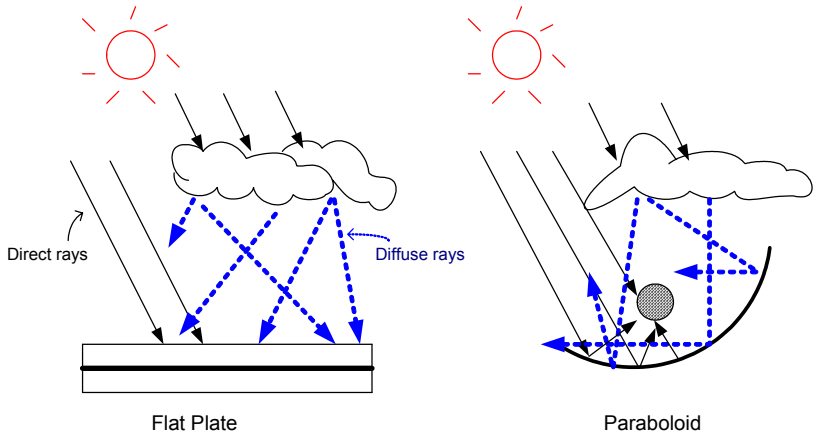

Figure 2-5 Solar Radiation on the Flat Plate Collector and the Parabolic Concentrating Collector

Evacuated Tube Solar Collectors

The evacuated tube solar collectors (ETC) are suitable for medium temperatures e.g. 100-150°C. They are generally made of a glass tube and are hermetically sealed. The glass tube contains an absorber with a working fluid circulating inside, or a heat-pipe system. The pressure inside is a partial vacuum (lower than 1kPa). This low pressure aims to reduce the convective heat loss. Most of these collectors are non-tracking and some use reflector enhancements. The obtained heat in the ETC-collector can be written as,

$$Q_{abs-\mathrm{cov}} = A_{abs}\varepsilon_{eff}\sigma(T_{abs}^4 - T_{\mathrm{cov}}^4) = A_{\mathrm{cov}}h_a(T_{\mathrm{cov}} - T_a) \quad \textit{Eq. 2-9}$$

where A_{abs} and A_{cov} correspond to the absorber and cover surface area. The effective emissivity (ε_{eff}) is given by the following equation.

$$\varepsilon_{eff} = \frac{1}{\frac{1}{\varepsilon_1} + \frac{1}{\varepsilon_2} - 1} \quad \textit{Eq. 2-10}$$

where ε_1 and ε_2 are the emissivity on surface 1 and 2.

$\varepsilon_{eff} \approx \varepsilon_{abs}$ for $\varepsilon_{cov} \approx 0.9$ and $\varepsilon_{abs} \leq 0.2$

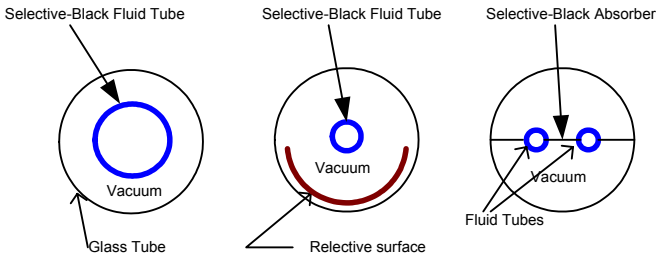

Figure 2-6 Design of Evacuated Solar Collector Tubes

Concentrating Solar Collectors

Two types of line-axis concentrating solar thermal collectors are commonly used today: a Compound Parabolic Concentrating (CPC) and Parabolic-through Concentrating (PTC). The simple structures of both of these types are shown in Figure 2-7.

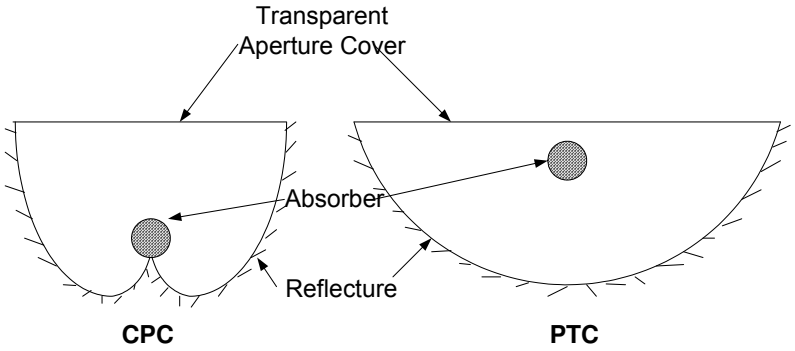

Figure 2-7 Structure of a Compound Parabolic Concentrating Solar Collector (CPC) and a Parabolic-Through Concentrating Solar Collector (PTC)

The concentration ratio (C) describes the characteristics of the concentrating solar collector. It is the ratio of the aperture area (A_a) to the receiver area (A_r).

$$C = \frac{A_a}{A_r} \qquad \textit{Eq. 2-11}$$

The concentrating optical solar collector is suitable for high temperature applications (e.g. tempertures >150°C). The large absorber area induces high heat losses. By concentrating the radiation incident of the aperture onto a smaller absorber, the heat losses per absorber area can be reduced. Tracking system is necessary to follow the movement of the sun in order to maintain concentration. The compound parabolic concentrator (CPC) is hovewer not necessary for tracking since the concentration ratio is quite low. The CPC can, therefore, play an important role in solar cooling in the future. The main contribution is the direct (not the diffuse) solar radiation which differs somewhat from the flat-plate solar collector.

Concentrators can be divided into two categories: non-imaging and imaging concentrators. The non-imaging concentrator does not produce a clearly defined image of the sun on the absorber; but distributes radiation from all parts of the solar disc onto all parts of the absorber. The values of the concentration ratio of linear non-imaging collectors are quite low, generally below ten. The imaging concentrator is similar to a simple camera lens, which can form images on the absorber.

For a concentrating collector with a reflectivity (ρ), the optical efficiency can be written as,

$$\eta_{opt} \cong \rho\tau\alpha \qquad \textit{Eq. 2-12}$$

The optical efficiency of the concentrating collector can also be written in an elaborate form, i.e. as shown in several literatures e.g. Norton, 1992 . These equations are placed here for reference but they are not used in the models in the thesis.

$$\eta_{opt,PTC} = \frac{\tau\rho\alpha\gamma(\beta_B I_B + \beta_B g_{D,PTC} I_D)}{I_B + I_D} \qquad \textit{Eq. 2-13}$$

and

$$\eta_{opt,CPC} = \left(\frac{G_u}{G_{tot}}\right)\tau_{\cos}\tau_{env}\alpha_{abs}\,p\,\rho_{ref}^{\bar{n}}\,(1-\rho_{abs}\rho_{env}\frac{A_{abs}}{A_{env}})^{-1} \quad \textit{Eq. 2-14}$$

Where:

A_{abs} = Absorber area, m²

A_{env} = Envelop area, m²

G_u = Exploitable absorbed solar radiation, W m^{-2}

G_{tot} = Total hemispherical solar radiation, W m^{-2}

p = Gap optical losses factor

β_D = Correction coefficient, which accounts for diffuse insolation, which reaches the absorber directly and it is not attenuated by reflection losses

β_B = Correction coefficient, which accounts for direct insolation, which reaches the absorber directly and it is not attenuated by reflection losses

γ = Interception factor

τ_{cov} = Transmissivity of cover

τ_{env} = Transmissivity of envelop

α_{abs} = Absorptivity of absorber

ρ_{ref} = Reflectivity of reflector

ρ_{abs} = Reflectivity of absorber

ρ_{env} = Reflectivity of envelop

2.2.3 Photovoltaic Efficiencies

The efficiency of a photovoltaic cell can be written as

$$\eta = \eta_R\left[1-\beta(T_c - T_R)\right] \qquad \textit{Eq. 2-15}$$

Where:

η_R = Reference efficiency at 0°C (about 0.12 for single crystalline cells)

β = Coefficient of variation of the solar cell efficiency (about 0.04 K-1 for single crystalline cells)

T_c = Cell Temperature (°C)

T_{ref} = Reference Temperature (°C)

Normally, one cell produces a potential difference of 0.5 volt and a current density of 200 Amp m^{-2} at 1 kW m^{-2} of solar radiation (Twidell and Weir, 1998). The efficiency of avaialable commercial photovoltaic cells is about 10-17% and they can produce 1-1.5 kWh m^{-2} per day (Twidell and Weir, 1998). The current is proportional to the light exposure area.

2.2.4 System Efficiencies

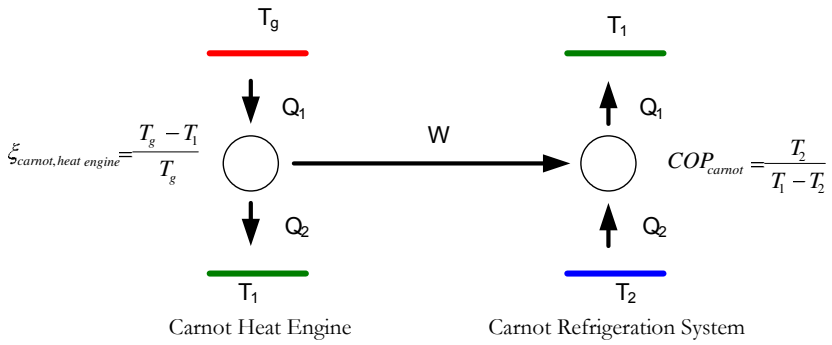

Figure 2-8 Definition of System Carnot Efficiency

In the case of an ideal heat engine and refrigerator, here referred to as Carnot cycles, the performance of the Carnot Heat Engine Cycle driving the Carnot Refrigeration Cycle can be written in terms of the Carnot efficiency and the Carnot Coefficient of Performance (COP_{Carnot}), as shown in Figure 2-8.

$$\xi_{Carnot\_Heat\_Engine} = \frac{T_g - T_1}{T_g} \qquad \textit{Eq. 2-16}$$

$$COP_{Carnot} = \frac{T_2}{T_1 - T_2} \qquad \textit{Eq. 2-17}$$

$$\eta_{carnot} = \xi_{carnot,heat\_engine} \cdot COP_{carnot} \qquad \textit{Eq. 2-18}$$

$$\eta_{carnot} = \left(\frac{T_g - T_1}{T_g}\right) \cdot \left(\frac{T_2}{T_1 - T_2}\right) \qquad \textit{Eq. 2-19}$$

For a PV-driven system, the simple Carnot Engine Efficiency (ξ) becomes the efficiency of the PV-array.

$$\eta_{system,el} = COP_{el} \times \eta_{PV} \qquad \textit{Eq. 2-20}$$

For the solar-driven refrigeration system, performance can, therefore, be depicted as the product of the COP and solar collector efficiency (η_{sc}) or the PV efficiency (η_{PV}). Alternatively, it can be defined as a ratio of the refrigeration effect and solar radiation input (G) for the thermal-driven system, which is designated as the 'system thermal ratio (STR)'. This term has been used by IIR, Guide to Solar Refrigerators for Remote Areas and Warm Countries (Fléchon, Lazzarin et al., 1999). This term will also be used in this thesis in describing the performance of the solar-thermal driven refrigeration machine.

$$STR = \frac{Q_e}{G \cdot A} = \frac{Q_e}{Q_g} \times \frac{Q_g}{G \cdot A} = COP \times \eta_{sc} \qquad \textit{Eq. 2-21}$$

Since the main energy source is free for solar cooling systems, the term 'solar fraction' is better suited for demonstrating the overall effectiveness of the system. Solar fraction is defined as the ratio of the total solar energy used to the total energy used in the system.

$$\text{Solar Fraction} = \frac{\text{Solar Energy Used in the System}}{\text{Total Energy Used in the System}} \qquad \textit{Eq. 2-22}$$

2.3 Solar Driven Refrigeration Systems in Brief

Table 2-2 illustrates an overview of some key characteristics for different system types. Thermally driven cycles dealt with are absorption, adsorption, chemical reaction, desiccant cooling, ejector and the Rankine refrigeration cycles. PV driven cycles are the Stirling, thermo-electric and vapour compression refrigeration cycles.

Table 2-2 Existing Solar-Driven Refrigeration Technologies

Refrigeration Cycle	Solar Technology		COP_{cycle}	Available Applications Today		
	Thermal Collectors (Tgen./ Tregen (°C))	PV Cells (Power for 3o L Cooling Box (W)		Refrigeration	A/C	Example Applications
Electricity/Work Driven Cycles						
Vapour-compression		✓ (16-40)	3-5	✓		HR, SR, CB
Thermo-electric		✓ (a few mW)	0.5[a]	✓		VT, CB, CT
Stirling		✓ (8-50)	3[b]	✓		CB, LT
Heat Driven Cycles						
Absorption	✓ (80-190)		0.6-0.8 (single stage)	✓	✓	AC, IP
Adsorption	✓ (80-300)		0.3-0.8	✓		CB, IP, VS
Chemical reaction	✓ (80-300)		0.1-0.2[a]	✓		IP, VS, FS
Duplex-Rankine	✓ (>120)		0.3-0.5[b]		✓	AC
Desiccant cooling	✓ (40-80)		0.5-1.5		✓	AC
Ejector	✓ (80-150)		0.3-0.8		✓	AC

Remark
a: Fléchon, Lazzarin et al., 1999, based on 5 kWh m^{-2} day^{-1} of the solar radiation, b: Gordon and Ng, 2000., AC: Air-Conditioning CB: Cooling Box, CT: Car, Transportation, FS: Food Storage, IP: Ice Production, HR: Household Refrigerator, LT: Low Temperature Applications, SR: Small Refrigerator VS: Vaccine Storage, VT: Vaccine Transportation

Most thermally-driven refrigeration systems found in the literature are suggested for air-conditioning purposes. Only adsorption and chemical adsorption cycles are used for applications serving lower temperatures (below 0°C). The temperature of the driving heat source varies, depending on type of cycle and the refrigerants used in the cycle. More details of each cycle with references to the literature can be found in the following sections.

This was the first type of solar refrigeration system to be introduced. It is now available on the market as small packaged systems. Heat is supplied to a device called the generator. The generator temperature can be lower than 100°C, depending on the refrigerant-absorbent pair, e.g., ammonia/water or water/lithium bromide. Low generator tempertures normally lead to significalty larger heat exchanger surfaces. Electricity is normally required for circulating the refrigerant-absorbent pair. The coefficient of performance (COP) of these refrigeration cycles is higher than the COP of other thermally operated cycles. With the single-stage cycle, a COP is obtained at about 0.6-0.8 and increased to 1.35 for a so-called double effect two-stage cycle (Gordon and Ng, 2000). It can be used in both refrigeration and air-conditioning applications. The absorption refrigeration cycle can be designed in different configurations as for example, the basic single effect cycle, the multi-stage absorption cycle, and the Platen Munters cycle which can be operated without a pump or the open cycle type.

Table 2-3 Comparison of Different Absorption Chillers for Solar-Driven Air Conditioning Systems (Grossman, 2002)

Type	Typical COP	Heat Source Temperature (°C)	Solar Heat Required per kW of Cooling Effect (kW)	Type of Solar Collectors
Single-effect	0.7	85	1.43	Flat plate
Double-effect	1.2	130	0.83	Flat plate / ETC
Triple-effect	1.7	220	0.59	ETC/CPC

Remark: ETC-Evacuated Tube Collector
CPC – Concentrated Parabolic Collector

The Single-Effect Absorption Cycle

The single effect absorption cycle can be either operated intermittently or continuously. An ammonia-water solution is used as the working fluid pair for low temperature applications and water-lithium bromide is used for air-conditioning applications. Commercial single effect absorption machines with an option of driving by solar energy are available by several companies such as Rotartica, Spain (Egilegor, Usbiaga et al., 2006; Rotartica, 2006) or LSCable, Korea (LSCable, 2006).

The Multi-Effect Absorption Cycle

The multistage design can improve the COP of the system at the cost of a higher driving temperature. There are several designs for multi-stage absorption systems: double effect, triple effect, absorber heat exchanger (AHX) or generator absorber heat exchanger (GAX) (Velázquez and Best, 2002). An example of the double effect absorption chiller is shown in Figure 2-9.

In general, the COP is improved by adding extra heat exchangers and arranging them in a way that heat can be utilised at different temperature levels. This means, in essence, that the same heat is utilised internally several times and of course, increaed complexity and cost. The solar driven double effect absorption system is quite promising and has been studied by several research groups (Berlitz, Lemke et al., 1998; Medrano, Bourouis et al., 2001; Saghiruddin, 2001; Ezzine, Barhoumi et al., 2004; Liu and Wang, 2004).

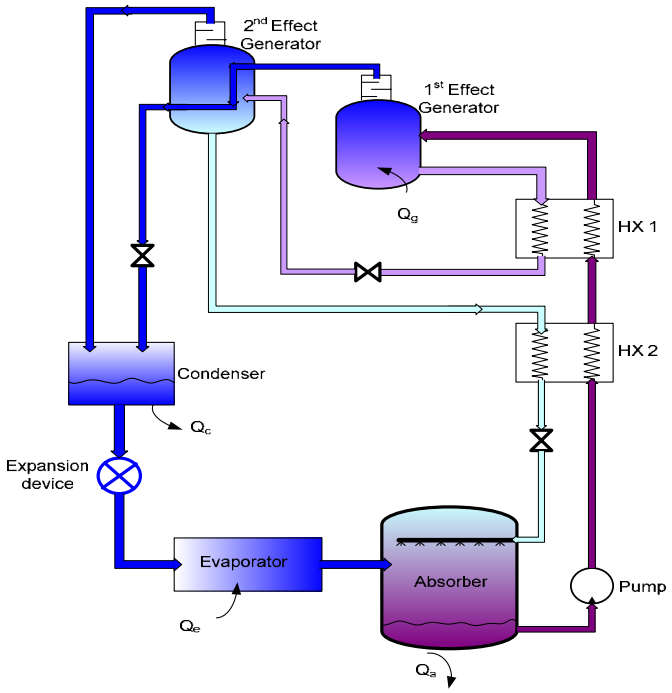

Figure 2-9 Double Effect Absorption Chiller

The Diffusion Absorption Cycle (Platen-Munters Cycle)

The system type is also called the Electrolux refrigerator. It was developed from the Carré absorption cycle and operates without a pump. It has been called a *no-moving part* and *no-auxiliary energy supply* system. An inert gas is used to maintain a constant total pressure in the whole system. The refrigerant partial pressure is allowed to be low in the evaporator, achieving the refrigeration effect. Ammonia is generally used as a refrigerant, water is used as an absorption media and hydrogen is used as the inert gas.

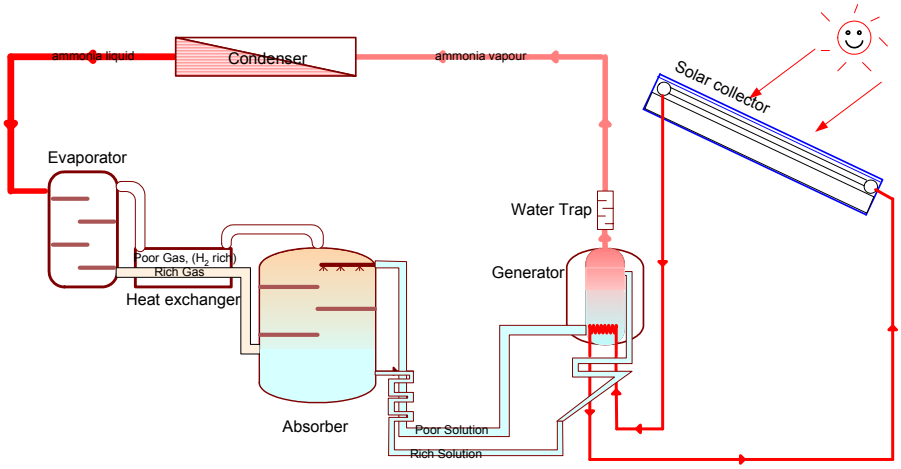

Figure 2-10 A Solar-Operated Diffusion Absorption Refrigeration System

The principle of the cycle is similar to the single stage absorption cycle. The difference is that the total pressure is the same in the entire system. Hydrogen is circulated between the evaporator and the absorber, compensating for the pressure difference between the high and low-pressure side. Ammonia vapour in the generator is condensed in the condenser before it flows to the evaporator. In the evaporator, liquid-ammonia is exposed to the hydrogen atmosphere, and a cooling effect is achieved when liquid ammonia evaporates due to its low partial pressure. Next, the ammonia-hydrogen mixture continues to the absorber (passing through the internal heat exchanger), in which ammonia will be absorbed in the water solution. The hydrogen returns to the heat exchanger and the evaporator while the aqueous ammonia solution is pumped to the generator by a thermosiphon pump. The poor ammonia aqueous solution, then, goes back to the absorber by gravitational flow. The generator temperature varies typically between 120 to 180°C, depending on the operating temperature. The typical energy sources are natural gas or kerosene, but also elec-

tricity. The practical COP varies between 0.2 to 0.3 at 25 to 100 W of cooling capacity (Granryd, 1998). Large capacity systems are not considered as attractive.

A schematic diagram of the solar-operated Platen-Munters absorption refrigeration system is shown in Figure 2-10. Valizadeh (1996) proposed a Platen-Munters system using ammonia-water and hydrogen (gas). This system can achieve an evaporator temperature of –19°C by using both an evacuated solar collector (at 200°C) and thermal storage (Valizadeh and Ashrafi, 1996).

The Thermochemical Generator, TCA

An interesting new technology is the Thermochemical generator, TCA, developed by the Swedish company Climate Well, patented in 2000 (Olsson, Kaarebring-Olsson et al., 2000) . The TCA is a three-phase absorption chiller/heat pump with the ability to store energy internally in the form of crystallised salt, in this case Lithium Chloride (LiCl) with water as the refrigerant.

The process operates under vacuum conditions as with standard absorption chillers using LiBr/water. The difference between the TCA and the traditional absorption chiller is that the TCA has an integral storage of energy in the form of crystallised salt to handle variations of available solar energy. It operates intermittently with a charge phase followed by a discharge phase, with an optional standby in between and two parallel systems can give a continously working process (Bales and Nordlander, 2005).

Figure 2-11 and Figure 2-12shows the schematic and the flow diagram of a TCA unit. The water/LiCl solution is pumped over the heat exchangers via spreader arms to increase the wetted area and improve heat transfer. During desorption the solution comes closer and closer to saturation, and when it reaches the saturation point further desorption results in the formation of solid crystals that fall under gravity into the vessel. At the bottom of the tank they are prevented from following the solutio by a sieve. The crystals form slurry in the bottom of the vessel.

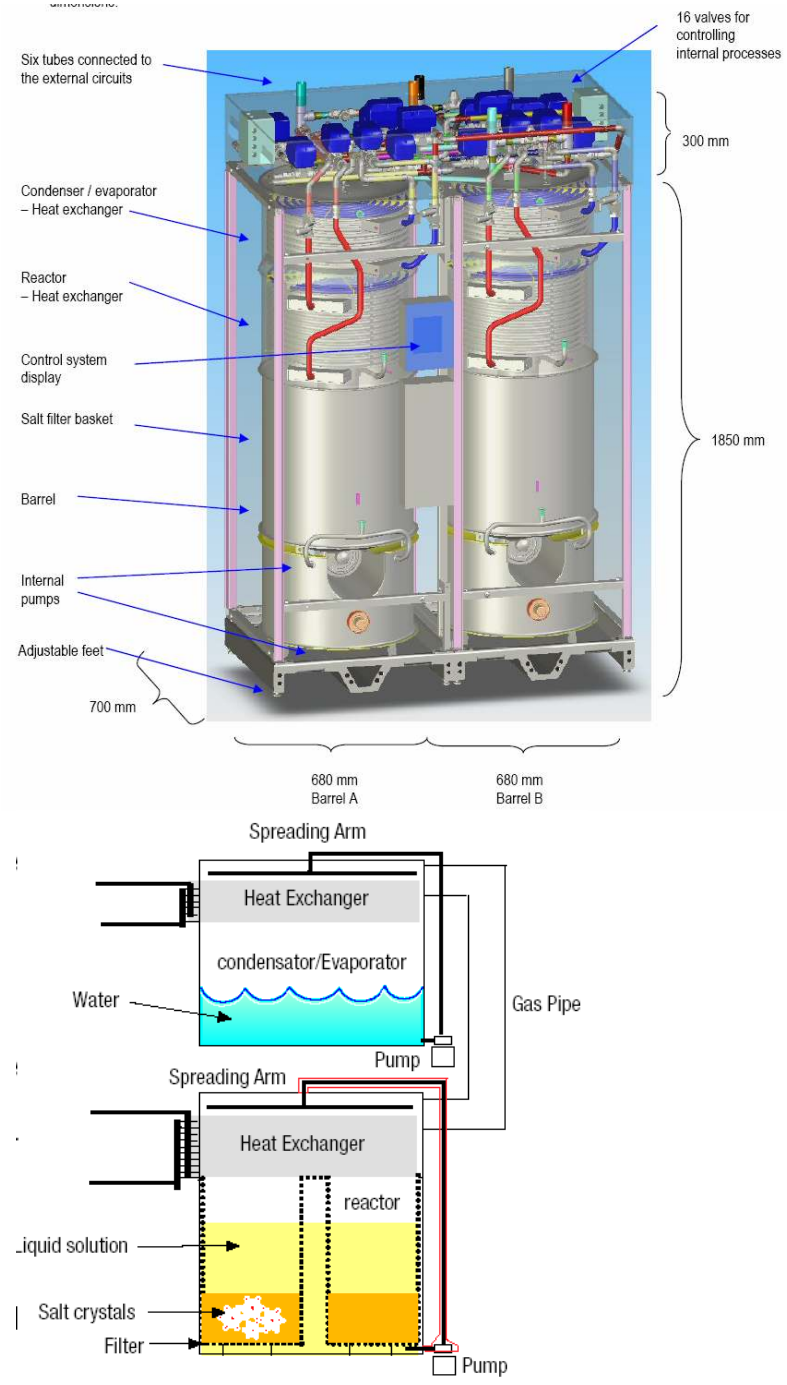

Figure 2-11 The Thermo Chemical Accumulator (Bales and Nordlander, 2005)

The benefits of the TCA are:

• High energy density storage in the solid crystals.

• Good heat and mass transfer, as this occurs with solution.

For discharging, when the process is reversed, saturated solution is pumped over the heat exchanger where it absorbs the vapour evaporated in the evaporator. The heat required for the phase change give the cooling effect (cooling mode) or if taken from the environment, the heat pumping function. The solution becomes unsaturated when passing the heat exchanger, but when falling into the vessel it again passes through the slurry of crystals whereby some of the crystals are dissolved thus making the solution fully saturated again.

In this way the solution is always saturated and the net result is a dissolving of the crystals into saturated solution. The heat of condensation and binding energy released is transferred to the environment (cooling mode) or to the building (heating mode). Thus there is a flow of energy from the evaporator at low temperature to the reactor at moderate temperature.

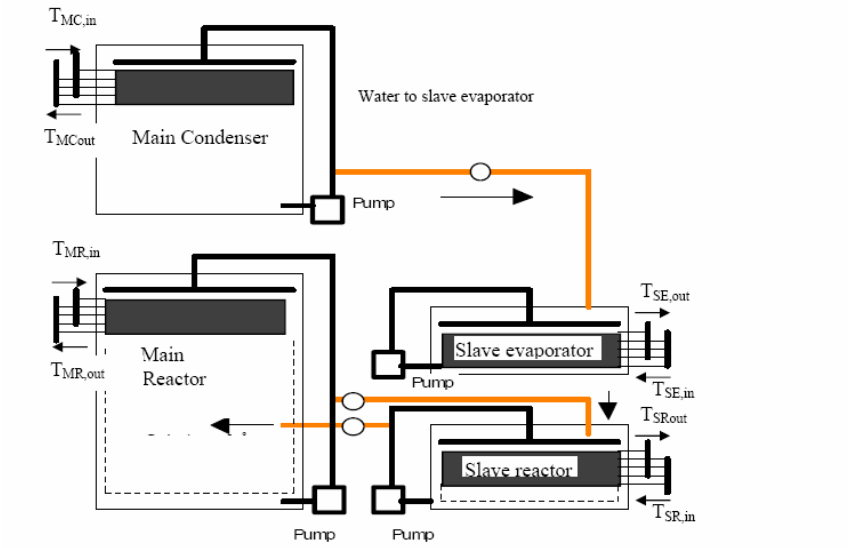

Figure 2-12 The TCA Flow Diagram (Bales and Nordlander, 2005)

Several protypes have been successfully developed and tested in the field. The COP of the system is projected to be as high as 0.7 and the fact that energy can be stored inernally with high energy density makes the system interesting. The technique was awarded with the first prize at the international conference in solar air conditioning in October 2005 in Bad Staffelstein Germany (ClimateWell, 2006).

The Open Absorption Cycle

The outstanding characteristic of this system is that there is no condenser. The weak absorbent solution is re-concentrated by an evaporating process in the solar collector. The rich solution is heated up until the water evaporates then the refrigerant vapour pressure and the absorbent concentration increase. The strong absorbent solution is collected in a storage tank before it is fed to the absorber (depending on the refrigeration effect). The refrigerants used in this system must be environmentally friendly since it is released to the environment. Furthermore, it should be cheap because make-up refrigerant is required in the entire operating time. Water is generally used as the refrigerant and LiBr, LiCl or $CaCl_2$ is used as the absorbent. A schematic diagram of the solar-operated open-absorption refrigeration system is shown in Figure 2-13.

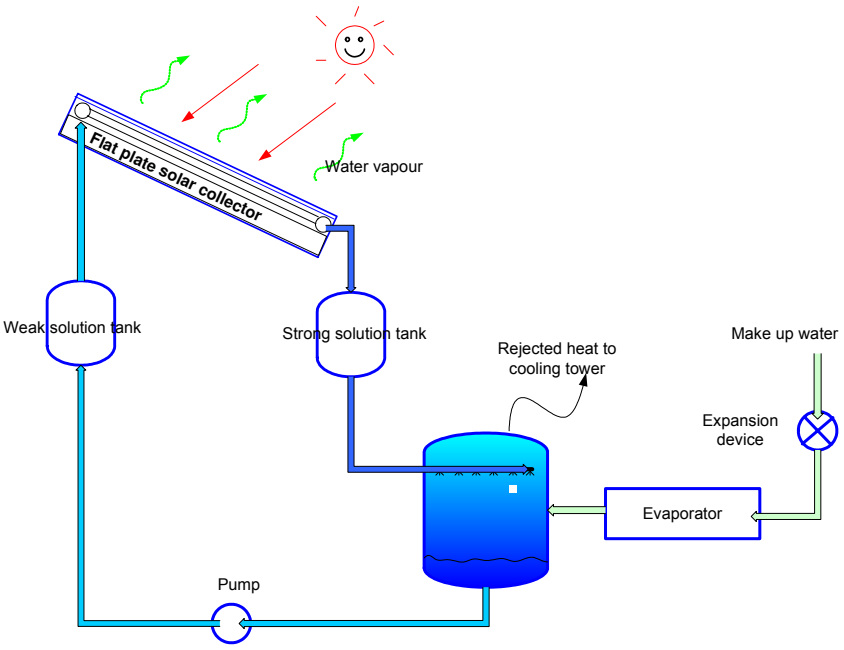

Figure 2-13 The Solar-Operated Open-Absorption Refrigeration System

Intermittent Cycles

The principle of these cycles is based on an absorption refrigeration cycle, but a solar collector is used as a generator and there is no pump.

There are two main processes, generation and refrigeration. Ammonia is generally used as the refrigerant. The generation process is initiated when the ammonia-water solution is heated up in the solar collector. The solution goes further into the storage tank by thermo siphon action. The ammonia vapour separates from the storage tank and passes through the rectifier to the condenser. After the generation process, the generator and condenser are isolated from the cycle and the weak solution in the generator is cooled to ambient temperature. The generator, containing a weak solution at ambient temperature now functions as the absorber. The refrigeration process originates when the liquid refrigerant (ammonia) is throttled through the expansion device to the evaporator. The refrigerant is evaporated and the vapour passes to the absorber.

There are both single-stage and two-stage ammonia-water intermittent solar refrigeration systems. The STRs of these systems at a generating temperature of 120°C are about 0.05 for the single-stage system (Venkatesh and Mani, 1989).

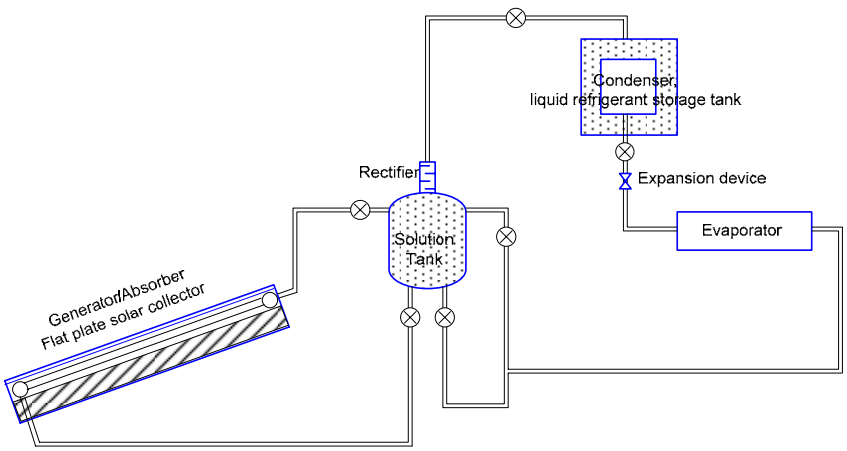

Figure 2-14 The Single-Stage Intermittent Absorption Refrigeration System(Venkatesh and Mani, 1989)

The two-stage intermittent system can be used to improve the operation and enhance the efficiency of the single stage system. The two-stage sys-

tem can solve the limiting operation temperature in the single stage system. The problem in the single-stage system is that it cannot operate when the generating temperature is too low or when the condensing temperature is too high for the given generating temperature or when the evaporation temperature is less than the design evaporation temperature.

In the two stage system there are two levels of generator pressures, a high-pressure generator (HPG) and a low-pressure generator (LPG). The generators are built into the flat plate solar collector. There are 2 weak solution storage tanks (Tank1 and Tank2) to store and supply to HPG and one tank (Tank3) to store and supply the weak solution to LPG. Tank1 and Tank2 don't supply the weak solution to HPG at the same time; they alternate daily. Tank3 is operated every day to supply the weak solution to Tank1 or Tank2, whichever is not suppling solution to HPG. The generation temperature is about 70-80°C. and the overall COP of this system is about 0.105 (Venkatesh and Mani, 1989).

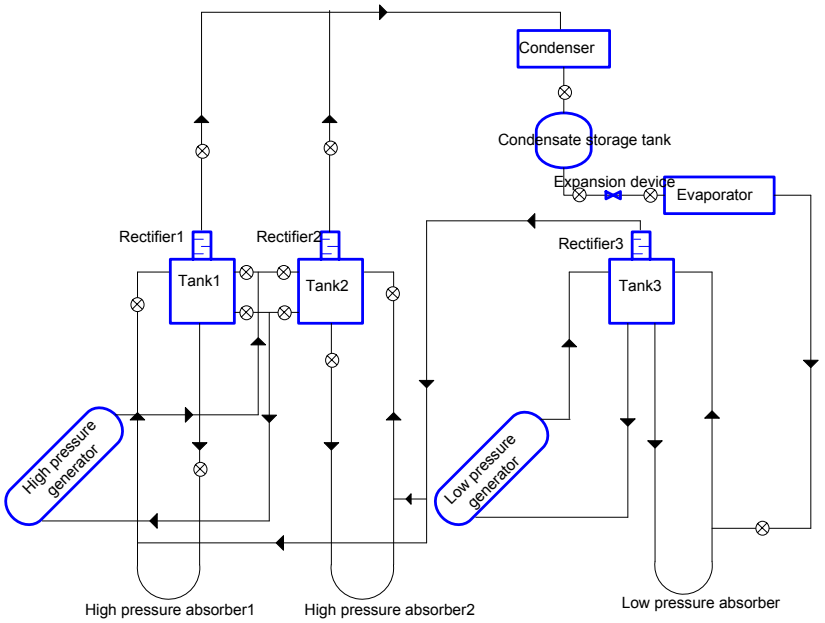

Figure 2-15 A two stages intermittent absorption cycle by Venkatesh and Mani, 1989

2.3.2 Solar-Driven Solid Adsorption and Chemical Reaction Refrigeration System

A solar-driven adsorption refrigeration system is a closed system, which consists of two main phases in the refrigeration cycle: refrigeration/adsorbtion and regeneration/desorbtion. The refrigerant is vaporized in the generator (or evaporator) and adsorbed by a solid substance, having a very high microscopic porosity. In the regeneration process, the adsorbent is heated until the refrigerant desorbs and goes back to the evaporator, then acts as a condenser. There are several pairs of refrigerants/absorbents such as water/zeolite and methanol/activated carbon.

Adsorption and chemical reaction adsorption cycles are similar to each other. The difference between these cycles is the processes which occur in the cycles. The force causing the adsorption process is a *physical adsorption force*; and the force causing the chemical adsorption process is a *chemical adsorption force*. Differences between the physical and chemical adsorption processes are described in Table 2-4.

Table 2-4 Comparisons between Physical and Chemical Adsorption Refrigeration Cycles

Physical Adsorption	Chemical Adsorption
1. Forces Causing the Adsorption Process	
The physical adsorption process occurs due to the Van der Waals force. This force binds the adsorbing molecules to the solid phase. This adsorption process on the surface of the adsorbent does not cause deformation or changes any macroscopic structure of the adsorbent (or solid). The binding molecules can be released by applying heat.	The chemical adsorption process occurs due to covalent or ionic bonds. The adsorbent and the adsorbate share electrons between each other and form a complex surface compound. The forces of these bonds are much stronger than the Van der Waal force.
2. The Thermodynamic Operation of the Cycle	
The physical adsorption is a reversible process. To complete the adsorption and desorption cycle, heat supply is required to the adsorber to increase the temperature of the absorbent. Heat of adsorption is usuall not exceed 80 kJ $mole^{-1}$(Webb, 2003).	The chemical adsorption process is very difficult to reverse. To complete the cycle, more heat supply to the adsorption cycle is required to achieve high kinetics of reaction. Heat of adsorption is upto 800 kJ $mole^{-1}$(Webb, 2003). The volume of the sorbent is also changed significantly during one period.
3. The Working Media	
Several pairs can be used e.g. - Activated carbon / ammonia - Activated carbon / methanol - Silicagel / water	There are 2 main groups of working pairs - Ammonia salts with alkaline compounds e.g. $BaCl_2$, $MnCl_2$, $SrCl_2$, etc. - Hydrogen and Methal hydrides with low-hysteris intermetallic or meshed metal compounds e.g. $LaNi_5$, $LaNi_{4.5}Al_{0.5}$ or $LaNi_{4.6}Al_{0.4}$.
4. Number of the Adsorbers	
One sorber is enough for the basic cycle. Enhancing the efficiency of the cycle can be achieved by increased the number of sorbers.	For methalhydride pairs, hydrogen does not change to the liquid phase; two sorbers are required.

The Intermittent Adsorption Refrigeration Cycle

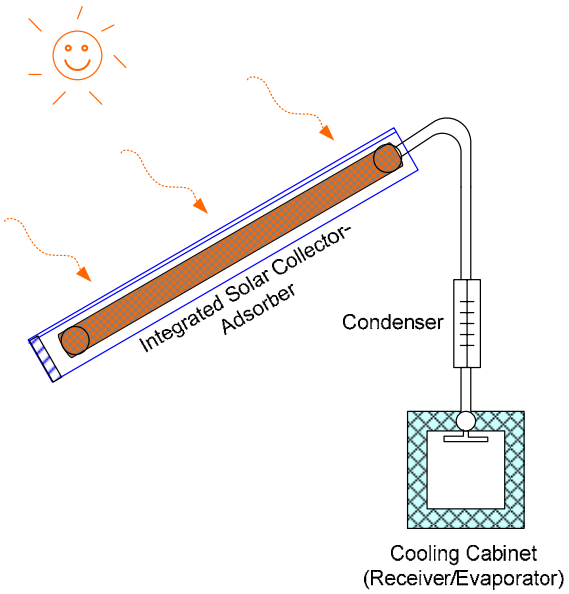

Figure 2-16 A valve-less daily activated carbon/methanol adsorption system by Hu, 1996

Most solid adsorption refrigeration systems installed worldwide are of the intermittent system type. Activated carbon/methanol is the most frequent working pair. The system is generally used for ice production.

Many systems integrate the adsorbent bed and the collector together. The adsorbent is, thus packed in the solar collector. Several special designs of both flat plate and evacuated tube solar collectors filled with adsorbent are proposed and tested such as a flat plate solar collector with activated carbon/methanol pair (Li and Wang, 2003), and an evacuated tube collector with activated carbon/methanol pair (Dai and Sumathy, 2003).

Ammonia can also be used as a refrigerant, but a special design with a steel or aluminium collector is needed. Li and Wang, 2002 studied the effect of design parameters and ambient conditions on the performance of a solar powered solid adsorption refrigerator. The results illustrated that the significant parameter which affects the system is equivalent to the number of collectors and the heat transfer between the metallic plate and the adsorbent. The ambient conditions also strongly affect the performance of the solar refrigerator.

A valve-less (also called non-valve system) solar ice maker is a system without valves, measure guages or moving parts. The example system is shown in Figure 2-16. The valve-less adsorption system with activated carbon/methanol was proposed and studied by serveral researchers such as Hu, 1996; Li, Sun et al., 2004; Sumathy, 2004; Li, Huang et al., 2005.

A recent study by Anyanwu and Ogueke, 2005 suggests that zeolite/water is the best pair of air-conditioning applications; while activated carbon/ammonia is better for applications requiring low temperature for e.g. food preservation and freezing. The most important parameters for system operations are the adsorption and condensation temperatures. The evaporation temperature has little affect on system performance.

Commercial products are provided by several companies such as Zeo-Tech GmbH, Germany with zeolite/water pairs (Schmidt, 2005), Zeo-power, USA (Tchernev, 2006) and BLM, France (Pons, Guilleminot et al., 2001).

The Continuous System

Even if the intermittent system is the most frequent configuration, it is also possible to operate the system continuously. A continuous system consists of a condenser, a throttle valve, an evaporator and a sorption reactor. Oertel and Fischer, 1998 built a continuous adsorption cooling system for cold storage by using silica gel/methanol. Flat plate solar collectors were used to supply heat for the sorption reactor. A refrigeration temperature of –2°C could be achieved with an 80-90°C reaction temperature.

Zhang and Wang, 2002a proposed a continuous solid adsorption system for heating and cooling. During the daytime, the system work on the heating mode, producing 30 kg of hot water at about 48°C with the $COP_{heating}$ of 0.34. At night, the cooling mode is performed at the cooling capacity of 0.13 MJ/m^2 of the heat-collecting area, providing the $COP_{cooling}$ of 0.18.

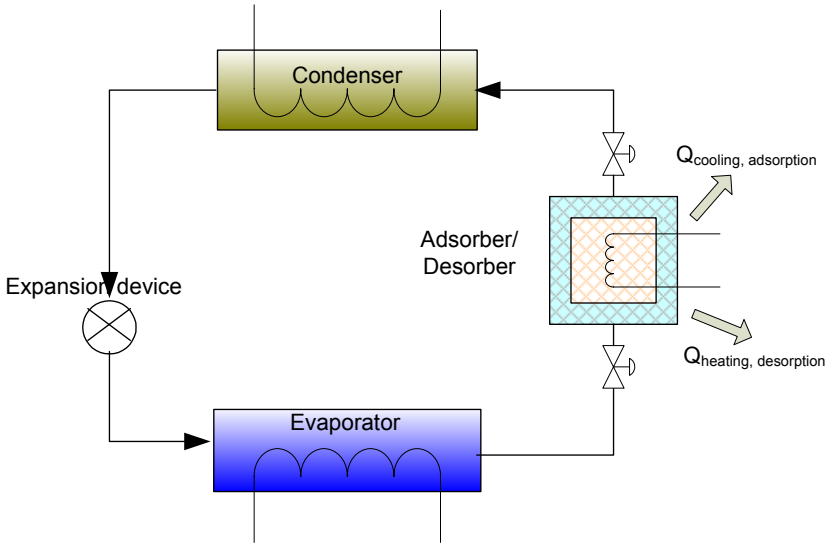

Figure 2-17 The Continuous Process

The Thermal Wave Cycle

The thermal wave cycle was proposed for the continuous system. Instead of only one adsorbent bed in the basic adsorption system, it consists of 2 absorbent beds and 2 heat exchangers, which are connected in a series. Between this equipment, a working fluid (e.g. high temperature oil), flows in the closed cycle at a low flow rate. It is assumed that a large temperature gradient persists along the adsorption beds.

Schematic of the system is shown in Figure 2-18. The operation of the cycle is divided into 2 phases. Sorption process occurs in one bed and desorption process occurs in another bed simultaneously. These sorption and desorption processes swaps between the beds when the next operating phase occurs.

In Phase 1, external heat is applied to heat exchanger 1. Bed 2 adsorbs the refrigerant from the evaporator, thereby releasing heat from the adsorbent to the oil. The oil is then pumped into heat exchanger 1, absorbing more heat and continues to bed 1. Bed 1 is heated up by the oil; the refrigerant is desorbed and flows to the condenser. The process continues until bed 2 reaches saturation.

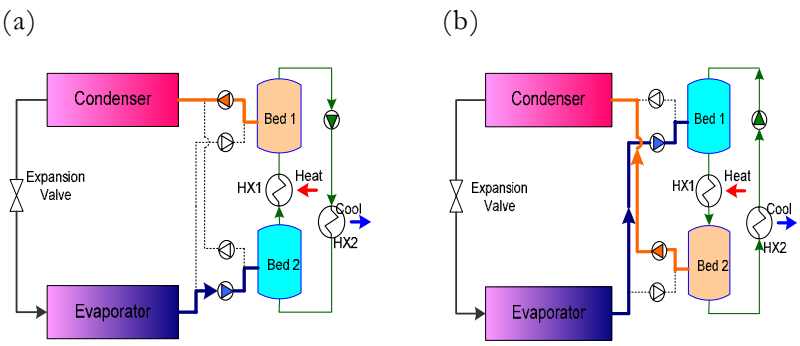

Figure 2-18 Thermal Wave Cycle, (a) Phase 1 and (b) Phase 2

In Phase 2 the pumps and the processes in both beds are reversed. Bed 1 adsorbs the refrigerant from the evaporator and releases heat to the oil. The oil then absorbs heat from bed 1 and from heat exchanger 1. The heat is released to bed 2; the refrigerant is then desorbed to the condenser.

Adsorption and desorption in both adsorbent beds are repeated, indicating that the thermal wave cycle can run continuously. Several numerical studies on this cycle have been carried out, e.g. Ben Amar, Sun et al., 1996; Sun, Feng et al., 1997.

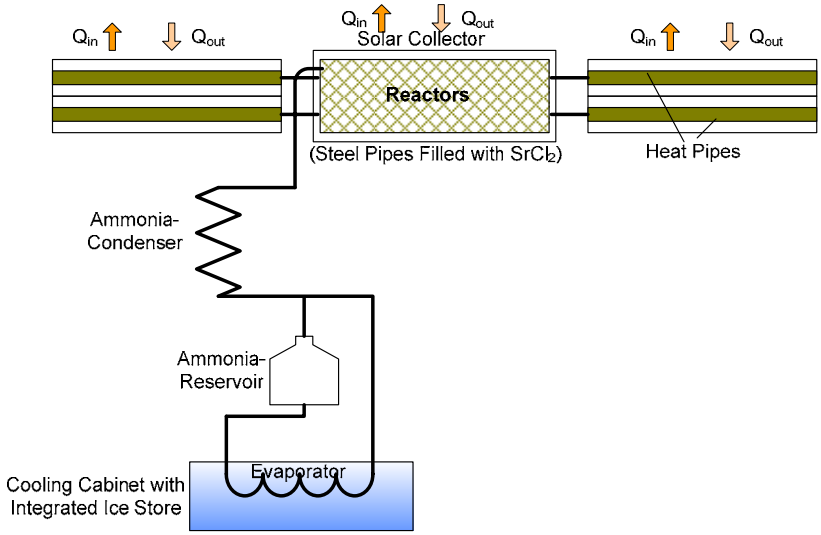

Figure 2-19 The Solid Sorption Cooling Machine Proposed by Erhard, Spindler et al., 1998.

The system thermal ratios (STR) of these prototypes vary from 0.06 to 0.14 (Fléchon, Lazzarin et al., 1999). An example of the chemical adsorption is shown in Figure 2-19 by Erhard, Spindler et al., 1998. The ammonia/$SrCl_2$ pair was used as a working media in this experiment. In the simulation, efficiency of this system could reach 0.05-0.08. Other prototypes that are reported by Fléchon, Lazzarin et al., 1999 are:

- Faradsy's refrigerator (1993)
- Andrew's refrigerated railway car (1951-1955)
- Muradov-Shadyev's ice machine (1971)
- Flechon's solar refrigerator (1984)
- Two prototypes (I and II) developed by Worsoe-Schmidt (1983)
- Iloeje's ice machine (1985)
- Balat-Crozat's ice machine
- Dornier GmbH's industrial prototype

Ammonia is not compatible with copper, thus systems with ammonia as a refrigerant generally use aluminum or steel. Enibe and Iloeje, 1997 designed solar collectors from aluminum and steel, filled with the adsorbent. Results illustrated that with a new type of steel collector, the COP could be improved by at least 30%. The authors also reported the limitations of

the COP in the tested condition to be 0.08. This limit could be improved by enhancing the cooling of the collector during the re-adsorption mode and upgrading the heat transfer characteristic of the evaporator.

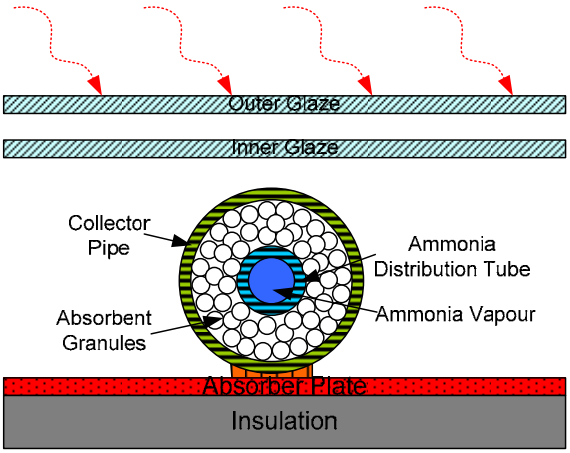

Figure 2-20 Solar Collector Filled Adsorbent (Acccording to Enibe and Iloeje, 1997)

Commercial Products of the Chemical Adsorption System Type

The solar thermal refrigerator is also used in World Health Organisation Projects (WHO, 2005). The product from Comesse Soudure SA, France coincides with the WHO's specification (Comesse_Soudure_SA, 2005). This product can store 38 litres of vaccines at the gross volume of 200 litres and 5 litres in freezing capacity. It is recommended this particular solar driven absorption unit be installed in places where the monthly solar radiation exceeds 5 kWh $m^{-2}day^{-1}$. The specification of this product is shown in Table 2-5 (WHO, 2005).

Fléchon, Lazzarin et al., 1999 reported on the commercial prototypes by Comesse Soudure, (France) under the trade name Coldfego (This prototype is used in the World Health Organisation project), by Dornier GmbH (Germany) and by Soby Sunice Company (Denmark).

Table 2-5 Specification of Thermal Driven Sorption Refrigerator (WHO, 2005)

	Refrigerator		Freezer		Unit
Ambient Temperature	32°C	43°C	32°C	43°C	°C
Icepack Freezing, with Vaccine	-	-	2/24	2/24	kg/hr
Icepack Freezing, without Vaccine	-	-	2/24	2/24	kg/hr
Internal Temperatures, Minimum	2	-1.5	-18	-12	°C
Internal Temperatures, Maximum	5	4	-10	-13	°C
No Sun Autonomy	9	5	-	-	days
Electric Power Consumption	0				
Temperatures Recorded During Day/Night (+43°C/+20°C) Tests:	Minimum 0°C; Maximum +4°C				
Price Per One Unit	5000				US$

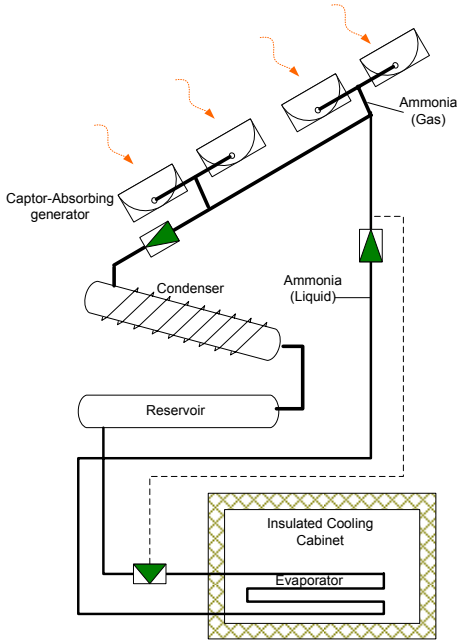

Figure 2-21 The Coldfego's Solar Refrigerator (Fléchon, Lazzarin et al., 1999)

The Combined Adsorption-Desiccant Refrigeration System

The combined adsorption-desiccant refrigeration system was proposed by Dai, Wang et al., 2002. The schematic of the system is shown in Figure 2-22. The system consists of 3 subsystems: solid intermittent adsorption refrigeration, desiccant dehumidification, and cold storage. Activated carbon and methanol are selected as a working pair. The desorption temperature of the adsorbent and the regeneration temperature of the desiccant wheel are in the range of 80-100°C.

This system is particularly designed for cooling of grain products. Grain usually releases moisture; therefore dehumidification of the air in the barn is required. A silica gel/water desiccant subsystem is consequently used. The air supply to the barn is obtained from the desiccant subsystem during the daytime. The dehumidified air is cooled by the evaporative cooler before it continues to the building. During the night, the dehumidified air is cooled in the evaporator by the adsorption subsystem before it enters the barn.

An auxiliary heater is needed for the regeneration of the desiccant material, in order to maintain a certain level of humidity of the inlet air in the barn. This heat also assists in the desorption process of the adsorbent.

The adsorption subsystem works intermittently. The desorption process is carried on during the daytime when solar radiation is available. The refrigerant (methanol) is collected in the receiver during the desorption process. The adsorption process is carried out during the night, while the pressure and temperature of the adsorbent bed decrease by natural convection and sky irradiation.

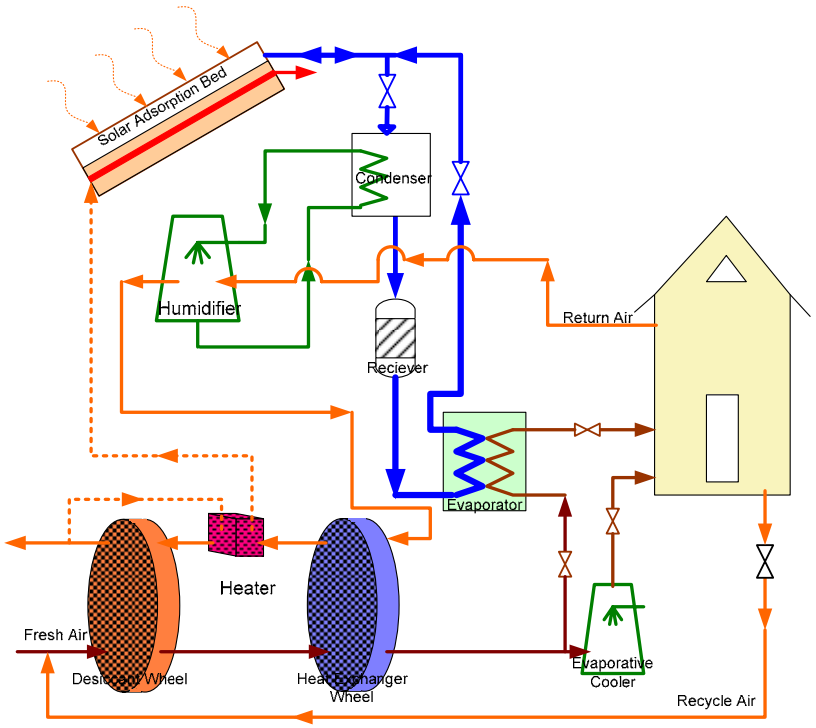

Figure 2-22 A Combined Adsorption-Desiccant Cooling System

The Combined Adsorption-Ejector Refrigeration System

This system was found in the literature by Li, Wang et al., 2002, and Zhang and Wang, 2002b. Both examples are from the same research group. Zeolite 13X and water are used as a working pair. Cooling is achieved by the ejector subsystem during the daytime and by the adsorption subsystem at night. Further details about this system can be found in the ejector refrigeration section.

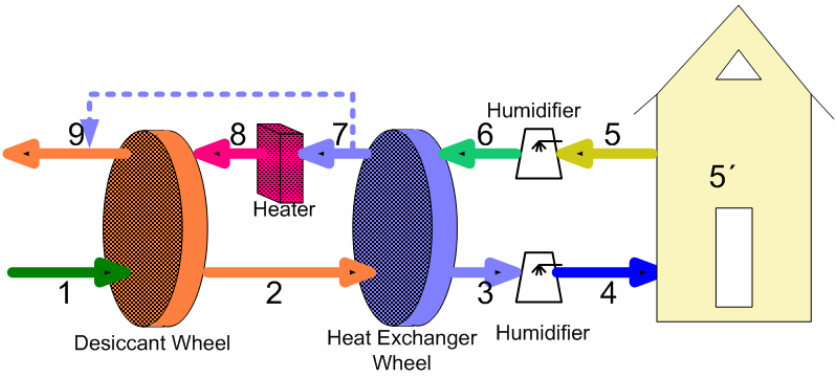

Figure 2-23 Solid Desiccant Cooling Integrated with the Ventilation System

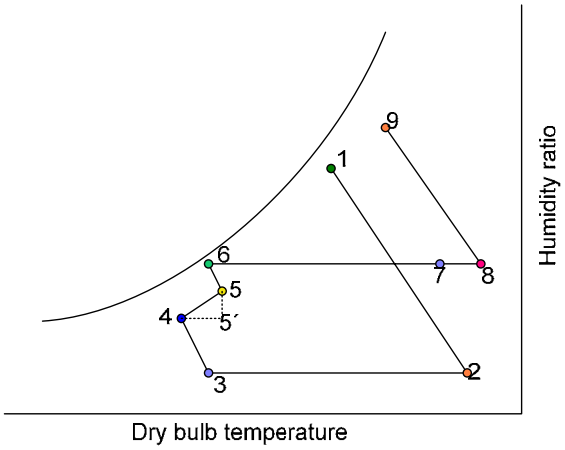

Figure 2-24 Desiccant Cooling Process (Numbers in the figure refer to the point in Figure 2-23)

Desiccant cooling is a combination of dehumidification and evaporative cooling processes. Moisture is removed from the air(1) by a desiccant material, thus the latent heat load is removed. The heated air (2) is then cooled in the heat exchanger wheel (3). The air temperature is further lowered and humidified by an evaporative cooling process (4). The desiccant material can be regenerated by heat. It can be classified into 2 types: solid desiccant and liquid desiccant. A small amount of electricity is required to run the pump, fan and rotor wheels. It may be very difficult to

run the system in an area where the humidity is high. However, additional components for removing sensible heat and drying may be installed.

Solid desiccant systems use adsorbents rather than absorbents e.g. silica gel, activated alumina or other molecular sieve materials. The solid sorbent is generally filled in a rigid body. This rigid body can either be rotated or fixed. Occasionally the desiccant is integrated with the solar collector. Solid desiccants generally have a higher degree of dehumidification than the liquid desiccants, but require a higher regeneration temperature. A conventional cooling machine can also be used as an additional component to increase tfurther lower the air temperature and take care the sensible load.

Liquid-Desiccant

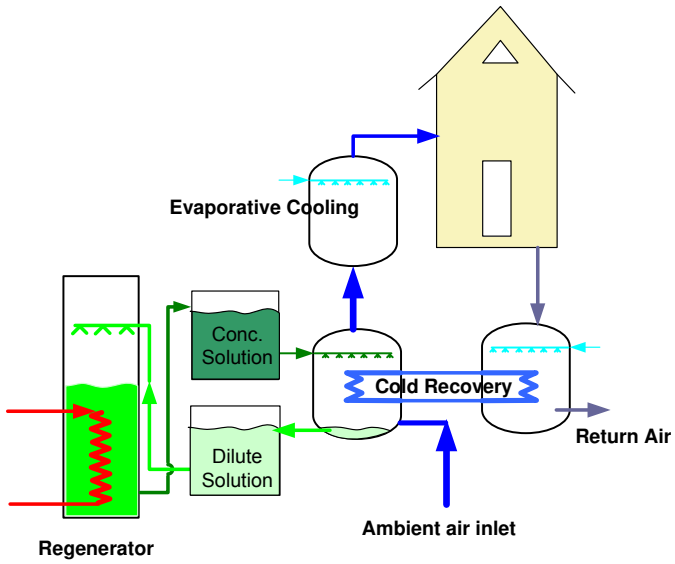

Figure 2-25 Liquid Desiccant Cycle

An aqueous solution of absorbents such as lithium bromide (LiBr), lithium chloride (LiCl), calcium chloride ($CaCl_2$) or triethylene glycol (TEG) can be used as the desiccant media. The dehumidifier is designed to converge the process air and the sorbent solution in order to absorb the humidity directly from the air. The regenerator is used to regenerate the sorbent solution by heating. The desiccant solution is in direct contacted with the ambient or exhaust air. An advantage of the liquid desiccants is that the liquid sorbent can be easily pumped, therefore allowing the pos-

sibility of connecting several small desiccant dehumidifiers to a larger regeneration unit (Öberg, 1998). Pressure drop in the liquid desiccant system is relatively low (Grossman, 2002). The system can run intermittently, the dehumidification of air and regeneration of the desiccant material does not need to occur simultaneously. The diluted desiccant solution can be accumulated until heat supply is available. Furthermore, the liquid desiccant material does not require a high temperature for the regeneration process. It is, therefore, possible to use flat-plate solar collectors. A disadvantage of this system is that there is a potential carryover of the sorbent to the air, which may lead to sorbent loss and contamination of the air (Grossman, 2002); salt solutions of the sorbents are corrosive; and relatively few liquid desiccant systems are available on the market. An excellent literature review on liquid desiccant cooling can be found in the literature by Öberg and Goswami, 1998.

Solar-Driven Desiccant Cooling System with Rotational Wheels (Dunkle Cycle)

A solar desiccant cooling system for humid, tropical or subtropical areas was proposed by Dunkle, 1965. The solid desiccant silica gel is used to dehumidify the process air and the desiccants are regenerated by the "solar-heated air". This cycle has additional sensible heat exchangers. The return air is treated and recirculated back to the building. The outdoor air is used for regeneration of the desiccant wheels. During hours of inadequate solar insolation, the system can be operated by a rock pile energy storage unit. A schematic of the Dunkle cycle is shown in Figure 2-26; and the process in Psychometric diagram is shown in Figure 2-27.

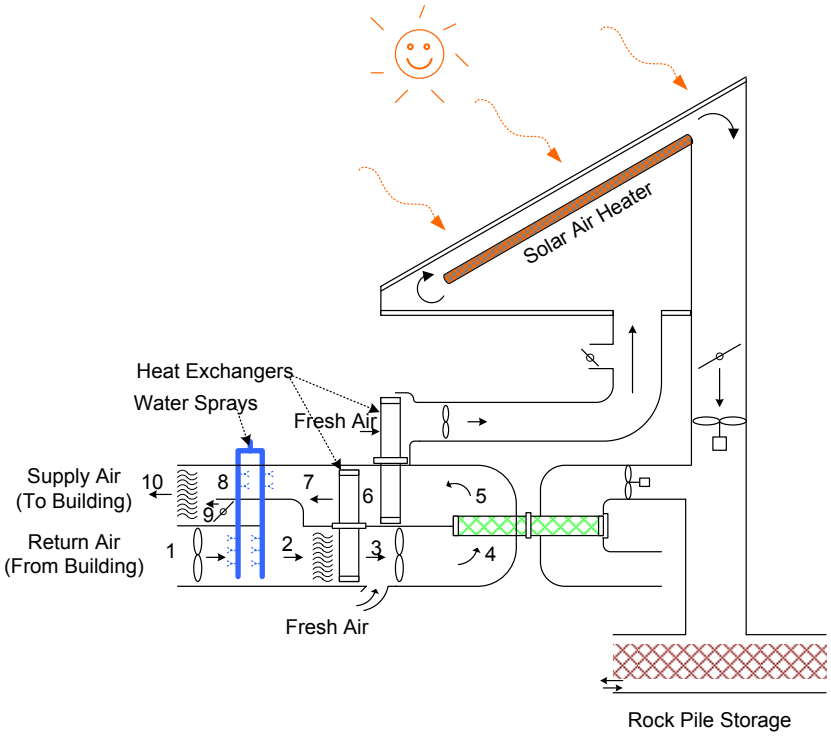

Figure 2-26 Desiccant Cooling System in a Humid, Tropical and Subtropical Area by Dunkle, 1965

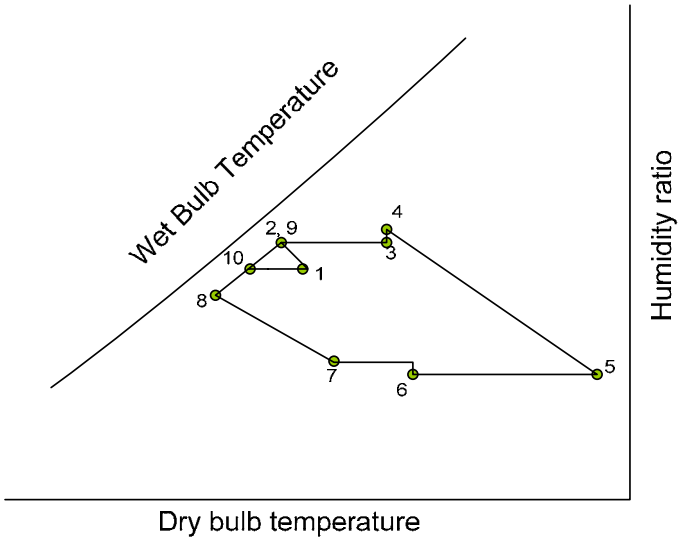

Figure 2-27 The Dunkle Cycle Process in Psychometrics Diamgram (Dunkle, 1965)

Solar-Driven Desiccant Cooling System with Rotational Wheels Integrated with the Ventilation System (MEC System)

Kanoglu, Carpinlioglu et al., 2004, developed a procedure for energy and exergy analyses of open-cycle desiccant cooling systems. The procedure was applied to an experimental unit operating in a ventilation mode with natural zeolite as the desiccant. The unit has a COP of 0.35 and an exergy efficiency of 11.1%. The largest exergy destruction in the system is from the processes in the desiccant wheel that accounted for 33.8% of the total exergy destruction in the system.

Different designs of the solid desiccant system have been proposed by various researchers. Almost all of these systems require an auxiliary heater for regeneration of the desiccant media during hours of low radiation. However, the backup system can be an auxiliary cooler e.g. a vapour compression machine.

The return air from the conditioned space can be recirculated or purged out, depending on the air quality requirement of each application. The MEC system can also be connected with the heat distribution network from the solar Combi-system (Wiemken, Motta et al., 2004). This can enhance the system capacity, especially during the heating season.

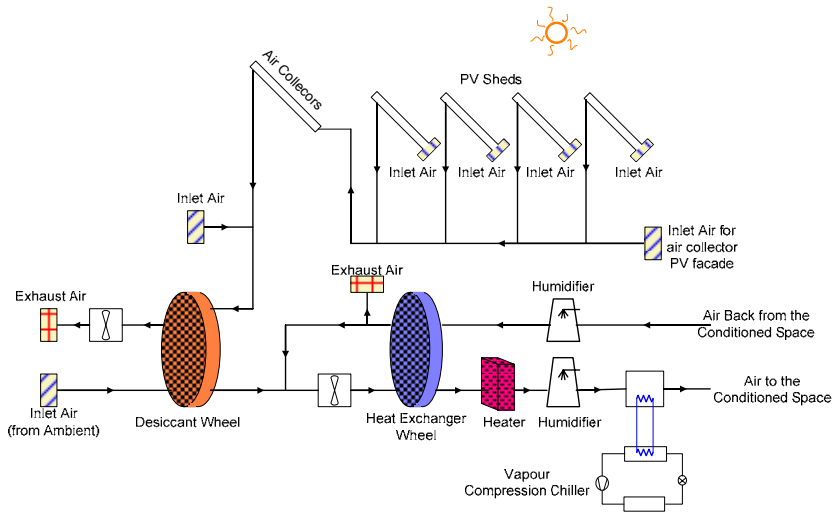

Figure 2-28 Desiccant System with Recirculation Air (Jakob, Eicker et al., 2003)

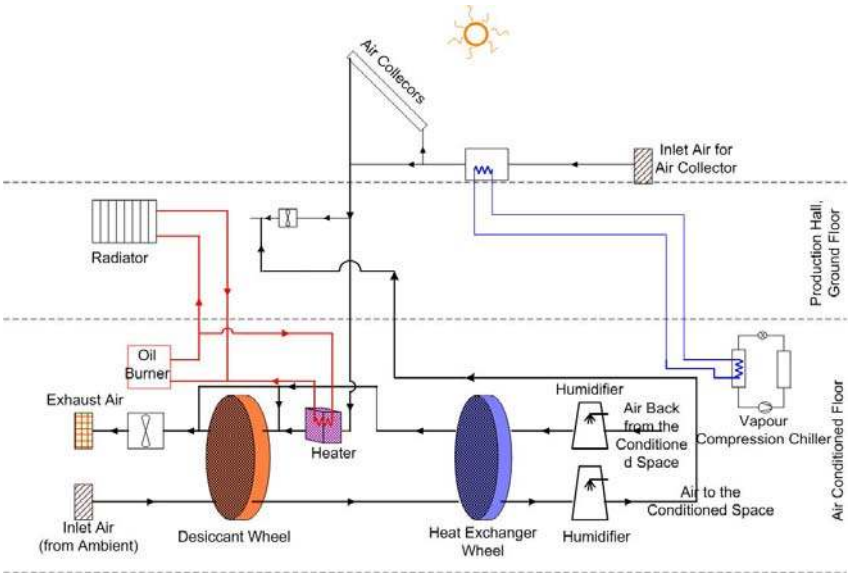

Figure 2-29 Desiccant System with Auxiliary Heater (Jakob, Eicker et al., 2003)

Schnabel, Hindenburg et al., 2004 has operated an autonomous solar-driven desiccant system with silica gel and air collector in Germany for 2 years. The performance of the system can be improved by better control of the energy supply from the solar collector, in order to avoid unfavourable heat transfer to the inlet air stream. The COP is strongly dependant on the plant design, operating and ambient conditions.

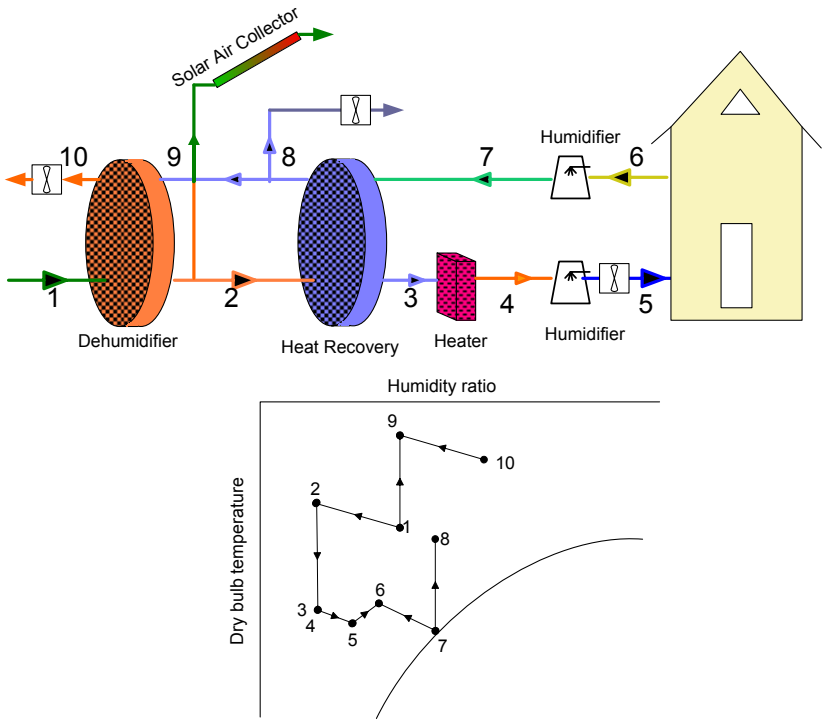

Figure 2-30 Solar-Driven Desiccant System by Schnabel, Hindenburg et al., 2004.

Solar-Driven Desiccant Cooling System with Integrated Desiccant-Solar Collector

Lucas, 1988 Lucas, developed a full scale solar desiccant enhanced radiative cooling system. The system consists of three independent subsystems. The desiccant bed is integrated in the solar collectors which are installed on the roof and 2 sides of the house. The regeneration process occurs during the daytime and the dehumidification process occurs at night. This system can continuously supply conditioned air 24 hours a day and is also suitable for humid areas.

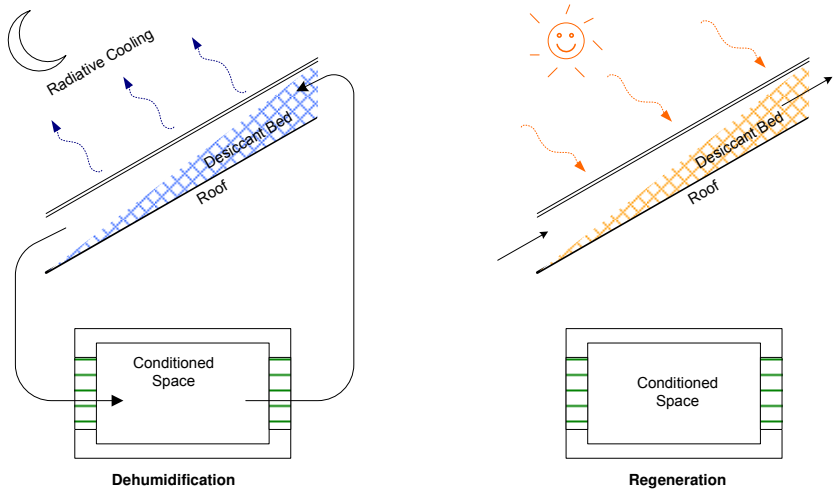

Figure 2-31 A Solar Desiccant Cooling System with Integrated Desiccant-Solar Collector (Lu and Yan, 1995).

Liquid Desiccant Technology

An early solar-driven liquid desiccant system was proposed by Löf, 1955. Triethylene glycol was used as the desiccant medium. Triethylene glycol was sprayed into an absorber, e.g. absorbing moisture from the conditioned air. The glycol became the weak solution and was then pumped through the heat exchangers to the regenerator. Air was heated by solar air collectors. This solar-heated air was used for regenerating the liquid desiccant. In the regenerator, water in the weak solution was evaporated and the weak solution became the strong solution. Several heat exchangers were used for recovering sensible heat, preheating the weak solution flowing into the regenerator and cooling the strong solution before spraying it into the absorber. The schematic of the liquid desiccant system with solar air collector is shown in Figure 2-32.

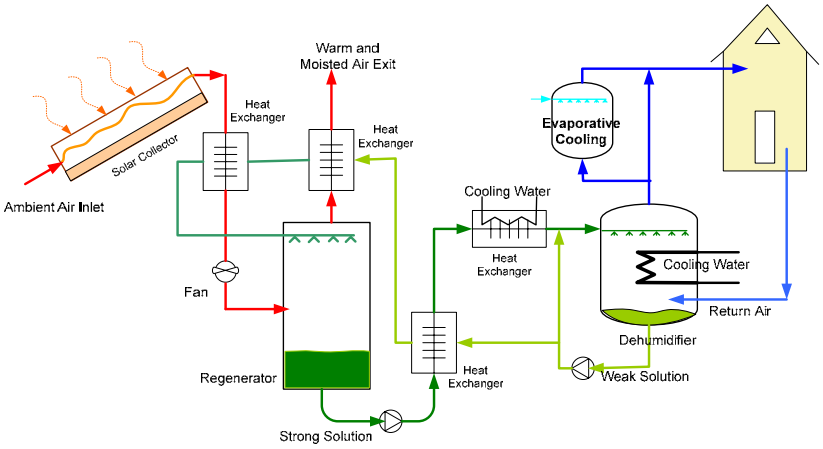

Figure 2-32 Solar Driven Liquid Desiccant System by Löf, 1955.

In 1973, Baum et al. proposed the LiCl-H_2O open cycle with flat plate collectors. Lithium chloride was subsequently used by several research groups, such as Kessling, Laevemann et al., 1998 and Gommed and Grossman, 2004.

Kessling, Laevemann et al., 1998, proposed a liquid desiccant cooling system with energy storage. The dehumidified air was cooled by the evaporation of water in order to create a desired temperature. The weak solution of the absorption process was regenerated to be a strong solution before being reused in the dehumidification process. Thermal energy from the solar collector was used for the regeneration process.

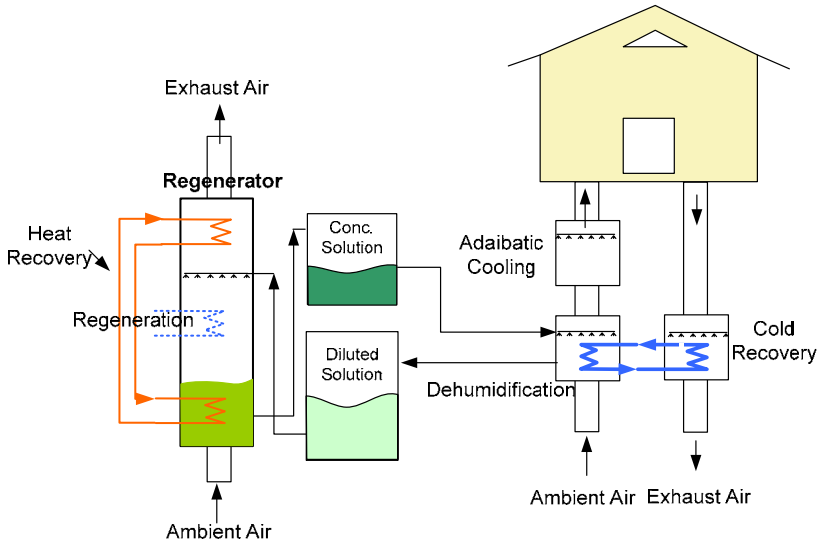

Figure 2-33 Liquid Desiccant Cooling System with Energy Storage by Kessling et al., (1998)

Lithium bromide was used by Khalid Ahmed, Gandhidasan et al., 1998 and Pohl, Hellmann et al., 1998. The former group performed an exergy analysis on a liquid-desiccant-based, hybrid air-conditioning system. The desiccant was regenerated by an open flat-plate solar collector. Results from the exergy analysis showed that the optimum desiccant mass flow rate through the solar regenerator was about 30 kg h^{-1} m^{-2} for an ambient temperature of 40°C. Irreversibilities in the absorber and the dehumidifier are almost equal since these two components have a similar function.

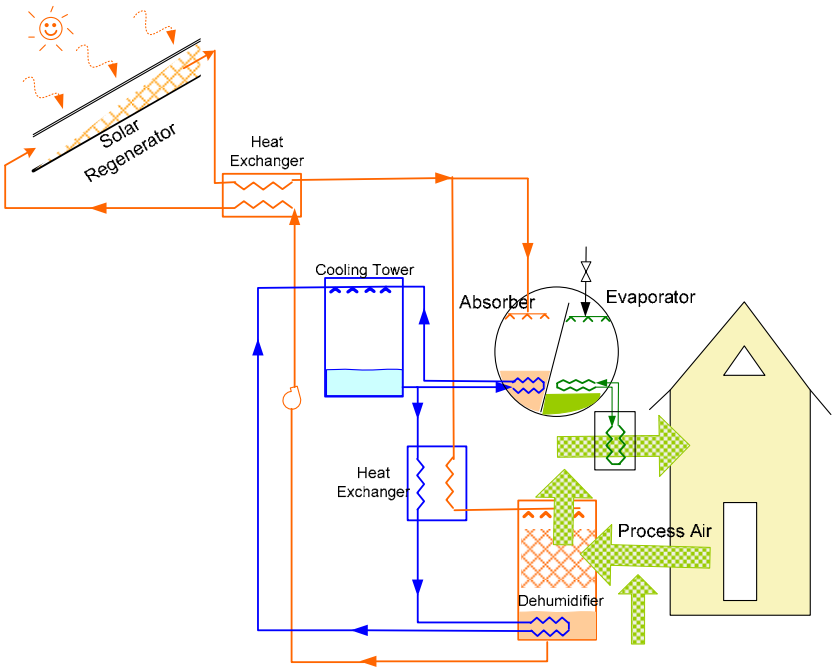

Figure 2-34 Hybrid Liquid-Desiccant Based Air Conditioning Cycle by Khalid Ahmed, Gandhidasan et al., 1998

Pohl, Hellmann et al., 1998 studied a dehumidifier-evaporative cooler-regenerator (DER) absorption chiller. This system is suitable to chill water at temperatures above 15°C. A maximum COP of about 0.8 was obtained. Both open dehumidifier-evaporative cooler-regenerator and semi-open dehumidifier-evaporative cooler-regenerator were studied. The open system is designed for small temperature lifts between heat source and heat rejection temperatures and is operated at atmospheric pressure. The semi-open yields better COPs but the open-DER operates well in daytime summer conditions with the refrigeration temperature higher than 15°C (COPs can be higher than 0.8). Low temperature heat down to 40°C can be utilised. The major components are a dehumidifier, an evaporative cooler and a regenerator; other additional components are two air to air heat exchangers and one liquid to liquid heat exchanger. The COP is quite low at typical relative humidities but the COP is lower for higher humidities. The schematic diagram of the novel open-cycle absorption refrigeration chiller by Pohl, Hellmann et al., 1998, is shown in Figure 2-35.

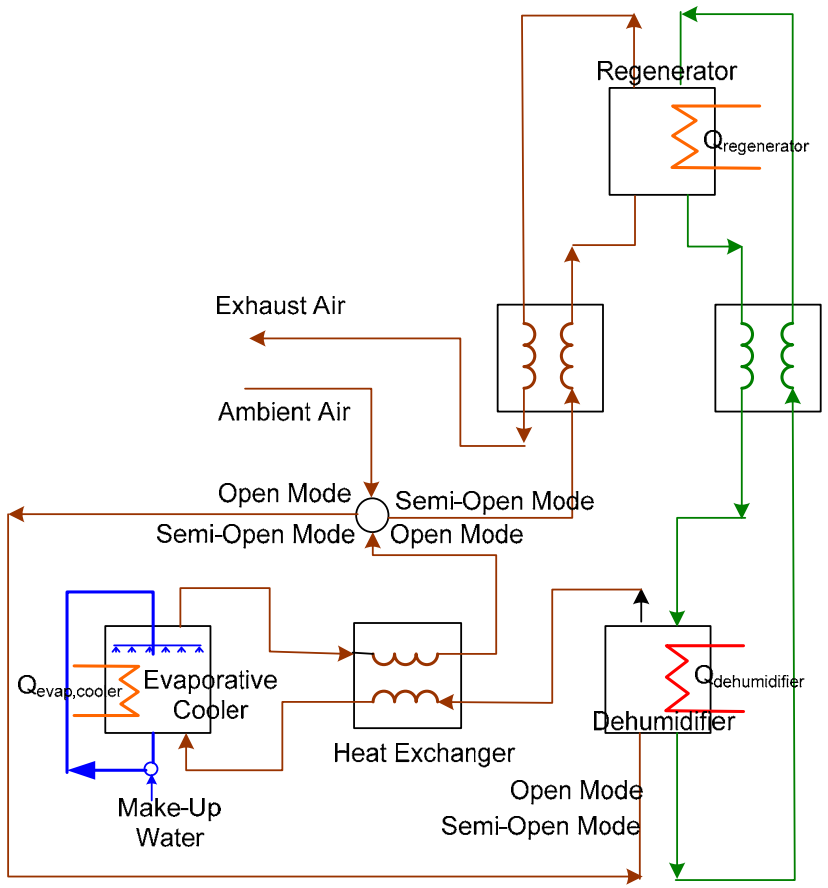

Figure 2-35 DER Absorption Chiller by Pohl et al., 1998

Calcium chloride is also a common liquid desiccant medium since it is cheaper than other desiccant media. Examples of researchers who use calcium chloride are Hamed, 2003 and Gandhidasan, 1990.

Gandhidasan, 1990 proposed a simple expression for the preliminary calculations of an open-cycle liquid desiccant system in order to predict the heat removed from the space. Ambient air conditions, desiccant concentration in the dehumidifier, and cooling water temperature were shown to have significant effects on the system performance.

The use of liquid absorbent requires an apparatus for continuous transportation of the liquid solution. To avoid this problem, Hamed, 2003,

proposed a solid porous stationary bed for carrying the liquid desiccant. A packed porous bed, containing porous granules of burned clay, was used. Calcium chloride was used as the absorbent. The regeneration process is intended to be driven by heat from the solar collector. The result of the experiments shows that the mass transfer rate has a significant effect on the concentration gradient in the bed. For specific conditions of operation, the desorption rate is found to be higher compared with adsorption, and consequently the effect of axial distance on the desiccant concentration can be neglected.

Hybrid Desiccant/Conventional Cooling System

More complicated hybrid systems such as a desiccant/absorption, a desiccant/vapour compression system are proposed in several papers. Several hybrid liquid desiccant systems are shown in the article by Öberg and Goswami, 1998. Conventional vapour compression and absorption systems are employed to handle the sensible cooling load. The coefficient of performance of the hybrid system was predicted to be larger than the desiccant and conventional refrigeration subsystems alone. Kinsara, Elsayed et al., 1996 proposed a combination of liquid desiccant, using a $CaCl_2$ solution with a vapour compression system. Results show that this system can be effectively used to reduce electric energy consumption in air-conditioning. For example: at an ambient temperature of 40°C, and humidity ratio of 0.015, STR=0.9, preserving about 30% more energy than a conventional AC system. The configuration of this system and the Psychometrics process are shown in Figure 2-36.

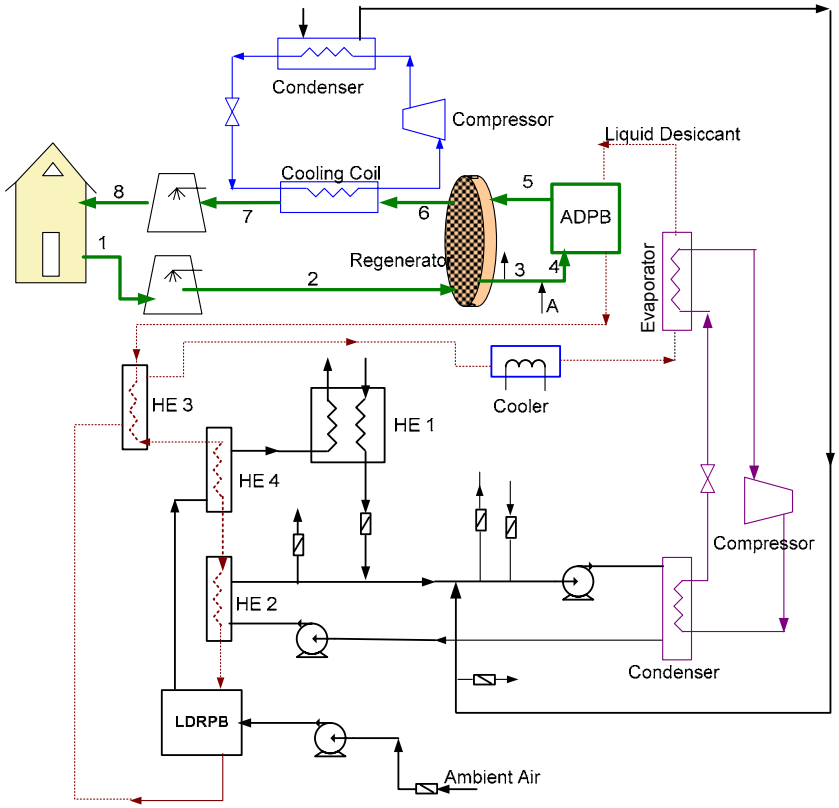

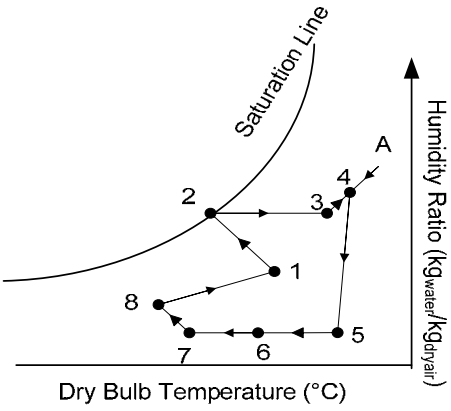

Figure 2-36 The Proposed Hybrid Desiccant/Vapour Compression System and the Psychometrics Process of the Air Loop from Kinsara, 1996.

A similar system was proposed by Dai, Wang et al., 2002; three experimental cases are compared among the vapour compression (VP), VP + desiccant(DEC), and VP + DEC + evaporative cooling (EC). Results show that the VP + DEC provide higher thermal COP than other systems, but the VP + DEC +EC yield the highest overall COP. The hybrid VP/DEC can produce more cooling than the VP alone by about 20-30%.

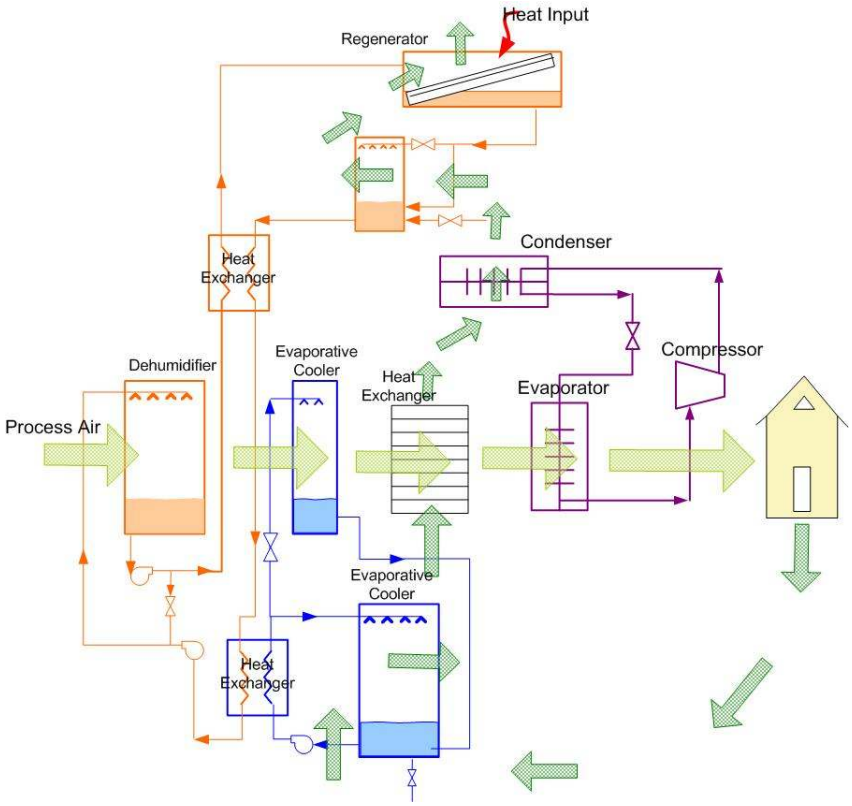

Figure 2-37 Hybrid Vapour Compression/Desiccant by Dai et al., 2001

2.3.4 Solar-Driven Duplex-Rankine Refrigeration Systems

A Rankine power cycle and a vapour compression refrigeration cycle can be put together as a Duplex-Rankine system. It uses the high-pressure vapour fluid to drive a turbine in the power cycle. Consequently, work from the turbine drives the compressor in the refrigeration cycle. The working fluid in the Rankine power cycle and the refrigeration cycle can be different. The COP of the refrigeration cycle is as high as that of vapour compression systems but the efficiency of the power cycle is quite low (about 10%). This system is quite complex and only suitable for large air-conditioning units.

Solar Rankine air-conditioning systems were suggested in the United States in 1975-1980 during the oil crisis. Numerous efforts have been made to develop similar solar cooling systems. The systems were, however, not economically competitive compared with conventional systems. One of the problems was the cost of the solar collector subsystem. In an early stage, water was considered to be an unsuitable fluid in many aspects e.g. excessive shaft speed, high turbine disc stresses, delicate machine, expensive, and required tight tolerances. Wali, 1980, suggested that only halocarbon compounds R-11, R-113 and R-114, and the fluorinated compounds FC-75 and FC-88 fulfilled safety requirements. Subsequently, the working media, which were previously recommended, were found not to be environmentally benign. Thus, the development of this system was detained until interest returned in the 21st century with new proposed cycles combining power and cooling cycles.

Prigmore and Barber, 1975 built a demonstration package of the solar operated Rankine cycle for electricity and cooling for Honeywell Inc. and the National Science Foundation. There were 2 cooling machines installed and results were compared: a LiBr-H_2O absorption chiller and a Rankine cycle (using R113/R12). For the Rankine cycle, the turbine efficiency was 80%, the Rankine cycle efficiency was 11.5%, the compressor efficiency was 85% and the overall COP was 0.71. A reciprocating compressor was used. The Rankine cycle system could become an economically attractive option in the future, since it performs very well when coupled with a CPC collector.

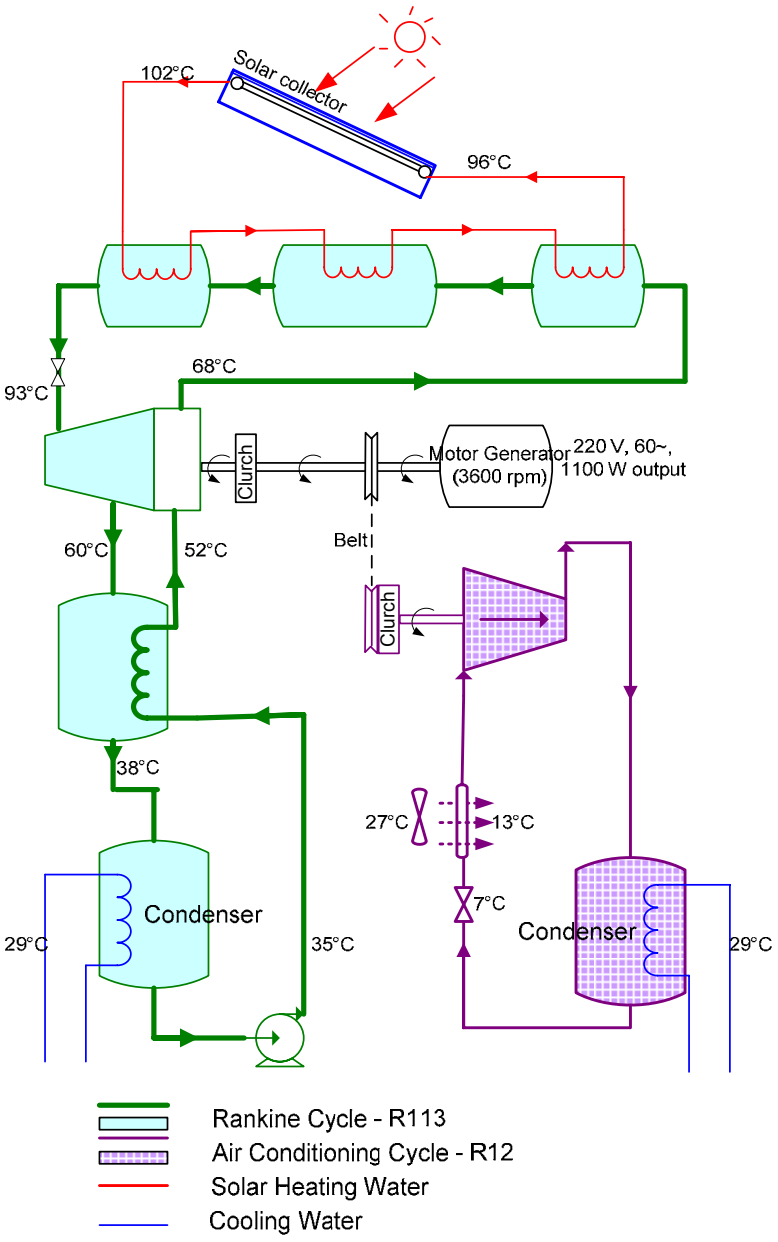

Figure 2-38 Solar Heated Rankine Cycle for Electricity/Cooling by (Prigmore and Barber, 1975)

Lior, 1977, studied the application of a solar-powered, fuel-superheated Rankine cycle incorporating a steam turbine. The fuel-fired combustion was used to superheat the working fluid to increase the efficiency of the system. This cycle would drive the heat pump in the cooling mode. Fuel-fired combustion would drive the heat pump in the heating mode, with system performance augmented by utilizing the waste heat from the cycle, as well as solar energy. In the cooling mode, resource energy savings of 50-60% were suggested. In the heating mode resource energy use is reduced about 3-to 4-fold.

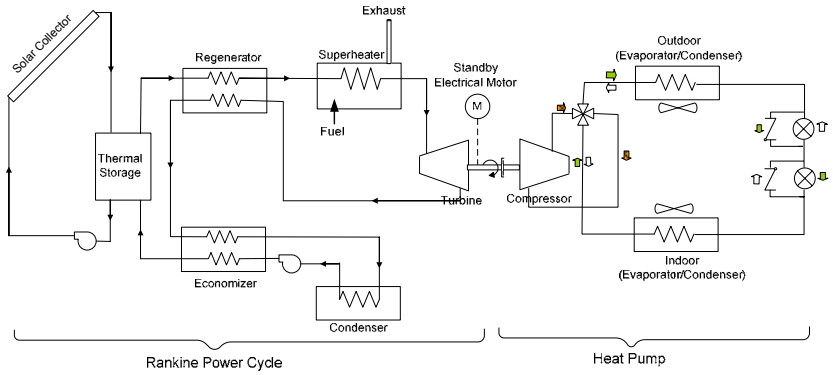

Figure 2-39 Combined Ejector/Rankine cycle by Lior, 1977

Biancardi, Sitler et al., 1982, designed and installed a laboratory test solar driven Rankine cycle heating and cooling system. The system could work in both heat pump and refrigeration mode. The COP in heat pump mode was claimed to be in the range of 1.5 to 3.0. R11 was used as the working fluid in both power and refrigeration cycle. The installation cost was too high for the application at that time.

Corcoleotes and Williamson, 1982, presented a solar cooling project within the Field of Solar Energy (SOLERAS) of the United States-Saudi Arabian Joint Commission on Economic Cooperation. There were both absorption systems and Rankine systems. These systems could also provide electricity during off-cooling load period.

Oliveira, Afonso et al., 2002, proposed a novel hybrid solar/gas system based on the combination of an ejector heat pump cycle with a Rankine cycle. The system was intended to provide cooling/heating and electricity generation for buildings. It is driven by solar energy and supplemented by

a gas burner. N-pentane was used as the refrigerant. Results from system computer modelling, prototype tests and economic analysis are reported. The system was judged to be viable and reliable.

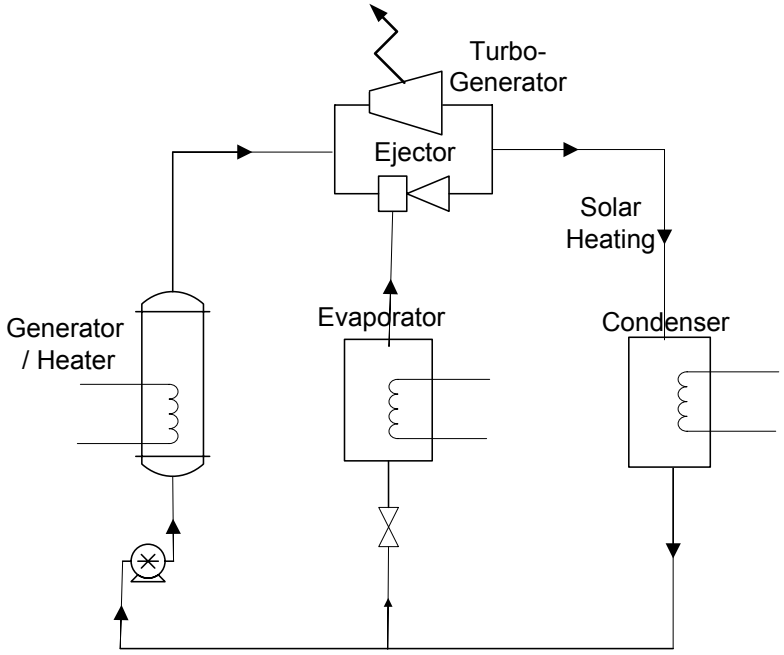

Figure 2-40 Combined Ejector/Rankine cycle by Oliveira, Afonso et al., 2002

Kane, Larrain et al., 2003, proposed an Organic Rankine Cycle (ORC) including a hermetic scroll expander-generator and solar tracking equipment. Heat sources for the system come from both exhaust gases and block cooling of the thermal engine. The thermal engine guarantees a minimum level of both power and heat availability at night or during cloudy periods. A few preliminary tests on the site of the solar power plant when coupled with an engine confirmed reasonable conduct and interest of the concept even at part load or during sharp variations of the thermal supply. Engine efficiency in the solar operation mode was reported to be 7.74%; and in the diesel mode 35%.

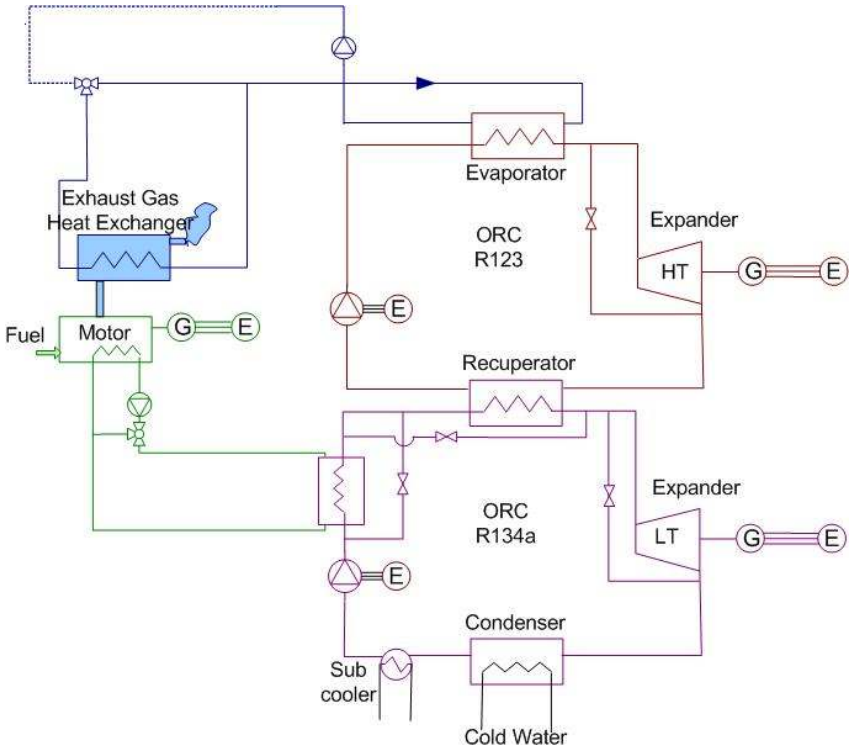

Figure 2-41 Schematic of the SPS Power Unit by Kane, Larrain et al., 2003.

One interesting system proposed by Xu, Goswami et al., 2000, was a combined power/cooling cycle using application of the Rankine power cycle and an ammonia-absorption refrigeration cycle. Both electricity and cooling are produced from the same machine. An ammonia-water mixture is used as the working media. The high concentration ammonia vapour expands to a very low temperature in the turbine without condensation, producing electricity and providing a cooling effect before condensing in the absorber by an absorption condensation process. This process is shown in Figure 2-42. The ammonia-water mixture is pumped to high pressure. The mixture is then heated in the boiler, enriching the ammonia vapour. Part of the vapour in a condenser/rectifier (state 6) is condensed and returned to the boiler while ammonia vapour is superheated after the condenser/rectifier, raising the temperature (state 7). The superheated ammonia vapour expands in the turbine, reaching a very low temperature (0°C or lower). The temperature of the ammonia is low enough to produce ice. Electricity is produced during the expansion process through the turbine. After the cooler, the low temperature ammonia is absorbed by

the weak solution in an absorber (from the boiler), converting again to an ammonia-water mixture.

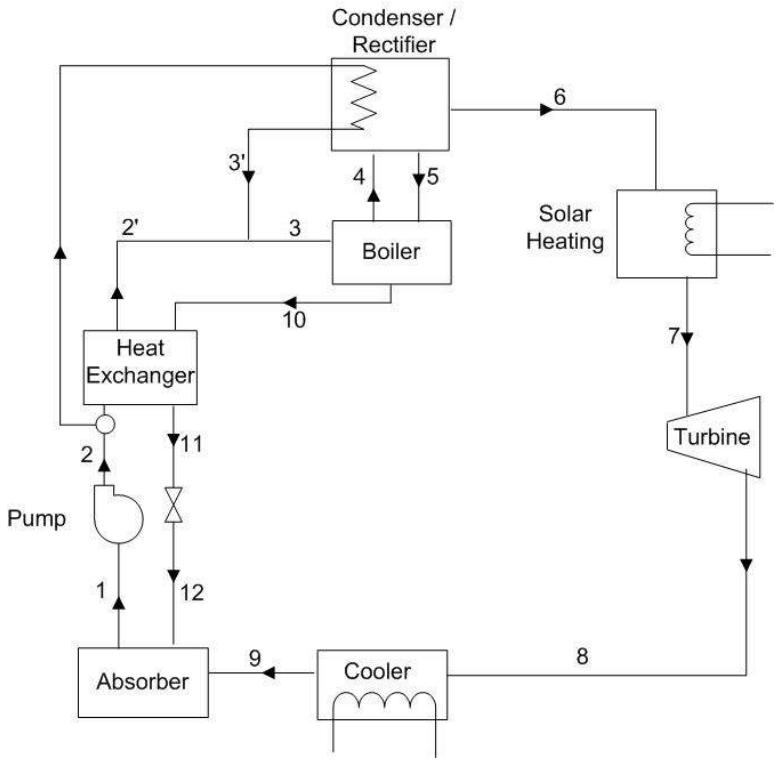

Figure 2-42 A Modified Ammonia-Based Combined Power/Cooling Cycle (Xu, Goswami et al., 2000)

The same principle as the above system was suggested by Tamm, Goswami et al., 2004. The proposed cycle combines the Rankine and absorption refrigeration cycles, using a binary ammonia–water mixture as the working fluid. This cycle can be used as a bottoming cycle using waste heat from conventional power cycles, or an independent cycle using low temperature heat sources. An experimental system was constructed. Results showed that the vapour generation and absorption condensation processes worked experimentally. There is thus a potential for simultaneous turbine performance and refrigerating effect for this system.

2.3.5 Solar-Driven Vapour Compression Systems

This system type comprises of a vapor-compression system and a photovoltaic panel. The system is still quite expensive due to high installation costs and low efficiency of the photovoltaic panels. It is, however, effective and simple in an area far from an electricity grid if the required cooling capacity is low. It is widely used for vaccine storage in remote areas. A mobile unit for a service temperature of 0-8°C is commercially available at a price of around 3000-7000 US$

Solar Refrigerators in Medical Applications

A major market for this type of solar refrigerators is for vaccine storage in developing countries, supported by the World Health Organisation (WHO). There are around 7000 systems installed world-wide at a capacity of about 1400 kWp in 1997 (IIR, 1999). Many manufacturers were certified by WHO/UNICEF in 1994 but due to environmental problems with CFC phase-out in many countries, the number of certified manufacturers has been reduced. The details of the WHO's specification can be downloaded from WHO's website (WHO, 2005).

The PV refrigerator for medical applications normally consists of a PV array, a controller set, a battery bank and a DC-refrigerator, and is comprised of 3 sizes of the PV refrigerator and freezer, according to the WHO's specification: < 30 litres, < 50 litres and > 50 litres. The system must be able to operate stand-alone completely. Detailed product requirements can be found in the supply equipment performance specifications and test procedure, E3: refrigerators and freezers of WHO-EPI WHO, 1999. Price examples for qualified PV refrigerators and icepack freezers are listed in Table 2-6.

Table 2-6 Price Examples and Specifications of Qualified WHO-Solar Refrigerators

Code / Model	Company	Storage Capacity		Gross Volume		Electricity Consumption at 43 °C		Hold-over time during power cut at 43°C	Price
		Refrigerator (litres)	Freezer (litres)	Refrigerator (litres)	Freezer (litres)	With Icepack (kWh/24h)	Without Icepack (kWh/24h)	(h)	(yr2004) (US$)
PIS E3/103-M / VC-65 F	Dulas Ltd.	37.5	16 x 0.6	68	25	0.67	0.34	3.8	1999-3499
PIS E3/104-M / Vacc-Pak XL 2100	Kyocera Solar Inc.	21	24 x 0.4	39	22	0.47	0.28	15.3	2985
PIS E3/105-M / XL 6000	Kyocera Solar Inc.	60	16 x 0.6	114	26	1.02	0.41	5	4985
PIS E3/106-M / PS65	Bright Light Solar Ltd.	37.5	16 x 0.6	66	24	0.7	0.3	2	1900-3400

WHO's standards for vaccine refrigerators are very high, refrigerators are therefore subjected to difficult conditions in remote areas. PV-vaccine refrigerators are quite successful in the WHO-EPI program, however they are very expensive and battery duration is short.

Table 2-7 Example Commercial PV Refrigerators

Company	Model	Volume (litres)	Energy Supply	Description	Price
SunDanzer (Sundanzer, 2005)	DCR165	164.24	8 Amp-hr day^{-1}	Battery Powered refrigerator, 12/24 VDC, refrigerant: R134a (SunDanzer 2005)	999 US$
	DCR225	229.37	10 Amp-hr day^{-1}		1099 US$
	DCF165	164.24	25 Amp-hr day^{-1}		999 US$
	DCF225	229.37	40 Amp-hr day^{-1}		1099 US$
PolarPower (PolarPower, 2005)	SPR-10-12/24 VDC	271.85		Freestanding Model, 12/24 VDC, 60" H, 25.5" W, 24" D	1980 US$
	SPR-10-120 VAC	271.85		Freestanding Model, 120 VAC, 60" H, 25.5" W, 24" D	1895 US$
	SPR-10B-12/24 VDC	271.85		53.5" H, 24" W, 24" D, 12/24 VDC	1875 US$
	SPR-10B-120 VAC	271.85		53.5" H, 24" W, 24" D, 120 VAC	1790 US$
Steca (Iliaktis, 2005)	900001	30.00	90 Wh day^{-1}	Refrigerator, 12 VDC, PV 35 Wp	1,069 €
	900002	50	200 Wh day^{-1}	Refrigerator + Freezer, 12 VDC, PV 80 Wp	1,184 €
	900003	60	90 Wh day^{-1}	Refrigerator, 12 VDC, PV 35 Wp	1,135 €
Global Solar Refrigerator (Low Keep, 2005)	2+ Global Solar Refrigerator	56.63	80 Wh day^{-1}	3 Amp x 12 VDC, makes up to 6 lbs of ice cubes per day	995 US$

The number of solar refrigerators used in household applications is still small. Several systems have been funded and installed by the Agency Francaise pour la Maitris de I' Energie in remote areas of French overseas territories in order to improve living conditions. The total capacity is claimed to be more than 220 kWp in Polynesia, Guyana and Martinique (Fléchon, Lazzarin et al., 1999). These refrigerators can also be found in remote areas of North America and the Middle East. Several companies

sell the solar refrigerators such as Sundanzer, Polar Power Inc., Steca. Price examples for these different commercial PV-refrigerators are given in Table 2-7.

Walk-in Solar Refrigerators

Solar refrigerators have also been installed in the transportation sector, for example in trucks for the transportation of food and vaccine. Generally, a transport refrigerator is powered by a diesel engine in the truck or car. The idea here is to reduce diesel consumption by using a solar powered refrigerator. Univ. of Southampton and Sainsbury (British supermarket chain) developed a solar-trailer refrigerator for carrying fresh fruit and vegetables in England in 1998 (Hague, 2000). The power supply from the PV modules mounted on the roof is 4.25 kWp. The storage compartment is divided into 2 temperature-level-dependent areas.

Polar Power Inc. has also developed and sells walk-in solar power refrigerators, designed to transport tree seedlings, and manufactured as a slip-in unit to be carried by a standard ¾ ton pick-up truck. This refrigerator was designed to be operated from the truck, or by use of a camper-jack. It may be removed from the truck and operated as an independent self-contained unit.

2.3.6 Solar-Driven Stirling Refrigeration Systems

A stirling system is suitable for specific applications requiring low temperatures. The principle of the stirling refrigeration cycle is based on volume changes caused by pistons, thus inducing changes in pressure and temperature of a gas (no phase change). This unit is expensive, complicated, and not yet commercially available. On the other hand, it yields very good performance at large temperature increases and can reach cryogenic temperatures (Lundqvist, 1993).

The solar-powered stirling engine has been suggested for both power generation and to drive refrigeration in so-called duplex systems since the 1970s. These engines require high quality heat at temperatures between 600 and 700°C. This, in turn, requires a high quality solar collector and absorber, e.g. a good solar concentrator with an advanced tracking system, therefore adding extra cost and complexity to the system. This technology holds, in fact a world record in efficiency for the conversion of direct sunlight to electricity (almost 30%). From an efficiency point of view, the solar thermal stirling engine may therefore be preferable, if costs can be managed in the future.

The stirling cooler driven by solar cells is, however, more competitive. Early research was funded by the Dutch Consortium of Environmental Groups and Utilities in an effort to build a Stirling cooled, solar powered, battery-free super efficient refrigerator in November 1993 (Mennink and Berchowitz, 1999). The prototype unit was first demonstrated in April 1994 at the 12th European Photovoltaic Conference. The COP of the Stirling cooler was claimed to be 3.0 at an ambient temperature of 25°C. . Two refrigerator sizes have been studied, 365 litres and 30 litres (1 cu. ft.) Capacity varies from 8 to 50 W at 0 to 30°C. It is a so-called free-piston machine driven by a linear motor and an AC voltage source. To avoid the need of batteries, 5 litres of water ice is produced for a "no-sun" operation time of 24 hours. This Stirling cooler is now being commercialized by Global Cooling BV (the Netherlands) and Twinbird Corporation (Japan).

2.3.7 Solar-Driven Thermoelectric Refrigeration Systems

A thermoelectric refrigeration cycle (Peltier) is as already mentioned suitable for small scale applications. Cooling is achieved by driving an electric current through the electric circuit containing junctions of different metals. This phenomenon is called the reversed Seebeck effect. There are no moving parts and no working fluid in this system. It is a small system, suitable for use in mobile refrigerators. A few examples are given here for completeness.

An early solar cooling system was proposed by Field, 1980. The refrigerator was designed for medical storage in developing countries. Thus, the unit is special and durable, since it must be operable in harsh conditions by unskilled personnel. Components of the system are commercially available. The current commercial unit operates on direct current, typical for PV´s; the supply voltage is 18 V D.C. with a lead-acid or advanced battery power system. The unit volume is 3.6 litres. The total cost for this unit in 1980 was about 8500 USD.

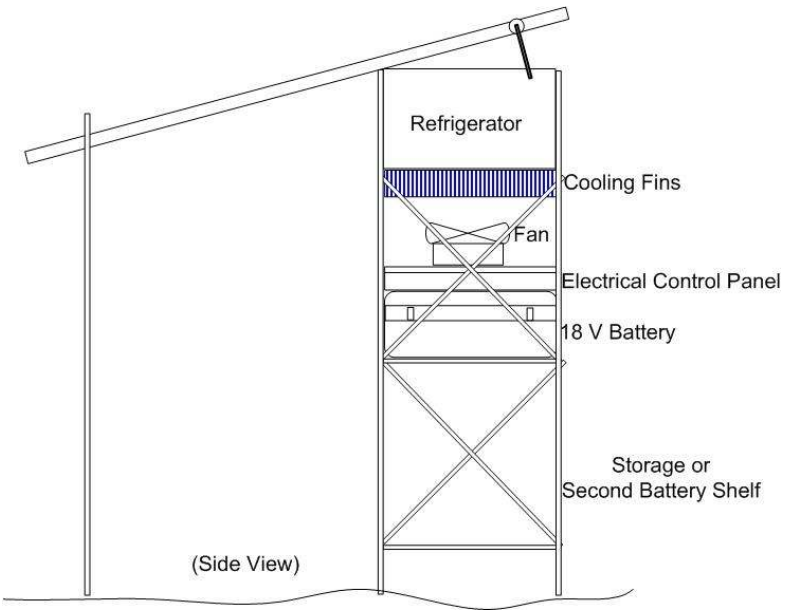

Figure 2-43 Side View of the PV-Driven Thermoelectric Refrigerator by Field, 1980.

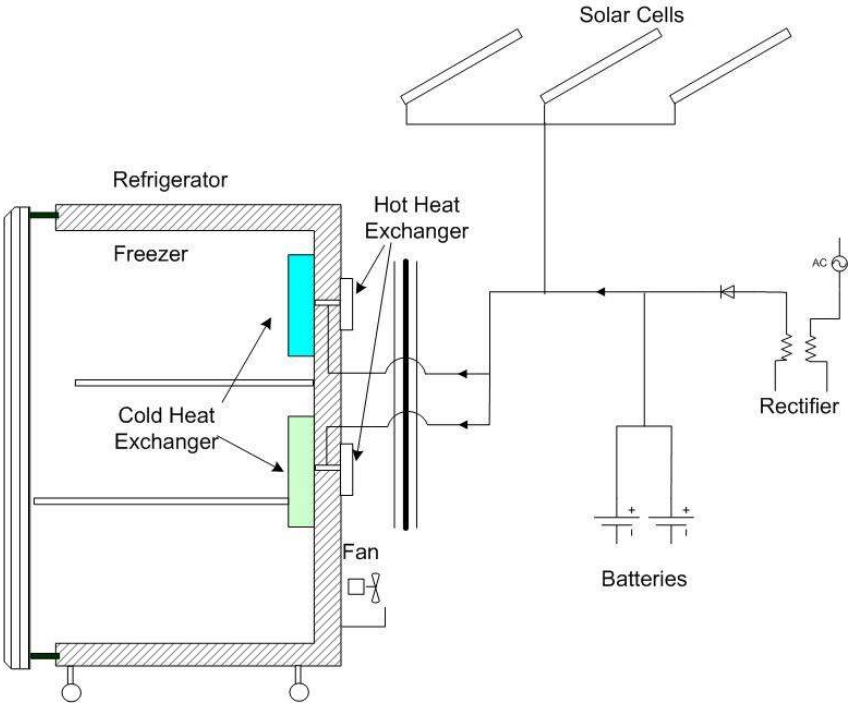

Figure 2-44 Thermoelectric Refrigerator and Power Supply Configuration by Sofrata, 1996

For curiosity, the thermoelectric cooling headgear for cooling of the forehead by Hara, Azuma et al., 1998 is included, It was driven by a small solar cell (amorphous type) as shown in Figure 2-45. Forehead temperature is claimed to be reduced by 4 K in order to accommodate thermal comfort.

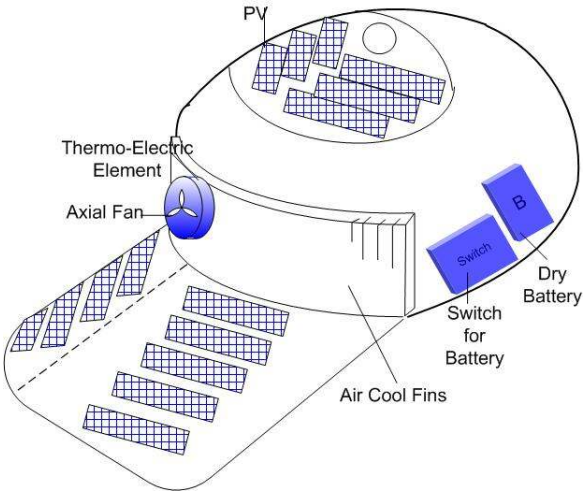

Figure 2-45 Thermoelectric Cooling Headgear Driven by Solar Cells, proposed by Hara et al., (1998).

The World Health Organisation (WHO) has proposed vaccine storage and transportation using a Peltier-effect refrigerator (Fléchon, Lazzarin et al., 1999). However, there are some problems concerning temperature levels, which is limited at +5°C at an ambient temperature of 30°C. The cooling compartment consequently heats up rapidly when the electric supply is cut off since Peltier's element itself becomes a thermal bridge.

Dai and Sumathy, 2003, tested the Peltier refrigerator driven by solar cell in different conditions. Electricity from the PV charged the batteries during the daytime, providing energy when sunshine was absent, expecting a refrigeration potential for cold storage of vaccine, foodstuffs and drinks in remote areas.

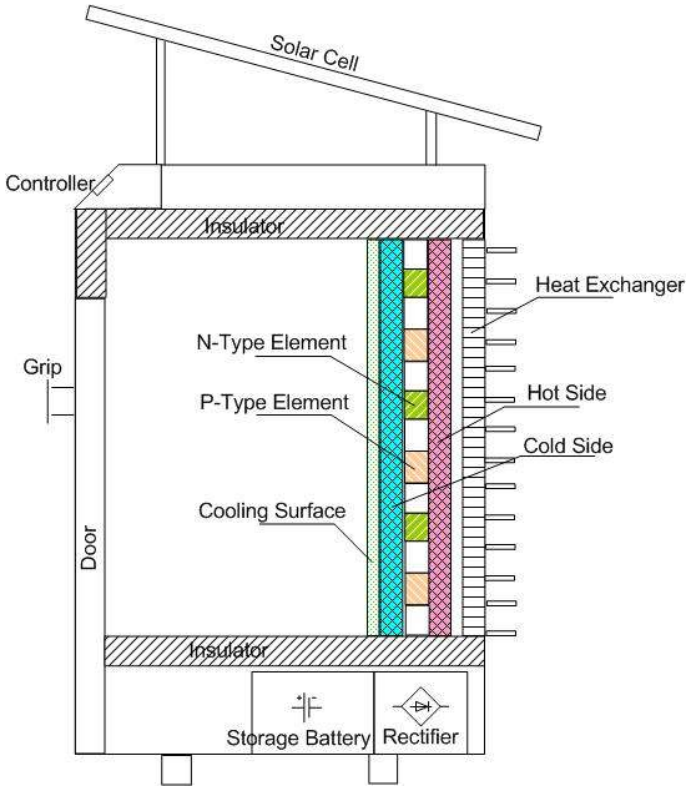

Figure 2-46 The PV-Driven Thermoelectric Refrigerator by Dai and Sumathy, 2003.

Khire, Messac et al., 2005 discussed an Active Building Envelope (ABE) system integrated with a thermoelectric heat pump. Solar energy is used to compensate passive heat loss or gain in building envelope or other enclosures. This paper focuses on the design and analysis of a key component—the thermoelectric heat pump unit, or the TE unit. This unit is an integral part of the generic enclosure, and is a collection of thermoelectric coolers, or heaters. A multi-objective optimization technique was implemented to design and evaluate different design configurations of the TE unit.

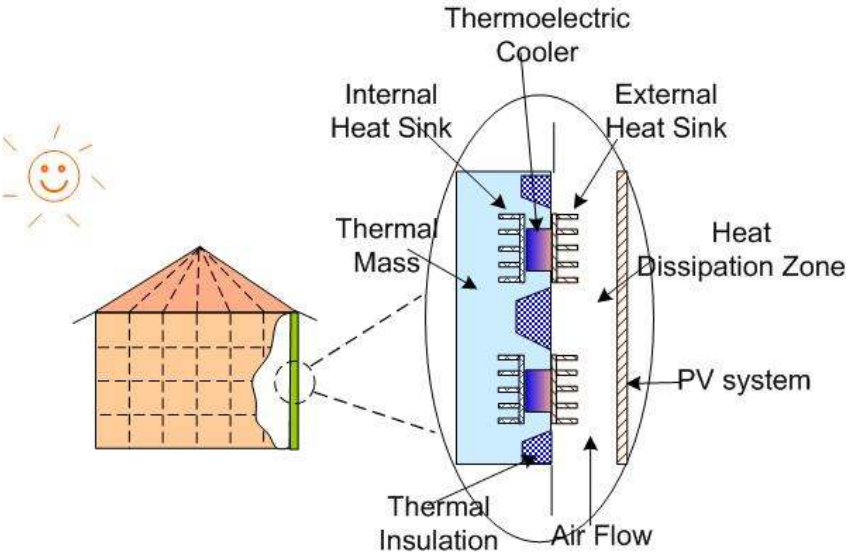

Figure 2-47 Active Building Envelop (ABE) with Thermoelectric Cooler by Khire, Messac et al., 2005

The single stage ejector system is the simpliest form of this technology and it is widely installed worldwide operating on low pressure steam generated from process heat typically in pulp and paper industry. Systems are often of MW size. The system presented in this thesis differs considerable from these. Firstly the driving steam is produced in the system for the ejector only and secondly the pressure is maintained with a pump. The system is closed whereas the systems in pulp and paper industry are more or less open. The working fluid of the systems presented here is not water and the size is much smaller.

There are several ongoing attempts to improve the performance of ejector systems using multi-stage ejectors or hybrid system where the ejector technology is combined with other technologies. Currently, the ejector refrigeration technology can roughly be classified into 3 main groups††:

1. Single stage ejector refrigeration systems
2. Multi-stage ejector refrigeration systems
3. Hybrid ejector and other technologies e.g. vapour compression, absorption and adsorption

Theoretical calculation, computer simulation and experimental work have been performed by many research groups worldwide.

Single Stage Ejector Refrigeration Systems

A majority of research and development studies regarding solar-driven ejector refrigeration systems deal with the single stage system type. Several experimental rigs have been built and tested in different parts of the world. Initially, chlorofluorocarbon (CFC) refrigerants e.g. R12 (Chang, Gravalos et al., 1986), R11 (Murthy, Balasubramanian et al., 1991), R113 (Al-Khalidy, 1997a) were used. After the CFC ban, the hydrochlorofluorocarbons (HCFCs) refrigerants e.g. R141b (Huang, Chang et al., 1998) was used. Subsequently, more environmentally friendly refrigerants were suggested e.g. the hydrocarbon refrigerant (Pridasawas and Lundqvist, 2003) or), as well as the hydrofluoroether (HFE) refrigerant (Wolpert, Riffat et al., 2003)

†† One use of the ejector gaining interst is to replace the expansion valve in vapour compression systems to revover exergy lost during expansion. This is especially of interst for cycles operating with the working fluid CO_2.

Al-Khalidy, 1997a, analysed the theoretical and experimental performance of a solar-driven ejector refrigeration system. Five refrigerants (R717, R12, R11, R113 and R114) were compared. From the theoretical analysis, it was found that R113 was more suitable than any other refrigerant. The COP of the refrigeration system and performance of the solar ejector refrigeration system as a whole, increased when the generating and the evaporating temperature increased and decreased when the condensing temperature increases. At a generating temperature of 87 °C, a condenser temperature of 43°C and an evaporating temperature of 10°C, the COP obtained was about 0.256 and the STR was 0.12.

Bejan, Vargas et al., 1995 designed a single-stage solar-driven ejector system with 3.5 kW (12 000 Btu hr^{-1}) of refrigeration capacity at an evaporating temperature of +4°C and a generating temperature of 90-105°C with R114. The overall COP was found to be around 0.126 - 0.26. The researchers discussed the importance of thermal storage. A cold storage was recommended based on consisting of phase-changing materials, cold water or ice storage instead of storing a large amount of heat on the warm side of the system. Efficiency of the system could be improved by an increase the generating temperature.

Murthy, Balasubramanian et al., 1991, tested different ejector dimensions at the cooling capacity about 0.5 kW. R12 was used as the refrigerant. A COP in the range of 0.08-0.33 was obtained.

Huang, Chang et al., 1998 developed a solar ejector cooling system using R141b as the refrigerant; obtaining the overall COP of around 0.22 at a generating temperature of 95°C, an evaporating temperature of 8°C and solar radiation of 700 W m^{-2}.

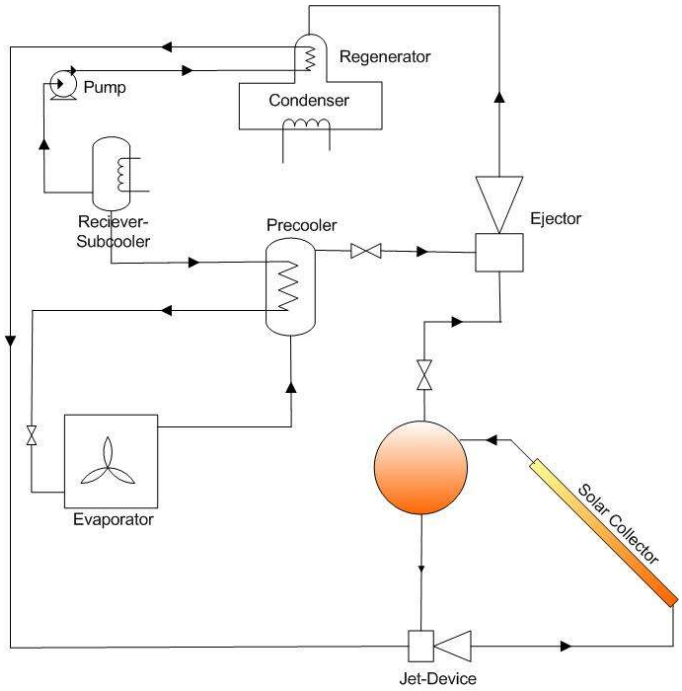

Figure 2-48 Single Stage Solar Driven Ejector Refrigeration System by Huang, Chang et al., 1998

Experiments on a solar-powered passive ejector cooling system were also performed in 2001 by Nguyen, Riffat et al., 2001. Water was used as the working fluid with an evacuated tube solar collector. Cooling capacity was designed for 7 kW. This system is also capable of delivering heat up to 20 kW during the winter period.

Several theoretical analyses and dynamic simulations of the single stage system using butane and iso-butane as refrigerants were performed by Pridasawas and Lundqvist, 2004c; 2004a. The optimum generating temperature was found to be in the range of 80 to 100°C, depending on the evaporation temperature. Therefore, high temperature solar collectors are not necessary for the solar-driven ejector refrigeration system being employed for air-conditioning applications.

Wolpert, Riffat et al., 2003 introduced the hydrofluoroether (HFE) as a refrigerant for a 13 kW single-stage system. From computer simulations, the COP obtained was about 0.62 at a suggested generating temperature

of 140-160°C, a condensing temperature of 32-40°C and an evaporator temperature of 5°C.

R134a was also proposed as a refrigerant for a solar-driven ejector system by Alexis and Karayiannis, 2005. The average STR was about 0.014-0.101 and the COP was found to be in the range of 0.05-0.199.

Multi-stage Ejector Refrigeration Systems

Although the single stage ejector refrigeration is simple, it is difficult to keep the system running at optimum conditions due to the variation of working conditions. For example, ambient temperatures above design conditions or low insolation often lead to operation difficulties. Attempts have been made to solve this problem by multi-stage ejectors. Several ejectors are placed in parallel before the condenser. One ejector operates at a time and the operation of each ejector is determined by the condenser pressure. An example of the ejector arrangement is shown in Figure 2-49. The overall entrainment ratio is the thick line. Ejector 1 operates when the condenser pressure is above P_{c1}; ejector 2 operates at a condenser pressure between P_{c1} and P_{c2}; and ejector 3 operates at a condenser pressure between P_{c2} and P_{c3}. This arrangement was proposed by Bejan, Vargas et al., 1995.

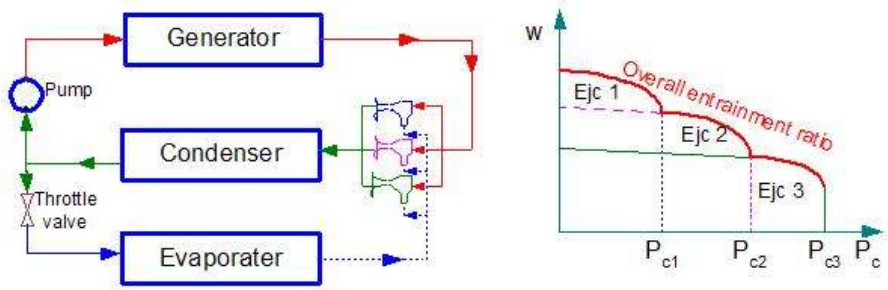

Figure 2-49 Multi-Stage Ejector System

Ejector Refrigeration System with Booster or Compressor

The low cycle's COP is the main disadvantage of the ejector system; several attempts have therefore been made to improve the performance of this system. A booster (a compressor) can be used to enhance the ejector system at the cost of additional driving energy. The booster is used to lift pressure of the refrigerant from the evaporator. There are several system configurations proposed by different research groups. An inter-cooler (internal heat exchanger) may be used for maintaining an intermediate pressure. Vapour refrigerant from the evaporator is first boosted to the intermediate pressure. The stream from the intercooler is then supplied to the ejector. A simple diagram of the ejector system with booster is shown in Figure 2-50.

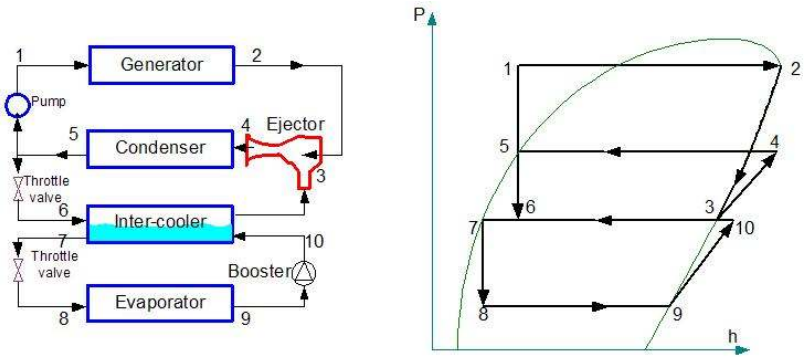

Figure 2-50 Ejector Refrigeration System with Booster

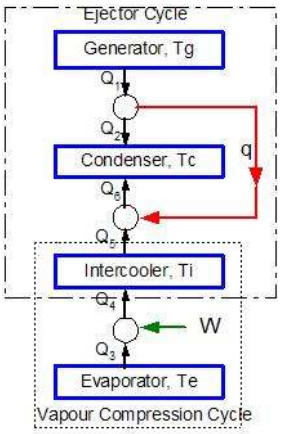

Figure 2-51 A Concept of a Combined Ejector Refrigeration System with Booster by Göktun, 2000.

Bejan, Vargas et al., 1995 proposed to use a booster and inter-cooler in an effort to improve the ejector cooling system. Heating, cooling and hot water supply could be the load of the ejector-power system, heating load during the winter and cooling load during the summer. This machine is called 'the solar-powered compression-enhanced ejector air conditioner'. The compression enhanced ejector system is used to boost the pressure of the secondary stream into the ejector. Mechanical energy or electricity is supplied to the booster. R114 is used as the working medium. Whole system performance can be improved. At 3.5 kW of the refrigeration capacity, 4°C evaporating temperature and 50°C condensing temperature, the theoretical COP of the ejector system can be up to 0.85 and the COP of the overall cycle can be up to 0.5. In 2004, this research group revised the system again with an HCFC refrigerant,Arbel and Sokolov, 2004. The previous CFC refrigerant (R114) was replaced by R142b.

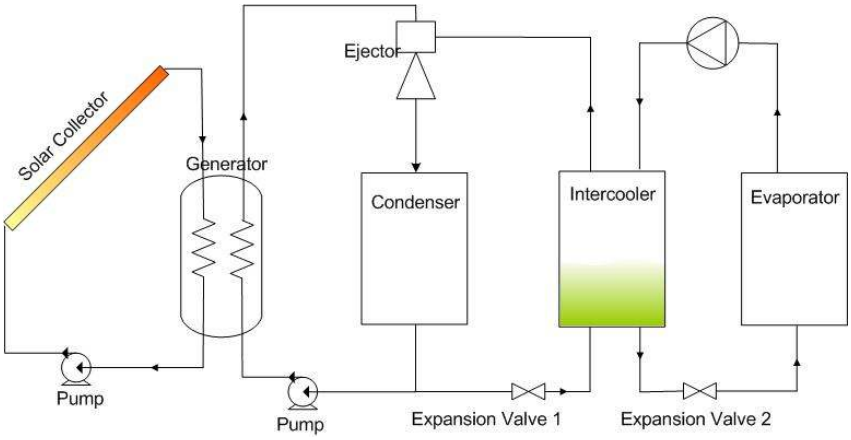

Figure 2-52 The Solar-Power Compression-Enhanced Ejector Air Conditioner Proposed by Bejan, Vargas et al., 1995

An ejector system with a booster using R142b was proposed by Dorantès, Estrada et al., 1996. There was no inter-cooler in the system. Dynamic simulations of the solar driven system demonstrated that the COP achieved was about 0.11 at an evaporating temperature of –10°C, condensing temperature of 30°C and generating temperature of 105°C. This system could produce 100 kg of ice per day at the capacity of 2 kW.

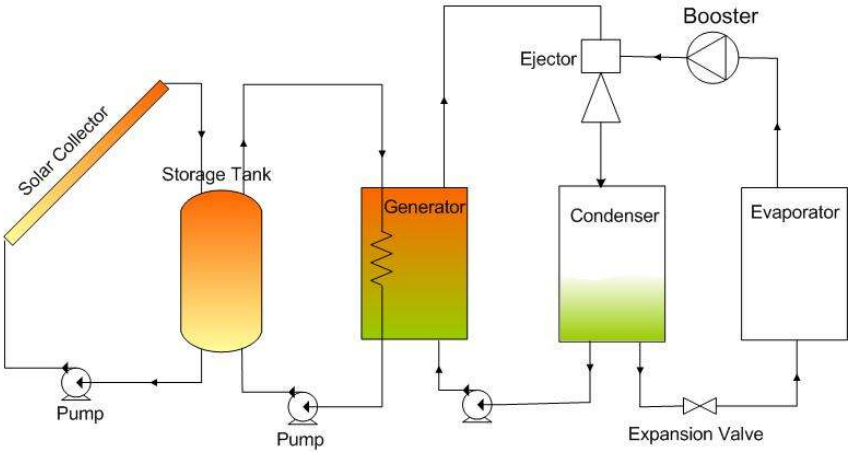

Figure 2-53 The Solar Driven Ejector with Booster System Proposed by Dorantès, Estrada et al., 1996

The system with 2 split methods: vapour compression and ejector system was proposed by Sun, Feng et al., 1997. Water was used as the refrigerant in the ejector system, and R134a was used in the vapour compression system. The condenser of the vapour compression system performed as the evaporator of the ejector system. This equipment is defined as an inter-cooler. Results from the theoretical analysis illustrated that this combined cycle can improve system efficiency by more than 50%.

A solar assisted ejector-vapour compression cascade system was proposed by Göktun, 2000. The inter-cooler was installed serving as a condenser for the vapour compression system and an evaporator for the ejector system. This paper also proposed an equation for calculating the optimum operating solar collector temperature and corresponding COP.

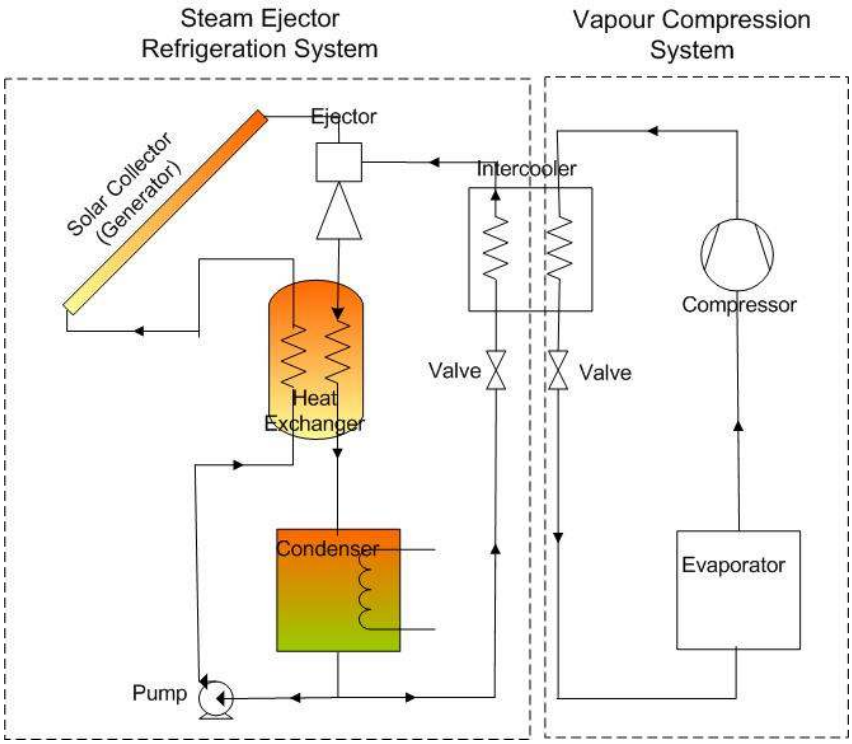

Figure 2-54 A Combined Ejector and Vapour Compression System, Proposed by Sun, Feng et al., 1997.

Solar-driven Combined Ejector and Absorption Refrigeration Systems

A conventional absorption refrigeration system consists of 2 pressure levels, a high pressure side in the condenser and the generator, and a low pressure side in the evaporator and the absorber. An expansion valve and pressure-reducing valve are the common equipment used to split the high and low pressure sides. Both valves operate on a throttle process causing inefficiency in the system. Thus, the idea of a combined cycle is to reduce throttle loss by using an ejector. The ejector is introduced in order to utilise energy from the high pressure side of the weak solution in the generator. The high-pressure weak solution in the generator expands through the nozzle in the ejector and creates a vacuum at the other end of the ejector. As a vacuum occurs, the vapour from the evaporator is drawn into the ejector. The mixing solution is then purged into the absorber. The schematic of the combined ejector-absorption cycle is shown in Figure 2-55.

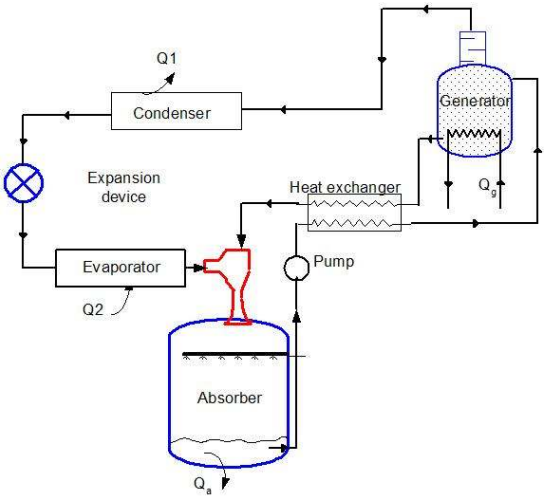

Figure 2-55 Schematic of a Combined Ejector-Absorption Refrigeration Cycle

A solar-driven ejector-absorption cycle was modelled by Sözen and Özalp, 2003. The proposed schematic is shown in Figure 2-57. As a result of the analysis, using the ejector, the COP improved by about 20%. A concentrating solar collector was used in this analysis. In 2005 the researchers investigated the possibility of using this system in Turkey, (Sözen and Özalp, 2005). According to the results obtained in this 8-9 month long study, (March–October), a CPC collector of 4 m^2 was sufficient for different typical applications of refrigeration all over Turkey.

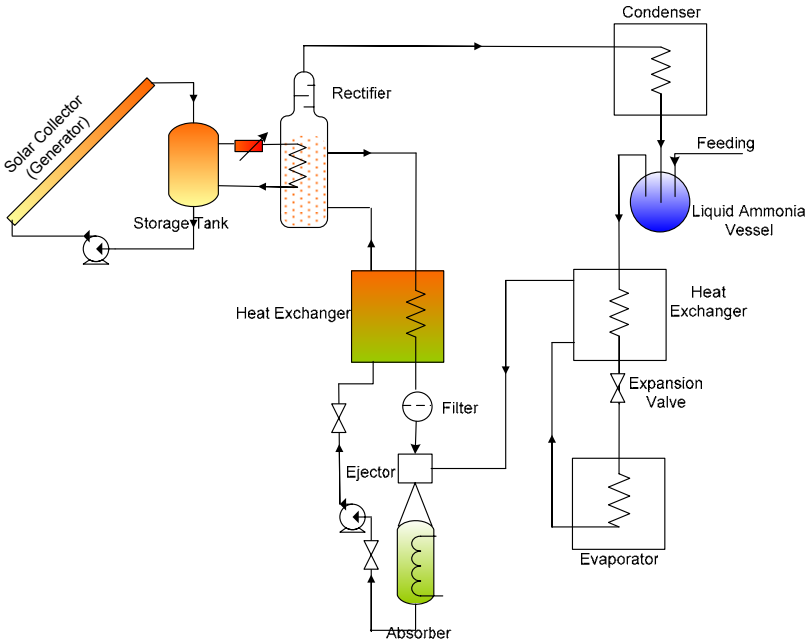

Figure 2-56 Schematic of a Combined Ejector-Absorption Refrigeration Cycle (Sözen and Özalp, 2003)

Solar-Driven Combined Ejector and Adsorption Refrigeration Systems

This system can be considered as 2 split cycles which work separately at different periods: an ejector cycle and an adsorption cycle. The system was proposed by Li, Wang et al., 2002 and Zhang and Wang, 2002b.

The theoretical analysis of a solar-driven continuous combined solar adsorption – ejector refrigeration and heating system was presented by Zhang and Wang, 2002b. A schematic of this system is shown in Figure 2-57. Zeolite – water were used as a working pair. This system is working on the same principle as the system proposed by Li, Wang et al., 2002. The difference is in the afternoon, when the temperature in the adsorber is high enough; the adsorber is used as a thermal collector for heating up tap water. The cooling capacity is 0.15 MJ/kg Zeolite during day-time and 0.34 MJ/kg Zeolite in the evening. This system can also heat up 290 kg of water to 45°C. A combined COP of about 0.33 was reached.

The proposed system by Li, Wang et al., 2002 is shown in Figure 2-58. Zeolite 13X and water are used as the working media. During daytime, the cooling effect is achieved by the ejector cycle; while the desorption process occurs in the adsorption cycle. The vapour from the desorption process of the adsorber enters the generator. During night time, the cooling effect is achieved by adsorption process; vapour refrigerant from the evaporator is adsorbed in the adsorber. The overall COP of this combined cycle is about 0.4, at the regeneration temperature 120°C, a desorption temperature of 200°C, a condensing temperature of 40°C and an evaporating temperature of 10°C.

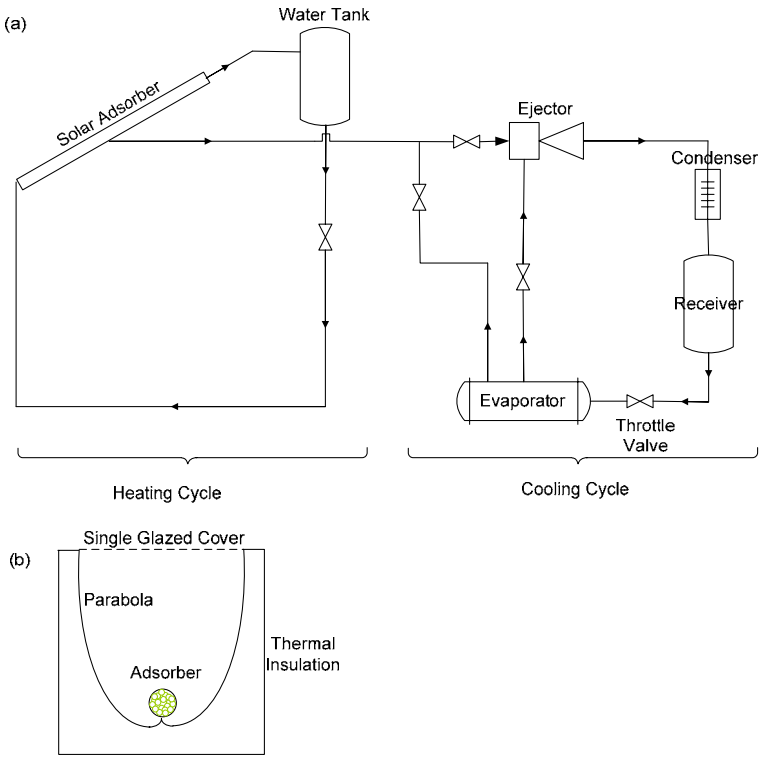

Figure 2-57 Solar Driven Ejector-Adsorption System and an Concentrating Adsorber Proposed by Zhang and Wang, 2002b.

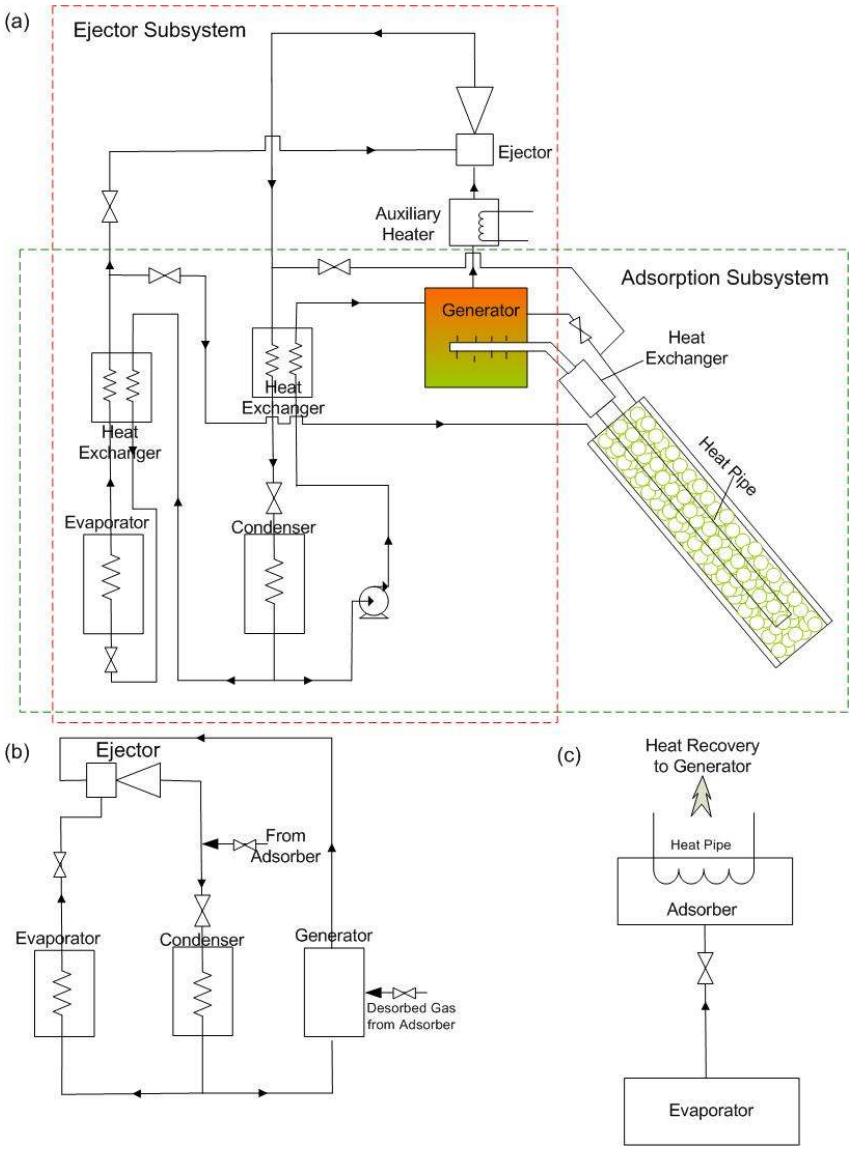

Figure 2-58 Solar Driven Ejector-Adsorption System Proposed by Li, Wang et al., 2002.
(a) System Layout
(b) Ejector Refrigeration System During Day Time
(c) Adsorption Refrigeration System During Night Time

2.3.9 Conclusions of the Reviews on Solar-Driven Refrigeration Systems

The main advantages and disadvantages of each solar-driven refrigeration system are shown in Table 2-8.

Table 2-8 Advantages and Disadvantages

Advantages	Disadvantages
Absorption Systems	
• Only one moving part (pump) with the possibly of no moving parts for small systems (e.g. Platen-Munters cycle) • Possible to utilise low-temperature heat supply	• It cannot achieve a very low evaporating temperature in using LiBr-H_2O as working media. • The system is quite complicated and difficult for service.
Adsorption Systems	
• No moving parts (except valves) • Low operating temperatures can be achieved.	• The high weight and poor thermal conductivity of the adsorbent make it unsuitable to use for high capacities and can cause long-term problems. • Low operating pressure requirement makes it difficult to achieve air-tight • Very sensitive to low temperature especially the decreasing temperature during the night. • It is an intermittent system.
Chemical Reaction Systems	
• No moving parts • Low evaporation temperatures can be achieved.	• Low COP • High weight of adsorbent, not suitable to use for high capacities. • The system design is complex especially due to the volume of the adsorber that changes when chemical reaction occurs. • Low operating pressure at a lower temperature, difficult to achieve air-tightness.

Table 2-8 (Cont.) Advantages and Disadvantages

Desiccant Cooling Systems	
• Environmentally friendly, water is used as the working fluid. • Can be integrated with a ventilation and heating system. • The driving temperature is quite low, thus possible to use low temperature solar collector. • In case of the liquid desiccant, the system doesn't need a condenser because the refrigerant can be released to the atmosphere	• It is difficult to have good control of the system in a humid area. • It is not appropriate for areas where water is scarce. • In case of the solid desiccant, the system requires maintenance due to moving parts in the rotor wheel of the solid desiccant system. • In case of the liquid desiccant, the liquid sorbent can contaminate the supplied air. • Crystallization generally occurs in liquid desiccant systems due to poor process control.
Ejector Refrigeration Systems	
• A low temperature heat source can be utilized. • Low operating and installation cost	• Low COP • Complicated design of the ejector • Difficult to operate in a wide range of ambient temperatures.
Rankine Cycles (Duplex Rankine Cycles)	
• Suitable for high capacity systems • Suitable for integration into polygeneration systems (heat, electricity and refrigeration).	• High installation cost • Large system • Regular maintenance required due to complications and many moving parts.

Table 2.8 (Cont.) Advantages and Disadvantages

Stirling/PV systems	
• Relatively high COP for high temperature lifts. • Can be used for cryogenic applications and is mechanically simpler than other applications for low temperature operations. • Environmentally friendly • Mobile and light weight	• High production costs • Complexity in design
Thermoelectric/PV systems	
• No working fluid and no moving parts (except fans) • Quiet • Small size and light weight	• Low COPs • Difficult to achieve a low refrigeration temperature • Low reliability especially when the power supply is cut off. • Requires efficient heat sink in order to reject heat from the thermo-electric module. • Not suitable for large cooling load • Induces thermal short circuiting when not operated
Vapour Compression/PV systems	
• High COP • Long term experience and widely available commercially • Scalable from small to a large systems	• For a PV system, installation cost is high and requires battery for energy backup. • Can be noisy.

While going through the material and by a discussion of the benefits and drawbacks of the various cycles, a number of observations can be made:

- All sorption cycles, including chemical sorption, are in the process beginning with research laboratory to the market, but much more work is needed on cost minimization and, design and packaging.

- Small-scale absorption cycles driven by solar thermal energy have already been recently launched in the market by several companies.

- Adsorption and chemical adsorption cycles appear to function well in small -scale applications such as small refrigerators; however, these cycles need to solve refrigerant/adsorbent problems due to corrosion and crystallization.

- An interesting option for the future is to integrate the desiccant cooling cycles into the ventilation system and, rendering the system to become more popular.

- The Duplex Rankine cycle is suitable for high cooling capacities where a large number of moving parts in the cycle, and the implied regular maintenance, can be accepted. The system type can be operated as part of a so-called polygeneration system.

- The ejector refrigeration cycle has the benefit of being simple, rreliable and feasible to operate with a low temperature heat source. The cycle COP is low, but only slightly lower than other heat operated cycles. This renders the system interesting from a cost point of view.

These conclusions were the major reasons for choosing the latter system for further studies.

It is obvious that each refrigeration cycle described has its own niche in application. Variations in local conditions can moreover limit the choice of refrigeration technology. The effects of local conditions does not strongly affect the function of the PV-driven refrigerators, often operating with a relatively constant cooling capacity, although large temperature lifts may cause malfunction. There are however, significant effects on local conditions for solar thermal driven air-conditioning systems. Chapter 5 will therefore, discuss the effects of local conditions in more detail.

3 Effects on Local Conditions

As discussed previously, it is important to consider local conditions when designing and installing a solar-driven refrigeration system. This is predominantly due to the different characteristics of each refrigeration cycle. Furthermore, cooling load characteristics for each location or building are not always similar. The differences in cooling load characteristics and available solar radiation in different locations from the southern to the northern hemisphere are discussed. Solar-driven single-stage absorption refrigeration systems are chosen as a case study in this chapter.

In warm urban regions, need for refrigeration is imperative for both prolonging the life of perishable products, as well as thermal comfort. An electric driven air-conditioning system is, therefore, often used to control the temperature and humidity for human thermal comfort. The demand for this application is fast growing in densely populated areas world-wide; serious infrastructure problems due to power shortage, associated with environmental problems related to electricity production are increasing.

In rural areas where thermal comfort can be obtained with passive ventilation, active air-conditioning is not essential. Refrigeration and freezing applications are however needed to store perishable material such as vaccines or food. PV-driven systems, already discussed, are highly effective for this application; however, installation costs are, frequently, too high for the local people to afford.

There are certain limitations for each solar cooling technique imposed by the local climate. Some of them are related to insolation, or rather lack of insolation, whereas others are related to temperature levels or humidity ratios. An example of the latter is the desiccant cooling system, which functions inefficiently at high humidity. The same goes for the passive evaporative cooling technique; the lowest temperature that can be reached is at dew point. The reason is that at the same dry bulb temperature, air with a low humidity ratio has a lower dew point temperature than air with a high humidity ratio. This implies that to reach the lower temperature, a considerable amount of heat is required to dehumidify the high humidity air be-

fore the evaporative cooling process. Therefore, this leads into poor system efficiency. Although low humidity is preferred for the desiccant cooling system, sufficient make up water is needed as the working medium for the evaporative cooling process.

The temperature of the heat sink significantly affects the performance of heat driven systems in general. A lower heat sink temperature can minimize the required driving temperature and improve system COP or STR. It is therefore critical to find a good heat sink in order to achieve a reasonably low temperature, especially in a hot environment. For ejector refrigeration cycles, systems with one fixed ejector dimension can only operate within a small range of condenser temperatures.

Subsequently, whenever discussing the potential for solar cooling, a thorough investigation of local conditions must be carried out.

3.1 Climate

The calculation of solar radiation in this chapter is based on climatic data from Meteonorm 4.10 (Remund, Lang et al., 2001). System calculations have been done in TRNSYS 16 (Klein, Beckman et al., 2004b). Total solar radiation on a horizontal surface at one specific location varies over the year due to the orbit and angle of the earth. Variations are obvious for locations located in the far north or southern hemisphere, as shown in Figure 3-1 and Figure 3-3. In the northern hemisphere, above the Tropic of Cancer (23° 26" 22' N), peak radiation is typically in July. Conversely, in the southern hemisphere, below the Tropic of Capricon (23° 26" 22' S), peak radiation is in January.

Total solar radiation on the horizontal surface of the area around the equator does not significantly change over the year. This does not, however, indicate that available solar energy is constant, since effects from the monsoon season must be taken into consideration. This is shown in Figure 3-1, the locations near the equator are represented by Singapore (latitude 1°N), Bangkok (latitude 13°N), and Brasilia (latitude 15°S).

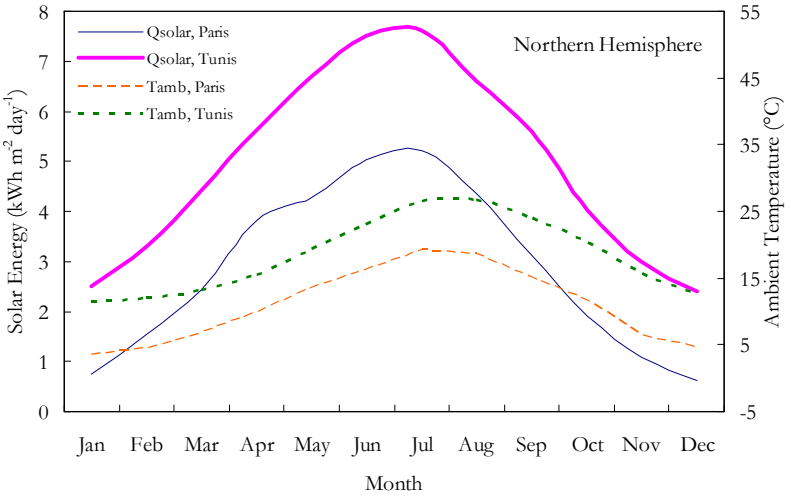

Figure 3-1 Total Solar Radiation on Horizontal Surface during One Day and the Ambient Temperature of Paris and Tunis as an Example of Locations in the Northern Hemisphere

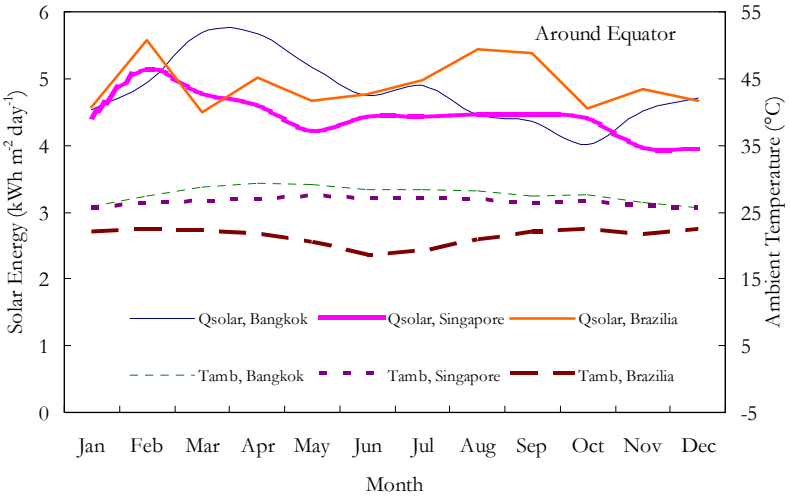

Figure 3-2 Total Solar Radiation on Horizontal Surfaces during One Day and Ambient Temperature of Bangkok, Singapore and Brasilia as an Example of Locations in the Tropical Region

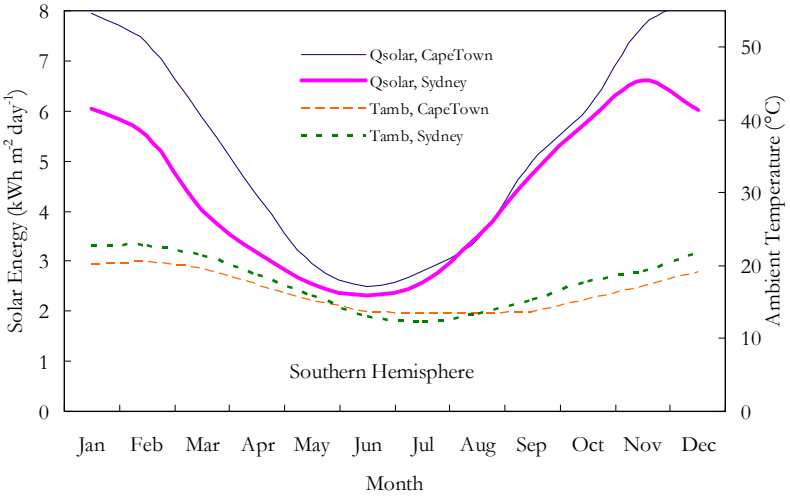

Figure 3-3 Total Solar Radiation on Horizontal Surfaces during One day and Ambient Temperature of Cape Town and Sydney as an Example of Locations in the Southern Hemisphere

The angle of incidence for solar radiation at any particular location relative to the earth changes at any given time, implying that solar collectors on different slopes (the angle between the plane of the collector surface and the horizontal) obtain a different amount of solar radiation. The total radiation in one year on different surface tilts at different locations is shown in Figure 3-4. The incident radiation at different locations reaches the maximum at different tilts depending on the latitude. In the northern hemisphere, higher radiation is obtained when the surface angle tilts southward. As rule of thumb, the surface angle of the solar collector is about 10-15 degrees lower than the latitude, but not less than 30 degrees. If the angle is too small, dust or scraps can accumulate on the collector panel. This dust shades the collector and decreases the incident solar radiation.

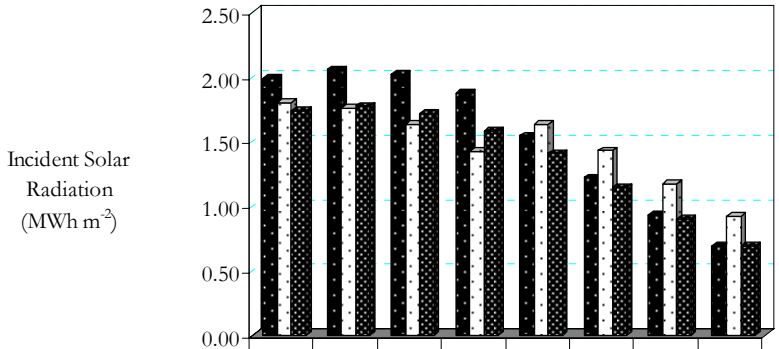

	S15	S30	S45	S60	N15	N30	N45	N60
Tunis	1.98	2.06	2.02	1.87	1.54	1.22	0.93	0.69
Bangkok	1.80	1.76	1.63	1.42	1.63	1.43	1.17	0.92
Sydney	1.73	1.77	1.72	1.58	1.41	1.15	0.90	0.69

Figure 3-4 Incident Solar Radiation on Solar Collector in One Year at Different Orientations and Tilt Angles for Tunis, Bangkok and Sydney

Unlike solar heating applications, cooling demand is generally high in summer when the solar radiation and the ambient temperature are high. The cooling demand in Figure 3-5 to Figure 3-7 is calculated using the building model described in Appendix B. The peak cooling load in the northern hemisphere above the Tropic of Cancer usually falls at the end of July or beginning of August, as shown in Figure 3-5, as the example for Tunis and Paris. Conversely, the peak cooling load in the southern hemisphere below the Tropic of Capricorn is usually in December and January, as shown in Figure 3-7. In tropic regions, cooling demands for air-

conditioning are generally high and unvaried all year, as shown in Figure 3-6.

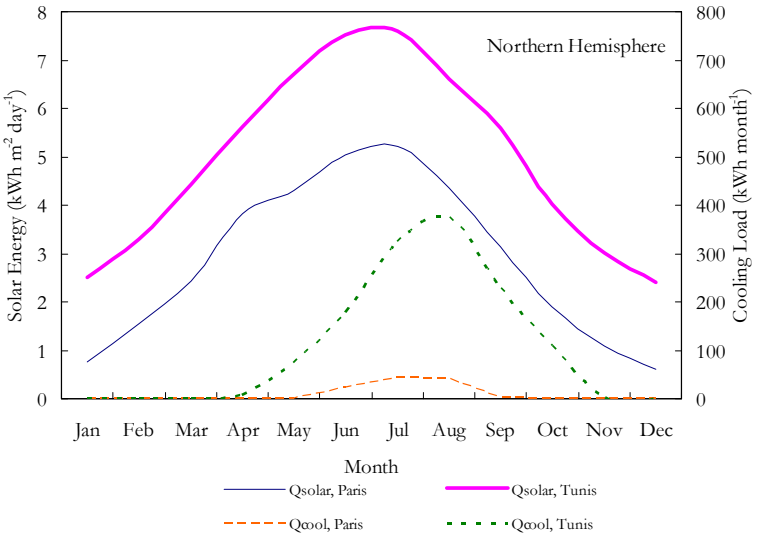

Figure 3-5 Solar Radiation and Cooling Load of Paris and Tunis, as an Example of Location in the Northern Hemisphere

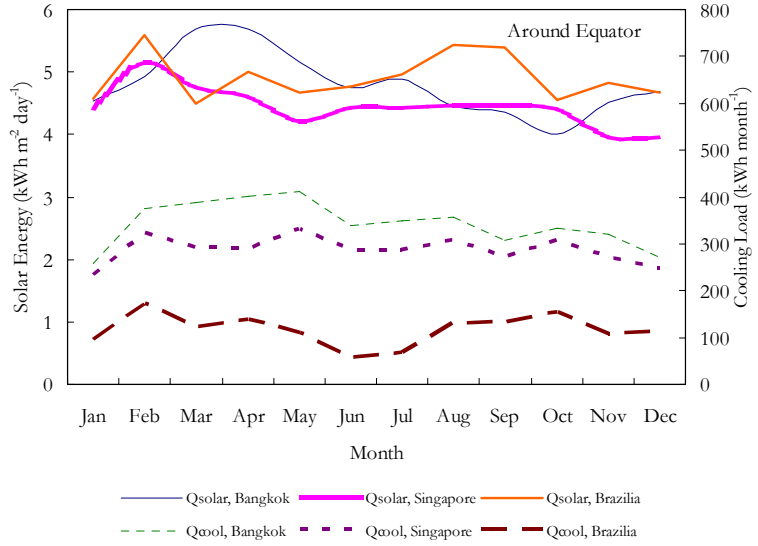

Figure 3-6 Solar Radiation and Cooling Load of Bangkok, Singapore and Brasilia, as an Example of Location in the Tropical Region

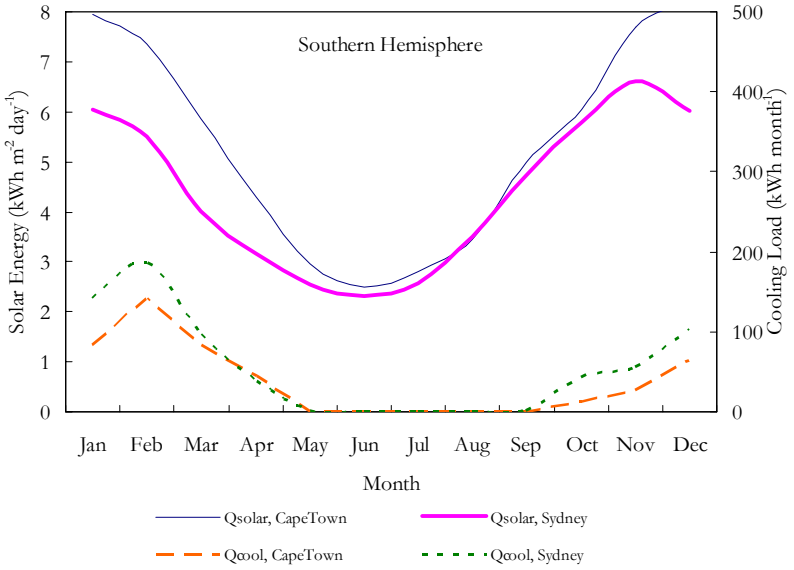

Figure 3-7 Solar Radiation and Cooling Load of Cape Town and Sydney, as an Example of a Location in the Southern Hemisphere

From the calculation using climatic data from Meteonorm 4.10 (Remund, Lang et al., 2001) for different tilt angles and locations, indicate that 15 degrees is the best angle yielding maximum incident radiation in one year in tropic regions and 30 degrees for locations above the Tropic of Cancer and below the Tropic of Capricorn. During the cooling season, the sun is however more perpendicular to the earth surface at this location, thus the best angle for obtaining radiation is quite low. Results show that the best angle for all locations is 15 degrees. In essence, the angle should however not be less than 30 degrees due to the aforementioned problems with dust and dirt. It can therefore be said that the best tilt angle for solar cooling purposes is 30 degrees. If the solar system is also designed for heating in winter, a suitable angle would most likely be different.

Table 3-1 Orientation and Suitable Tilt Angle of Solar Collectors for Solar Cooling Applications

Locations	Latitude	Angle at Maximum Incident Radiation in a Year	Angle at Maximum Incident Radiation During Cooling Season	Practical Angle for Solar Cooling
Stockholm	59° 21' N	45 S	30 S	30 S
Paris	48° 51' N	30 S	15 S	30 S
Beijing	39° 54' N	30 S	15 S	30 S
Tunis	36° 50' N	30 S	15 S	30 S
Los Angeles	34° 03' N	30 S	15 S	30 S
Delhi	28° 34' N	30 S	15 S	30 S
Bangkok	13° 44' N	15 S	15 S	30 S
Singapore	01° 17' N	15 S	15 S	30 S
Brasilia	15° 45' S	15 S	15 S	30 S
Cape Town	33° 55' S	30 S	15 S	30 S
Sydney	33° 52' S	30 S	15 S	30 S

3.2 Solar Cooling in Different Locations

If a small building of 150 m³ (building's details are described in Appendix B) is modelled for different locations, the cooling demand of the building would obviously depend on the local conditions. Results in the following figures are based on a simulation using TRNSYS 16 (Klein, Beckman et al., 2004b). The model of the building is described in Appendix B. Figure 3-8 to Figure 3-10 illustrate the result of cooling demand using the same building model at different locations, where the cooling system operates only during working hours of the weekday in one year. Demand is greater in the area near the equator and lower in an area further away from the equator; this is in line with the results in Figure 3-8. For example, the cooling load in Singapore (Latitude 0.5° N), Bangkok (Latitude 11.3° N) and Delhi (Latitude 25° N) is higher than that in Tunis, Los Angeles or Paris, which are situated on latitudes higher further up north.

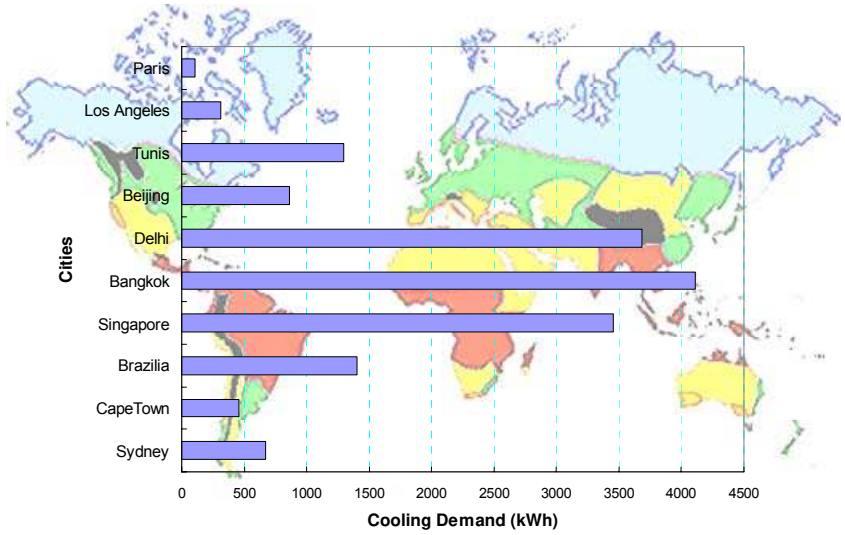

Figure 3-8 Cooling Demand for a 150 m³ Building at Different Locations

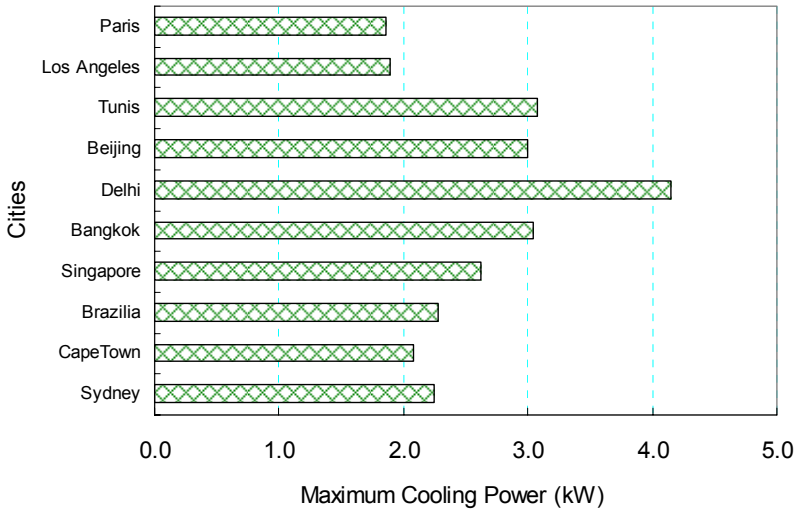

Figure 3-9 Maximum Cooling Power for a 150 m³ Building at Different Locations

The maximum cooling power needed is shown in Figure 3-9. Note that there are huge differences in energy needed and peak power.

Assuming that the building is cooled by a solar-driven absorption system with an unlimited capacity, the required evacuated tube solar collector area meeting the solar fraction of 95% is shown in Figure 3-10. The simulation is based on the baseline building with 150 m³ volume, roof facing north and south. A hot water storage tank of 2 m³ and a 5 kW electric auxiliary heater are installed. TRNSYS component TYPE 680, hot water 'fired' absorption chiller, is used for the absorption cooling unit.

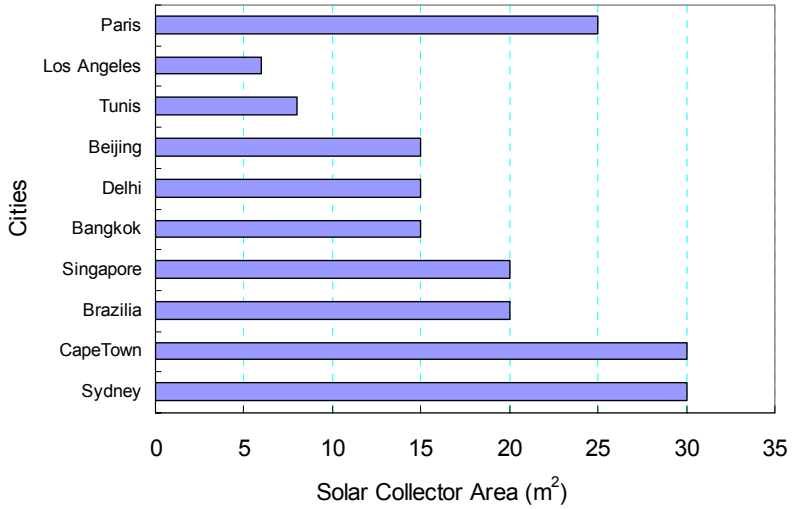

Figure 3-10 Required Solar Collector Area, Evacuated Tube, for Driven Absorption Cooling Machine in a 150 m³ Building with Total Solar Fraction of 95%.

In an area where cooling demand is high, the system works more efficiently and requires less solar collector area per cooling effect (in kW). The ambient temperature (heat sink) affects the condenser conditions, and the condenser temperature strongly influences the performance of the absorption chiller. In an area where the ambient temperature is not extremely high, the solar-driven cooling systems work more efficiently and dry condensers (air-liquid condenser) may be used. In very hot climates, liquid-liquid condensers or cooling towers are needed. The required area of solar collectors per 1 kW of cooling capacity is shown in Figure 3-11. In the tropical regions, the required solar collector area averages 7 m² per kW of cooling capacity. For Paris and Cape Town, the required solar collector is higher than for other selected cities in this simulation; this is primarily due to the fact that the total solar radiation in Paris in the summer is about 30% lower than the solar radiation in the cities which are located further south, e.g. Tunis. The required maximum cooling effect is however high, almost as high as for Los Angeles (see Figure 3-9). Therefore, a large solar collector area is required. In New Delhi, the maximum cooling effect and the cooling demand are high, but the solar radiation is also high all year round. Thus, the solar collector area per cooling load is lower. This suggests that this particular location is suitable for installation of a solar cooling system.

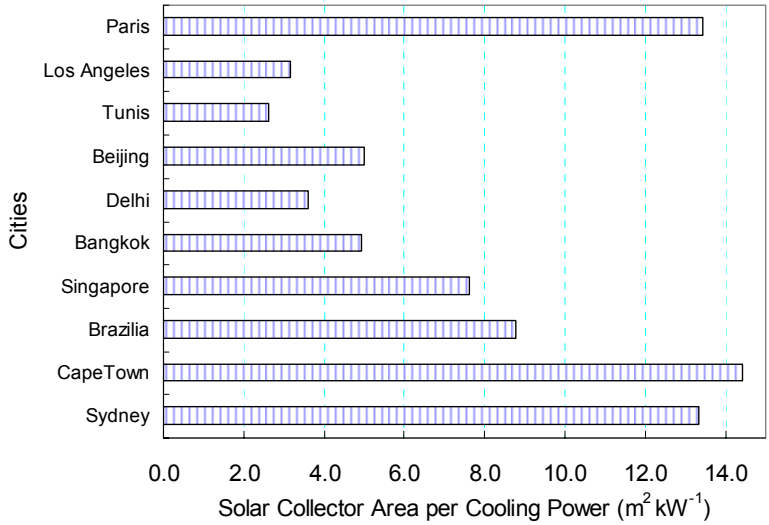

Figure 3-11 Required Solar Collector Area per 1 kW of Cooling Power in One Year, Evacuated Tube, for Driven Absorption Cooling Machine in the 150 m³ Building at at Different Locations and a Minimum Total Solar Fraction of 95%

3.3 Conclusions

Characteristics of the cooling demand are different at various locations. The performance of the whole system depends on both the cooling subsystem and solar converter efficiency. To provide cooling for one specific application, the right cooling cycle must be chosen in order to meet the desired cooling characteristics and temperature level. A suitable solar collector must also be selected in order to provide the right driving temperature for the chosen cycle. The dimension (size) of the solar collector strongly depends on the climate. An additional storage tank or auxiliary heater may be required to secure the cooling supply. The cooling demand in tropical regions is generally higher than in locations to the north or south, but the required peak capacity may not much differ. Furthermore, the cooling load does not vary considerably in tropical regions over the course of the year for tropical regions. Therefore, the price of a cooling supply per kilowatt hour of cooling energy is lower for these locations. In some cities, such as Paris, the cooling demand in summer is quite high; therefore a system with a high cooling power is required in order to fulfill the desired cooling demand. The cooling load, however, lasts for a relatively short period of time, e.g. a few months at the most. Assuming that only the cooling demand is taken into account, the system might not be economically competitive to conventional cooling systems. On the other hand, the solar collector subsystem can provide heating in winter thus promoting project economy considerably.

In this thesis, one specific technology will be further investigated, the solar-driven ejector refrigeration system. The next chapter will describe the models used for a system analysis of the solar-driven ejector refrigeration system.

PART II:
Theoretical Studies of the Solar-Driven Ejector Refrigeration system

This part consists of:

4 The Solar-Driven Ejector Refrigeration System

The models of the various parts of the solar-driven ejector refrigeration system, which are used for simulation in this thesis, are described in this chapter. The schematic of the system is shown in Figure 4-1. A solar thermal collector is used to supply heat to the generator as a major energy source for the ejector refrigeration subsystem, via a thermal storage and an auxiliary heater. An evaporator provides cooling to the conditioned space. In this case, the cooling load is assumed to be the already introduced small 150 m^3 office building. Details of each subsystem are described in the following section, starting with the model of the solar collector subsystem, followed by the ejector refrigeration subsystem, and the cooling load.

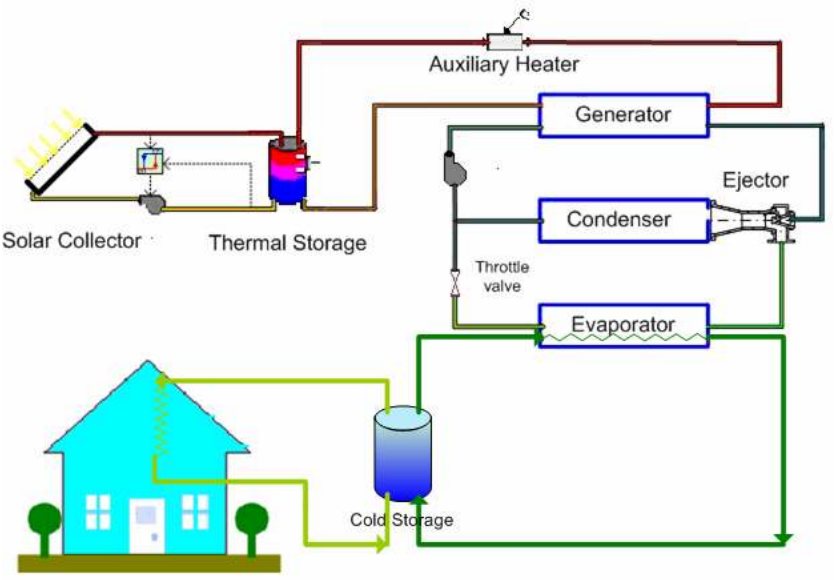

Figure 4-1 A Solar Driven Ejector Refrigeration System

In this study, TRNSYS and EES simulation tools are used to model and analyse the performance of a solar-driven ejector refrigeration system utilizing so-called co-solving. TRNSYS is a transient systems simulation program with a modular structure (Klein, Beckman et al., 2004b). It is widely used for the analysis of time dependent systems such as solar systems and HVAC systems. The whole system is modelled in the TRNSYS studio and it is divided into 3 main subsystems: solar collector subsystem, refrigeration subsystem and cooling load (building). The model of the ejector refrigeration subsystem is developed in Engineering Equations Solver, EES (Klein, 2004), since it is suitable for cycle calculations requiring good access to thermophysical properties of the working fluid.

4.1 The Solar Collector Subsystem

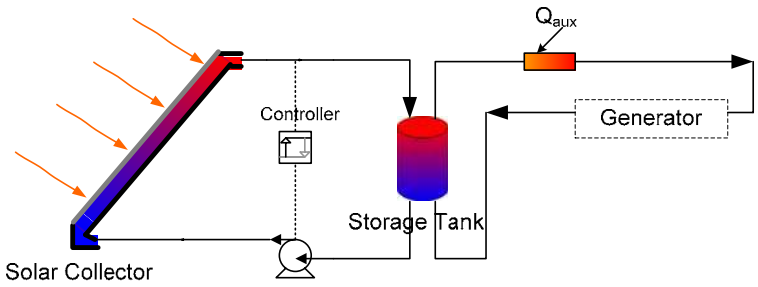

Figure 4-2 The Solar Collector Subsystem

This subsystem consists of the solar collector, a storage tank, a pump, a controller and an auxiliary heater. Solar radiation is converted to heat by the solar collectors. The storage tank is used as thermal storage when solar radiation is not sufficient. The auxiliary heater is placed between the storage tank and generator of the refrigeration subsystem. If the temperature of the liquid coming from the storage tank is lower than the lowest generator temperature set point, the auxiliary heater will start.

The useful heat gained by the solar collector, Q_u, is calculated from the heat balance in the solar collector by the Hottel-Whillier-Bliss equation (Duffie and Beckman, 1991) as shown in equation 4-1.

$$Q_u = \eta_{sc} Q_s = A_{sc} F_R \left[G(\tau\alpha)_e - U_L (T_i - T_a) \right] \qquad \textit{Eq. 4-1}$$

The solar collector efficiency is defined as the ratio of the useful heat gain over any time period to the incident solar radiation over the same period. The instantaneous energy efficiency of the solar collector can also be expressed in the form of the average Bliss coefficient ($F_R(\tau\alpha)_e$) and the heat loss coefficient (F_RU_L), as shown in equation 4-2.

$$\eta_{sc} = \frac{Q_u}{A_{sc}G} = F_R(\tau\alpha)_e - \frac{F_RU_L(T_i - T_a)}{G} \qquad \textit{Eq. 4-2}$$

Three types of solar collectors are selected in this study, a single-glazed flat plate, a double-glazed flat plate and an evacuated tube solar collector (ETC). The compound parabolic concentrating solar collector (CPC) is not considered in this thesis. This is due to high installation costs, and unnecessarily high temperature output from the CPC collector for the selected application. The assumed values of $F_R(\tau\alpha)_e$ and F_RU_L for each type of solar collector used in this simulation are shown in Table 4-1.

Table 4-1 The Value of $F_R(\tau\alpha)_e$ and F_RU_L for Each Type of Solar Collector Using in Chapter 6, 7 and 8

Solar Collector Type	$F_R(\tau\alpha)_e$	F_RU_L ($Wm^{-2}K^{-1}$)
Flat-plate, selective-surface, single-glass cover	0.80	5.00
Flat-plate, selective-surface, double-glass cover	0.80	3.50
Evacuated tubular collectors	0.80	1.5

4.2 The Ejector Refrigeration Cycle Subsystem

Different configurations and designs of solar driven ejector refrigeration systems have been previously discussed in Chapter 2, Section 2.3.8. More details of the models for this subsystem are mentioned in this section.

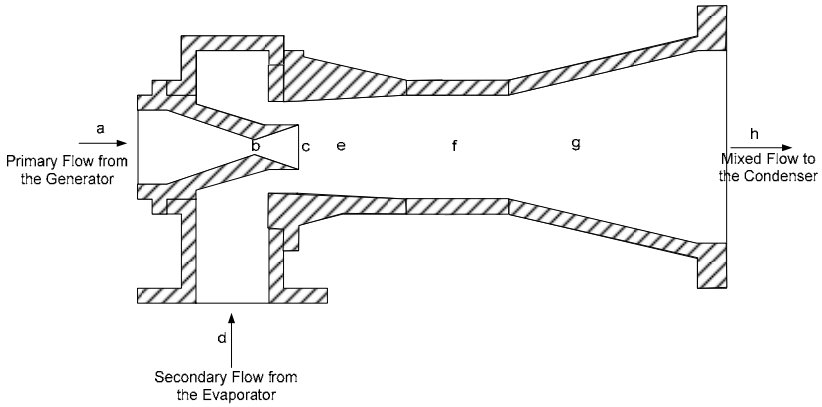

Figure 4-3 The Ejector in the Ejector Refrigeration Subsystem

In the ejector, the primary vapour stream from the generator (a, Figure 4-3) accelerates through the nozzle of the ejector (b, Figure 4-3), creating a low pressure at the nozzle exit (c, Figure 4-3). This pressure is lower than the pressure in the evaporator (d, Figure 4-3), thus the vapour is drawn from the evaporator. In a mixing zone (e, Figure 4-3), at the end of the converging section, the two streams are mixed. After mixing, the combined stream becomes a transient supersonic stream. A transverse shock occurs along the constant area (f, Figure 4-3) and the diffuser sections (g, Figure 4-3) to balance the pressure difference. After the shock, the velocity of the combined stream becomes subsonic and is further reduced in the diffuser. The vapour from the ejector then goes to the condenser (h, Figure 4-3). After the condenser, one part of the liquid working fluid is pumped to the generator and the rest goes to the evaporator, reaching the evaporation pressure by throttling in the expansion device.

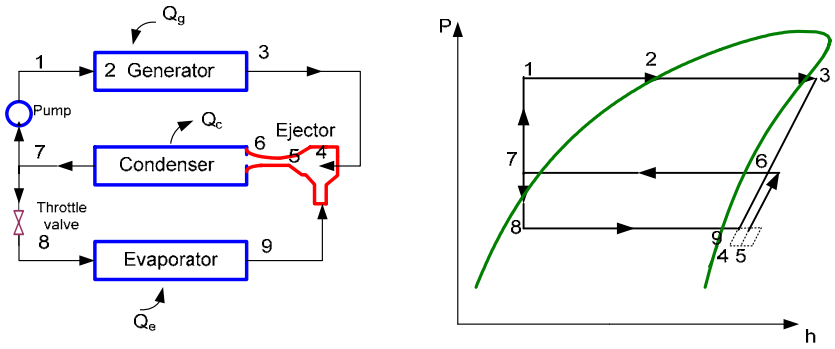

Figure 4-4 An Ejector Refrigeration Cycle

The processes of the ejector refrigeration subsystem are represented in a pressure-enthalpy diagram in Figure 4-4. The model of the ejector refrigeration subsystem is based on the thermodynamic states in each operating point according to Figure 4-4 and the following equations. In the following nomenclatures in this section (section 4.2), the numbers in the subscription refer to the condition according to Figure 4-4 and,

- subscription 'm' refers to the condition in the mixing chamber of the ejector,
- subscription 'g' refers to the condition in the generator
- subscription 'c' refers to the condition in the condenser
- subscription 'e' refers to the condition in the evaporator
- subscription 'is' refers to the isentropic condition.

The energy balance at the mixing point of the ejector can be written as:

$$(m_g + m_e) \cdot h_5 = m_e \cdot h_9 + m_g \cdot h_3 \qquad \textit{Eq. 4-3}$$

Mass conservation and the law of impulse at the mixing section of the ejector yields:

$$m_g \cdot c_g + m_e \cdot c_e = (m_g + m_e) \cdot c_m \qquad \textit{Eq. 4-4}$$

Assuming that the inlet area from the evaporator is large enough, the inlet velocity c_e can be set to zero thus simplifying equation 4-4 to:

$$\frac{m_e}{m_g} = \frac{c_g}{c_m} - 1 \qquad \textit{Eq. 4-5}$$

The nozzle's isentropic efficiency (η_N) is defined as,

$$\eta_N = \frac{h_3 - h_4}{h_3 - h_{4,is}} \qquad \textit{Eq. 4-6}$$

From the energy conservation equation, with the assumption of adiabatic conditions (q = 0), no work (ε_t =0), and no influence of elevation change ($z_B = z_A$), the velocity of the stream at the nozzle exit (c_g) can be expressed as,

$$c_g = \sqrt{2 \cdot (h_3 - h_4)} = \sqrt{2 \cdot \eta_N \cdot (h_3 - h_{4,is})} \qquad \textit{Eq. 4-7}$$

The diffuser isentropic efficiency (η_D) is defined as,

$$\eta_D = \frac{h_{6,is} - h_5}{h_6 - h_5} \qquad \textit{Eq. 4-8}$$

The pressure of the mixing stream rises along the diffuser, and the velocity of the mixing stream can be expressed as,

$$c_m = \sqrt{2 \cdot (h_6 - h_5)} = \sqrt{2 \cdot (1/\eta_D) \cdot (h_{6,is} - h_5)} \qquad \textit{Eq. 4-9}$$

4.2.1 Entrainment Ratio and Coefficient of Performance

The mass ratio or so called the entrainment ratio can be written as,

$$\omega = \frac{m_e}{m_g} = \sqrt{(\eta_N \cdot \eta_D) \cdot \left(\frac{h_3 - h_{4,is}}{h_{6,is} - h_5} \right)} - 1 \qquad \textit{Eq. 4-10}$$

The product of the isentropic efficiency of the nozzle (η_N) and the isentropic efficiency of the diffuser (η_D) may be referred to as the ejector isentropic efficiency (λ),

$$\lambda = \eta_N \cdot \eta_D \qquad \textit{Eq. 4-11}$$

Another important criterion for the ejector is the compression ratio, which is defined as the pressure ratio between the condenser and the evaporator.

$$r_p = \frac{p_c}{p_e} \qquad \textit{Eq. 4-12}$$

The back pressure or the condenser pressure at critical conditions is called as the critical condenser pressure. The ejector refrigeration system is generally operated at the critical condenser temperature. The compression ratio at the critical condition is called the critical compression ratio, r_p^*.

$$r_p^* = \frac{p_c^*}{p_e} \qquad \textit{Eq. 4-13}$$

This chapter does not focus on the details of ejector design and dimensioning. The analysis in this part of the thesis assumes that all losses along the ejector are included in the terms of isentropic efficiency of the nozzle and the diffuser as described above. Further details on ejector design and geometry can be found in Chapter 9.

The efficiency of the ejector cooling subsystem is generally expressed in terms of both the entrainment ratio, ω, and a coefficient of performance (COP_{ejc}). The COP of an ideal thermal refrigeration system can be written as the product of the Carnot heat engine efficiency and the ideal COP of the Carnot refrigeration cycle, as previously defined in Equation 2-4.

Neglecting the work input to the pump, the thermal COP of the ejector refrigeration system is defined as the ratio between cooling capacity and necessary heat input, as shown in Equation 4-10 and Equation 4-11.

$$COP_{ejc} = \frac{Q_e}{Q_g} \qquad \textit{Eq. 4-14}$$

$$COP_{ejc} = \frac{m_e(h_9 - h_8)}{m_g(h_3 - h_1)} \qquad \textit{Eq. 4-15}$$

4.3 The Cooling Load

The purpose of the building model is to illustrate the hourly variation of cooling load over a year. There are 2 thermal zones in the model: working space and attic. The cooling "produced" by the refrigeration submodel is coupled to the zones as an internal negative gain.

To maintain the stability of the cooling supply to the building, a cold storage tank is proposed. The cooling load subsystem includes a cold storage tank and building model. The cold storage tank provides cooling to the building; and the working media in the tank is cooled by the ejector subsystem.

The selected building is a small office building with a square footprint of 5 x 10 m and an internal volume of 150 m^3. More details of the building can be found in Appedix B. The cooling supply subsystem operates only during working hours on weekdays, from 9:00 to 18:00. The building model is a non-geometrical balance model with one air node per zone. The model is created in TRNBuild, the visual building interface of TRNSYS16 (Klein, Beckman et al., 2004b). The TRNBuild model is then executed and generates the input files for TRNSYS component type 56 (multi-zone building). Heat gain into the building comes from both convective heat flow to the air node and radiative heat flow to the walls and windows. Convective and radiative heat balances around the building are shown in Equations 4-12 and 4-13.

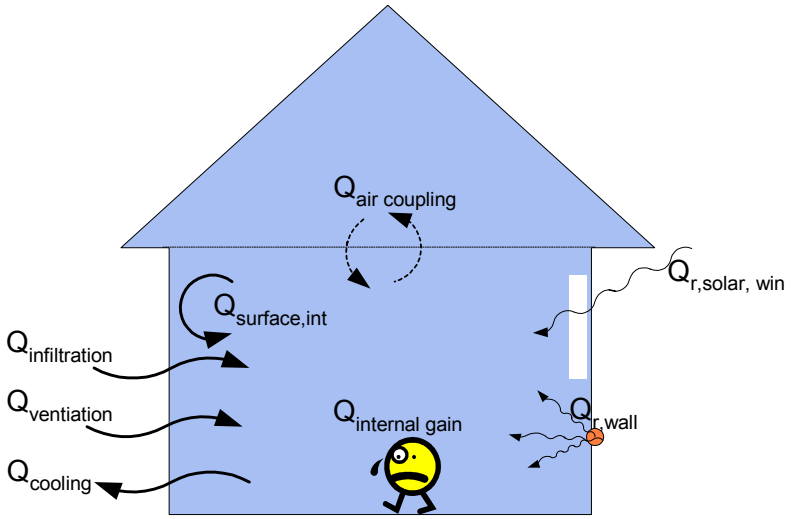

Figure 4-5 Heat Balance on the Cooling Zone

Convective heat flow to the zone air node:

$$Q_{conv,i} = Q_{surface,i} + Q_{\inf iltration,i} + Q_{ventilation,i} + Q_{\int ernal\_gain,i} + Q_{air\_coupling,i}$$

Eq. 4-16

Radiative heat flow to the walls and windows:

$$Q_{r,w_i} = Q_{r,wall,\int} + Q_{r,sol,wall} + Q_{r,long,wall} \qquad \textit{Eq. 4-17}$$

The walls are modelled according to the transfer function relationship of Mitalas and Arseneault (Klein, Beckman et al., 2004a), in which the wall is considered a black box. The wall in this case is considered to be a heavy wall with a high thermal mass. More details about this thermal zone can be found in the TRNSYS16 manual, component type 56 (Klein, Beckman et al., 2004a).

4.4 System Performance

Energy performance of the system is expressed as the system thermal ratio (STR), and the solar fraction as shown in section 2.2.4, Equation 2-21 and Equation 2-22 respectively.

4.5 Climatic Data

Climatic data used in this thesis comes from Meteonorm 4.10 Software (Remund, Lang et al., 2001). Climate data from various locations was selected and generated hourly in the Typical Meteological Year 2 (TMY2) format. TMY2 is an hourly metrological data set for a 1-year period. It is widely used in computer simulations of solar energy conversion and building systems. Data provided in the TMY2 format consists of local standard time (year, month, day, hour), solar radiation (global, direct, diffuse, extraterrestrial), zenith luminance, sky cover factor (total, opaque), temperature, humidity, atmospheric pressure, wind speed, wind direction, visibility and precipitation. More details about the TMY2 format can be found in the User's Manual for TMY2s (Marion and Urban, 1995).

4.6 Conclusions

In this thesis, the solar driven ejector refrigeration system is analysed in five different ways: a steady-state analysis, a specific working fluid analysis, an exergy analysis, the full year dynamic analysis and, finally, the detailed ejector design and analysis. Different models are thus required in order to perform these analyses. Four different sub-models used in this thesis:

Model 1: the solar collector subsystem (section 4.1 – three different collector types, flat plate single glazed, flat plate double glazed and evacuated tube)

Model 2: an ejector model with constant isentropic efficiency (section 4.2)

Model 3: a cooling load (section 4.3, Appendix B)

Model 4: an ejector design model with one fixed dimension (will be explained in Chapter 9)

The solar collector subsystem (model 1) provides thermal energy to the refrigeration subsystem. In the steady-state analysis and the exergy analyis, model 1 is used without the thermal storage tank. The storage tank is included in the dynamic analysis (Chapter 8).

The second model (model 2) is the model of the ejector refrigeration cycle with constant isentropic efficiency. This model is relatively straightforward and good enough to show the thermodynamic characteristics of the cycle provided that reliable thermophysical data is available for the various working fluids. This model is developed in EES and used for exergy analysis and analysis of the working fluid. The cooling load is assumed to be constant in the steady-state analysis, the working fluid analysis and exergy analysis.

In reality, the cooling load is not constant; it changes with atmospheric and ambient conditions. Therefore, in the dynamic analysis, the cooling load model (model 3) must be taken into consideration.

An ejector system with one fixed dimension ejector does not operate at constant istentropic efficiency over a wide variety of operating conditons. The performance of the ejector strongly depends on back pressure (in this case, back pressure is the condenser pressure). Therefore, a more detailed analysis of the ejector is necessary, and is provided in model 4. This detailed model of the ejector, including some preliminary test results for one fixed dimension ejector is described in Chapter 9.

The analyses performed by use of different models summarized in Table 4-2.

Table 4-2 Models Used in Different Analyses

Analysis	Chapter	Model 1	Model 2	Model 3	Model 4
Steady State Analysis	6	☼	☼		
Working Fluid Analysis	5	☼	☼		
Exergy Analysis	7	☼	☼		
Dynamic Analysis	8	☼		☼	☼
Ejector Design	9				☼

The choice of the appropriate working fluid (refrigerant) is one of the most important parts in the design of the ejector refrigeration system. The appropriate refrigerant should yield good performance in the selected operating ranges. There are, however, issues other than thermodynamic performance to consider, such as safety and environmental impact. In this thesis, the analysis of the solar-driven ejector refrigeration system therefore starts with the working fluid selection, followed by the steady state analysis and exergy analysis. The steady-state analysis is performed in Chapter 6, in order to determine the effects of the operating conditions. Optimum operating conditions and loss analysis are performed in Chapter 7, by the exergy analysis. The dynamic analysis is performed in Chapter 8. This analysis is necessary for the practical design and dimensioning of the system. Finally, a detailed analysis of the ejector is described in Chapter 9.

5 Working Fluid Selection

As previously mentioned in Chapter 4, working fluid is an essential part in the ejector refrigeration cycle. Different refrigerants have distinct characteristics and perform differently. Appropriate refrigerants can provide good system performance in selected operating conditions. In this chapter, the criteria for working fluid selection for the ejector refrigeration cycle are provided. The performances of the ejector refrigeration cycle using several refrigerants are compared for different operating conditions.

Various kinds of refrigerants can be used with this system. The most common way of classifying the refrigerant is by the chemical compounds in the refrigerant molecules. They can be classified into 4 main groups:

1. Halocarbon Group, e.g. R11, R113, R114, R134a, R245ca, R245fa and R152a

2. Hydrocarbon Group, e.g. methane (R50), ethane (R170), propane (R290), cyclopropane (RC270), butane (R600), isobutane (R600a), and ethyleneglycol

3. The Compound Refrigerants, e.g. R407A, R407B, and R410A

4. Other Refrigerants, e.g. water (R718) and ammonia (R717)

The following criteria should always be taken into consideration when choosing a working fluid.

- *Environmental Effect:* Ozone Depletion Potential (ODP), Global Warming Potential (GWP)

Several refrigerants suggested in the literature yielding high performance, are not environmentally friendly. Some have a high ODP (an impact on the stratospheric ozone layer compared to R11) or a high GWP (a factor indicating the relative effect on global warming compared to CO_2)

Many working fluids suggested in the literature for ejector refrigeration systems are now, in fact, forbidden due to their environmental effect, such as R11, R113, or R114. New refrigerants are now studied, for example, R123, R134a, R152a and ammonia. R123 is, however, a HCFC working fluid, thus forbidden on many markets. R134a is a relatively strong climate gas and R152a is a weak flammable working fluid with low GWP.

- *Safety:* toxicity, flammability

Toxicity can be identified by some numbers such as TLV (Threshold Limit Value). Flammability is generally identified by the lower flammability limit (LFL). The ASHRAE standard 34 classifies refrigerants into 2 classes of toxicity (A=no toxicity identified and B=evidence of toxicity), and three groups of flammability characteristics (1= no flame propagation in the air at 10°C and 101 kPa, 2= LFL more than 0.10 and 3=LFL less than or equal to 0.10).

- *Economics and availability:* price and availability

The refrigerant should be cheap and available on the market. Various possible fluids for the ejector refrigeration cycles are shown in Table 5-1 and Figure 5-8. Property charts were created by the author using data from the database in the Engineering Equation Solver program, EES (Klein, 2004), the Thermodynamic and Transport Properties of Refrigerants and Refrigerant Mixtures, REFPROP (Lemmon, McLinden et al., 2002).

5.1 Working Fluids for Ejector Cycles in the Literature

Huang, Chang et al., 1998, developed a solar ejector cooling system using R141b as the refrigerant; the overall COP obtained is around 0.22 at a generating temperature of 95°C, an evaporating temperature of 8°C and solar radiation at 700 W m^{-2} . Several simulation models are found in literature, such as Dorantès, Estrada et al., 1996, and Sokolov and Hershgal, 1993. Halocarbon refrigerants such as R142b (Dorantès, Estrada et al., 1996; Huang, Chang et al., 1998), R114 (Sokolov and Hershgal, 1993) or R113 (Al-Khalidy, 1997b), were recommended due to high performance. Cizungu (Cizungu, Mani et al., 2001) studied the performance of vapour jet refrigeration systems with several working fluids such as R123, R134a, R152a and ammonia. He concluded that the COP and entrainment ratio

of the system depended primarily on the ejector geometry and compression ratio. Sun, 1999, studied eleven different refrigerants including water, halocarbon compounds, a cyclic organic compound and an azeotrope. His results show that the system using R152a has better performance. Some environmentally benign refrigerants for solar-driven ejector refrigeration systems were introduced in the literature of Pridasawas and Lundqvist, 2002, including a comparison of the technical feasibility and performance of each refrigerant. Among natural refrigerants, normal butane is an interesting working fluid. Small vapour volume after expansion through the ejector signifies that a system using butane does not require large ejector dimensions. Iso-butane, the isomeric structure of butane produced similar results. The cost of butane is, however, higher than that of iso-butane. Despite their high flammability characteristic, hydrocarbons should therefore be considered as competitors to chlorinated refrigerants.

Halocarbon compounds are, or have been, widely used as refrigerants in ejector cycles such as R12, R13, R113, R114, R134a R141b, R142b or R152a. R113 is a low-pressure refrigerant having high molecular weight; producing a high mass ratio, good ejector efficiency and high compressibility factor which is relatively close to an ideal gas (Al-Khalidy, 1997b). R141b was used in the solar-ejector cooling system by Huang et al., 1998. For a +8°C evaporating temperature a COP of around 0.22 is reported at an insolation of 700 Wm^{-2}. R142b and R11 are also used in solar applications as described by Dorantès, Estrada et al., 1996, and Chen and Hus, 1987.

Hydrofluoroether (HFE) was considered for use by Wolpert, Riffat et al., 2003, for a solar-powered ejector air-conditioning system at a cosmetic factory in Mazunte, Mexico. The 13 kW cooling power was designed with an estimated COP of 0.62.

Rusly, Charters et al., 2002 combined ejector and vapour compression refrigeration systems. Refrigerant R152a was suggested to yield a good performance compared to other refrigerants such as ammonia, R245ca, R245fa and R500. R245fa was chosen by Rusly, Charters et al., 2002 to be used in the ejector cycle of a combined ejector-vapour compression refrigeration system.

Hydrocarbons are appealing refrigerants for small refrigeration systems. These refrigerants, though natural products, are however, explosive and flammable. They are nevertheless environmentally friendly, with zero ozone depletion potential and low GWP. R600 or N-butane is an interesting refrigerant. Small vapour volume after expansion implies that a large ejector size is not required. Calculations in the following section of this

chapter indicate that the COPs of the systems vary from 0.09 to 0.34 for generating temperatures between 70°C and 152°C. R600a or iso-butane yields a somewhat lower COP than R600, but other properties are almost identical.

Compound refrigerants, mixtures, such as R407A (20%R32 + 40%R125 + 40%R134a) or R410A (50%R32 + 50%R125)) can also be used.

Ammonia has been used as a refrigerant for many years, and is still an interesting alternative, yielding good performance in many applications. It is an environmentally friendly fluid (no ODP and GWP) but quite toxic (TLV is 25 ppm). However, it has a strong smell that can be easily detected when released into the environment. The pressure-enthalpy characteristic curve of ammonia indicates that it requires more superheating than other refrigerants due to a negative slope of the saturated vapour line, thus condensation may occur inside the ejector causing failure in operation. Higher generating temperatures also require a high superheating temperature. Rogdakis and Alexis, 2000, simulated the performance of a single-stage ammonia ejector refrigeration system at a constant superheated temperature (100°C); the maximum COP obtained was between 0.042 and 0.446.

Methanol as a working fluid was suggested in the paper by Wolpert and Riffat, 1999. They designed and installed a 5 kW solar-driven ejector air conditioning system in Mexico. Preliminary tests indicated that it would be possible to operate at the evaporating temperature of 11°C. Performance of the system was not mentioned in the reference (Wolpert and Riffat, 1999).

Water has been widely used and studied. Large capacity commercial systems driven by low pressure steam have been installed and operated since since 1945 by the Ingersoll-Rand Company (Ingersoll-Rand, 1945) , for example for 20 to 1 200 tons of refrigeration effect and evaporationtemperatures could be as low as 1.67°C (35°F). Later, many research groups such as Eames, Aphornratana et al., 1995, Chen and Sun, 1997, Grazzini and Mariani, 1998, and Chang and Chen, 2000, have studied this refrigerant for various applications. A 200 kW cooling capacity steam jet driven ejector cooling plant was installed in 1998 in Denmark in 1998 for district cooling purposes (Sør and Lund, 1999).

A drawback already mentioned for water when used as refrigerant is the high specific vapour volume; indicating a very high volumetric flow rate and consequently demand of a large size of ejector. For example, for one

ton of refrigeration effect (~3.52 kW) at an evaporating temperature of +8°C, 665 m^3h^{-1} of volumetric flow rate is needed when using water as a refrigerant, compared to R12, which requires only 7 m^3/h (Al-Khalidy, 1997b). Another obvious drawback is that evaporation temperatures below 0°C cannot be reached, due to the freezing point. Figure 5-14 clearly illustrates the difference in volumetric flow rate per kilowatt of the refrigeration load between water and other refrigerants. The volumetric flow rate per kilowatt of cooling capacity is generally higher than other refrigerants by more than 150 times.

Vapour volume after expansion dictates the size of the ejector, the higher the vapour volume, the larger the ejector size. Viscosity should be low in order to reduce friction loss along the pipe. The critical temperature and pressure of the working fluid influences the design philosophy. At a low generating temperature, pump work decreases when the generating pressure rises relative to the critical pressure; however it does not significantly increase at a high generating temperature. Supercritical operating conditions are not considered in this thesis.

5.2 The Characteristic of the Saturated Vapour Line in T-S Diagram

A particularly important characteristic for ejector systems is the shape of the saturated vapour line in a T-S diagram. The first derivative of temperature with respect to entropy should be positive in order to avoid condensation during expansion in the ejector and minimize the degree of superheat necessary in the generator.

The shape of the saturated vapour line in a T-S diagram can thus be used to classify working fluids alternatively into 3 main groups: "dry working fluids, isentropic fluids, and wet fluids". Characteristic curves of each group are shown in Figure 5-1, Figure 5-2 and Figure 5-3 respectively. The saturation vapour line of the dry fluid type has a positive slope in the T-S diagram. For wet fluids it is the opposite, the saturation vapour line has a negative slope. For the isentropic fluids, the saturation vapour line is vertical in the T-S diagram.

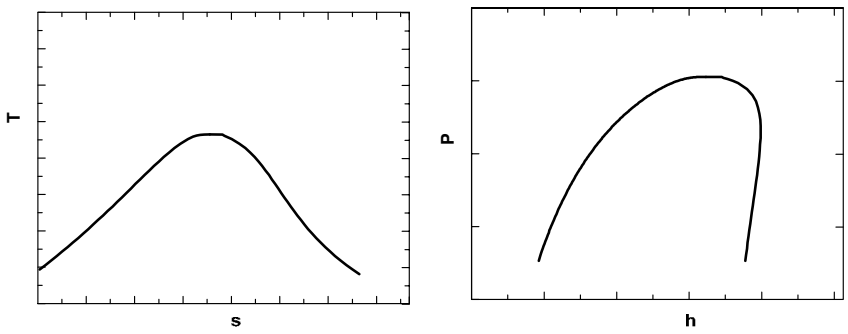

Figure 5-1 Thermodynamic Diagrams of the "Wet Fluid"

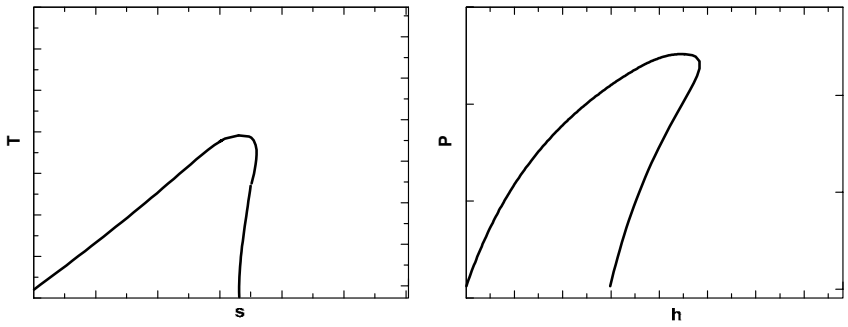

Figure 5-2 Thermodynamic Diagrams of the "Isentropic Fluid"

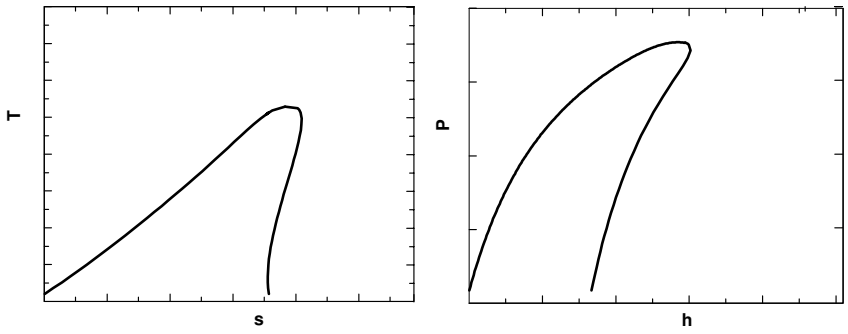

Figure 5-3 Thermodynamic Diagrams of the "Dry Fluid"

Ammonia, water, methanol, R22 and R142b are examples of "wet working fluids". R114 is an example of an isentropic working fluid. R113 and iso-butane are examples of dry working fluids. Examples in the P-H diagrams of some working fluids e.g. iso-butane, ammonia and R134a are shown in Figure 5-4 to Figure 5-6.

If the slope is negative (i.e. ammonia); superheat in the generator should be high enough to avoid condensation and droplet formation in the ejector, which may otherwise lead to poor operation.

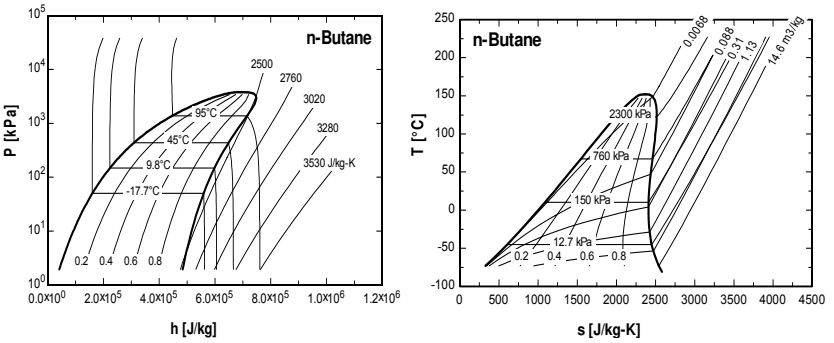

Figure 5-4 Pressure-Enthalpy Diagram of N-Butane[‡‡]

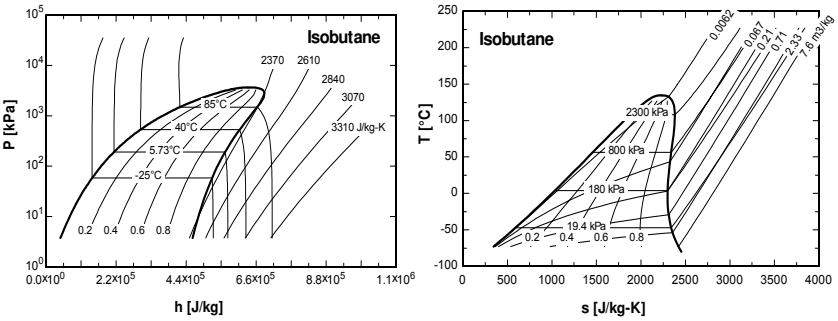

Figure 5-5 Pressure-Enthalpy Diagram of Iso-Butane[§§]

‡‡ The diagrams are generated using Engineering Equation Solver (EES) Software. Details of the equations of state of the refrigerant can be found in the program's manual (Klein, 2004).

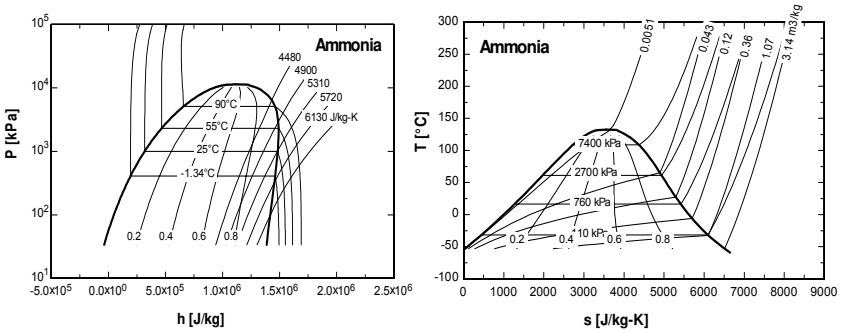

Figure 5-6 Pressure-Enthalpy Diagram of Ammonia[#]

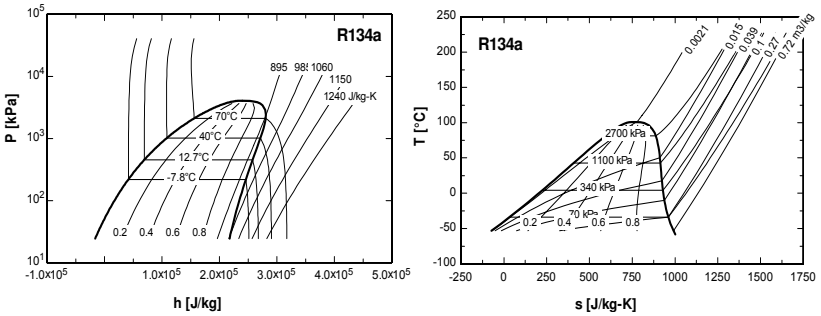

Figure 5-7 Pressure-Enthalpy Diagram of R134a[#]

A high refrigerating effect per kilogram of evaporated refrigerant is also preferred. The product of latent heat of vaporisation and vapour density can estimate the capacity of the system. A high pressure system yields high capacity since vapour density is high; however, critical pressure compared to the pressure in the system will be low, thus leading to a low COP.

---

§§ The diagrams are generated using the Engineering Equation Solver (EES) Software. Details on the equations of state of the refrigerants can be found in the program's manual (Klein, 2004).

Table 5-1 Characteristics of Various Candidate Refrigerants for the Ejector Refrigeration Cycle

No	Fluid Name	R-no.	Formula	M.W. (kg/kmol)	n.B.P. (°C)	C.P. (bar)	C. T. (°C)	Flamm-ability?	GWP rel. CO_2	ODP rel. R11	first use as wf	atm life year	r *** (kJ/kg)	n.B.P./C.T.	ASHRAE class.
1	1-(difluoromethoxy)-1,1,1-trifluoroethane	R-E245	$CF_3CH_2OCHF_2$	150.0	29.2	34.2	170.9	?	640	0	-	6.5	171.28	0.68	-
2	1.1-dichloro-1-fluoroethane	R141b	CH_3CCl_2F	117.0	32.0	42.1	204.2	No	630	0.1	1990	9.4	221.69	0.64	A2
3	2,2-dichloro-1,1,1-trifluoroethane	R123	CHCl2CF3	152.89	27.6	36.68	183.7	No	93	0.02			167.20	0.66	B1
4	1-(methoxy)-1,1,2,2,3,3,3-heptafluoropropane	R-E347 mcc1	$CH_3OCF_2CF_2CF_3$	200.1	34.2	24.8	164.6	No	485	0	-	6.4	130.59	0.70	-
5	1,1,1-trifluoroethane	R143a	CH_3CF_3	84.0	-47.2	37.8	72.9	Yes	5400	0		53.5	228.53	0.65	A2
6	1,1,2-trichloro-1,2,2-trifluoroethane	R113	$CFCl_2$-$CClF_2$	187.4	47.7	34.6	214.4	No	4800	0.9	1933	85	145.52	0.66	A1
7	1,2-dichloro-1,1,2,2-tetrafluoroethane	R114	CF_2ClCF_2Cl	170.9	3.7	32.5	145.7	No	9200	0.85	1934	300	137.66	0.66	A1
8	2-(methoxy)-1,1,1,2,3,3,3-heptafluoropropane	R-E347	$CH_3OCF_2CF_2CF_3$	200.1	29.4	25.5	160.2	No	368	0	-	4.9	128.55	0.70	-

Remark: ***) heat of vaporisation, estimated with Troutons "rule"

**) Many R-no are based on the ASHRAE designation number system but they are not official

Table 5-1 (Cont.): Characteristics of Various Candidate Refrigerants for the Ejector Refrigeration Cycle

No	Fluid Name	R-no.	Formula	M.W. (kg/kmol)	n.B.P. (°C)	C.P. (bar)	C. T. (°C)	Flamm-ability?	GWP rel. CO_2	ODP rel. R11	first use as wf	atm life year	r *** (kJ/kg)	n.B.P./C.T.	ASHRAE class.
9	Ammonia	R717	NH_3	17.0	-33.3	132.3	113.3		<1	0	-	?	1197.14	0.62	B2
10	Butane	R600	C_4H_{10}	58.1	-0.5	37.9	152.0	Yes	0	0	?	-	398.69	0.64	A3
11	Cyclobutane	RC390	$(-CH_2-)_4$	56.1	12.0	x	x	Yes	low	0	-	?	431.99	x	-
12	Dodecafluorocyclohexane	-	C_6F_{12}	300.1	52.2	x	x	No(?)	x	x	-	-	92.18	x	-
13	Cyclopentane	HC-C41-10	$(-CH_2-)_5$	70.1	49.4	45.1	238.6	Yes	11	0	-	"few days"	390.94	0.63	-
14	Decafluorobutane	R-31-10	$CF_3CF_2CF_2CF_3$	238.0	4.0	x	x	No	7000	0	1995	2600	98.97	x	-
15	Decafluorocyclopentan	-	C_5F_{10}	250.0	22.2	x	x	No	x	x	-	-	100.39	x	-
16	Difluoromethoxy-difluoromethane	R-E134	CHF_2OCHF_2	118.0	6.2	42.3	147.0	No	6900	0	-	23-24	201.15	0.66	-

Remark: ***) heat of vaporisation, estimated with Troutons "rule"

**) Many R-no are based on the ASHRAE designation number system but they are not official

Table 5-1 (Cont.): Characteristics of Various Candidate Refrigerants for the Ejector Refrigeration Cycle

No	Fluid Name	R-no.	Formula	M.W. (kg/kmol)	n.B.P. (°C)	C.P. (bar)	C. T. (°C)	Flamm-ability?	GWP rel. CO_2	ODP rel. R11	first use as wf	atm life year	r *** (kJ/kg)	n.B.P./C.T.	ASHRAE class.
17	Difluoroethane	R152a	CHF_2CH_3	66.0	-25.0	44.92	113.5	No	140	0	-		319.59		A2
18	Dodecafluoropentane	R-41-12	$CF_3CF_2CF_2CF_2CF_3$	288.0	57.7	x	x	No	7500	0	1995	4100	97.63	x	?
19	Heptafluorobutane	R347scc	$CH_3CF_2CF_2CF_3$	184.1	15.1	25.7	144.2	No(?)	?	0	-	?	133.12	0.69	-
20	Heptafluoropentane	R227ea	CF_3CHFCF_3	170.0	-17.5	29.5	102.0	No	2900	0	Jan-96	36.5	127.81	0.68	app pend.
21	Hexafluoropropane	R236ea	$CF_3CHFCHF_2$	152.0	6.5	35.3	139.3	No	1000	0	-	8.1	156.34	0.68	-
22	Hexafluoropropane	R236fa	$CF_3CH_2CF_3$	152.0	-1.4	32.0	124.0	No	6300	0	oct 1996	209	151.91	0.68	app pend.
23	Tetrafluoroethane-1,1,1,2	R134a	CH_2FCF_3	102.0	-26.1	40.7	101.1	Yes	1600	<0.0005	1990	13.6	205.88	0.66	A1
24	Isobutane	R600a	C_4H_{10}	58.1	-11.6	36.4	134.7	Yes	0	20	-	-	382.50	0.64	A3

Remark: ***) heat of vaporisation, estimated with Troutons "rule"

**) Many R-no are based on the ASHRAE designation number system but they are not official

Table 5-1 (Cont.): Characteristics of Various Candidate Refrigerants for the Ejector Refrigeration Cycle

No	Fluid Name	R-no.	Formula	M.W. (kg/kmol)	n.B.P. (°C)	C.P. (bar)	C. T. (°C)	Flamm-ability?	GWP rel. CO_2	ODP rel. R11	first use as wf	atm life year	r *** (kJ/kg)	n.B.P./C.T.	ASHRAE class.
25	Nonafluorobutane	R329pcc	$CHF_2CF_2CF_2CF_3$	220.0	15.1	23.9	140.2	No(?)	?	0	-	?	111.35	0.70	-
26	Octaflourocyklobutane	RC318*	C_4F_8	200.0	-7.0	27.78	115.0	No	8700	0	1961	3200	113.10	0.69	A1*
27	Octafluorobutane	R338mee	$CF_3CHFCHFCF_3$	202.0	25.4	24.8	148.5	No(?)	?	0	-	?	125.60	0.71	-
28	Octafluorobutane	R338qcc	$CH_2FCF_2CF_2CF_3$	202.0	27.8	25.5	160.5	No(?)	?	0	-	?	126.61	0.69	-
29	Octafluorobutane	R338pcc	$CF_2CHF_2CHF_2CF_2$	202.0	42.5	28.3	186.4	No(?)	?	0	-	?	132.79	0.69	-
30	Pentafluorobutane	R365scf	$CH_3CF_2CH_2CF_3$	148.1	40.0	x	x	Yes	<1200	0	-	7.5	179.76	x	-
31	Pentafluoropropane	R245ca	$CHF_2CF_2CH_2F$	134.0	25.2	39.25	174.0	No	720	0	-	6.6	189.21	0.67	-
32	Pentafluoropropane	R245fa	$CHF_2CF_2CF_3$	134.0	14.9	36.4	154.1	No	820	0	-	7.6	182.66	0.67	

Remark: *) RC318 have been suggested for removal from class A1

***) heat of vaporisation, estimated with Troutons "rule"

**) Many R-no are based on the ASHRAE designation number system but they are not official

Table 5-1 (Cont.): Characteristics of Various Candidate Refrigerants for the Ejector Refrigeration Cycle

No	Fluid Name	R-no.	Formula	M.W. (kg/kmol)	n.B.P. (°C)	C.P. (bar)	C. T. (°C)	Flamm-ability?	GWP rel. CO_2	ODP rel. R11	first use as wf	atm life year	r *** (kJ/kg)	n.B.P./C.T.	ASHRAE class.
33	Pentane	R601, N-C5	C_5H_{12}	72.2	36.2	33.59	196.4	Yes	12	0	-	"few days"	364.45	0.66	-
34	Iso-Pentane	R601a, I-C5	C_5H_{12}	72.2	27.8	33.7	187.0	Yes	-	0	-	?	354.60	0.65	-
35	Tetradecafluorohexane	R-51-14	C_6F_{14}	338.0	57.1	x	x	No	7400	0	1995	3200	83.04	x	?
36	Tetrafluoropropane	R254cb	$CH_3CF_2CHF_2$	116.1	-0.8	37.5	146.2	No	?	0	-	1.6	199.47	0.65	-
37	Trifluoroethanol	RE143	$C_2H_3F_3O$	100.0	-23.8	35.9	104.9	?	x	0	1989	4.1-5.1	x	x	-
38	Tricloroflouormethane	R11	$CFCl_3$	137.4	23.8	44.7	198.1	No	3800	1	1932	50	183.72	0.63	A1
39	Water	R718	H_2O	18.0	100.0	221.0	374.2	No	-	0	-		2257.10	0.58	A1
40		R-E227ca2	$CHF_2CF_2OCF_3$	186.0	-3.1	22.9	114.6	No(?)	?	0	-	?	123.39	0.70	-

Remark: ***) heat of vaporisation, estimated with Troutons "rule"

**) Many R-no are based on the ASHRAE designation number system but they are not official

Table 5-1 (Cont.): Characteristics of Various Candidate Refrigerants for the Ejector Refrigeration Cycle

No	Fluid Name	R-no.	Formula	M.W. (kg/kmol)	n.B.P. (°C)	C.P. (bar)	C. T. (°C)	Flamm-ability?	GWP rel. CO_2	ODP rel. R11	first use as wf	atm life year	r *** (kJ/kg)	n.B.P./C.T.	ASHRAE class.
41	(Zeotrope mixture)	R407a	20% R32+40% R125 + 40%R134a	90.1	-45.2	44.9	81.9	No	2340	2E-05	1993		215.02	0.64	A1
42	(Azeotrope mixture)	R500	73.8% R12+26.2% R152a	99.3	-33.6	41.7	102.1	No	7870	0.605	1950		205.01	0.64	A1

Remark: ***) heat of vaporisation, estimated with Troutons "rule"

**) Many R-no are based on the ASHRAE designation number system but they are not official

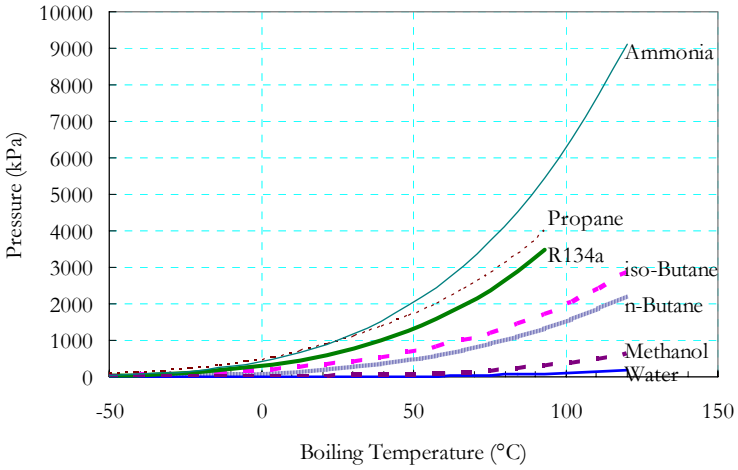

Figure 5-8 Pressure-Temperature Diagram of Some Interesting Working Fluids (Plot Based on Data of the Refrigerant Properties Provided by EES (Klein, 2004))

5.3 Characteristic of Different Working Fluids in the Ejector Refrigeration Cycle

Results in the following figures are based on the model of the ejector refrigeration cycle, previously described in Chapter 4, section 4.2 (model 2). Several refrigerants e.g. butane, iso-butane, ammonia, propane, methanol, water, R134a, R113, R114 and R141b are used in the calculation. If the operating conditions are not stated under the figure, the calculations assume a constant isentropic efficiency of the ejector, +10°C evaporation temperature, 35°C condensing temperature and +120°C of the temperature from the generator entering the ejector.

The stream from the generator entering the nozzle part of the ejector is assumed to be superheated, so that the expansion takes place in the super-saturated region. Therefore, the degrees of superheat for each selected refrigerants are different due to the differences in the saturated vapour line in the T-S diagram. The degrees of superheat for each refrigerant are shown in Table 5-2.

Table 5-2 Degrees of Superheat for Each Selected RefrigerantUsed in Calculations in this Chapter

Refrigerants	Degree of Superheat (K)
Butane (R600)	5
Iso-Butane (R600a)	5
R113	5
R114	5
R141b	5
R134a	50
Ammonia (R717)	50
Propane (R290)	50
Methanol	50
Water (R718)	60

Performance of the system increases as expected for all working fluids when the generating temperature increases, as shown in Figure 5-9. The COPs of the dry refrigerants are significantly higher than the wet refrigerants at the same temperature if the extra superheat is taken into account. The wet refrigerants require a higher degree of superheat, this indicating that more heat is required. The driving temperature at which the system can start operation is thus higher in the case of the wet working fluids. R141b, an HCFC, yields the best performance among the selected dry refrigerants.

Increasing the evaporating temperature increases the COP significantly, as shown in Figure 5-10. In contrast, increasing the condensing temperature decreases the COP as shown in Figure 5-9. The COPs of the refrigerants in the dry working fluid group are not significantly different from each other; this is also similar for the wet working fluids. Changing the evaporating or condensing temperature affects the COP of the system more than the shift of generating temperature. One Kelvin change of evaporating or condensing temperature changes the COP by approximately 6%, while one Kelvin change of the generating temperature only changes the COP by approximately 0.4%. The evaporator temperature is normally a design parameter. The condenser temperature depends on the ambient conditions. Therefore, this clearly illustrates the importance of ambient conditions, i.e. the coupling to good heat sink with a low ΔT and an efficient cooling supply system.

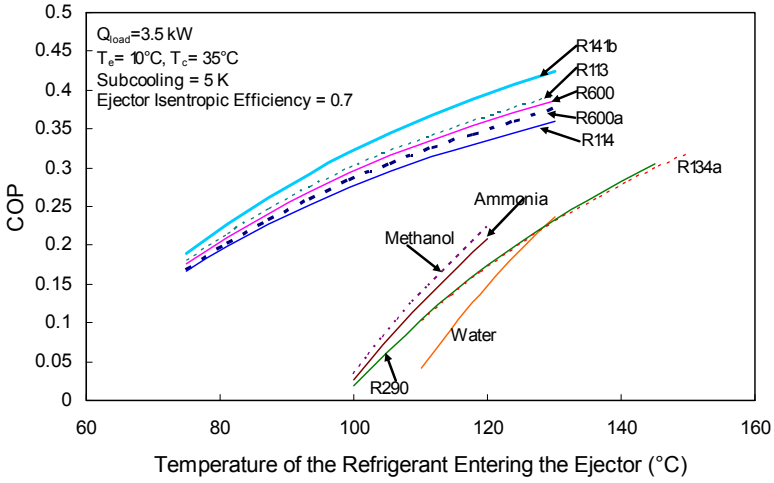

Figure 5-9 COP of an Ejector Refrigeration Cycle as a Function of the Generator Temperature (Calculated with the Model Described in Section 4.2. Evaporation Temperature +10°C, Condensing Temperature 35°C and Degree of Superheat Described in Table 5-2)

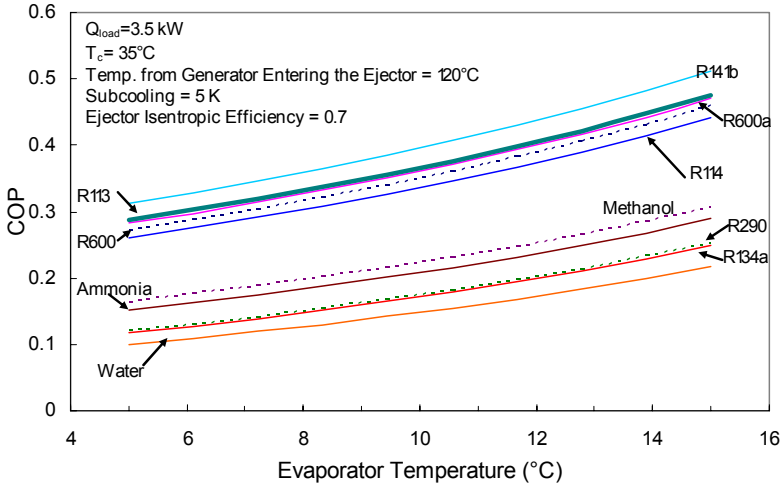

Figure 5-10 COP of an Ejector Refrigeration Cycle as a Function of the Evaporating Temperature for Various Working Fluids (Calculated with the Model Described in Section 4.2, Condensing Temperature 35°C, Temperature from the Generator Enters the Ejector at 120°C and Degree of Superheat Described in Table 5-2)

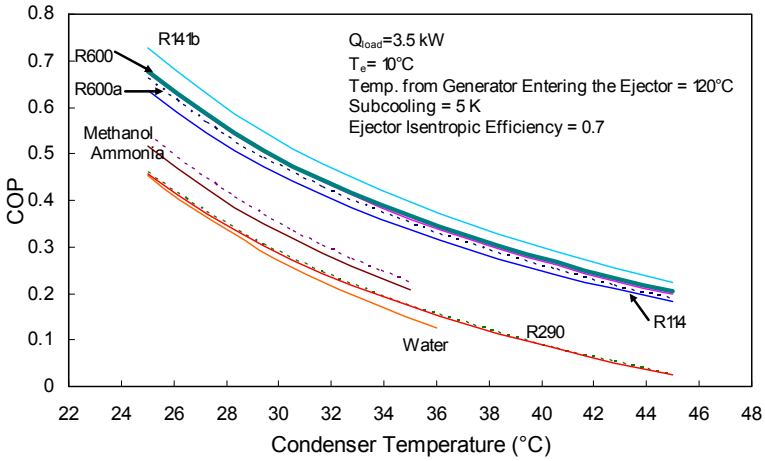

Figure 5-11 Effect of Condensing Temperature to COP (Calculated with the Model Described in Section 4.2, Evaporator Temperature 10°C, Temperature from the Generator Enters the Ejector at 120°C and Degree of Superheat Described in Table 5-2)

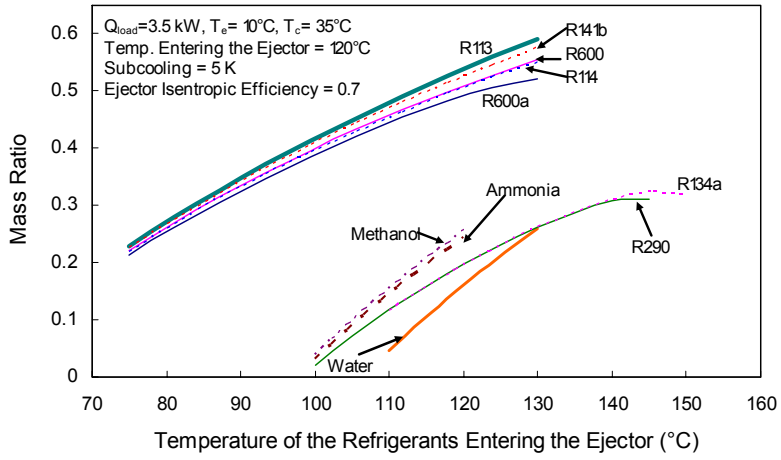

Figure 5-12 Entrainment Ratio at Different Evaporating Temperatures (Calculated with the Model Described in Section 4.2., Evaporation Temperature +10°C, Condensing Temperature 35°C and Degree of Superheat Described in Table 5-2)

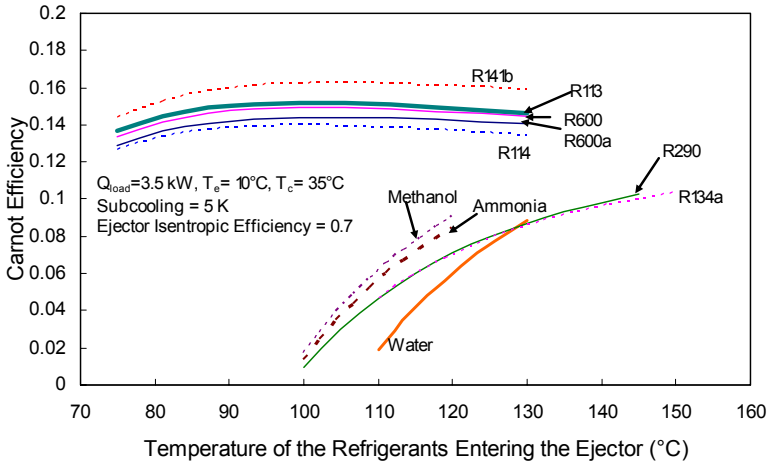

Figure 5-13 Carnot Efficiency at Different Generator Temperatures (Calculated with the Model Described in Section 4.2. Evaporation Temperature +10°C, Condensing Temperature 35°C and Degree of Superheat Described in Table 5-2)

Increasing generator temperature increases the mass ratio as shown in Figure 5-12. In the case of wet and the isentropic fluids, the trend for the Carnot efficiency is similar to the trend for COP; i.e. increasing the generator temperature increases the Carnot efficiency. The influence of the generating temperature on the Carnot efficiency is not significant for dry working fluids which yield high efficiency such as R141b, R113, R114, R600, and R600a.

The volume of the refrigerant after expansion in the ejector does not change extensively when the generating temperature changes in the case of the dry working fluids. An increase in generator temperature slightly decreases the volume of refrigerant for a given cooling load. This is due to the fact that the operating pressure also increases, thus resulting in the decrease of specific vapour volume.

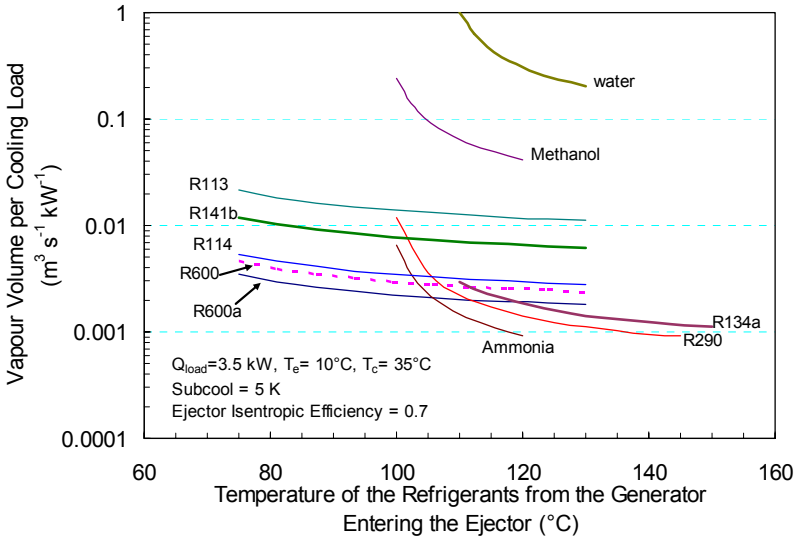

Figure 5-14 Volumetric Flow Rate of Refrigerant per Kilowatt of Refrigeration Load at 3.5 kW Cooling Power, 10°C Evaporation Temperature, 35°C Condenser Temperature

5.4 Concluding Discussion in Working Fluid Selection

There are obviously various candidate refrigerants for the ejector refrigeration cycle. Several candidate fluids suggested in the literature are however no longer allowed due to environmental constraints.

Dry fluids e.g. butane, iso-butane, R113, R114, and R141b yield better performance than wet fluids and isentropic fluids at the same operating temperatures, and require less excessive energy for superheating.

However, not only the efficiency that should be considered when choosing the refrigerant, but also vapour volume after the expansion through the ejector, since it influences the size of the ejector.

Operating conditions affect the performance of the system, and vapour volume of the refrigerant per refrigeration load generally affects the dimension of the ejector. This will be further investigated in Chapter 9. Non-CFC and non-HCFC refrigerants such as water, butane, ammonia,

R152a, or R134a yield an impressive performance, regardless of various drawbacks.

For a system driven by electricity the COP will vary, depending on changes in ambient conditions and load. For a solar driven system the influence of variations in solar insolation will further complicate the picture. The first step, however, is to use the steady-state analysis to identify the effect of varying operating conditions on the performance of the system. Furthermore, general guidelines can be obtained for optimizing operating conditions or choosing working fluid. Interesting natural working fluids e.g. butane, iso-butane, propane, methanol, water, ammonia are selected for the steady-state analysis of the solar-driven ejector refrigeration system in the next chapter.

6 Steady-State Analysis of the Solar-driven Ejector Refrigeration System

In this chapter, a steady-state analysis of the solar-driven ejector refrigeration system will be performed. The system consists of the ejector refrigeration subsystem and solar collector, as shown in Figure 6-1. Only major components are considered in this case. These include a solar collector, ejector, condenser, regenerator, evaporator, expansion device and pump. The system can be divided into 2 sub-systems: the ejector refrigeration subsystem and the solar thermal collector. Six natural working fluids are selected for the case study: water, methanol, ammonia, propane, butane and isobutane.

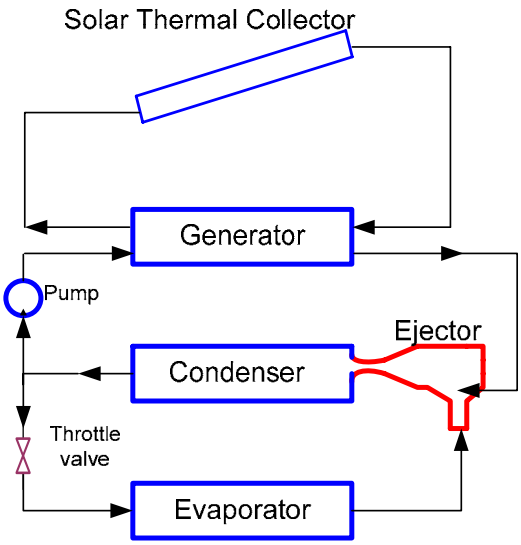

Figure 6-1 A Solar-Driven Ejector Refrigeration System for Steady-State Analysis

6.1 Assumptions

Analysis in this chapter is peformed by use of a computer program developed in Engineering Equation Solver (EES) software. The program is based on the model of the ejector refrigeration cycle explained in Section 4.2, the solar thermal collector model without storage tank and auxiliary heater, together with the following assumptions:

- Flat plate, double glazed solar collector with an area of 50 m^2, Bliss constant $F_R(\tau\alpha)_e$ =0.8 and $F_R U_L$=1.5, water is used as working medium between the solar collector and the generator. Insolation is assumed constant during the day at 17 506 kJ/m^2 day. Solar collector efficiency is calculated by the Bliss equation, as previously mentioned in section 4.1, Equation 4-1 and Equation 4-2.

- The degree of superheat in the generator is 5 K for butane (R600), iso-butane (R600a), 50 K for ammonia, methanol***, propane†††, and 60 K for water. The refrigerant is subcooled in the condenser by 5 K.

- Simulation of refrigerants at various generating temperatures was done limiting the range of the generator temperatures to under the critical point.

- The outlet temperature from the solar collector is higher than the temperature of the refrigerant from the generator that enters the ejector by 10 K.

- Properties of the refrigerants are taken from the database of EES (Klein, 2004). Six natural refrigerants are used in the simulation: water, methanol, ammonia, propane, butane and iso-butane.

*** Ammonia, methanol, and water are classified as wet fluids, according to the slope of the positive slope of the saturation pressure line, see Figure 5-1

††† R134a and propane are classified as isentropic fluids, according to the slope of the positive slope of the saturation pressure line, see Figure 5-2

6.2 Results

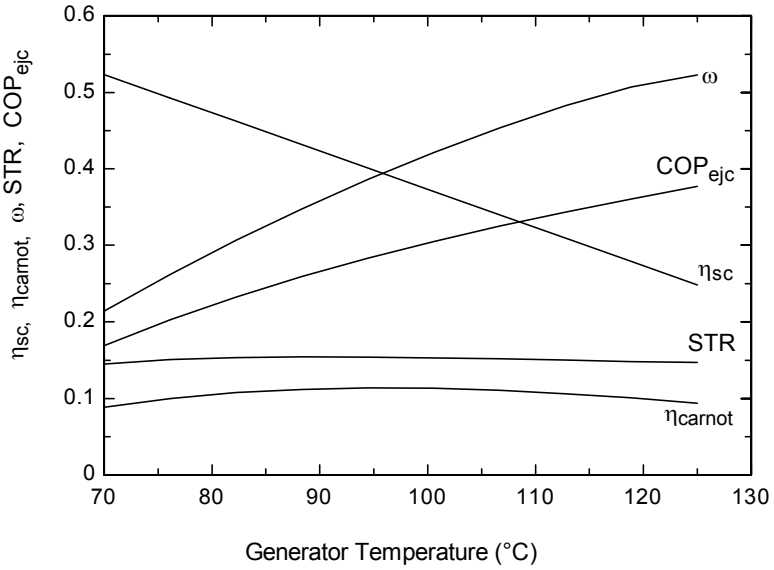

Figure 6-2 Performance of the Solar-Driven Ejector Refrigeration System with ETC, Using Iso-Butane as the Refrigerant at 10°C Evaporating Temperature, 35°C Condensing Temperature, 30°C Ambient Temperature and 5 K superheating

Figure 6-2 illustrates the performance of iso-butane when used as a refrigerant. The principal behaviour of other refrigerants is similar. The COP of the ejector refrigeration sub-system increases when the generating temperature increases as shown in the lines for COP_{ejc} and entrainment ratio in Figure 6-2 and Figure 6-3. Real performance of the refrigeration cycle (COP_{ejc}), compared to ideal performance (COP_{carnot}), is referred as Carnot efficiency (η_{carnot}).

Dry fluids (R600 and R600a) yield higher COP_{ejc} at the same generator temperature compared to the COP_{ejc} of wet and isentropic fluids. In order to reach the same value of COP_{ejc}, the wet fluids require a higher driving temperature, as can be seen in Figure 6-3.

Total system performance, the system thermal ratio (STR), depends on the COP_{ejc} and the efficiency of the solar collector. Contrary to the

COP_{ejc}, the solar collector efficiency decreases when the output temperature increases; thus resulting in the curve shown in Figure 6-4.

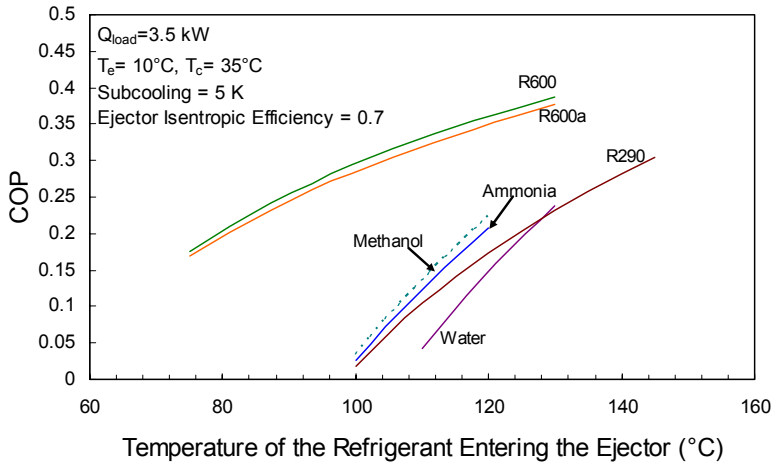

Figure 6-3 COP_{ejc} When Changing the Generating Temperature to 10°C Evaporating Temperature and 35°C Condensing Temperature

Since condensing and evaporating temperatures do not affect the solar collector efficiency, the COPs of the ejector cycle and the system thermal ratio have an identical slope. Increase of the condensing temperature decreases the STR, while on the other hand, an increase of the evaporating temperature increases the STR as shown in Figure 6-5 and Figure 6-6.

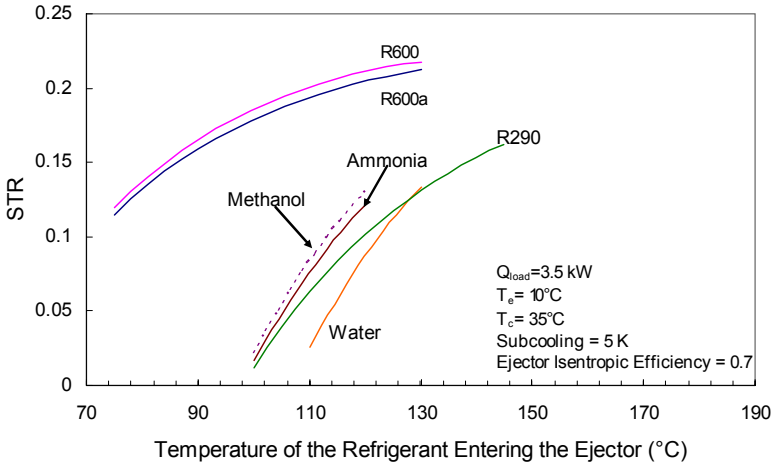

Figure 6-4 System Thermal Ratio (STR) at 10°C Evaporating Temperature, 35°C Condensing Temperature using an ETC collector

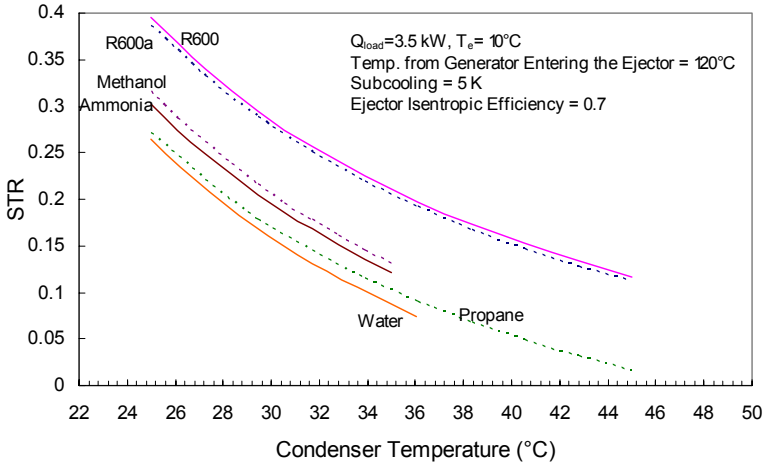

Figure 6-5 System Thermal Ratio (STR) at Evaporating Temperature 10°C, Temperature from Generator Entering the Ejector at 120°C, and using an ETC collector

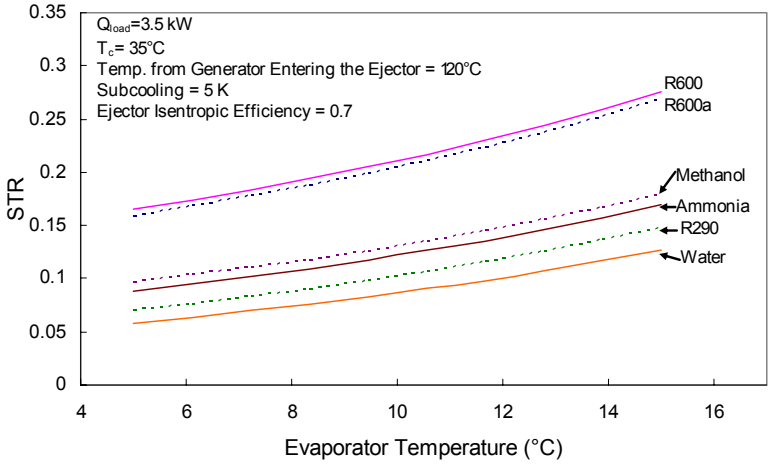

Figure 6-6 System Thermal Ratio (STR) at Condenser Temperature 35°C and Temperature from Generator Entering the Ejector at 120°C and using an ETC collector

Butane and iso-butane are obviously two interesting refrigerants. The characteristics of both refrigerants are previously shown in Table 5-1. The saturated vapour line in the T-S diagram of both butane and iso-butane has a positive slope, thus superheat in the generator is not necessary, as shown in Figure 5-4 and Figure 5-5. At the same boiling temperature, butane gives a somewhat higher pressure than iso-butane as shown in Figure 5-8. The analysis in the following section will focus on butane and iso-butane as the working fluids.

Butane and iso-butane present similar results. The COPs of the n-butane refrigeration subsystem vary from 0.18 to 0.39 at generating temperatures between 70°C and 120°C. Iso-butane yields a little bit lower COP than butane, but other properties and the performances are almost identical to normal butane.

Performance of the theoretical refrigeration cycle, taking losses into account (COP_{ejc}), compared to the ideal performance (COP_{carnot}), also called the Carnot efficiency (η_{carnot}), slightly decreases when the generating temperature increases. The mass ratio (entrainment ratio) also increases with the generating temperature as shown in Figure 6-8.

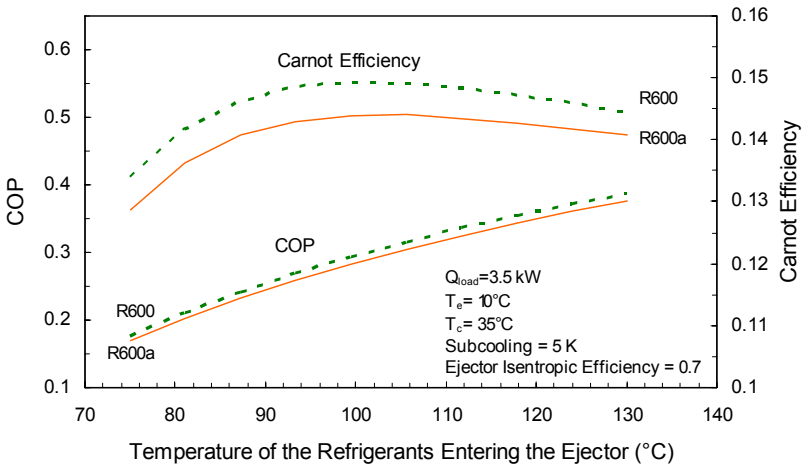

Figure 6-7 COP and Carnot Efficiency of Butane and Iso-butane

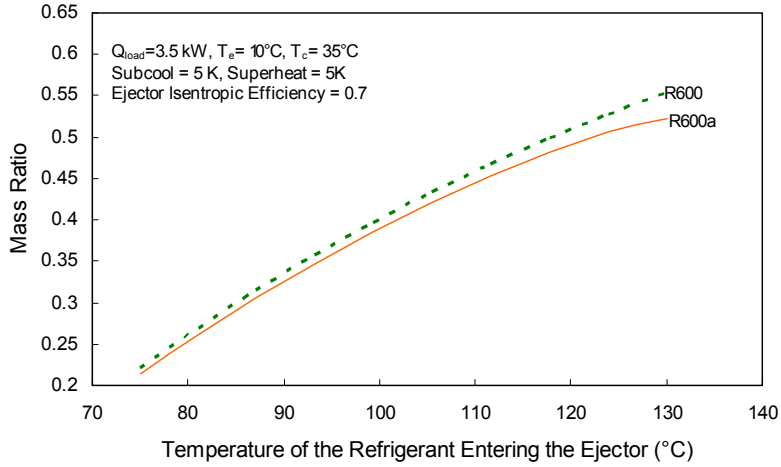

Figure 6-8 Mass Ratio of Butane and Iso-butane

The ambient temperature affects the condenser temperature and the collector efficiency. The evaporation temperature is less affected and more dependant on the application and the systems choosen for distribution of the cold. An increase of the ambient temperature increases the condensing temperature and decreases the COP and the STR. On the other hand, an increase of the evaporating temperature increases the COP and the STR as shown in Figure 6-9 and Figure 6-10. The condensing temperature should therefore be kept as low as the ambient conditions allow increasing the system performance.

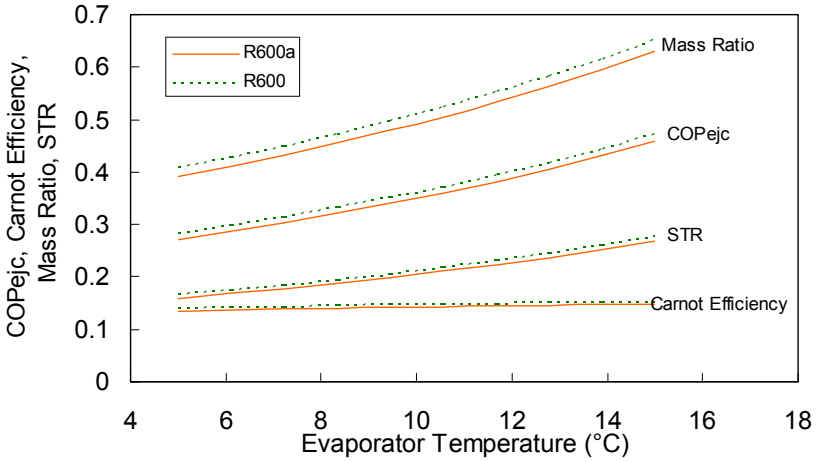

Figure 6-9 Performance of the Solar-Driven Ejector Refrigeration System versus the Evaporating Temperature of Butane and Iso-butane

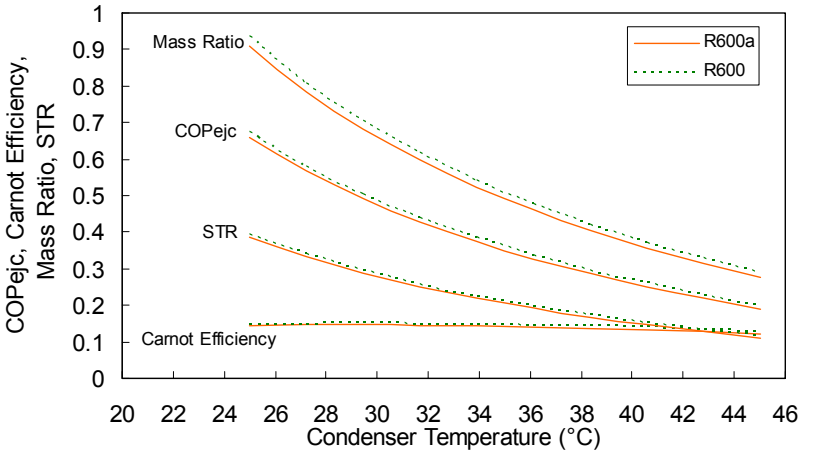

Figure 6-10 Performance of the Solar-Driven Ejector Refrigeration System versus the Condensing Temperature of Butane and Iso-butane

From the results illustrated above, performance of the system using butane as the refrigerant is only slightly higher than the system using iso-butane. Iso-butane can be considered a competitive option since the cost of the fluid, 35 €/kg, is about a third of the cost for n-butane.

Performance of the ejector refrigeration cycle does not solely depend on generating temperature or refrigerant, it is also strongly dependant on the geometry of the ejector. In this chapter, the isentropic efficiency of the ejector is assumed to be constant at 0.7, thus the size of the ejector is adjustable in this case. The size of the ejector depends primarily on vapour volume of the refrigerant after expanding through the ejector. More details on ejector geometry and design can be found in Chapter 9.

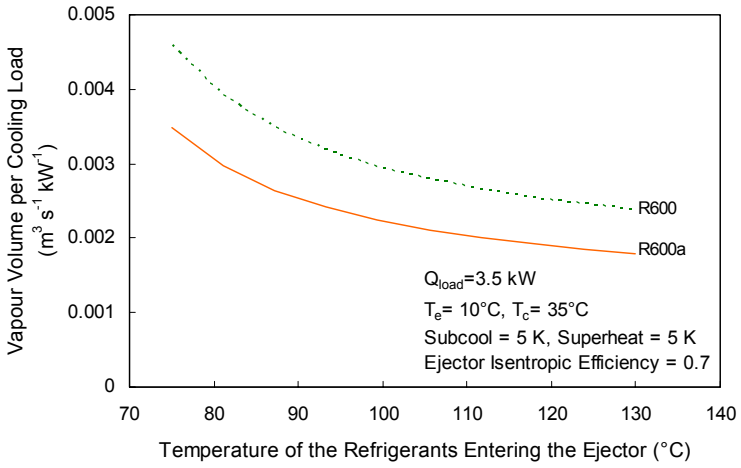

Figure 6-11 Vapour Volume per Cooling Load of Butane and Iso-butane

Variation of the solar collector and the system thermal ratio (STR) during daytime operation is shown in Figure 6-12. Results in this figure come from the assumption that the refrigeration cycle operates at constant generator, condenser and evaporator temperatures, thus the COP of the refrigeration subsystem is constant and it is assumed to be 0.27. Given the above assumption, the STR varies by the insolation and the solar collector efficiency. The highest STR can be achieved between 12:00-14:00, when the highest insolation is gained. This assumption is very simplified, since insolation and ambient conditions change during the day. Therefore, an in-depth dynamic analysis is required for more realistic results.

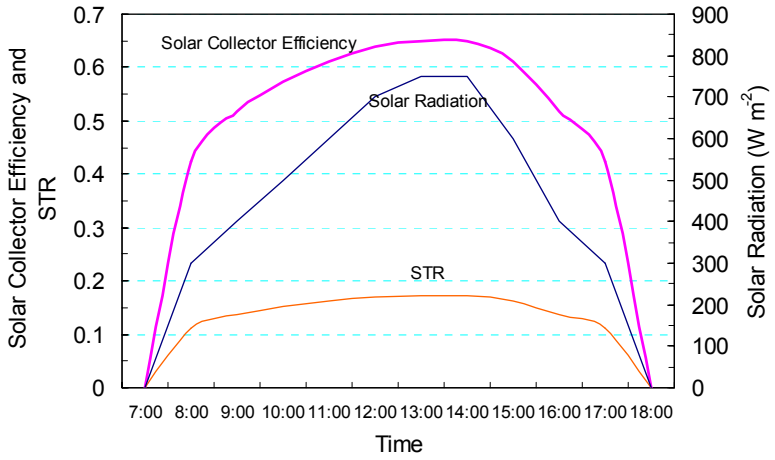

Figure 6-12 The Performance of the Solar-Driven Ejector Refrigeration System during Daytime Operation. The COP of the Ejector Refrigeration System Is Assumed at 0.27. It Works at the Generating Temperature 90°C, Condensing Temperature 35°C and the Evaporating Temperature 10°C, Iso-Butane as the Refrigerant.

6.3 Conclusions

This chapter demonstrates how system performance in terms of COP depends on refrigerant, and operating conditions. The coefficient of performance (COP_{ejc}) of the refrigeration cycle is strongly influenced by operating temperatures; and the system thermal ratio (STR) is further influenced by both the generating temperature and solar collector efficiency. The cycle COP (COP_{ejc}) increases with generator and evaporating temperature, but decreases with increasing condensing temperatures. The condensing temperature should therefore be kept as low as possible for maintaining the function of the ejector and increasing system performance.

The STR is dependant on the choice of collector type and may very well increase for lower generating temperatures due to a more efficient solar collector. For the specific solar collector, the outlet fluid temperatures depend on the fluid inlet temperature and the insolation. High insolation results in high temperature output and consequently, a high refrigeration subsystem performance.

As for all refrigeration systems, the ejector system is more efficient at high evaporating temperatures, therefore a greater fraction of solar energy can be utilised. From the results of the simulation for water, ammonia, butane, iso-butane, methanol and propane, butane yields the highest performance, followed by iso-butane, propane, water, methanol and ammonia. The system size by using normal-butane or iso-buante is manageable and the fluids give dry expansion without excessive superheat. Normal-butane yields a slightly better thermodynamic performance than iso-butane. Since the cost of normal-butane is higher than iso-butane, therefore, iso-butane is proposed as the working fluid.

Steady-state analysis reveals the characteristics and performance of the overall system. A few guidelines for choosing desired operating conditions can therefore be specified. In order to improve the system further, it is necessary to know more in detail where the most inefficient process occurs within the system. One way of doing so is by aid of exergy analysis, which will be performed in Chapter 7.

Another way to further analyse the system is by a more detailed dynamic analysis taking into account variation in insolation, cooling demand and ambient conditions. This is done in Chapter 8.

7 Exergy Analysis

Steady-state analysis demonstrates the performance of a system at different operating conditions in terms of the COP of the refrigeration subsystem. The process, including losses, is hardly identified by steady-state analysis. This can, however, be investigated by exergy analysis. Furthermore, exergy analysis is especially useful when analysing systems with several different categories of driving energy, such as solar+electricity driven refrigeration systems.

The objective of this chapter is to identify optimum operating conditions for the solar-driven ejector refrigeration system by investigating the impact of various losses in the system. Analysis is performed by implementing an energy and exergy balance for the system. This analysis will not focus on details of the ejector. Irreversibilities in each component of the system are calculated and the results discussed. This chapter is based on the publication by the author entitled 'An Exergy Analysis of a Solar-Driven Ejector Refrigeration System' (Pridasawas and Lundqvist, 2004b).

As discussed previously at the beginning of Chapter 2, energy inputs to a solar-driven ejector refrigeration system are derived from three different forms; solar radiation, heat and electricity. Three different forms of energy used in the equation: heat, radiation and electricity leading to three possible definitions of system performance:

$$SP_1 = \frac{Q_e}{Q_{su} + W_{p,el}} \qquad \textit{Eq. 7-1}$$

or,

$$SP_2 = \frac{Q_e}{Q_{su}} \qquad \textit{Eq. 7-2}$$

or,

$$SP_3 = \frac{Q_e}{W_{p,el}} \qquad \textit{Eq. 7-3}$$

Exergy Analysis in the Literatures

Parrott, 1978, studied conversion efficiency of a solar collector on the terrestrial surface by assessing energy transport from the sun to the solar collector. He presented the equations as a function of the ambient temperature and solar temperature. Jeter, 1981, defined the efficiency of exergy transport from the sun to the solar collector as the Carnot coefficient ($1-T_{ref}/T$) by assuming that the process functions as a heat engine. Bejan, Kearney et al., 1981, presented irreversibilities in solar collectors due to heat transfer processes and illustrated operating conditions producing the highest possible exergy delivery rate for a certain size of solar collector. Said and Zubair, 1993, presented an analysis of the performance of solar thermal collectors and photovoltaic panels based on experimental measurements. He presented the maximum second-law efficiency of the photovoltaic panel as being 17% and the maximum exergetic efficiency of the solar thermal collector as 11%. Izquierdo Millán, Hernandez et al., 1996, performed work on available solar exergy in an absorption cooling process. Results demonstrated that maximum hourly exergetic efficiency of available heat varies from 11% to 14.6%, while the maximum daily exergetic efficiency of the full conversion of solar radiation to cooling is approximately 3% when the maximum daily available exergy varies between 810 kJ $m^{-2}day^{-1}$ and 940 kJ $m^{-2}day^{-1}$. Torres R, Picon Nunez et al., 1998, worked on a theoretical and experimental exergy analysis of a solar-assisted heat pump for air heating. Solar collectors were used as an evaporator. The largest irreversibilities occurred in the collector-evaporator. Exergetic efficiency of this system is lower than 3.5%.

There are several studies on the exergy analysis of a solar subsystem (Parrott, 1978; Bejan, Kearney et al., 1981; Jeter, 1981; Fujiwara, 1983; Said and Zubair, 1993) and a few papers that present the entire solar-driven air-conditioning system (Izquierdo Millán, Hernandez et al., 1996; Torres R, Picon Nunez et al., 1998).

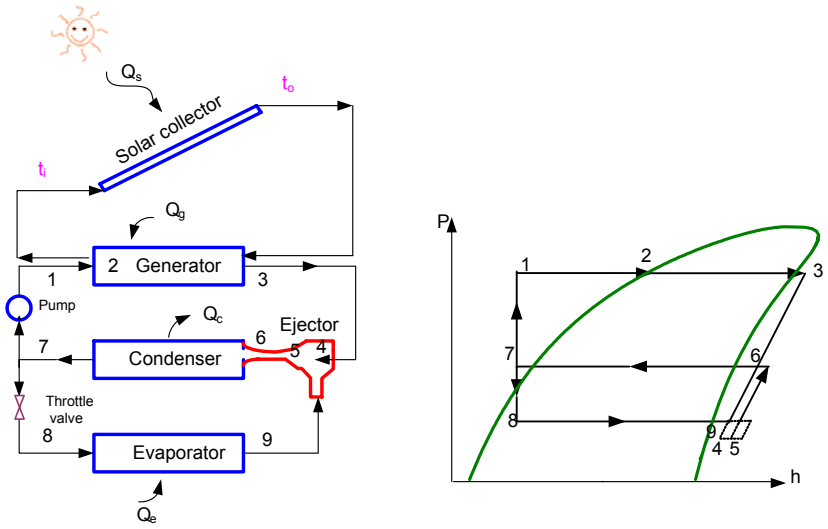

Figure 7-1 Ejector Refrigeration System for Exergy Analysis (the Picture is Similar to Figure 4-4 and Figure 6-1, Repeated for the Convenience of the Reader)

7.1 System Descriptions

The system consists of the same solar collector subsystem and ejector refrigeration subsystem previously described in Chapter 4. The thermodynamic cycle model is described in section 4-1 and 4-2. The exergy model is described in the following sections.

7.1.1 Solar Collector Subsystem

De Vos, 1992, established equations for calculating the exergy input to the collector per unit area as a function of the exergy emitted from the sun minus the albedo of the earth and the radiation emitted from the solar collector:

$$E_s = f\sigma T_{sun}^4 + (1-f)\sigma T_{planet}^4 - \sigma T_{sc}^4 \qquad \textit{Eq. 7-4}$$

Where f is the sunlight dilution factor, which is equal to 2.16 x 10^{-5} on the earth.

The incident radiation on the solar collector ($E_{s,h}$), the exergy heat load to the evaporator (E_e) and the electricity used by the pump ($W_{p,el}$) are the inputs to the system. The rejected exergy from the condenser ($E_{c,out}$) and the total irreversibilities from every component in the system (I_{total}) are the outputs. The exergy balance for the system can be written as:

$$E_{s,h} + E_e + W_{p,el} = E_{c,out} + I_{total} \qquad \textit{Eq. 7-5}$$

The solar radiation that reaches the solar collector is transformed to heat. This heat is partly absorbed by the thermal fluid and the surrounding equipment and partly lost to the environment. The available solar radiation (G_{ava}) is transformed into available heat for the process (Q_{ava}) and the second law of thermodynamics governs the transformation of thermal energy into exergy:

$$E_{s,h} = Q_{ava} \cdot (1 - (T_{ref} / T_{sc})) \qquad \textit{Eq. 7-6}$$

The exergy loss during the transformation from solar radiation to heat on the solar collector is given as

$$I_{sc,r} = E_s - E_{s,h} \qquad \textit{Eq. 7-7}$$

Exergy transferred from the absorbing material increases the exergy of the working fluid. Assumed that there is no loss of the energy transferred from the absorbing plate to the thermal fluid (Q_u=Q_{ava}), the exergy gain by the solar collector is

$$E_{su} = Q_u \cdot (1 - (T_{ref} / T_{sc})) \qquad \textit{Eq. 7-8}$$

where (Q_u) is the useful steady state energy gain to the solar collector. Q_u is calculated from the heat balance in the flat plate solar collector by the Hottel-Whillier-Bliss equation as

$$Q_u = AF_R\left[G(\tau\alpha)_e - U_L(T_i - T_a)\right] \qquad \textit{Eq. 7-9}$$

The exergy loss related to the heat transfer in the collector, from the exergy absorbed by the solar collector to the exergy supplied to the working fluid can be calculated using the equation

$$I_{sc} = E_{s,h} - E_{su} \qquad \textit{Eq. 7-10}$$

7.1.2 Refrigeration Subsystem

The exergy loss in each component of the solar-driven ejector refrigeration system can be described by the equations shown in Table 7-1. These equations are used for calculating exergy losses by performing an exergy balance for each component. The refrigeration subsystem is modelled through an energy and momentum balance over the ejector. The pressure drop in the heat exchangers is neglected, and heat transfer is modelled by assuming typical temperature differences. The details of the ejector are not included in this section and the full description of the model used can be found in Chapter 4. The isentropic efficiency of the ejector is 70%, as suggested by Lundqvist, 1987.

Table 7-1 Equations Used in the Exergy Analysis (Nomenclature in Figure 7-1)

Solar collector		
Exergy (radiation) input	$E_s = f\sigma T_{sun}^4 + (1-f)\sigma T_p^4 - \sigma T_{sc}^4$	*Eq. 7-11*
Exergy (heat) input	$E_{s,h} = Q_{ava} \cdot (1-(T_{ref}/T_{sc}))$	*Eq. 7-12*
Loss (transformation process)	$I_{sc,r} = E_s - E_{s,h}$	*Eq. 7-13*
Useful exergy gain	$E_{su} = Q_u \cdot (1-(T_{ref}/T_{sc}))$	*Eq. 7-14*
Loss (heat transfer)	$I_{sc} = E_{s,h} - E_{su}$	*Eq. 7-15*
Generator		
Exergy available	$E_{gin} = Q_g \cdot (1-(T_{ref}/T_g))$	*Eq. 7-16*
Exergy loss	$I_s = T_{ref} \cdot (m_g(S_3 - S_1) + m_{sc}(S_{g,sc\_out} - S_{g,sc\_in}))$	*Eq. 7-17*
Ejector		
Exergy loss	$I_j = T_{ref} \cdot \left[\left(m_e + m_g\right) \cdot S_6 - m_g \cdot S_3 - m_e \cdot S_9 \right]$	*Eq. 7-18*
Condenser		
Exergy loss	$I_c = T_{ref}\left[(m_e + m_g) \cdot (S_7 - S_6) + (Q_c/T_{ref})\right]$	*Eq. 7-19*
Pump		
Exergy loss	$I_p = W_{pump} + m_g \cdot \left((h_1 - h_7) - T_{ref} \cdot \left(S_1 - S_7\right)\right)$	*Eq. 7-20*
Expansion device		
Exergy loss	$I_{\exp} = m_e \cdot \left(T_{ref} \cdot (S_8 - S_7)\right)$	*Eq. 7-21*

Evaporator		
Exergy delivered	$E_e = Q_e \cdot (1-(T_{ref}/T_{room}))$	*Eq. 7-22*
Exergy loss	$I_e = T_{ref}\left(m_e \cdot \left(S_9 - S_8\right) - \left(Q_e / T_{room}\right)\right)$	*Eq. 7-23*
Total irreversibility	$I_{total} = I_{sc} + I_{gen} + I_c + I_p + I_{\exp} + I_e$	*Eq. 7-24*

7.2 Performance

The alterative definitons of COP for the refrigeration subsystem have been previously defined in Chapter 2.

$$COP_{el} = \frac{Q_e}{W} \qquad \textit{Eq. 2-1}$$

$$COP_{thermal} = \frac{Q_e}{Q_g} \qquad \textit{Eq. 2-2}$$

$$\eta_{carnot} = \left(\frac{T_g - T_1}{T_g}\right) \cdot \left(\frac{T_2}{T_1 - T_2}\right) \qquad \textit{Eq. 2-19}$$

The Energy performance of the system is defined as the system thermal ratio (STR) and previously defined in Chapter 2 as,

$$STR = \frac{Q_e}{G \cdot A} = \frac{Q_e}{Q_g} \times \frac{Q_g}{G \cdot A} = COP \times \eta_{sc} \qquad \textit{Eq. 2-21}$$

The exergetic efficiency of the ejector refrigeration cycle (REE) is defined as the ratio of cooling exergy to exergy inputs to the generator and pump.

$$REE = \frac{E_e}{E_g + E_{p,el}} \qquad \textit{Eq. 7-25}$$

The system exergetic efficiency (SEE) is defined as the ratio of cooling exergy to exergy of the available solar heat input plus electricity input to the pump.

$$SEE = \frac{E_e}{E_{s,h} + E_{p,el}} \qquad \textit{Eq. 7-26}$$

7.3 Methodology

The mathematical model is implemented in the Engineering Equation Solver Environment (EES, Klein, 2004). Properties for the refrigerant(s) are taken from the NIST reference database REFPROP (Lemmon, McLinden et al., 2002). The exergy analysis of the solar-driven ejector refrigeration system was performed assuming the following conditions:

- the incident solar radiation is 700 W m^{-2} , and a double-glazed flat-plate solar collector is used with an area of 63.5 m^2, $F_R(\tau\alpha)_e$ = 0.8 and $F_R U_L$ = 3.5 W m^{-2} K^{-1},
- butane is used as the refrigerant,
- water is used as the heat carrier between the solar collector and the generator,
- the outlet temperature of the solar collector is assumed to be 10 K above the generating temperature,
- the cooling capacity is 5 kW,
- the ambient air temperature is 30°C which also is used as the reference temperature for the analysis,
- the generating temperature is 90°C,
- the condensing temperature is 37°C,
- the evaporation temperature is 10°C,
- the pump efficiency is assumed to be 25%,
- the total isentropic efficiency of the ejector is assumed to be 70%.

The average heat removal factor and heat loss coefficient ($F_R(\tau\alpha)_e$ and F_RU_L) for the flat plate and the evacuated tube solar collectors are shown in Table 4-1.

7.4 Results

The overall thermal energy efficiency or the system thermal ratio (STR) at a generating temperature of 90°C is about 11%.

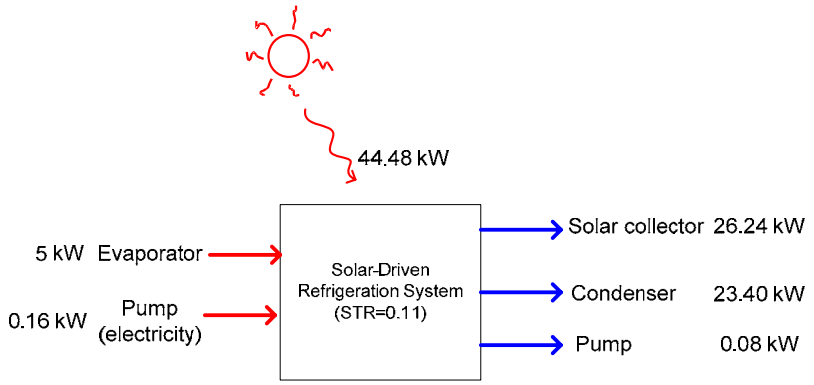

Figure 7-2 Energy Balance for the Solar-Driven Ejector Refrigeration System

The energy balance for the whole system is shown in Figure 7-2. The coefficient of performance (COP) of the ejector cycle is 0.27 and the solar collector efficiency is about 41% for the conditions simulated. The system thermal ratio (STR) is quite low. If the performance measure is based on supplied electricity (cooling load per electricity input to the pump), it is as high as 32. Figure 7-3 illustrates that the ideal Carnot efficiency is significantly higher than the actual system thermal ratio, which indicates large losses occurring in the system. The Carnot efficiency of the system (as defined in Eq. 2-6) decreases slightly when the generation temperature increases. The decrease of the Carnot efficiency is due to the heat losses in the system. The solar collector efficiency decreases when the output temperature increases due to the heat loss in to the environment. The STR decreases slightly after the generator temperature

reaches levels above 110°C. This decrease in STR is due to a decrease in solar collector efficiency at high generating temperatures.

Table 7-2 Energy Balance

	Energy Received (kW)	Energy Delivered (kW)	Energy Losses (kW)	Energy (thermal) Efficiency (%)
Solar collector	44.48	18.24	26.24	41.01
Refrigeration cycle	18.40	5.00	0.08	27.41
(from solar)	(18.24)			
(from pump)	(0.16)			
Overall	44.64	5.00		11.24

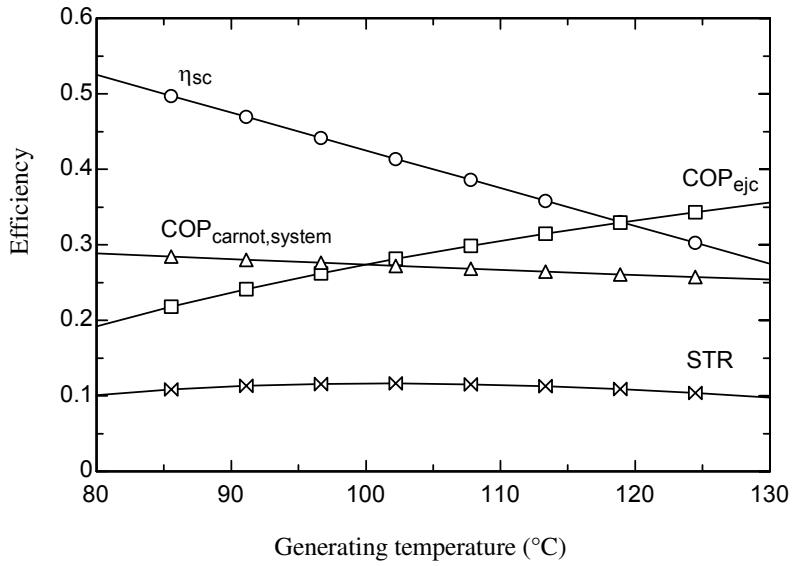

Figure 7-3 System Energy Efficiency

Table 7-3 Exergy Balance

	Exergy Received (kW)	Exergy Delivered (kW)	Exergy Losses (kW)	Exergy Efficiency (%)
Solar collector				
(from radiation to heat)	44.48	8.10	36.38	18.21
(from heat to refrigeration cycle)	8.10	3.85	4.25	47.53
Refrigeration cycle	4.01	0.17	4.01	4.23
(from solar collector)	(3.85)			
(from pump)	(0.16)			
Total	44.64	0.17	44.47	0.38
(Total, if considering only exergy, in the form of heat, received in the solar collector)	(8.26)	(0.17)	(8.09)	(2.06)

The exergy balance, the exergy losses in the ejector refrigeration cycle and the exergy efficiency of the whole system are shown in Table 7-3 Table 7-4 and Figure 7-4. Overall exergetic efficiency is less than 1%. The extremely low exergetic efficiency is due to the fact that cooling is performed at a temperature level near the reference state for the exergy analysis. In essence, cooling an object at the reference temperature yields zero exergetic efficiency by definition since no exergy is delivered to the object (heat is removed at the reference temperature). This indicates that the concept of overall exergetic efficiency is better suited to prime movers. Nevertheless, since this section focuses on the distribution and relative magnitude of losses in the system rather than overall exergetic efficiency the results are still useful. The highest loss, 51%, is found in the solar collector, followed by loss in the ejector, which is 16%. Exergy loss of each component is shown in Table 7-4. Focusing on the components solely in the ejector refrigeration subsystem, the largest loss (32%) occurs in the ejector followed by the generator (22%), and condenser (21%). The remaining exergy losses occur in the pump, evaporator and expansion valve.

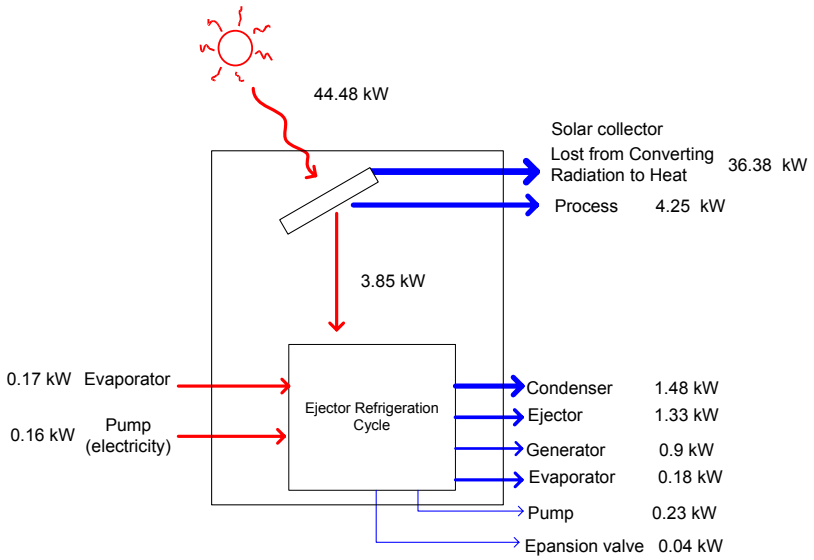

Figure 7-4 Exergy Balance of the Solar-Driven Ejector Refrigeration System for the Generating Temperature of 90°C and Evaporation Temperature of 10°C

The significant loss in the ejector further emphasizes the need for a suitable ejector design. The exergy loss in the ejector is caused by the friction losses of the flow inside the ejector through the converging-diverging nozzle, the non-ideal adiabatic expansion in the nozzle and the corresponding irreversibilities. The performance of the ejector increases immensely at increased evaporator temperatures. Refrigeration should therefore be provided at the highest evaporating temperature possible in the given application.

The entrainment ratio strongly influences the efficiency of the refrigeration subsystem. The entrainment ratio has previously defined in Equation 4-10. A more efficient ejector design would lead to a higher entrainment ratio and therefore, redistribution of losses in the system. This would imply that optimum efficiency would be obtained at lower generating temperatures since the collector losses would be reduced (see Figure 7-5 and Figure 7-6).

The second largest irreversibility in the refrigeration subsystem occurs in the generator. The major loss here is due to heat transfer over a finite

temperature difference. Both the condenser and the evaporator are exchanging heat over a finite temperature difference.

Table 7-4 Exergy Losses

	Exergy Loss	Exergy Loss in the Whole System (%)	Loss in Refrigeration Subsystem (%)
Solar Collector**	4.25	50.50	
Refrigeration Subsystem			
Generator	0.90	10.69	21.59
Ejector	1.33	15.79	31.90
Condenser			
(loss)	0.89	10.62	21.45
(rejected)	0.59	7.02	14.19
Pump	0.23	2.73	5.52
Expansion Valve	0.04	0.47	0.96
Evaporator	0.18	2.17	4.39
Total	8.42		100.00

Note**: Exergy loss from converting the solar radiation to heat (36.38 kW) is not taken into account in this table because it cannot be avoided. Furthermore large amount of irreversibilities occur in this process compared to the losses in other processes.

The exergy of the stream leaving the pump is equal to the exergy difference between the electricity input and the losses. The losses in the pump are associated with the electrical and mechanical inefficiencies.

The expansion device is used in the refrigeration cycle to decrease the pressure of the refrigerant from the condenser pressure to the evaporator pressure. The throttling process in the expansion valve causes a loss that is the smallest one in this system.

A slightly higher overall efficiency is obtained in this example at a generating temperature of about 80°C due to lower heat losses in the solar collector (see Figure 7-6 and Figure 7-7). The optimum generating temperature for the selected evaporation temperature of 10°C is about 80°C. Below this value the total irreversibilities increase. The main reason for this behaviour is the increase of the required mass flow rate of the primary

stream in the generator-ejector-pump loop, to maintain the same cooling capacity. The mass flow rate of the primary stream must be higher to be able to induce the secondary stream from the evaporator to the ejector. A higher mass flow rate thus needs a higher energy supply to the generator. For generator temperatures over 80°C the losses in the ejector decrease, but the losses in the solar collector increase due to the decrease in solar collector efficiency, as shown in Figure 7-5 and Figure 7-6. The optimum generator temperature thus depends on the evaporation temperature and other operating conditions such as condensing temperature, working fluid, and the ejector efficiency.

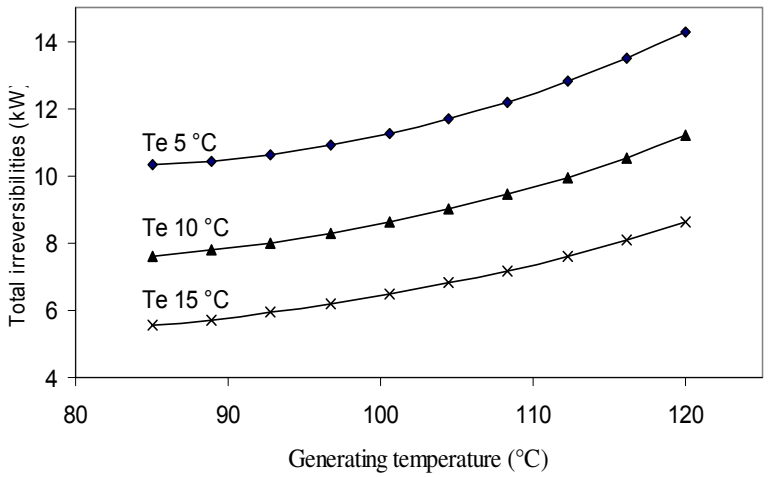

Figure 7-5 Total Irreversibilities vs. Generating Temperature at Different Evaporation Temperatures and the Condensing Temperature of 37°C

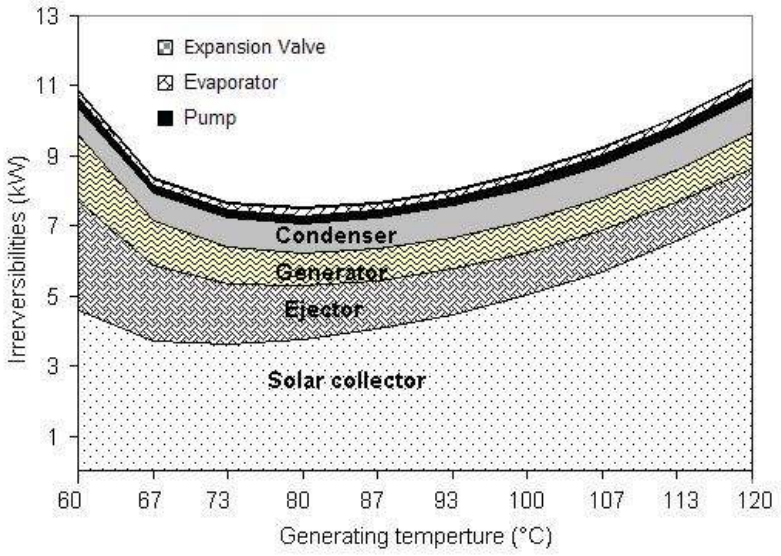

Figure 7-6 Irreversibilities in Each Component vs. Generating Temperature, at the Condensing Temperature of 37°C and the Evaporting Temperature of 10°C

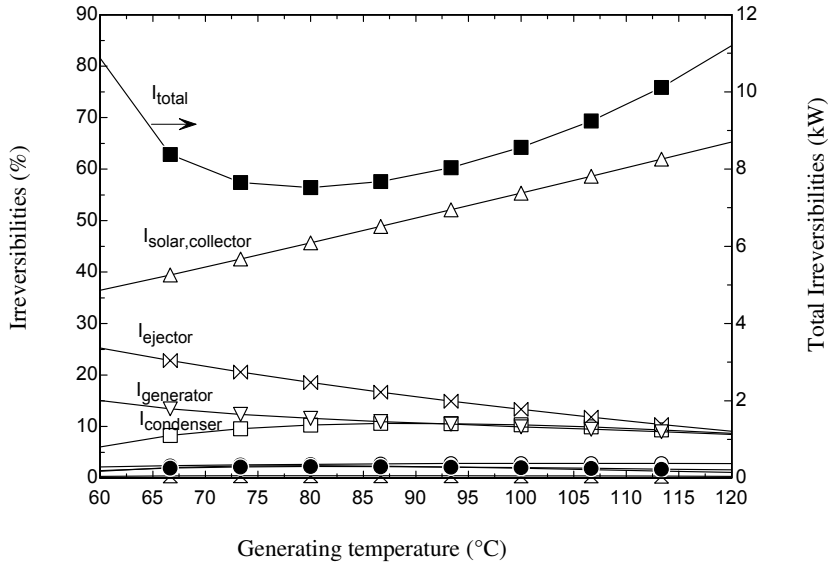

Figure 7-7 The Percentage of the Exergy Loss in Each Component as a function of the Generator Temperature, at the Condensing Temperature of 37°C and the Evaporting Temperature of 10°C

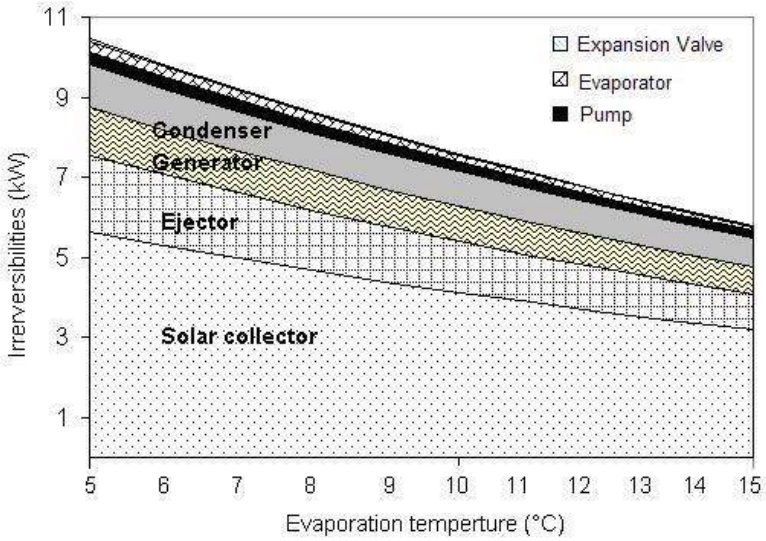

Figure 7-8 The Irreversibility in Each Component as a function of the Evaporation Temperature, at the Condensing Temperature of 37°C and the Generating Temperature of 90°C

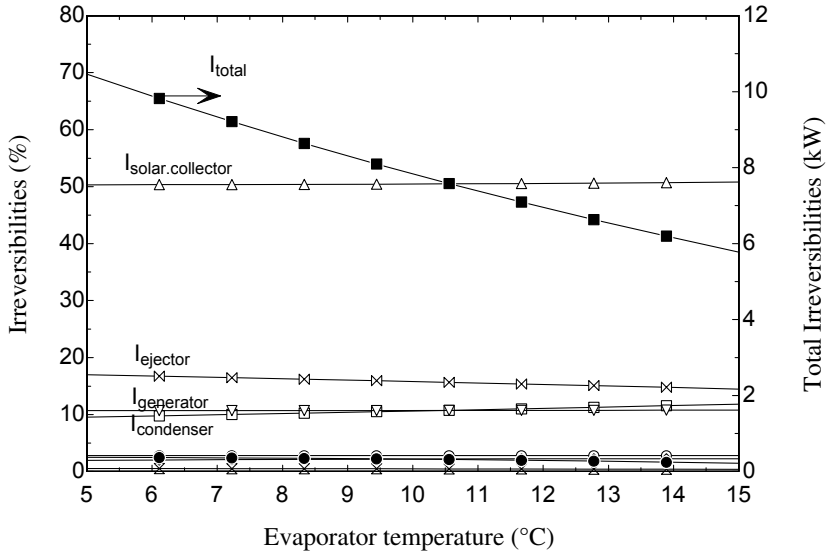

Figure 7-9 Percentage of Irreversibility in Each Component as a function of the Evaporation Temperature, at the Condensing Temperature of 37°C and the Generating Temperature of 90°C

An increase of the evaporation temperature decreases the total irreversibility mainly due to the reduction of the pumping power, the required heat to the generator and the rejected heat from the condenser. At a generating temperature of 90°C, the total loss decreases about 0.5 kW when the evaporation temperature increases 1 K; but at an evaporating temperature of 10°C, the total loss changes only about 0.1 kW when the generating temperature changes 1K. The optimum generating temperature for the 10°C evaporation temperature is around 80-100°C, depending on the type of the solar collector. For a given operating temperature, the evacuated-tube solar collector generates the lowest irreversibilities among the types of solar collectors analysed here. To optimise the system efficiency, a suitable solar collector should be chosen together with an appropriate generating temperature in order to reduce installation costs and gain the highest efficiency.

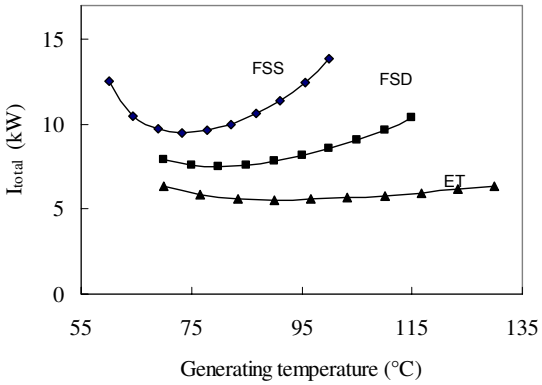

Figure 7-10 Exergy Loss vs. Generating Temperature for Different Types of Solar Collectors (FSS=Flat-Plate, Single-Glaze Solar Collector, FSD=Flat-Plate, Double-Glaze Solar Collector and ET=Evacuated Tubular Collector)

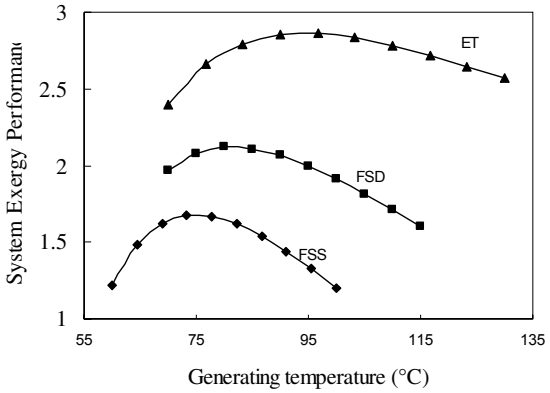

Figure 7-11 System Exergetic Efficiency vs. Generating Temperature for Different Types of Solar Collectors (Note Earlier Comments on Usability of the Concept for Refrigeration Systems)

The calculations in this section of the thesis are based on the average efficiency of different solar collector types.

7.5 Conclusions

Exergy analysis is used as a tool in analysing the performance of an ejector refrigeration cycle driven by solar energy. The analysis is based on the following conditions: a solar radiation of 700 W m^{-2}, an evaporator temperature of 10°C, a cooling capacity of 5 kW, butane as the refrigerant in the refrigeration cycle, an ambient temperature of 30°C, and the reference temperature of 30°C (the same as the ambient temperature).

Irreversibilities occur among components and depend on the operating temperatures. The largest portion of the exergy is lost in the solar collector followed by the ejector, the generator, the condenser, the evaporator and the expansion valve. The irreversibilities decrease with increasing the evaporation temperature, which is also the parameter that most strongly affects the total irreversibilities of the whole system. Minimum losses for a specific evaporation temperature can be obtained at the optimum generating temperature. The evacuated tube solar collector provides the highest efficiency and lowest total irreversibilities compared to the flat-plate double-glazed and the flat-plate single-glazed solar collector. How-

ever, the optimum generating temperature is about 80 – 100°C, depending on the evaporation temperature. Therefore, a high temperature solar collector is not necessary for solar-driven ejector refrigeration systems for the given conditions.

In practice, the cooling load and the solar radiation are not constant. Therefore, the steady-state analysis may not demonstrate system dimensions properly. The load variation and the solar radiation characteristic are better understood in a dynamic analysis. This is therefore paramount for system design, especially when dimensioning the solar collector subsystem with energy storage tanks. Dynamic analysis of the solar-driven ejector refrigeration system can be found in Chapter 8.

8 Dynamic Simulation of a Small Scale Solar-Driven Ejector Refrigeration System

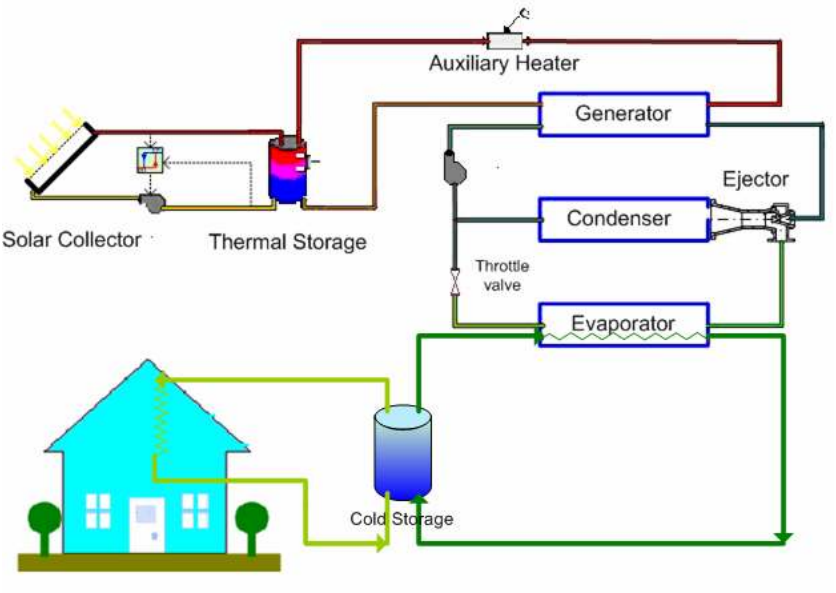

Figure 8-1 System Descriptions for Dynamic Simulation

The discussion in Chapter three showed that the performance of the solar-driven refrigeration system is strongly dependant on the climate, i.e. solar insolation and ambient conditions, as previously discussed in Chapter 3. The dynamic nature of the climate may necessitate a more in-depth analysis. The steady-state analysis, as performed in Chapter 5 and 6, may not fully represent the real system performance. In the real system, the solar collector subsystem must be able to supply enough energy to the

refrigeration subsystem, even when solar energy is unavailable, at least for a shorter period of time. A storage tank is therefore recommended to enhance the security of supply. Heat transfer media, circulating between the solar collectors, the storage tank and the generator, will always perform as a thermal mass, smoothing out small variations in insolation, thus avoiding fluctuation in temperature level for the supply to the generator. Dynamic simulation is very useful in the design point of view, especially for dimensioning the tank sizes.

In the first section, the climate data of Bangkok, Thailand is chosen for the analysis because the cooling load during the whole year at this location is quite constant. Later, the results from the analysis of different locations are presented. A schematic of the system is shown in Figure 8-1.

8.1 Simulation Parameters and Methodology

The model of the whole system is developed in TRNSYS 16 (Klein, Beckman et al., 2004b), but the mathematical model of the refrigeration subsystem is implemented in Engineering Equation Solver (EES) Klein, 2004. TRNSYS calls the refrigeration sub-model, built in EES, through component type 66. Component type 66 calls the EES file; passing it information and receiving output from EES by using the dynamic data exchange method and text files in order to exchange information and commands. Properties for the refrigerants are taken from the library of EES, which uses equations of state for iso-butane (R600a) based on Miyamoto and Watanabe, 2002. The system is divided into three main subsystems: the solar collector subsystem, the refrigeration subsystem and the cooling load. The solar collector subsystem and the cooling load models are previously described in Chapter 4 and Appendix B. The model of the ejector refrigeration subsystem is based on the model described in Section 4.2, together with the assumption of the mass ratio, shown in Figure 8-2. Details of each subsystem are shown in Table 8-1 and Appendix B.

Table 8-1 Simulation Parameters

Simulation Parameters	
Tolerance Convergence	0.001
Time Step	0.5 h
Climatic Data	Short description of TRNSYS components: Type 109 reads the weather data from weather data files and recalculates the solar radiation at different wall orientation. Effective sky temperature for long-wave radiation exchange is calculated by Type 69. Psychometric properties e.g. dew point temperature, wet bulb temperature, humidity ratio and enthalpy of the air are calculated by Type 33. Weather data from METEONORM version 4.10 Location : Bangkok Latitude : 13.44 Longitude : -100.34
Cooling Load Subsystem	Short description of TRNSYS components: Thermal behaviour of the building with 2 thermal zones is modelled and calculated by TRNSYS Type 56, multizone building. Overhang and wing-wall shading is modelled by Type 34. The temperature of the building is controlled by a three-stage room thermostat, Type 8, at the maximum indoor air temperature of 26°C. Maximum required cooling capacity : 3.5 kW Average cooling capacity : 2.5 kW Floor area: 50 m^2 Wall/Window area : Wall/Window North: 30/3 m^2 Wall/Window East: 15/1.5 m^2 Wall/Window South: 30/1.5 m^2 Wall/Window West: 15/1.5 m^2 Roof area: 22.4 m^2 Volume : 150 m^3

Simulation Parameters	
	Ventilation : ACH = 0.8
	Maximum indoor air temperature: 26 °C
	(for more details, please see Appendix B)
Cold Storage Tank	Short description of TRNSYS components:
	The cold storage tank is modelled by TRNSYS Type 4, Stratified Fluid Storage Tank. The tank has 6 thermal stratified nodes. Each node has the same volume and is assumed to be fully-mixed. The warmer fluid enters or leaves the tank from the top and the cooler fluid enters or leaves the tank from the bottom.
	Volume: 1 m^3
Solar Collector Subsystem	
	Flow rate: 3600 kg/hr
Collector	Short description of TRNSYS components:
	TRNSYS Types 1 and 71, are used for modelling the flat plate, and evacuated solar collector with the performance as shown in the following table.
	Collector types: Flat plate single glaze, Flat plate double glaze, and Evacuated Tube Collector (ETC)
	Collector angle: 15°
	Collector azimuth: south direction
	Collector area: varies in simulations
Pump	Short description of TRNSYS components:
	TRNSYS type 3 represents the circulation pump with a power coefficient of 0.5.
	Maximum power: 1 kW
Storage Tank	Short description of TRNSYS components:
	The hot storage tank is modelled by a TRNSYS type 4, Stratified Fluid Storage Tank. The tank has six thermal stratified nodes. Each node has the same volume and is assumed to be fully-mixed. The

Simulation Parameters	
	warmer fluid enters or leaves the tank from the top and the cooler fluid enters or leaves the tank from the bottom. Volume: 0.5, 1, 2, 3 m^3
Auxiliary Heater	Maximum heating capacity: 6 kW Setting temperature: the heater starts when the temperature of the fluid supply to the generator falls below 80°C. Efficiency: 100%
Refrigeration Subsystem	TRNSYS type: TRNSYS Type 60 calls external model which is built in EES. Refrigerant: iso-butane (R600a) Heat exchanger mean temperature difference: 10°C Operation time: 7:00-17:00, Monday to Friday
Generator	Minimum driven temperature: 70°C Maximum driven temperature: 120°C
Pump	Pump efficiency: 0.5
Ejector	One fixed-dimension ejector for which the characteristic curve is provided in Figure 8-2, Figure 8-3, and Figure 8-4.
Condenser	Condenser temperature: 5°C above the ambient temperature
Evaporator	Evaporator temperature: 15°C

Note: TRNSYS is an open source code program, more details of TRNSYS components can be found in the TRNSYS manual (Klein, Beckman et al., 2004b).

8.2 System Performance

The system performance is presented as the system thermal ratio, STR. The STR is defined as the ratio between the cooling capacity and the solar energy input to the collectors. The ideal system thermal ratio can also be written as the product of the collector efficiency and the COP_{ejc}. For a year-round operation, the performance of the system is presented as the solar fraction, previously defined in Equation 2-22.

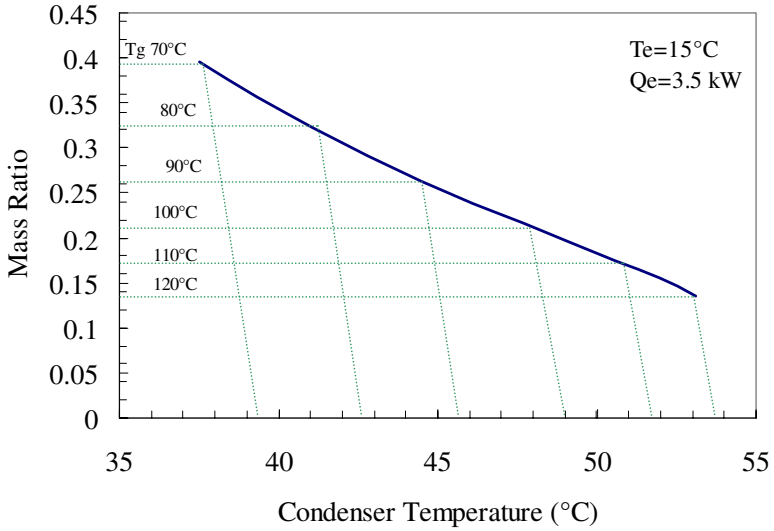

Figure 8-2 Mass Ratio at Evaporator Temperature 15°C

Figure 8-2, Figure 8-3, Figure 8-4 and Figure 8-5 illustrates the functions of the selected ejector at different operating conditions. All data in these graphs are used as the assumptions for the ejector using in the simulation of this chapter.

At a specific generator pressure and evaporator pressure, the mass ratio depens on the condenser pressure. The mass ratio will suddenly decrease if the back pressure is over the critical point. The critical condenser temperature depends on the ejector geometry, type of working fluid and generator temperature. For a more detailed discussion of the critical condenser temperature, please refer to chapter 9. Figure 8-2 illustrates the mass ratio of one selected ejector at different generators and con-

denser temperatures. This figure comes from the assumption of a fixed ejector dimension, as described in the next chapter at Section 9.1. The dash lines in the figure show the mass ratio at a certain gernerator temperature when operate at different condenser temperature. The connection between the critical point of each dash line becomes the thick line, showing the mass ratio at the critical condenser temperature and the specific generator temperature.

The mass ratio at different critical condenser pressure is plot as the function of the compression ratio in Figure 8-3. The COP and the mass ratio as the function of the generator temperature are shown in Figure 8-4. The required heat supply to the generator at different generator temperature is shown in Figure 8-5.

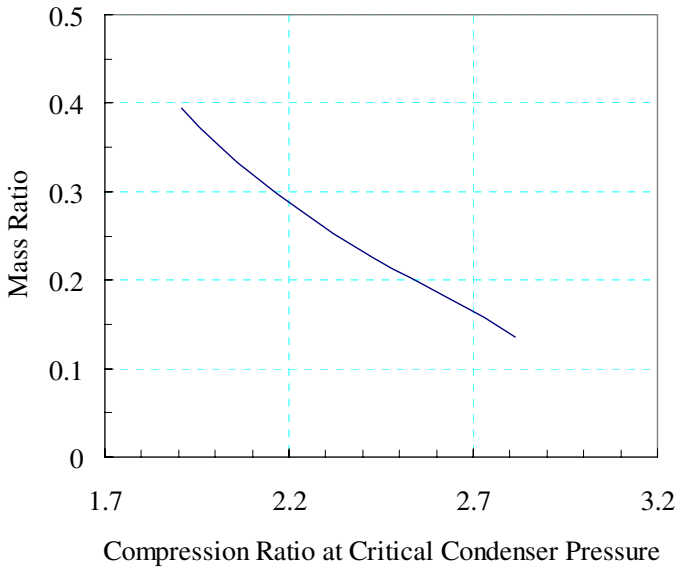

Figure 8-3 Mass Ratio (Entrainment Ratio) at Critical Compression Ratio

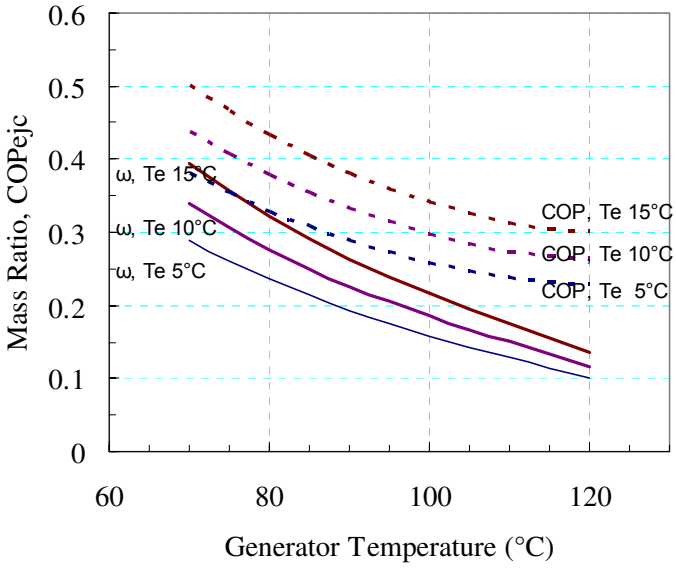

Figure 8-4 Mass Ratio and COP_{ejc} at Different Generator and Evaporator Temperatures

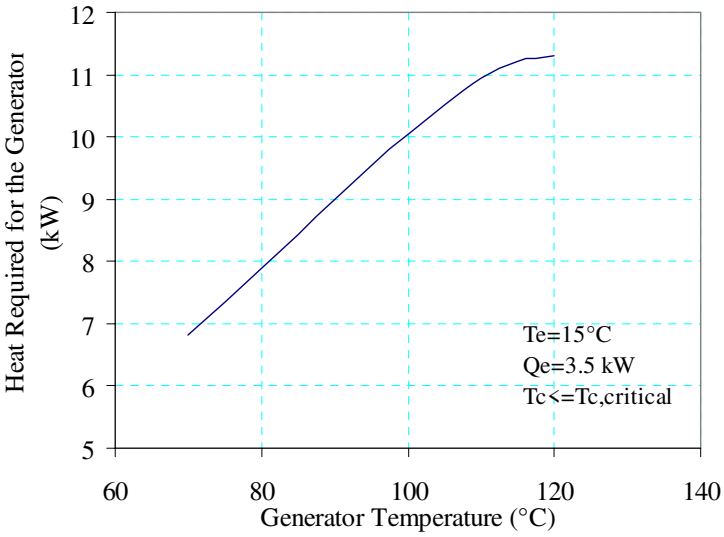

Figure 8-5 Heat Required for the Generator at Different Generator Temperatures

8.3 Results

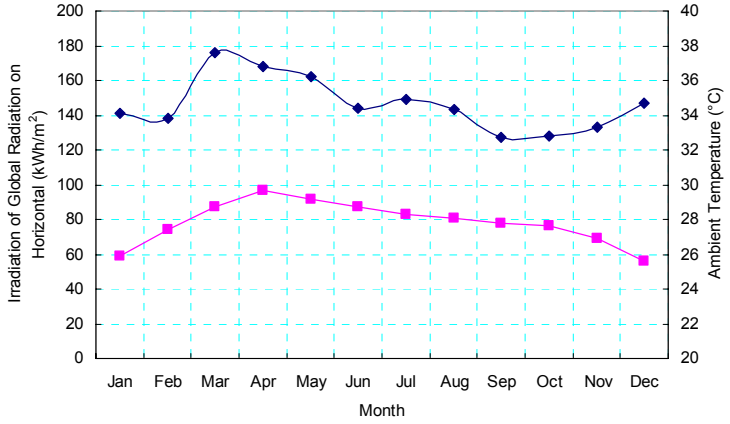

Figure 8-6 Average Solar Radiation and Ambient Temperature in One Year for Bangkok, Thailand

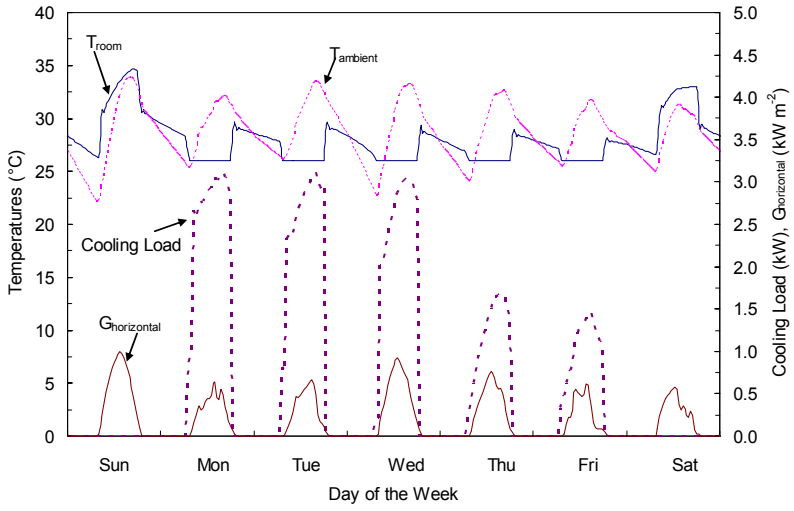

Figure 8-7 Solar Radiation and Load Characteristic in One Random Week

The average monthly solar radiation and ambient temperatures are shown in Figure 8-6 for the selection location, Bangkok. The climate data shown in Figure 8-6 comes from Meteonorm Software (Remund, Lang et al., 2001). Solar radiation and load characteristics in one random week are shown in Figure 8-7. The maximum cooling load is about 3.5

kW. The room temperature is maintained at a maximum of 26°C during work time on weekdays (8:00-18:00). The generator temperature will vary between 70-120°C due to variations in insolation. The instantaneous STR is thus changing due to both the available generator temperature and the variation of the solar radiation. The lowest generator temperature allowed is set at 70°C in the model. This minimum temperature level is maintained by energy from the auxiliary heater when the solar radiation is low. Previous analysis has shown the importance of a low condenser temperature to maintain the operation of the ejector. In this case, the condenser temperature is therefore set to 5K above the ambient temperature. Again, a higher evaporator temperature is favourable if possible.

Figure 8-2 and 8-3 clearly indicate that an efficient ejector system can only work in a region with decent incident solar radiation and where a sufficiently low condenser temperature can be maintained.

Average yearly system performance in terms of solar collector efficiency, COP_{ejc} and STR is shown in Figure 8-9. In this case, the evaporator temperature is varied, while the condenser temperature is assumed to be 5 K above the ambient temperature. The generator temperature depends on the solar radiation but the minimum is set at 70°C in this simulation.

Effects of operating temperatures on the performance of the system have been shown in the previous chapter. Due to the fact that the main energy source for this system is free, thus the solar fraction, defined in Equation 2-22, is better suited for showing the effectiveness of the system. Results from the dynamic simulation are shown in Figure 8-8, Figure 8-9 and Figure 8-10.

The size of the storage tank does not considerably influence the system performance as can be seen in Figure 8-9. However, a proper storage tank is recommended in order to increase the stability and performance of the system. By using a larger storage tank, less auxiliary heat is required, therefore solar fraction is somewhat higher.

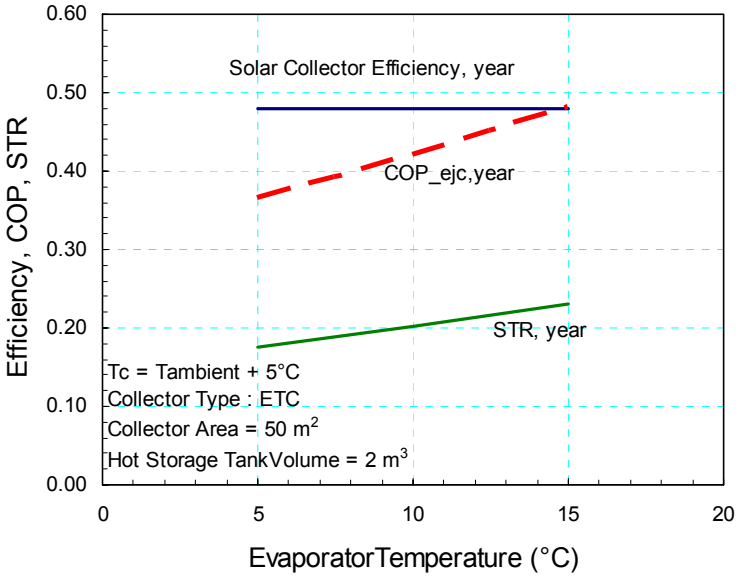

Figure 8-8 Average Solar Collector Efficiency, COP and STR in One Year

The condenser temperature significantly affects the performance of the system, especially if the condenser temperature is near the critical point. At condenser temperatures higher than the critical temperature, the performance of the system is dramatically decreased and the system is likely to stop completely‡‡‡ (will be discussed in Chapter 9, Figure 9-2). Lower condenser temperatures can minimize the required driving temperature, implying that the system must use a cooling tower or must be installed near a pond, a river or a sea.

The COP of the ejector refrigeration subsystem increases with the evaporator temperature as presented in Figure 8-8. For yearly simulation, an increase of the evaporator temperature by 5K, results in an increase of the yearly COP by 15% and an increase of the STR by 15%.

Figure 8-9 and Figure 8-10 illustrate the solar fraction over the period of one year when the system is operated with different types of solar collectors. The evacuated tube solar collector yields much higher solar fraction values than the flat plate solar collectors. A flat plate collector can be

‡‡‡ A so-called transcritcal cycle is possible for some refrgerants but it is not treated here.

considered to minimise the installation costs, but the solar fraction is very poor thus resulting in high operational costs for auxiliary heat. In regions where a low condenser temperature can be maintained (e.g. <=30°C), it is not necessary to provide a high generator temperature, consequently, the flat plate solar collector can be considered.

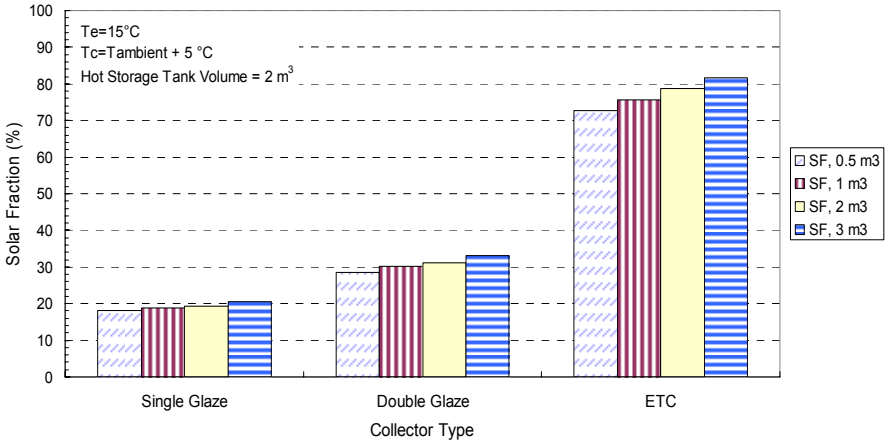

Figure 8-9 Effect of Storage Tank Size for Different Types of Solar Collectors at Collector Area of 80 m^2, T_c 5 K above the Ambient Temperature

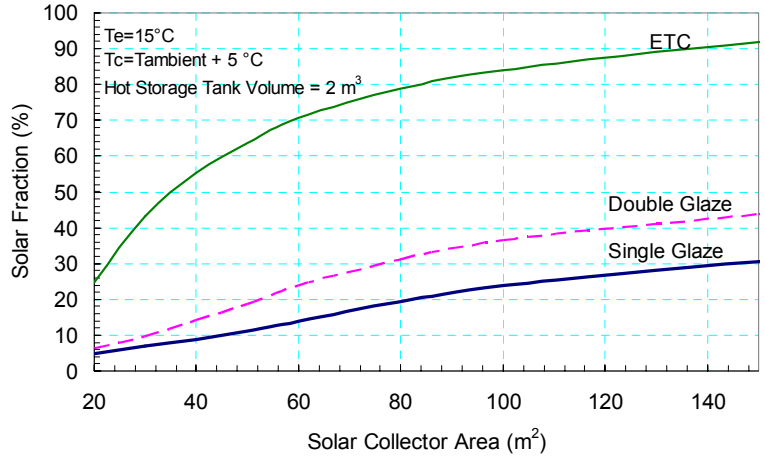

Figure 8-10 Solar Fraction for Different Types of Solar Collectors and Solar Collector Areas at Hot Storage Tank Volume of 2 m^3, T_c 5 K above the ambient temperature, and T_e +15°C

In the previous chapters, a flat plate double glaze solar collector was selected in the calculations. The calculation in the early stage showed that the temperature supply by the flat plate collector is enough to drive the refrigeration cycle using butane as the refrigerant. After performing the dynamic simulation, by using the flat plate collector yields a low solar fraction, in average of 30%. This means that high parasitic energy is required to operate the system. Due to low efficiency of the ejector refrigeration system, it is not economically advantageous if the solar fraction is too low. If the major part of the driving energy is supplied by an auxiliary heater it is better to choose a cycle with higher efficiency, such a double-effect absorption chiller.

The real challenge is however not the energy supply through the solar collector but rather the difficulty in maintaining the condenser temperature lower than the corresponding maximum back pressure. The hypothesis that the ejector refrigeration system can be installed with low quality solar collectors must therefore be abandoned for locations where the ambient temperature is too high. A large amount of poor economy auxiliary heat will be required unless the waste heat is free from industries etc.

Installation costs should always be taken into consideration. The cost of solar thermal collectors varies depending on type and quality. A flat plate collector costs between 55 - 615 Euro /m², which is relatively less than an evacuated tube, i.e. about 510 - 1300 €/m², (ISES-Germany, 2005). This thesis does however not deal with the economic optimization dilemma.

8.4 The Solar-driven Ejector Refrigeration Systems at Different Locations

The same 150 m³ building modelled in Chapter 3 and 4 in different locations is used in this sections simulation. Cooling demand in one year (in kWh) was shown previously in Figure 3-8. The maximum cooling effect (in kW) is the same as in Figure 3-9.

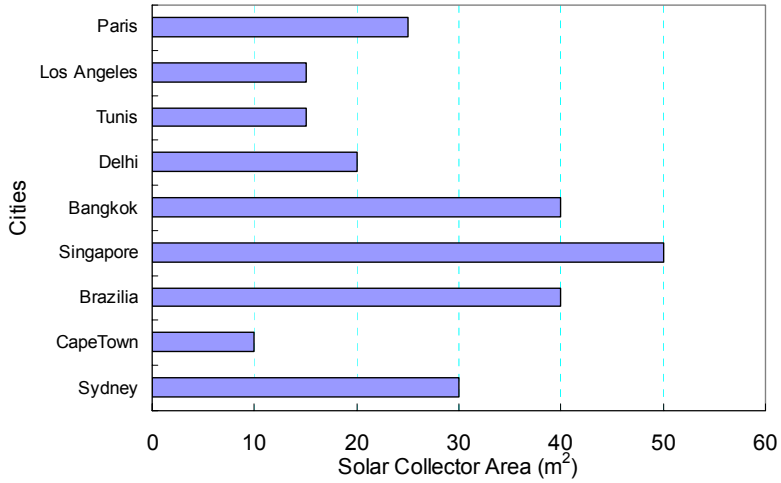

Figure 8-11 Solar Collector Area Required for the Solar-Driven Ejector Refrigeration System for Different Locations Using ETC collector at a Solar Fraction of 95%

The required solar collector area, corresponding to 95% of the solar fraction for the solar-driven ejector refrigeration system is shown in Figure 8-11. Cities located nearest the equator, require the largest solar collector area. The required solar collector area is smaller at higher latitude, but beyond the latitude of about 45°, the required collector area increases again, as the example of Paris. However, the required solar collector area per kW of cooling power in tropic regions is in average 15 m² per kW on a yearly basis. For latitudes above 45°N, or below 45°S the cooling season is short, even the collector area per cooling power is comparable with other locations, but the solar collector area per cooling load is high. Solar-driven ejector refrigeration systems may therefore not appear to be economically beneficial in this region due to high installation costs of the solar collector unless the avoided use of electricity is extremely highly valued. The system, however, can be competing with the conventional system on other terms because the solar collector subsystem can provide

heat in winter, as well as tap water heating. An interesting city for such an application is Cape Town. The ambient temperature of Cape Town is quite low, compared to other selected cities, even on a summer day. A comparison of the solar collector area per cooling load between the absorption cycle (Figure 3-11) and ejector cooling cycle (Figure 8-12), illustrates that in most locations, the ejector cooling cycle requires more collector area per cooling power than the absorption cycle. In a very hot environment, as in a tropical region, the absorption cycle requires less collector area per cooling power and is much more beneficial in terms of energy efficiency and installation costs. In the case of Cape Town, the average ambient temperature is quite mild compared to the ambient temperature of other selected locations (see Figure 3-7), thus the condenser temperature is lower than other locations. Low condenser temperature indicates that less driving energy is required, signifying that with high insolation, the system would require a relatively small solar collector area.

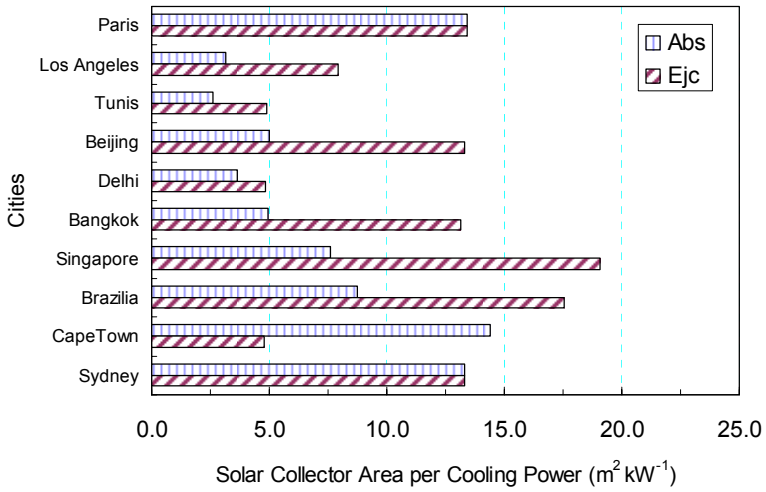

Figure 8-12 Solar Collector Area per Cooling Power (in kW) Required for Different Locations at a Minimum Solar Fraction of 95%

8.5 Conclusions

A change of the condenser temperature strongly influences system performance. In order to maintain the function of the system, condenser temperature must be kept equal or lower than the critical condenser temperature. The higher the condenser temperature, the higher generator temperature is needed. In tropical regions, the ambient temperature is constantly high; it is therefore difficult to maintain the required condenser temperature. Even if the system can be operated at a sufficiently low generator temperature, and installation costs of the system using a flat plate collector are cheaper than the evacuated tube; results from the dynamic simulation of the solar-driven ejector refrigeration system clearly show that the system using evacuated tube solar collectors yields a higher solar fraction than the flat plate solar collector. In this case, it is not likely to be economically competitive using the flat plate collector due to the high amount of auxiliary heat required unless waste energy from industries is available.

Larger storage tanks give better solar fraction. Even though the increasing value of the solar fraction is not significantly high, but the thermal storage tanks are necessary to secure the operation.

Compared with solar-driven absorption systems, the solar-driven ejector refrigeration system illustrates a favorable benefit in areas where the ambient temperature is mild and the insolation is high e.g. Cape Town. The system illustrates a comparable benefit in Paris and Sydney.

Results from the exergy analysis (Chapter 7) illustrate that the highest irreversibility in the ejector refrigeration cycle occurs in the ejector. Together with results from the dynamic simulation in this chapter one can argue that a better understanding of the ejector will improve functionality and performance of the system. Therefore, it is important to go further into detail regarding ejector design, which will be done in the next chapter.

PART III:
Ejector Design and Experimental Studies

This part consists of:

Chapter 9 Ejector Design

9.1 Theoretical Analysis

9.2 Test Results of the Ejector

9 Ejector Design

Results from the exergy analysis and dynamic simulation have demonstrated that a better understanding of the ejector is vital for the design of solar-driven ejector refrigeration systems. It is additionally the most complicated part to design in an ejector refrigeration cycle. The design of ejectors is typically based on the theoretical expression of ideal gas dynamics together with experimental data. Empirical equations for steam ejectors, on the other hand, are quite well known and can be found in several handbooks e.g. ASHRAE, 1983. Empirical design data for other working fluids i.e. water, is however, rarely presented. In this chapter a theoretical analysis of the ejector is performed. The design procedure for each section is based on the theoretical expression of ideal gas behaviour and some empirical equations found in literature. One ejector has been tested in the project with refrigerant R134a and the result is presented at the end of this chapter.

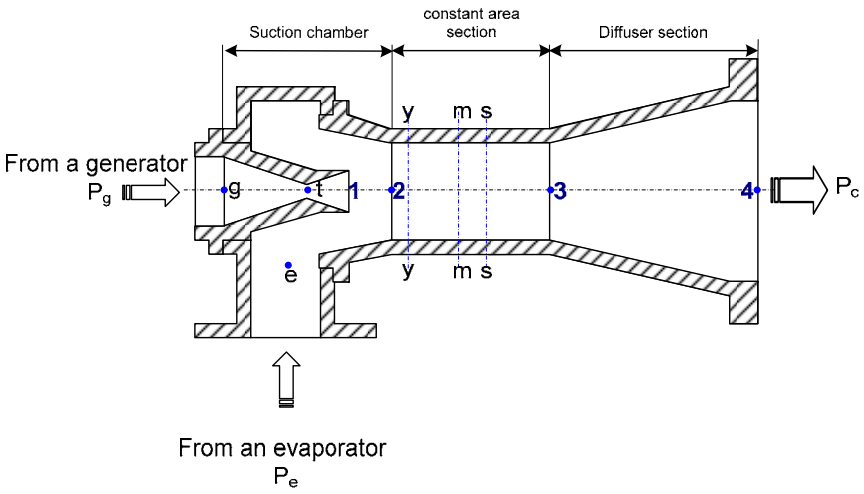

Figure 9-1 Ejector Geometry and Sections

9.1 Theoretical Analysis

An ejector is a device in which a higher pressure fluid (also called primary fluid) is used to induce a lower pressure fluid (called secondary fluid) into the ejector. Fluids from these two streams mix together and discharge to a pressure that lies between the pressures of these two fluids. In an ejector refrigeration cycle, the ejector and a pump are used instead of a compressor (in a vapour-compression system) for producing a cooling power.

An ejector consists of 3 main parts: a suction chamber, a constant area and mixing chamber and a diffuser. A schematic of ejector geometry is shown in Figure 9-1. When the primary flow goes through a converging-diverging nozzle in the ejector; vapour is drawn from the evaporator. The secondary flow is accelerated to a high velocity vapour stream and reaches subsonic velocity. Mixing starts at the onset of the constant-area section (section y-y, hypothetical throat, in Figure 9-1). In section y-y, both streams develop uniform pressure; choking of the secondary flow occurs. A combined stream develops into a transient supersonic stream and shocks at section s-s. The velocity of the mixing fluid must be high enough to increase the pressure after deceleration in the diffuser to a suitable condensing pressure.

Different ejectors generally have contrasting characteristics, producing a variety of performances. Ejector performance is primarily dependant on design and operating conditions. For the best performance, double choking should be considered. Design principle of the steam ejector can be used as a guideline for other working fluids, but cannot be exclusively applied for every case. There is no unique solution for every single ejector. Hypothetical throat analysis can be used as a key for calculating performance and dimensioning the ejector when operating the ejector in a critical mode.

Ejector design is generally classified into two categories, depending on the position of the nozzle, as

1. "*Constant-Area Mixing Ejector*": the exit of the nozzle is inside the constant area of the ejector. Primary and secondary fluids mix at the constant area.

2. "*Constant-Pressure Mixing Ejector*": the exit of the nozzle is in the suction chamber, before the constant area. Primary and secondary flows mix in the suction chamber at a specific pressure. Pressure of the mixing streams remains constant along the chamber from the nozzle exit to the inlet of the constant area section.

The constant-pressure mixing ejector is more promising than the constant-area mixing ejector because it generates better performance. With this design concept, mixing occurs in the constant-area section (Keenan, Neumann et al., 1950; Huang and Chang, 1999). Choking phenomena can be observed in 2 places: the primary flow through the nozzle and the secondary flow. Choking in the secondary flow is due to acceleration of the flow from the stagnant state; this happens in the suction chamber at the inlet of the supersonic flow to the constant-area section. Performance of the ejector is as described previously, generally measured by a mass flow ratio between the streams from the evaporator and generator, called the entrainment ratio (ω).

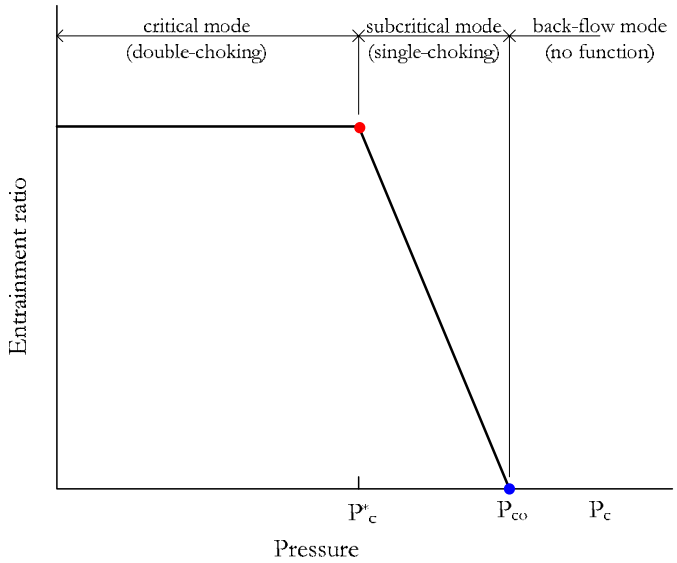

Figure 9-2 Operation Modes

At a specific primary pressure (P_g) and secondary pressure (P_e), the entrainment ratio is dependent on a back pressure (also called condenser pressure, P_c). There are 3 operation modes, according to the back pres-

sure. Best performance can be obtained at the critical mode, where the back pressure is lower than the critical pressure. In this state, the entrainment ratio is constant and choking phenomenon occurs both in the primary and entrained flow. The entrainment ratio decreases when the back pressure increases higher than the critical pressure; choking exists only in the primary flow but not in the secondary flow. If the back pressure is higher than P_{co}(see Figure 9-2), there will be no choking phenomena in either flow. P_{co} is considered as the limiting pressure of ejector operational mode. The operation would then subsequently fail.

The following analysis originates with the expansion process of the primary flow through the nozzle, followed by the analysis of secondary flow and mixed flow at different cross sections, and the flow through the diffuser at the end.

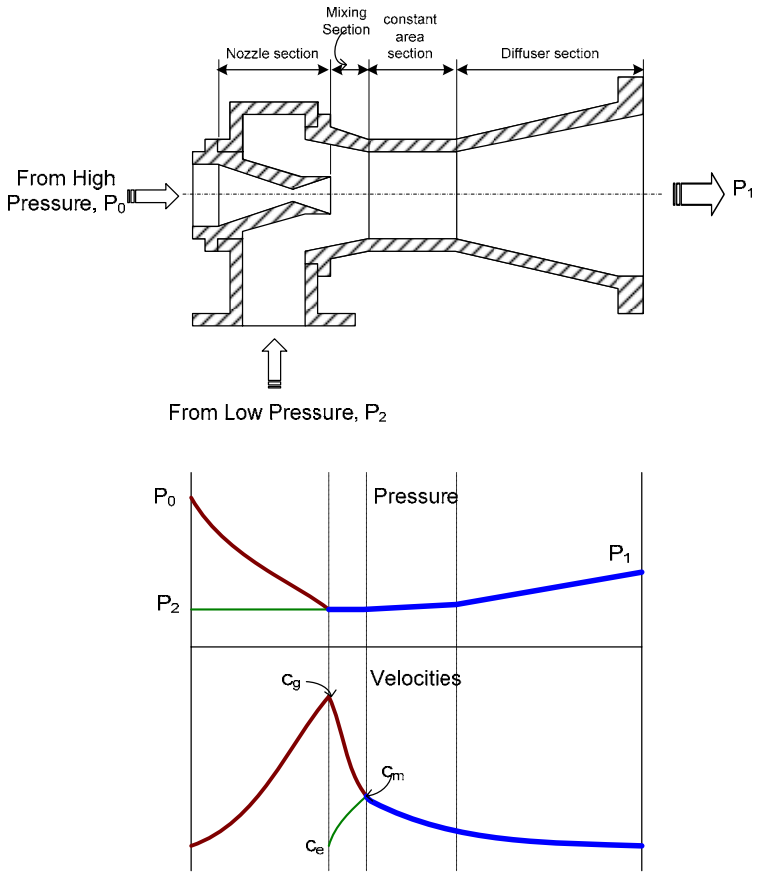

Figure 9-3 The Geometric, Pressure and Velocity Diagram in an Ejector

Analysis assumes the process in the ejector to be adiabatic. Kinetic energy of the inlet and outlet flows is not considered. Friction and mixing loss is accounted in the form of isentropic efficiency. Flow inside the ejector is assumed to be steady and the working fluid has constant properties along the ejector.

The expansion process of the primary flow through the nozzle

Vapour from the generator expands irreversibly in the primary nozzle creating a partial vacuum at the nozzle exit. Applying the first law of thermodynamics by using the energy balance equation:

$$q = \varepsilon_t + h_B - h_A + \frac{c_B^2 - c_A^2}{2} + g \cdot (z_B - z_A) \qquad \textit{Eq. 9-1}$$

With the assumption of adiabatic condition (q = 0), no work (ε_t =0), and no influence of elevation change ($z_B = z_A$), the velocity of the stream at the nozzle exit (c_g) can be expressed as;

$$c_g = \sqrt{2 \cdot (h_g - h_m)} \qquad \textit{Eq. 9-2}$$

$$= \sqrt{2 \cdot \eta_N \cdot (h_g - h_{gm,is})} \qquad \textit{Eq. 9-3}$$

Where a nozzle's isentropic efficiency (η_N) can be defined as;

$$\eta_N = \frac{h_g - h_m}{h_g - h_{gm,is}} \qquad \textit{Eq. 9-4}$$

where

h_m = enthalpy of the mixing fluid at mixing point

h_g = enthalpy of the driving (primary) fluid from the generator

$h_{gm,is}$ = enthalpy of the driving fluid (primary) from the generator expanded isentropically to the mixing pressure.

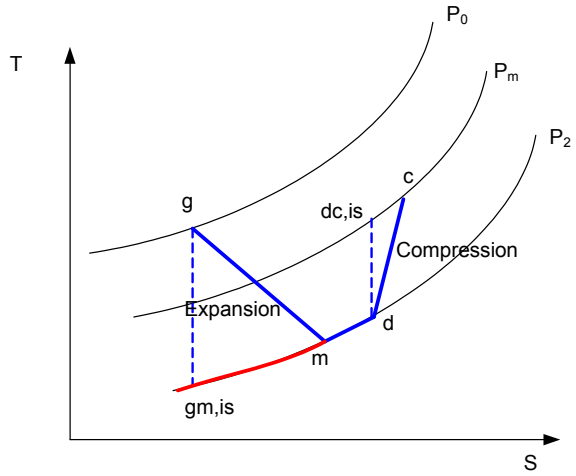

Figure 9-4 The T-S Diagram for Expansion and Compression Process

The mass flow from the generator through the nozzle at choking condition can be expressed as,

$$m_g = P_g \cdot A_t \cdot \sqrt{\frac{\eta_N \gamma}{T_g R}\left(\frac{2}{\gamma+1}\right)^{\gamma+1/\gamma-1}} \qquad \textit{Eq. 9-5}$$

The mach number of the fluid from the generator ($Ma_{g,1}$), which expands through the nozzle can be depicted as,

$$Ma_{g,1} = \sqrt{\frac{2 \cdot \eta_N}{\gamma - 1}\left[1 - \left(\frac{p_1}{p_g}\right)^{\frac{\gamma-1}{\gamma}}\right]} \qquad \textit{Eq. 9-6}$$

The relation between the Mach number and the cross sectional area can be depicted as,

$$\left(\frac{A_{g1}}{A_t}\right)^2 \approx \frac{1}{Ma_{g1}^2}\left[\frac{2}{\gamma+1}\left(1+\frac{\gamma-1}{2}Ma_{g1}^2\right)\right]^{(\gamma+1)/(\gamma-1)} \quad \textit{Eq. 9-7}$$

$$\frac{P_g}{P_{g1}} \approx \left(1+\frac{(\gamma-1)}{2}Ma_{g1}^2\right)^{\frac{\gamma}{\gamma-1}} \quad \textit{Eq. 9-8}$$

The Mach number of the primary flow at cross section y-y can be calculated from

$$\frac{P_{gy}}{P_{g1}} \approx \left(\frac{1+\left(\frac{\gamma-1}{2}\right)Ma_{g1}^2}{1+\left(\frac{\gamma-1}{2}\right)Ma_{gy}^2}\right)^{\gamma/(\gamma-1)} \quad \textit{Eq. 9-9}$$

The area of the primary flow core at the y-y section is calculated by using the isentropic relation including an arbitrary coefficient,ϕ, signifying loss in the flow from section 1-1 to y-y.

$$\frac{A_{gy}}{A_{g1}} \approx \frac{\phi_g / Ma_{gy}}{1/Ma_{g1}}\left(\frac{\frac{2}{\gamma+1}\cdot\left(1+\left(\frac{\gamma-1}{2}\right)Ma_{gy}^2\right)}{\frac{2}{\gamma+1}\cdot\left(1+\left(\frac{\gamma-1}{2}\right)Ma_{g1}^2\right)}\right)^{(\gamma+1)/2\cdot(\gamma-1)} \quad \textit{Eq.9-10}$$

The arbitrary coefficient for the primary flow (ϕ_g) leaving the nozzle can be assumed to be around 0.88, according to Huang and Chang, 1999.

In essence, the throat area of the primary flow can be calculated by first assuming the throated pressure and calculating the mass flux through this throat. Calculations will be done until the maximum mass flux through this throat is displayed. The first assumed throated pressure could be the throated pressure which generates the unity Mach number (Eq. 9-11). The procedure for calculating the nozzle throat area is shown in Figure 9-5.

$$P_t = P_g\left(1+\frac{(\gamma-1)}{2}\right)^{\gamma-1/\gamma} \qquad \textit{Eq. 9-11}$$

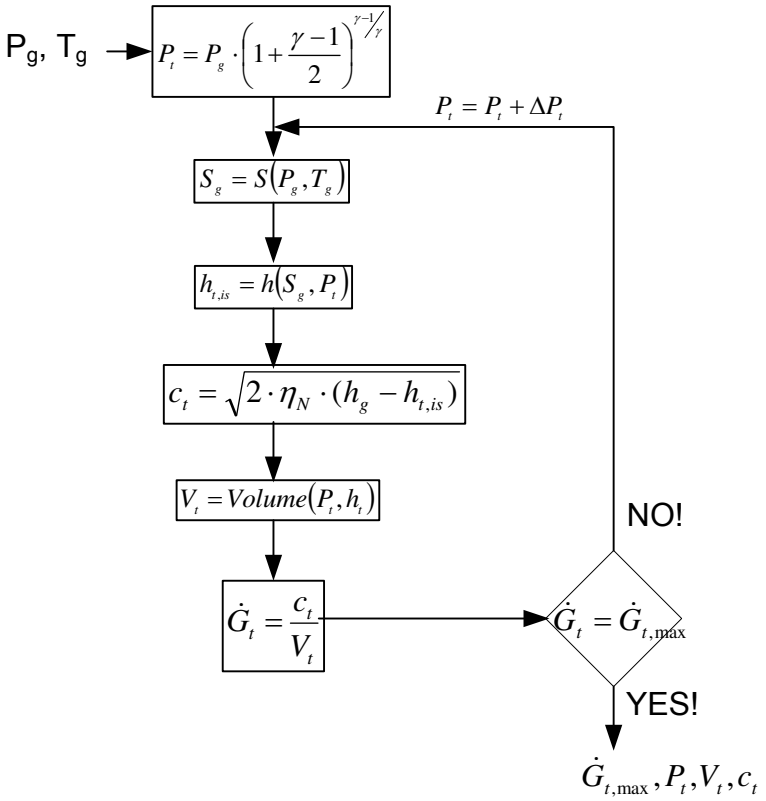

Figure 9-5 Procedure for Calculating Nozzle Throat Diameter

The Secondary Flow

The secondary flow rate at choking condition (section y-y) is illustrated as,

$$m_e = \frac{P_e A_{ey}}{\sqrt{T_e}}\sqrt{\frac{\gamma}{R}\left(\frac{2}{\gamma+1}\right)^{\lambda+1/\gamma-1}}\sqrt{\eta_{Ne}} \qquad \textit{Eq. 9-12}$$

Assuming that the entrained flow reaches choking conditions, the Mach number of the secondary flow at section y-y is approximately one,

$$Ma_{ey} = \sqrt{\frac{2}{\gamma - 1}\left[1 - \left(\frac{P_e}{P_{ey}}\right)^{\gamma-1/\gamma}\right]} \qquad \textit{Eq. 9-13}$$

The area at the entrance of the secondary flow to the mixing zone can be calculated in a similar way by calculating the throat diameter of the nozzle. The procedure is shown in Figure 9-6.

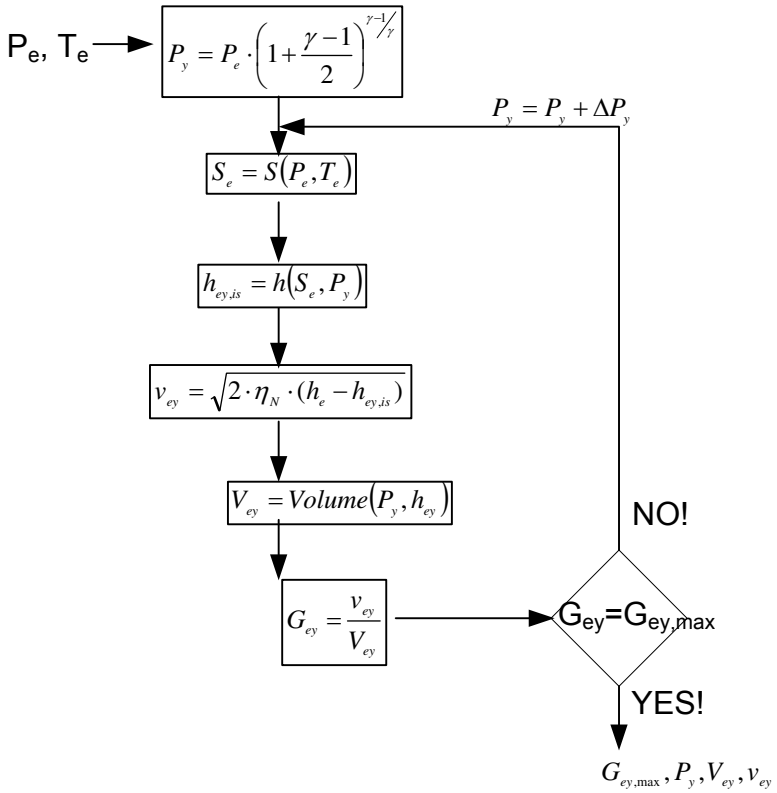

Figure 9-6 Procedure for Calculating Throat Diameter of the Secondary Flow

Cross-sectional area at section y-y (A_3)

A cross-sectional area at y-y is the summation of the area for primary flow (A_{gy}) and entrained flow (A_{ey}),

$$A_3 = A_{ey} + A_{gy} \qquad \textit{Eq. 9-14}$$

Mixing Section

Energy balance at the mixing point can be expressed as;

$$(m_g + m_e) \cdot h_m = m_e \cdot h_e + m_g \cdot h_{g,\exp} \qquad \textit{Eq. 9-15}$$

where

h_m = enthalpy of the mixing fluid at the mixing point

h_e = enthalpy of the entrained refrigerant (secondary fluid) from the evaporator

$h_{g,exp}$ = enthalpy of the driving fluid from the generator after expansion through the nozzle.

The temperature and the Mach number of the streams at section y-y can be written as,

$$\frac{T_g}{T_{gy}} = 1 + \frac{\gamma - 1}{2} Ma_{gy}^2 \qquad \textit{Eq. 9-16}$$

$$\frac{T_e}{T_{ey}} = 1 + \frac{\gamma - 1}{2} Ma_{ey}^2 \qquad \textit{Eq. 9-17}$$

A vacuum exists at the exit of the nozzle, thus the stream from the evaporator is sucked to the ejector. The entrained stream then mixes perfectly with the higher-pressure stream from the generator. For simplicity we assume that the mixing pressure is constant. Pressure remains unchanged while mixing of the two streams takes place.

The mass conservation law of impulse can be written as:

$$\phi_m (m_g \cdot c_{g,\exp} + m_e \cdot c_e) = (m_g + m_e) \cdot c_m \qquad \textit{Eq. 9-18}$$

where

m_g = mass flow of driving (primary) fluid from generator

m_e = mass flow of the entrained (secondary) refrigerant from the evaporator

$c_{g,exp}$ = velocity of driving (primary) fluid from the generator after expansion in the nozzle entering the mixing section

c_e = velocity of entrained (secondary) refrigerant from the evaporator

c_m = velocity of mixing fluid leaving the mixing section

An arbitrary coefficient accounting for friction loss ϕ_m, varies with the ejector area ratio (A_3/A_t). Huang and Chang, 1999, reported that

$$\phi_m = 0.80 \; for \; \frac{A_3}{A_t} > 8.3 \qquad \textit{Eq. 9-19}$$

$$\phi_m = 0.82 \, for \; 6.9 \le \frac{A_3}{A_t} \le 8.3 \qquad \textit{Eq. 9-20}$$

$$\phi_m = 0.84 \; for \; \frac{A_3}{A_t} < 6.9 \qquad \textit{Eq. 9-21}$$

It can also be expressed as an equation:

$$\phi_m = 1.037 - 0.02857 \cdot \frac{A_3}{A_t} \qquad \textit{Eq. 9-22}$$

The length of the mixing section is generally defined in terms of the throat diameters. For steam jet ejectors, the recommended lengths are

different, depending on the research groups. However, all of them are in the range of 6-10 times the throated diameter.

$$L_{mix} = 7 \cdot D_3, \text{ (ASHRAE, 1983)} \qquad \text{Eq. 9-23}$$

$$L_{mix} = 6 \cdot D_3, \text{ (Chang and Chen, 2000)} \qquad \text{Eq. 9-24}$$

The angle of the mixing section is also important. Ejector efficiency will be reduced if the angle is too large, contrarily, if the angle is too small, the ejector will not be able to compress the vapour flow to design condensing pressure. Angles of the mixing section cone are about 7-10 degrees for the first portion and 3 to 4 degrees for the second portion (ASHRAE, 1983).

The velocities of the primary and secondary flows at section y-y can be expressed as:

$$c_{gy} = Ma_{gy} \cdot \sqrt{\gamma \cdot R \cdot T_{gy}} \qquad \text{Eq. 9-25}$$

$$c_{ey} = Ma_{ey} \cdot \sqrt{\gamma \cdot R \cdot T_{ey}} \qquad \text{Eq. 9-26}$$

Constant Area Section

In the constant area section, supersonic shock occurs around section s-s (Figure 9-1). The shock is that happens here includes complex oblique shock patterns (ASHRAE, 1983); this is due to a thick boundary layer and a very peaked velocity profile.

For an efficient ejector, the length of the constant-area throat section is recommended to be three to five throat diameters long (ASHRAE, 1983). Chang and Chen, 2000, recommended this length to be five throat diameters long.

Assuming that the mixed flow after the shock undergoes an isentropic process, the pressure of the mixed flow from m-m to 3-3 is constant at P_3.

$$P_3 = P_m \cdot \left[1 + \frac{2\gamma}{\gamma+1}\left(Ma_m^2 - 1\right)\right] \qquad \textit{Eq. 9-27}$$

$$Ma_3^2 = \frac{1 + \left(\frac{\gamma-1}{2}\right)Ma_m^2}{\gamma Ma_3^2 - \left(\frac{\gamma-1}{2}\right)} \qquad \textit{Eq. 9-28}$$

The Mach number of the stream after the shock flow is,

$$Ma_3 = \sqrt{\frac{Ma_2^2 + \frac{2}{\gamma-1}}{\left(\frac{2\gamma}{\gamma-1}\right)Ma_2^2 - 1}} \qquad \textit{Eq. 9-29}$$

In ASHRAE, 1983, it is mentioned that the constant-area section diameter is a critical design parameter. Several methods for calculating this dimension are given in the literature; however, none are accurate. The only way to determine this is by experiment or, possibly, an analysis of manufacturer data.

Diffuser

After mixing, the mixing stream forms a single supersonic stream and moves forward through a constant-area section with transverse shock to the diffuser. In the diffuser section, the stream will be compressed to condensing pressure and the velocity of the stream will decrease.

The subsonic diffuser is conical in shape. For the steam ejector, the angle can be in the range of 5 to 12 degrees with an axial length of 4 to 12 throat diameters (ASHRAE, 1983). Chang and Chen, 2000 recommended the axial length to be 6 times the throat diameter.

From the equation of energy conservation, the velocity of the mixing stream can be written as,

$$c_m = \sqrt{2 \cdot (h_c - h_d)} = \sqrt{2 \cdot (1/\eta_D) \cdot (h_{dc,is} - h_d)} \qquad \textit{Eq. 9-30}$$

The nomenclature 'c, d and dc,is' here refers to the point in Figure 9-4.

A diffuser isentropic efficiency (η_D) is defined as,

$$\eta_D = \frac{h_{dc,is} - h_d}{h_c - h_d} \qquad \textit{Eq. 9-31}$$

The stream is compressed to a higher pressure, based on an assumption of a reversible adiabatic process in the subsonic flow. The velocity at the exit is assumed to be zero, the pressure lift in the diffuser can thus be estimated as:

$$\frac{P_4}{P_3} = \left(\frac{\eta_D(\gamma - 1)}{2} Ma_3^2 + 1 \right)^{\gamma/\gamma - 1} \qquad \textit{Eq. 9-32}$$

Performance

The performance of an ejector is generally defined in terms of the mass flow rate ratio between the streams from the evaporator and generator, called the entrainment ratio (ω). The following equations of the entrainment ratio have been previously defined in Section 4-2. They are repeated again here for the convenient of the reader.

$$\omega = \frac{m_e}{m_g} \qquad \textit{Eq. 9-33}$$

From the mass conservation law of impulse (Equation 9-1) and the velocity equations;

$$\omega = \frac{c_g}{c_m} - 1 \qquad \textit{Eq. 9-34}$$

$$\omega = \sqrt{\frac{h_g - h_m}{h_c - h_d}} - 1 \qquad \textit{Eq. 9-35}$$

$$\omega = \sqrt{(\eta_N \cdot \eta_D) \frac{h_g - h_{gm,is}}{h_{dc,is} - h_d}} - 1 \qquad \textit{Eq. 9-36}$$

In addition, the entrainment ratio can be described by the ratio of the Mach number between the streams of the evaporator and generator (Riffat and Holt, 1998).

$$\omega = \frac{Ma_e}{Ma_g} \qquad \textit{Eq. 9-37}$$

The nozzle position is an important parameter. The distance between the nozzle exit and constant area (section x-x) is suggested by Huang, Chang et al., 1999 to be about 1.5 times the constant-area chamber diameter.

Equations for ejector design are illustrated as procedure in Figure 9-7. This procedure can be used after the throat diameters in both primary and secondary flow have been selected or calculated (see Figure 9-5 and Figure 9-6).

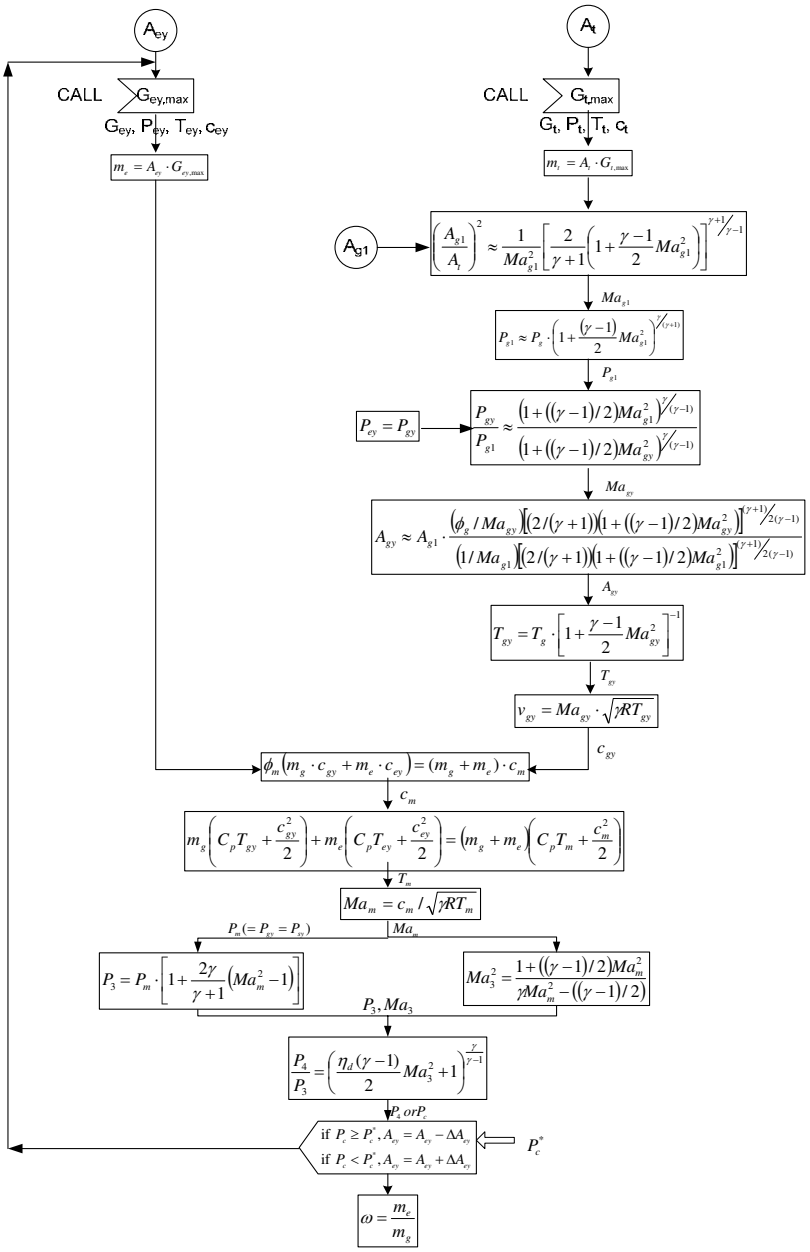

Figure 9-7 Procedure for Calculating Ejector Dimension

9.2 Test Results of the Ejector

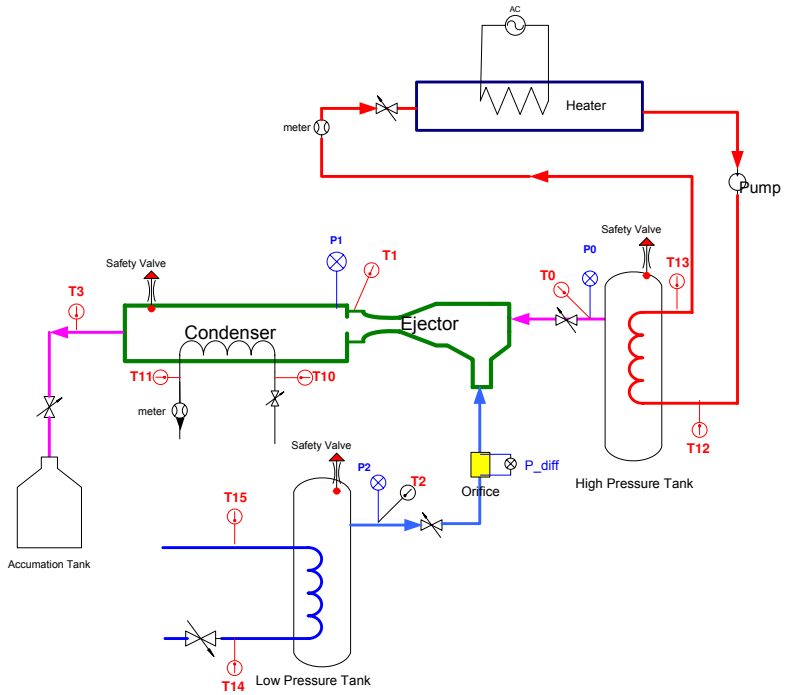

Figure 9-8 Schematic of the Experiment

The schematic of the test rig is shown in Figure 9-8. The high pressure tank is adapted from a shell and tube heat exchanger, consisting of 11.8 litres. The refrigerant is always kept saturated and the pressure and temperature in the tank is controlled by hot water. Hot water is heated by the electric heater at the rated capacity of 12 kW; the heat supply is adjusted by the flow rate of the heating media (water) and electric power controller. The low pressure tank is modified from a 5.1 litre shell and tube heat exchanger. The flow from the ejector is purged to the condenser and collected in the accumulator, which is connected at the end of the condenser.

Pressure in the low pressure tank and condenser are measured by the pressure transducer from 'Druck' (Druck, 2006), model PTX 610-0I. High pressure from the generator is measured by the pressure transducer series 22S from 'ClimaCheck' (ClimaCheck, 2006). The pressure differ-

ence over the orifice is detected by a differential pressure transducer from 'Druck', model PDCR 2160. All thermocouples are T-type. Thermocouples are connected to a Hewlett Packard data logger, via an isothermal box. The reference temperature in the isothermal box is measured by a Pt-100 element. Uncertainty in absolute temperature readings is expected to be less than 0.1 K. The ejector with one fix dimension as shown in Table 9-1and Figure 9-9, was tested. The ejector was built in seven parts. All parts were assembled in an aluminium chamber. Dividing the ejector in many parts makes it easy to fabricate and convenient to change the dimension of each section, which may not be suitable for some operating conditions. R134a was chosen as the test fluid for safety reasons (R600a and R600 were not possible to use, due to laboratory safety measures).

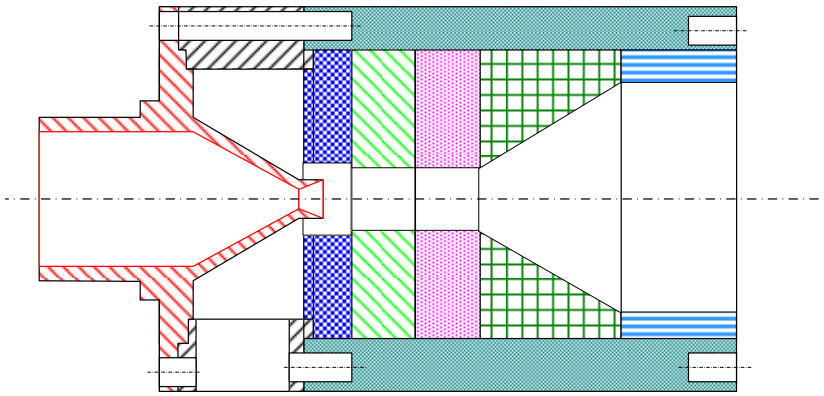

Figure 9-9 Schematic of the Tested Ejector (not in the Right Scale)

Table 9-1 Ejector Geometry

Parts	Dimension (mm)
Primary Nozzle	
Nozzle diameter	2
Nozzle inlet diameter	25
Nozzle outlet diameter	7
Secondary Inlet	
Inlet of the secondary flow	21
Area of the secondary flow to the mixing chamber	40.07 mm^2
Mixing Section	
Mixing Chamber Diameter	8
Minxing Chamber Length	16
Constant Area Section	
Constant Area Chamber Diameter	5
Constant Area Length	12
Diffuser	
Diffuser Inlet Diameter	5
Diffuser Outlet Diameter	50
Diffuser Chamber Length	15

Mass flow rate of the primary flow from the ejector is calculated from the pressure of the working fluid in the generator. The flow is assumed to be choked when the refrigerant flows through the nozzle. The velocity and the mass flow rate are independent of the downstream conditions. Velocity of the fluid at the throat of the nozzle is equal to the velocity of sound at prevailing conditions. Velocity and mass flow rate cannot be increased further even by reducing downstream pressure. The choke flow rate depends primarily on the specific heat capacity ratio (C_p/C_v), throat diameter and pressure. It can be calculated according to Equation 9-11.

$$m_g = P_g \cdot A_t \sqrt{\frac{\eta_N \gamma}{T_g R}\left(\frac{2}{\gamma+1}\right)^{\gamma+1/\gamma-1}} \qquad \textit{Eq. 9-38}$$

Specific heat capacity ratio and saturation pressure of R134a are shown in Figure 9-10. Critical temperature and pressure of R134a are at 101° and 40.59 bar. At saturated pressure higher than 90°C, the specific heat capacity ratio of R134a increases exponentially.

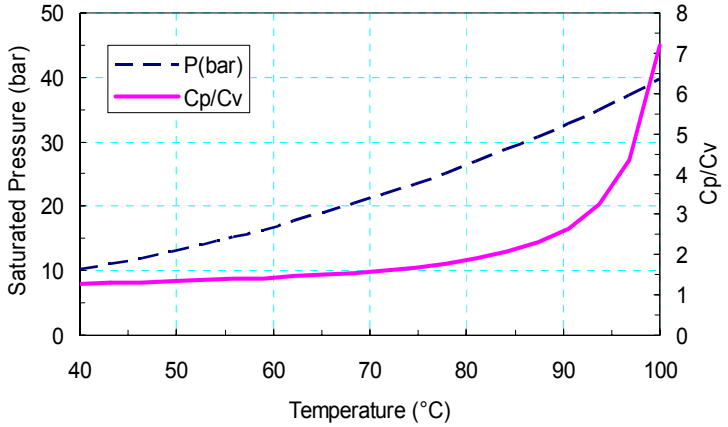

Figure 9-10 Saturation Pressure and Specific Heat Capacity Ratio of R134a

At the tested dimension, the 2 mm nozzle throat diameter, choked flow rate at various pressures of R134a is shown in Figure 9-11.

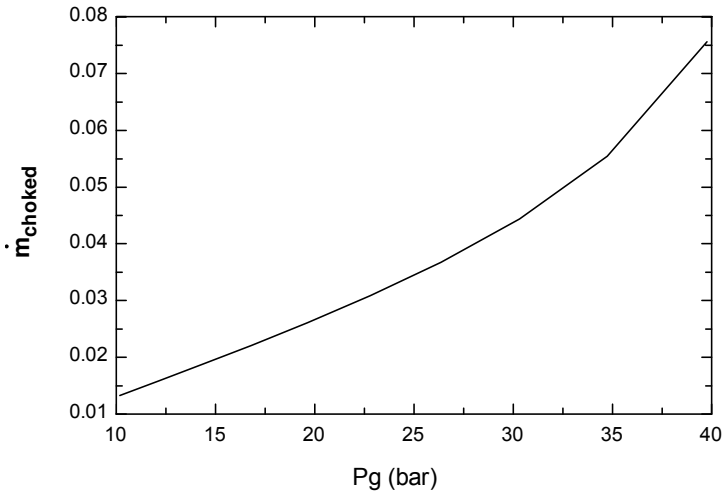

Figure 9-11 Mass Flow Rate of the Primary Flow from the Generator

Secondary mass flow rate in this experiment is calculated from the pressure difference over the orifice. Mass ratio at different generator and condenser pressures is shown in Figure 9-12. Mass flow rate of the primary flow becomes choked at the nozzle throat, and the choked flow rate increases when the driven pressure increases (as shown in Figure 9-11). Maximum secondary flow cannot exceed the choked flow through the secondary flow inlet, and pressure of the secondary flow does not change notably. Mass ratio is then lower at the higher generator temperature. Conversely, critical back pressure (condenser pressure) is higher. This indicates that in an environment of high ambient temperature, condenser temperature is generally high; therefore high generator temperature is required.

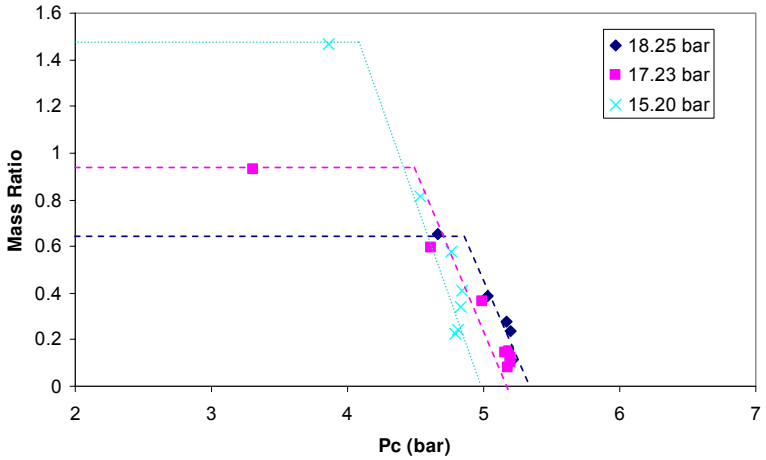

Figure 9-12 Mass Ratio of the Tested Ejector at Different Generator Temperatures

In this test, the author could not conduct an analysis of the driven pressure higher than 20 bar in the lab due to security regulations. This notably limits the range of the test. Increasing driving pressure increases the compression ratio, but decreases the mass ratio as shown in Figure 9-13 and Figure 9-14.

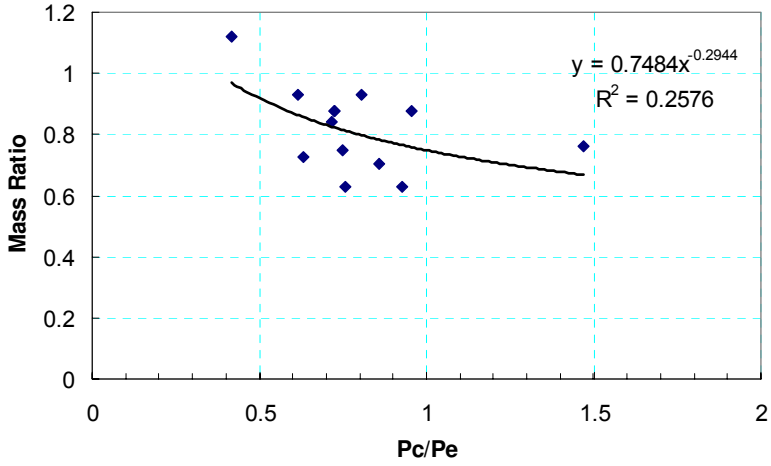

Figure 9-13 Mass Ratio of the Tested Ejector at Different Compression Ratio

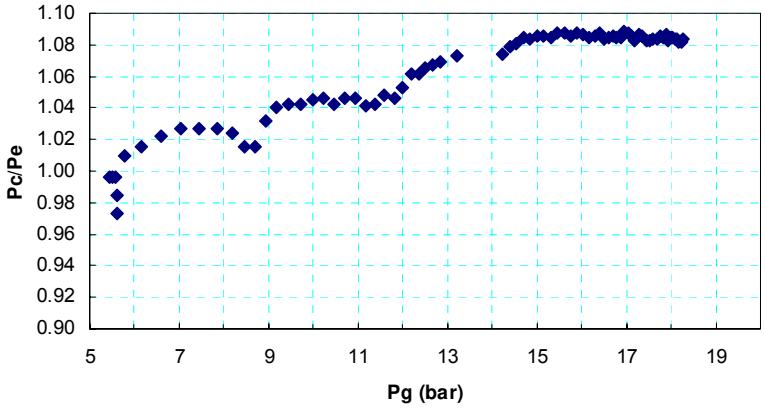

Figure 9-14 Compression Ratio of the Tested Ejector at Different Generator Temperature

Results of the test indicate that the function of the ejector is strongly dependant on the back pressure or condenser pressure. Thus in real operating condition it is critical to provide efficient condenser cooling at start up to maintain the functionality of the ejector. One fixed dimension ejector can only operate in a limited range of generator/condenser temperatures. This implies that, in a real case, an ejector with adjustable dimensions or multi-ejectors in parallel might be required. Furthermore, a good control system with valves is needed to direct the flow to the right ejector or change the dimension of the ejector. This will add undesired complexity to the system.

10 Conclusions & Future Work

10.1 Conclusions

Solar energy as a renewable energy source for driving cooling machines has for a long time been a favourite topic for many researchers. In the early stages of development, solar cooling focused on refrigeration of perishable goods and vaccine storage. Today, the demand for air-conditioning for human thermal comfort is growing rapidly and occasionally influences the power supply structure in a negative manner. The European Solar Thermal Industry Federation (ESTIF) reported that solar cooling capacity was about 6.3 MW for 70 installation units survey time (2004) and was predicted to increase to about 12% in 2004 and 2005 (IIR, 2006).

Many novel and innovative solar-driven refrigeration systems are presented, most of which are designed for a specific application, and also based on different thermodynamic cycles. All electricity-driven systems so far are designed for refrigerating perishable materials. Most thermal-driven systems are designed for air conditioning in different climates and different capacities. Absorption cooling, by far the most common system, plays an important role in this business, followed by desiccant evaporative cooling and the adsorption refrigeration cycle. Other novel refrigeration systems have been proposed, most of which are still under development.

Solar cooling systems strongly depend on local conditions e.g. solar radiation, ambient temperature, or cooling load. Systems should therefore be specifically designed for each location, thereby obtaining the best performance. For thermally-driven systems, a solar cooling system requires less solar collector area per cooling demand (kWh) in tropical areas than in areas above the Tropic of Cancer or below the Tropical of Capricorn, provided that the building has a reasonable climate shell. One severe restriction for solar cooling in general and the ejector system in particular,

is the heat rejection temperature. Heat sink temperatures must be kept as low as possible in order to maintain a stable operation and high performance. A good local heat sink such as a lake, a river or the sea or even a cooling tower can be used with additional parasitic energy consumption for the latter. The best solar cooling locations are therefore located near sufficient solar radiation and a good heat sink.

Solar-driven ejector refrigeration system is a thermally operated cycle, i.e. driven by any form of low temperature heat. Various kinds of working fluids can be used in the cycle; each of these providing different performance and characteristics. Choosing a working fluid concerns several issues, particularly physical and thermodynamic characteristics. Apart from general issues such as chemical stability, environmental impact or toxicity, the curve of the saturated vapour line in a Temperature – Entropy diagram (T-S) should be taken into consideration. Dry fluids e.g. butane, iso-butane, R113, R114, and R141b require less excessive energy for superheating, therefore, they yield better performance than wet fluids and isentropic fluids at the same operating temperatures.

In steady-state analysis of the ejector refrigeration sub-system it has been shown that system performance depends on the type of refrigerant, the operating conditions and theejector geometry. The system thermal ratio (STR) is influenced by the ejector refrigeration subsystem and the solar collector efficiency. In a certain range of generator temperatures, up to a certain temperature, the STR increases with the generator temperature due to an increase in the refrigeration subsystem´s coefficient of performance, COP. After a certain point, increase in the generator temperature does not increase the STR. This is due to high heat losses from the solar collector at high output temperatures. Exergy analysis can further be used as a tool to analyse losses in the system.

Results from the exergy analysis illustrate that irreversibilities occur most in the solar collector, follow by the ejector, the generator, the condenser, the pump and the expansion valve. For butane as the refrigerant, the optimum generating temperature is about 80-100°C.

In practice, the cooling load and the climate are dynamic. Thus, dynamic simulations are required for the dimensioning of the equipments in the system, rather than steady state analysis. Furthermore, the designer can better understand the influence of the local conditions on the function of the system. Due to the low efficiency of the ejector cycle, it is not economically competitive to operate the system with low solar fraction. Results from the dynamic analysis show that the solar-driven ejector refrigeration system using evacuated tube solar collectors is better suited

since higher solar fraction can be achieved compared with the system using flat plat collectors.

The ejector is a key component of the ejector refrigeration system. Both thermodynamic performance and practical function of the system is strongly dependant on the dimensioning of the ejector. This is also the most complicated part to design. The design of the ejector can be assisted by theoretical expressions of the isentropic behaviour of an ideal gas if it is systematically validated with empirical data. There is, however, a lack of empirical data of the ejector design for refrigerants other than water.

The increasing of demand of energy for cooling in many parts of the world can be decreased if we take advantage of the abundant solar radiation in solar-driven refrigeration systems. It can be a remarkable system in the future with potential for rapid growth and a high capacity for primary energy savings. Research and development in this field are still needed to overcome barriers such as lack of experience in design, high costs and too low efficiency.

10.2 Suggested Future Development

The ejector refrigeration cycle requires further development in several respects, particularly ejector design. To utilize solar energy as a heat source for an ejector refrigeration cycle over a wide range of operating conditions is truly a challenge. Additionally, a delicated control system is needed. Systems with one fixed dimension ejector operate only within a small operating temperature range. Furthermore, the system is vulnerable to condenser temperatures, which are strongly related to the ambient temperature. Climate conditions, particularly insolation and ambient temperature, vary constantly, thus temperature supply to the generator and condenser temperatures are not constant, signifying the need for development in the design of ejectors with adjustable dimensions and control for multi-ejector systems, especially in areas of varying climate.

Since it is not economically beneficial to design and install any solar driven system with too high solar fraction, it is important to develop systems with a supplementary energy source such as biomass or process heat from industries.

Heat from solar collectors can also be used for domestic heating of tap water or houses in winter, when there is no cooling demand. The system of combined heating and cooling should enhance the economy of solar cooling systems, and similar systems should be studied for various locations and types of dwellings worldwide, in order to determine the best locations for combined solar heating and cooling.

11 Nomenclature

A_3	Cross sectional area of the constant area chamber in the ejector (see Figure 9-1)	m^2
A_a	Aperture area of the concentrating collector	m^2
A_{abs}	Absorber area	m^2
A_{cov}	Cover surface area of the ETC collector	m^2
A_{sc}	Solar collector area	m^2
A_{env}	Envelop area of the CPC collector	m^2
A_{ey}	Cross sectional area, required for the secondary flow at the constant area chamber in the ejector (see Figure 9-1)	m^2
A_{g1}	Cross sectional area at the exit of the primary nozzle (see Figure 9-1)	m^2
A_{gy}	Cross sectional area, required for the primary flow at the constant area chamber in the ejector (see Figure 9-1)	m^2
A_r	Receiver area of the concentrating collector	m^2
A_t	Nozzle Area	m^2
ACH	Air Changer per Hour	h^{-1}
atm	Atmospheric	
C	Concentration ratio	
c_0	Optical efficiency	-
c_1	Linear heat loss coefficient	-
c_2	Quadratic heat loss coefficient	-
c_e	Velocity of the entrained (secondary) re-	$m\ s^{-1}$

	frigerant from the evaporator	
c_{ey}	Velocity of the secondary flow in the constant area chamber, at section y-y	m s^{-1}
c_g	Velocity of the primary fluid from the generator, expanded through the nozzle in the ejector	m s^{-1}
$c_{g,exp}$	Velocity of the primary fluid from the generator, after expansion through the nozzle in the mixing section	m s^{-1}
c_{gy}	Velocity of the primary flow in the constant area chamber, at section y-y	
c_m	Velocity of the mixing fluid leaving the mixing section	m s^{-1}
c_t	Velocity of the primary flow through the nozzle throat	m s^{-1}
C_p	Specific heat	kJ kg^{-1} K^{-1}
COP_{ejc}	Coefficient of Performance of the ejector refrigeration subsystem	-
COP_{carnot}	COP of the Carnot refrigeration machine	-
COP_{el}	COP of the electricity/work driven refrigeration system	-
$COP_{thermal}$	COP of the thermal driven refrigeration system	-
C.P.	Critical Pressure	bar
C.T.	Critical Temperature	°C
D_3	Diameter of the mixing section	m
$E_{c,out}$	Exergy output from the condenser	kW
E_e	Exergy cooling load	kW
E_g	Exergy input to the generator from the solar collector	kW
$E_{p,el}$	Exergy (electricity) input to the pump	kW
E_s	Exergy (radiation) input to the solar collector	kW
$E_{s,h}$	Exergy (heat) input to the solar collector	kW

E_{su}	Useful exergy input to the solar collector	kW
EPI	Expanded Programme of Immunization by the World Health Organisation	
ETC	Evacuated Tube Solar Collector	
f	Sunlight dilution factor	
F_R	Collector heat removal factor	
FSS	Flat plate, single-glazed solar collector	
FSD	Flat plate, double-glazed solar collector	
g	Gravitational constant	kg N m s^{-2}
G	Solar flux density, solar energy irradiation	W m^{-2}
G_{ava}	Available solar radiation	W m^{-2}
$G_{horizontal}$	Total Solar Radiation on Horizontal	W m^{-2}
$\dot{G}_t$	Refrigerant mass flux through the throat of the nozzle	kg m^{-2}
$\dot{G}_{t,max}$	Maximum refrigerant mass flux through the throat of the nozzle	kg m^{-2}
$\dot{G}_{ey}$	Secondary refrigerant mass flux to the constant area chamber	kg m^{-2}
$\dot{G}_{ey,max}$	Maximum secondary refrigerant mass flux to the constant area chamber	kg m^{-2}
G_{total}	Total hemispherical insolation on the plane of the collector	kW m^{-2}
G_u	Insolation absorbed by the absorber	kW m^{-2}
GWP	Global Warming Potential, relative to CO_2	
H, h	Enthalpy, specific enthalpy	kJ kg^{-1}
h_a	Enthalpy of the ambient air	kJ kg^{-1}
h_c	Enthalpy of the mixing fluid from the ejector entering the condenser (see Figure 9-4)	kJ kg^{-1}
h_d	Enthalpy of the mixing fluid entering the diffuser in the ejector (see Figure 9-4)	kJ kg^{-1}
$h_{dc,is}$	Enthalpy of the mixing fluid, isentropically compressed and entering the dif-	kJ kg^{-1}

	fuser in the ejector (see Figure 9-4)	
$h_{e,in}$	Enthalpy of the fluid entering the evaporator	kJ kg^{-1}
$h_{e,out}$	Enthalpy of the fluid leaving the evaporator	kJ kg^{-1}
$h_{g,\ exp}$	Enthalpy of the primary fluid from the generator, after expansion through the nozzle	kJ kg^{-1}
$h_{g,exp}$	Enthalpy of the driving fluid from the generator, expanded through the nozzle in the ejector (see Figure 9-4)	kJ kg^{-1}
$h_{g,in}$	Enthalpy of the fluid entering the generator	kJ kg^{-1}
$h_{gm,is}$	Enthalpy of the driving fluid from the generator, expanded isentropically through the nozzle in the ejector (see Figure 9-4)	kJ kg^{-1}
$h_{g,out}$	Enthalpy of the fluid leaving the generator	kJ kg^{-1}
$h_{t,is}$	Enthalpy of the primary fluid expanded isentropically through the nozzle	kJ kg^{-1}
h_{ey}	Enthalpy of the secondary fluid to the constant area chamber	kJ kg^{-1}
$h_{ey,is}$	Enthalpy of the secondary fluid expanded isentropically to the constant area chamber	kJ kg^{-1}
h_m	Enthalpy of the mixing fluid at the mixing point	kJ kg^{-1}
I	Irreversibility or exergy loss	kW
I_c	Irreversibility in the condenser	kW
I_e, I_{evap}	Irreversibility in the evaporator	kW
I_{exp}	Irreversibility in the expansion device	kW
I_g	Irreversibility in the generator	kW
I_j	Irreversibility in the ejector	kW
I_p	Irreversibility in the pump	kW

I_{sc}	Irreversibility in the solar collector	kW
I_{total}	Total irreversibilities from every part in the system	kW
IEA	International Energy Agency	
IIR	International Institute of Refrigeration	
ISES	International Solar Energy Society	
$K(\Theta)$	Incident angle modifier	
L_{mix}	Length of the mixing section	m
m	Mass flow rate	kg s^{-1}
m_e	Mass flow of the entrained refrigerant from the evaporator	kg s^{-1}
m_g	Mass flow of driving fluid from generator	kg s^{-1}
Ma	Mach number	
Ma_2	Mach number of the mixed flow at the entrance of the constant area chamber, at section 2-2 (see Figure 9-1)	
Ma_3	Mach number of the mixed flow in the constant area chamber, at section m-m to 3-3 (see Figure 9-1)	
Ma_e	Mach number of the secondary flow from the evaporator	
Ma_{ey}	Mach number of the secondary flow in the constant area chamber in the ejector, section y-y (see Figure 9-1)	
Ma_g	Mach number of the primary flow from the generator	
Ma_{g1}	Mach number of the fluid from the generator, which expands through the nozzle	
Ma_{gy}	Mach number of the primary flow in the constant area chamber in the ejector, section y-y (see Figure 9-1)	
Ma_m	Mach number of the mixed flow in the constant area chamber, at section m-m to 3-3 (see Figure 9-1)	

M.W.	Molecular weight	Kg kgmole^{-1}
n.B.P.	Normal Boiling Point	°C
ODP	Ozone Depletion Potential, relative to R11	
p	Gap optical losses factor	
P_3	Pressure of the mixed flow in the constant area chamber, along section m-m to 3-3 (see Figure 9-1)	Pa
P_4	Pressure of the mixed flow at the exit of the ejector, section 4-4 (see Figure 9-1)	Pa
P_c	Condenser pressure	Pa
P_{co}	Condenser pressure as the entrainment ratio falls to zero; the ejector stops working if the pressure is higher than this point	Pa
P_e	Evaporator pressure	Pa
P_{ey}	Pressure of the secondary flow at the entrance of the constant area chamber in the ejector (see Figure 9-1)	Pa
P_g	Generator pressure	Pa
P_{g1}	Pressure at the exit of the primary nozzle (see Figure 9-1)	Pa
P_{gy}	Pressure of the primary flow at the entrance of the constant area chamber in the ejector (see Figure 9-1)	Pa
P_m	Pressure of the mixed flow in the constant area chamber, at section m-m to 3-3 (see Figure 9-1)	Pa
P_t	Pressure at the throat of the nozzle	Pa
P_y	Pressure at the entrance of the constant area chamber (see Figure 9-1)	Pa
PV	Photovoltaics	
$Q_{abs\text{-}cov}$	Heat absorbed into the absorber by convection	kW
Q_{ava}	Available heat for the process in the solar	kW

	collector	
$Q_{air\ coupling,\ i}$	Convective heat flow from the air coupling to the zone air node	kW
Q_{conv}	Convective heat flow to the zone air node	kW
Q_e	Cooling capacity	kW
Q_g	Energy input to the generator	kW
$Q_{infiltration,\ i}$	Infiltration heat flow to the zone air node	kW
$Q_{internal\ gain}$	Internal heat gain in the zone	kW
$Q_{r,\ long,\ wall}$	Long wave radiation from the wall to the zone air node	kW
$Q_{r,\ sol,\ wall}$	Solar radiation through the wall to the zone air node	kW
$Q_{r,\ w}$	Radiative heat flow to the walls and windows	kW
$Q_{r,\ wall,\ int}$	Internal radiation from the wall to the zone air node	kW
Q_s	Energy gain from solar radiation	kW
Q_{su}	Useful solar radiation input to the collector	kW
$Q_{surface,\ i}$	Convective heat flow from the surface to the zone air node	kW
Q_u	Useful energy gain at the solar collector	kW
$Q_{ventilation,\ i}$	Convective heat flow from the air ventilation to the zone air node	kW
r	Heat of vaporization, estimated by 'Troutons rule'	kJ kg^{-1}
r_p	Compression ratio, ratio of the pressure between the condenser and the evaporator	-
r_p^*	Compression ratio at the critical condenser temperature	-
REE	Refrigeration Exergetic Efficiency	
S	Entropy	kJ $kg^{-1}K^{-1}$
S_e	Entropy of the refrigerant secondary flow	kJ $kg^{-1}K^{-1}$

	from the evaporator	
S_g	Entropy of the refrigerant primary flow from the generator	kJ $kg^{-1}K^{-1}$
$S_{g\_sc,in}$	Entropy of the stream from solar collector to generator	kJ $kg^{-1}K^{-1}$
$S_{g\_sc,out}$	Entropy of the stream from generator back to solar collector	kJ $kg^{-1}K^{-1}$
SEE	System Exergetic Efficiency	-
SF	Solar Fraction	-
SP	System Performance	-
STR	System Thermal Ratio	-
T	Temperature	K
T_1	Temperature of the heat sink for the Carnot heat engine and	K
	Temperature of the heat sink for the Carnot refrigeration system (see Figure 2-8)	
T_2	Temperature of the heat source for the Carnot refrigeration system, low temperature level (see Figure 2-8)	K
T_a	Ambient temperature	°C
$T_{abs,avg}$	Average temperature of the absorber plate in the solar collector	°C
T_c	Condenser temperature	°C
	Or	
	Solar cell temperature (in Chapter 2)	
$T_{c,\ critical}$	Critical condenser temperature	°C
T_{cov}	Temperature of the cover in the ETC collector	°C
T_e	Evaporator temperature	°C
T_{ey}	Temperature of the secondary flow in the the constant area chamber, section y-y	K
T_g	Generator temperature	K
t_g	Generator temperature	°C

T_{gy}	Temperature of the primary flow in the constant area chamber, section y-y	K
T_i	Temperature of the working medium entering the solar collector	°C
T_o	Temperature of the working medium leaving the solar collector	°C
$T_{platnet}$	Temperature of the planet	K
T_r	Room temperature	°C
T_{ref}	Reference temperature	K
T_{sc}	Average temperature of the solar collector	K
T_{sun}	Temperature of the sun	K
U_L	Heat loss coefficient	W m^{-2} K^{-1}
UNICEF	United Nations International Children's Emergency Fund	
V	Vapour volume of the refrigerant	m^3 kg^{-1}
V_{ey}	Vapour volume of the secondary refrigerant flow to the constant area chamber	m s^{-1}
V_t	Vapour volume of the primary refrigerant flow through the nozzle throat	m s^{-1}
$W_{p,el}$	Electricity input to the pump	kW
WHO	World Health Organisation	
z_A	Height at level A	m
z_B	Height at level B	m

Greek alphabets

α	Absorptivity factor	-
α_{abs}	Absorptivity of an absorber	-
β	Coefficient of variation of the solar cell efficiency	-
β_D	Correction coefficient for diffuse insolation	-
β_B	Correction coefficient for direct insolation	-

γ	Heat capacity ratio	-
	Or Intercept factor (Chapter 2)	
ε_1	Emissivity on surface 1 in the solar collector	-
ε_2	Emissivity on surface 2 in the solar collector	-
ε_{abs}	Emimissivity of the absorber	-
ε_{eff}	Effective emimissivity	-
ε_t	Work	kW
ϕ_g	Arbitrary coefficient for the primary flow	-
ϕ_m	Arbitrary coefficient for the friction loss	-
η_D	Diffuser efficiency	-
η_N	Nozzle efficiency	-
η_{Ne}	Nozzle efficiency at the entrance of the sec-ondary flow inlet	
η_{opt}	Optical efficiency of the solar collector	-
$\eta_{opt,PTC}$	Optical efficiency of the PTC solar collector	-
η_{PV}	Photovoltaic efficiency	-
η_R	Reference efficiency of a photovoltaic cell at-0 °C	
η_{sc}	Solar collector efficiency	-
$\eta_{system,Carnot}$	Carnot system Efficiency	-
$\eta_{system,el}$	Efficiency of the electricity driven system	-
ρ	Reflectivity	-
ρ_{abs}	Reflectivity of an absorber	-
ρ_{env}	Reflectivity of an envelop	-
ρ_{ref}	Reflectivity of a reflector	-
λ	Ejector isentropic efficiency	-
σ	Stefan-Boltzmann constant	-
τ	Transmissivity factor	-
τ_{cov}	Transmissivity of a cover	-

τ_{env}	Transmissivity of an envelop	-
$(\tau\alpha)_e$	Effective transmittance-absorbance product	-
ω	Mass ratio	-
$\xi_{carnot,heatengine}$	Efficiency of the Carnot heat engine	-

12 References

Al-Khalidy, N. (1997a). "Experimental Investigation of Solar Concentrating Collectors in a Refrigerant Ejector Refrigeration Machine." *International Journal of Energy Research* 21(12): 1123-1131.

Al-Khalidy, N. (1997b). "Performance of Solar Refrigerant Ejector Refrigerating Machine." *ASHRAE Transactions* 103(1): 56-64.

Alexis, G. K. and Karayiannis, E. K. (2005). "A Solar Ejector Cooling System Using Refrigerant R134a in the Athens Area." *Renewable Energy* 30(9): 1457-1469.

Anyanwu, E. E. and Ogueke, N. V. (2005). "Thermodynamic Design Procedure for Solid Adsorption Solar Refrigerator." *Renewable Energy* 30: 81-96.

Arbel, A. and Sokolov, M. (2004). "Revisiting Solar-Powered Ejector Air Conditioner– the Greener the Better." *Solar Energy* 77: 57–66.

ASHRAE (1983). Steam-Jet Refrigeration Equipment, Chapter 13. *Ashrae Handbook*. Atlanta, American Society of Heating, Refrigerating and Air-Conditioning Engineers, Inc. Equipment: 13.1-13.6.

Bales, C. and Nordlander, S. (2005). *Tca Evaluation, Lab Measurements, Modelling and System Simulations*. No. 3-9809656-4-3, Högskolan Dalarna, Borlänge, Sweden.

Bejan, A., Kearney, D. W. and Kreith, F. (1981). "Second Law Analysis and Synthesis of Solar Collector Systems." *Journal of Solar Energy Engineering, Transactions of the ASME* 103: 23-28.

Bejan, A., Vargas, J. V. C. and Sokolov, M. (1995). "Optimal Allocation of a Heat-Exchanger Inventory in Heat Driven Refrigerators." *International Journal of Heat and Mass Transfer* 38(16): 2997-3004.

Ben Amar, N., Sun, L. M. and Meunier, F. (1996). "Numerical Analysis of Adsorptive Temperature Wave Regenerative Heat Pump." *Applied Thermal Engineering* 16(5): 405-418.

Berlitz, T., Lemke, N., Satzger, P. and Ziegler, F. (1998). "Cooling Machine with Integrated Cold Storage." *International Journal of Refrigeration* 21(2): 157-161.

Biancardi, F. R., Sitler, J. W. and Melikian, G. (1982). "Development and Test of Solar Rankine Cycle Heating and Cooling Systems." *ASHRAE Transactions* 88: 971-985.

Chang, V., Gravalos, J. and Chitty, A. (1986). Thermal Performance of an Ejector-Compressor Solar Cooling System. *Proceedings of the*

Ninth Biennial Congress of the International Solar Energy Society, Montreal, Canada**:** 744-748.
Chang, Y.-J. and Chen, Y.-M. (2000). "Enhancement of a Steam-Jet Refrigerator Using a Novel Application of the Petal Nozzle." *Experimental Thermal and Fluid Science* 22: 203-211.
Chen, F. C. and Hus, C.-T. (1987). "Performance of Ejector Heat Pumps." *International Journal of Energy Research* 11(2): 289-300.
Chen, Y.-M. and Sun, C.-Y. (1997). "Experimental Study of the Performance Characteristics of a Steam-Ejector Refrigeration System." *Experimental Thermal and Fluid Science* 15: 384-394.
Cizungu, K., Mani, A. and Groll, M. (2001). "Performance Comparison of Vapour Jet Refrigeration System with Environment Friendly Working Fluids." *Applied Thermal Engineering* 21: 585-598.
ClimaCheck (2006). *Climacheck Peizoresistive Transmitters for Industrial Applications*, Clima Check Sweden AB. **Series 22S**.
ClimateWell. (2006). "*Frist Prize in Solar Ac to Climatewell.*"Last Update, Retrieved: 20 September 2006, from http://www.climatewell.com/index.php?pageId=7&newsId=79&howold=12.
Comesse_Soudure_SA (2005). *Comesse Soudure Sa.*
Corcoleotes, G. and Williamson, J. S. (1982). "Soleras Solar Cooling Project." *ASHRAE Transactions* 88: 1017-1025.
Dai, Y. J. and Sumathy, K. (2003). "Heat and Mass Transfer in the Adsorbent of a Solar Adsorption Cooling System with Glass Tube Insulation." *Energy* 28: 1511-1527.
Dai, Y. J., Wang, R. Z. and Xu, Y. X. (2002). "Study of a Solar Powered Solid Adsorption–Desiccant Cooling System Used for Grain Storage." *Renewable Energy* 25: 417-430.
De Vos, A. (1992). *Endoreversible Thermodynamics of Solar Energy*. New York, Oxford University Press.
Dorantès, R., Estrada, C. A. and Pilatowsky, I. (1996). "Mathematical Simulation of a Solar Ejector-Compression Refrigeration System." *Applied Thermal Engineering* 16(8/9): 669-675.
Druck. (2006). "*Druck Pressure Transducer.*" 26 May 2006, from http://www.druck.com/.
Duffie, J. A. and Beckman, W. A. (1991). *Solar Engineering of Thermal Process*. Wisconsin, John Wiley&Sons Inc.
Dunkle, R. V. (1965). "A Method of Solar Air Conditioning." *Mech. and Chem. Engr. Trans., Inst. Engrs.* MC1(73).
Eames, I. W., Aphornratana, S. and Haider, H. (1995). "A Theoretical and Experimental Study of a Small-Scale Steam Jet Refrigerator." *International Journal of Refrigeration* 18(6): 378-386.
Egilegor, B., Usbiaga, M., Loubet, R. and Fernández, R. (2006). Rotartica Unit, a Small Scale Thermally Driven Heat Pump Providing Of-

fice Cooling & Heating. *61st ATI National Congress, International Session on 'Solar Heating and Cooling'*, Perugia, Italy.

Enibe, S. and Iloeje, C. (1997). "Design Optimization of the Flat Plate Collector for a Solid Absorption Solar Refrigerator." *Solar Energy* 60(2): 77-87.

Erhard, A., Spindler, K. and Hahne, E. (1998). "Test and Simulation of a Solar Powered Solid Sorption Cooling Machine." *International Journal of Refrigeration* 21(2): 133-141.

Ezzine, N. B., Barhoumi, M., Mejbri, K., Chemkhi, S. and Bellagi, A. (2004). "Solar Cooling with the Absorption Principle: First and Second Law Analysis of an Ammonia-Water Double-Generator Absorption Chiller." *Desalination* 168: 137-144.

Field, R. L. (1980). "Photovoltaic/Thermoelectric Refrigerator for Medicine Storage for Developing Countries." *Solar Energy* 25(5): 445-447.

Fléchon, J., Lazzarin, R., Spinner, B., Dicko, M., Charters, W., Kleinmeier, H. and Hammad, M. A. (1999). *Guild to Solar Refrigerators for Remote Areas and Warm Countries*. Paris, International Institute of Refrigeration (IIR).

Fujiwara, M. (1983). "Exergy Analysis for the Performance of Solar Collectors " *Journal of Solar Energy Engineering, Transactions of the ASME* 105: 163-167.

Gandhidasan, P. (1990). "Analysis of a Solar Space Cooling System Using Liquid Desiccants." *Journal of Energy Resources Technology* 112(4): 246-250.

Göktun, S. (2000). "Performance Analysis of a Heat Engine Driven Combined Vapor Compression-Absorption-Ejector Refrigerator." *Energy Conversion & Management* 41: 1885-1895.

Gommed, K. and Grossman, G. (2004). Experimental Study of a Liquid Desiccant System for Solar Cooling and Dehumidification. *Eurosun2004, 14. Interna. Sonnenforum*, Freiburg, Germany, **03 – Solar Cooling:** 2-043-050, PSE GmbH, 79072 Freiburg, Germany.

Gordon, J. M. and Ng, K. C. (2000). "High-Efficiency Solar Cooling." *Solar Energy* 68(1): 23-31.

Granryd, E. (1998). *Introduction to Refrigerating Engineering*. Stockholm, Dept. of Energy Technology, KTH.

Grazzini, G. and Mariani, A. (1998). "A Simple Program to Design a Multi-Stage Jet-Pump for Refrigeration Cycles." *Energy Conversion & Management* 39(16-18): 1827-1834.

Grossman, G. (2002). "Solar-Powered Systems for Cooling, Dehumidification and Air-Conditioning." *Solar Energy* 72(1): 53-62.

Hague, B. (2000). "*Sainsbury's Tests Solar Refrigeration*."Last Update**:** February 2000, Retrieved: July 18, 2005, from http://www.dti.gov.uk/NewReview/nr43/html/sainsbury.html.

Hamed, A. M. (2003). "Desorption Characteristics of Desiccant Bed for Solar Dehumidification/Humidification Air Conditioning Systems." *Renewable Energy* 28: 2099-2111.

Hara, T., Azuma, H., Shimizu, H., Obora, H. and Sato, S. (1998). "Cooling Performance of Solar Cell Driven, Thermoelectric Cooling Prototype Headgear." *Applied Thermal Engineering* 18(11): 1159-1169.

Henning, H.-M. (2004). *Solar-Assisted Air-Conditioning in Buildings, a Handbook for Planners*. Wien, Springer-Verlag.

Hu, E. J. (1996). "Simulated Results of a Non-Valve, Daily-Cycled, Solar-Powered Carbon/Methanol Refrigerator with a Tubular Solar Collector " *Applied Thermal Engineering* 16(5): 439-445.

Huang, B. J. and Chang, J. M. (1999). "Empirical Correlation for Ejector Design." *International Journal of Refrigeration* 22: 379–388.

Huang, B. J., Chang, J. M., Petrenko, V. A. and Zhuk, K. B. (1998). "A Solar Ejector Cooling System Using Refrigerant R141b." *Solar Energy* 64(4-6): 223–226.

Huang, B. J., Chang, J. M., Wang, C. P. and Petrenko, V. A. (1999). "A 1-D Analysis of Ejector Performance." *International Journal of Refrigeration* 22: 354–364.

IIR (2006). *Solar Cooling on the Rise*. IIF-IIR News letter. **25**.

Iliaktis. (2005). "*Pv Sunfreezer Refrigerators*."Last Update, Retrieved: July 18, 2005, from http://www.iliaktis.com/Fridge/Fridge.htm.

Ingersoll-Rand (1945). *Water-Vapor Refrigeration, Steam-Jet Cooler Type*. New York, Ingersoll-Rand company.

ISES-Germany. (2005). "*Solar Collectors: Different Types and Fields of Application*."Last Update**:** 12 May 2005, Retrieved: 15 June 2005, from http://www.solarserver.de/wissen/sonnenkollektoren-e.html.

Izquierdo Millán, M., Hernandez, F. and Martin, E. (1996). "Available Solar Exergy in an Absorption Cooling Process." *Solar Energy* 56(6): 505-511.

Jakob, U., Eicker, U., Taki, A. H. and Cook, M. J. (2003). "*Development of an Optimised Solar Driven Diffusion-Absorption Cooling Machine*."Last Update, Retrieved: 10 December 2003, from http://www.zafh.net/dokumente/diffusion%20absorption%202003.pdf.

Jeter, S. M. (1981). "Maximum Conversion Efficiency for the Utilization of Direct Solar Radiation." *Solar Energy* 26(3): 231-236.

Kane, M., Larrain, D., Favrat, D. and Allani, Y. (2003). "Small Hybrid Solar Power System." *Energy* 28(14): 1427-1443.

Kanoglu, M., Carpinlioglu, M. Ö. and Yildirim, M. (2004). "Energy and Exergy Analyses of an Experimental Open-Cycle Desiccant Cooling System." *Applied Thermal Engineering* 24: 919-932.

Keenan, J. H., Neumann, E. P. and Lustweek, F. (1950). "An Investigation of Ejector Design by Analysis and Experiment." *Journal of Applied Mechanics*(September): 299-309.

Kessling, W., Laevemann, E. and Kapfhammer, C. (1998). "Energy Storage for Desiccant Cooling Systems Component Development." *Solar Energy* 64(4-6): 209-221.

Khalid Ahmed, C. S., Gandhidasan, P., Zubair, S. M. and Al-Farayedhi, A. A. (1998). "Exergy Analysis of a Liquid-Desiccant-Based, Hybrid Air-Conditioning System." *Energy* 23(1): 51-59.

Khire, R. A., Messac, A. and Van Dessel, S. (2005). "Design of Thermoelectric Heat Pump Unit for Active Building Envelope Systems." *International Journal of Heat and Mass Transfer* 48(19-20): 4028-4040.

Kinsara, A. A., Elsayed, M. M. and Al-Rabghi, O. M. (1996). "Proposed Energy-Efficient Air-Conditioning System Using Liquid Desiccant." *Applied Thermal Engineering* 16(10): 791-806.

Klein, S. A. (2004). *Ees, Engineering Equation Solver*. S. A. Klein. Madison, F-Chart Software.

Klein, S. A., Beckman, W. A., Mitchell, J. W., Duffie, J. A., Duffie, N. A., Freeman, T. L., Mitchell, J. C., Braun, J. E., Evans, B. L., Kummer, J. P., Urban, R. E., Fiksel, A., Thornton, J. W., Blair, N. J., Williams, P. M., Bradley, D. E., McDowell, T. P. and Kummert, M. (2004a). *Trnsys 16 User Manual*. Wisconsin, Solar Energy Laboratory, Univ. of Wisconsin-Madison.

Klein, S. A., Beckman, W. A., Mitchell, J. W., Duffie, J. A., Duffie, N. A., Freeman, T. L., Mitchell, J. C., Braun, J. E., Evans, B. L., Kummer, J. P., Urban, R. E., Fiksel, A., Thornton, J. W., Blair, N. J., Williams, P. M., Bradley, D. E., McDowell, T. P. and Kummert, M. (2004b). *Trnsys 16, a Transient System Simulation Program*. Wisconsin, Solar Energy Laboratory, Univ. of Wisconsin-Madison.

Lemmon, E. W., McLinden, M. O. and Huber, M. L. (2002). *Reference Fluid Thermodynamic and Transport Properties, Nist Standard Reference Database 23, Version 7.0*. USA, Physical and Chemical Properties Division, NIST.

Li, C. H., Wang, R. Z. and Lu, Y. Z. (2002). "Investigation of a Novel Combined Cycle of Solar Powered Adsorption–Ejection Refrigeration System." *Renewable Energy* 26: 611-622.

Li, M., Huang, H. B., Wang, R. Z., Wang, L. L., Yang, W. M. and Cai, W. D. (2005). "Study on Intermittent Refrigeration Phenomenon for Solar Solid Adsorption Refrigeration." *Applied Thermal Engineering* In Press: In Press.

Li, M., Sun, C. J., Wang, R. Z. and Cai, W. D. (2004). "Development of No Valve Solar Ice Maker." *Applied Thermal Engineering* 24: 865-872.

Li, M. and Wang, R. Z. (2002). "A Study of the Effects of Collector and Environment Parameters on the Performance of a Solar Powered Solid Adsorption Refrigerator." *Renewable Energy* 27: 369-382.

Li, M. and Wang, R. Z. (2003). "Heat and Mass Transfer in a Flat Plate Solar Solid Adsorption Refrigeration Ice Maker." *Renewable Energy* 28: 613-622.

Lior, N. (1977). "Solar Energy and the Steam Rankine Cycle for Driving and Assisting Heat Pumps in Heating and Cooling Modes." *Energy Conversion* 16(3): 111-123.

Liu, Y. L. and Wang, R. Z. (2004). "Performance Prediction of a Solar/Gas Driving Double Effect Libr–H_2o Absorption System." *Renewable Energy* 29: 1677-1695.

Löf, G. O. G. (1955). Cooling with Solar Energy. *World Symposium on Applied Solar Energy*, Phoenix, Arizona.

Low Keep. (2005). "*Low Keep (Tm) Super Efficient Alternative Energy Products*."Last Update**:** November 4, 1999, Retrieved: July 18, 2005, from http://www.datawise.net/~lowkeep/specs.htm.

LSCable. (2006). "*Ls Absorption Machine*."Last Update, Retrieved: 15 September 2006, from http://www.lsaircondition.com:2222/english/index.htm.

Lu, S.-M. and Yan, W.-J. (1995). "Development and Experimental Validation of a Full-Scale Solar Desiccant Enhanced Radiative Cooling System." *Renewable Energy* 6(7): 821-827.

Lucas, L. (1988). "Iir News." *International journal of refrigeration* 21(2): 88.

Lundqvist, P. (1987). *A Steam Ejector for Heat Recovery Form Flue Gases*. No. 261, Värmeforsk, Stockholm.

Lundqvist, P. (1993). *Stirling Cycle Heat Pumps and Refrigerators*. Applied Thermodynamics and Refrigeration. Stockholm, Royal Institute of Technology**:** 284.

Marion, W. and Urban, K. (1995). *User's Manual for Tmy2s, Typical Meteorological Years*. Colorado, A National Laboratory of the U.S. Department of Energy.

Medrano, M., Bourouis, M. and Coronas, A. (2001). "Double-Lift Absorption Refrigeration Cycles Driven by Low Temperature Heat Sources Using Organic Fluid Mixtures as Working Pairs." *Applied Energy* 68: 173-185.

Meyer, J. P. (2005). *Solar Cooling*. Sun & Wind Energy.

Miyamoto, H. and Watanabe, K. (2002). "A Thermodynamic Property Model for Fluid-Phase Isobutane." *International journal of thermophysic* 23(2): 477-499.

Murthy, S. S., Balasubramanian, R. and Murthy, M. V. K. (1991). "Experiments on Vapour Jet Refrigeration System Suitable for Solar Energy Applications." *Renewable Energy* 1(5/6): 757-768.

Nguyen, V. M., Riffat, S. B. and Doherty, P. S. (2001). "Development of a Solar-Powered Passive Ejector Cooling System." *Applied Thermal Engineering* 21: 157-168.

Norton, B. (1992). *Solar Energy Thermal Technology*. Germany, Springer-Verlag.

Öberg, V. and Goswami, Y. (1998). A Review of Liquid Desiccant Cooling. *Advances in Solar Energy*. K. W. Böer. 12: 431-470.

Oertel, K. and Fischer, M. (1998). "Adsorption Cooling System for Cold Storage Using Methanol/Silicagel." *Applied Thermal Engineering* 18: 773-786.

Oliveira, A. C., Afonso, C., Matos, J., Riffat, S., Nguyen, M. and Doherty, P. (2002). "A Combined Heat and Power System for Buildings Driven by Solar Energy and Gas." *Applied Thermal Engineering* 22(6): 587-593.

Olsson, R., Kaarebring-Olsson, M. and Jonsson, S. (2000). *A Chemical Heat Pump*. No: WO0037864, Sweden.

Parrott, J. E. (1978). "Theoretical Upper Limit to the Conversion Efficiency of Solar Energy." *Solar Energy* 21(3): 227-229.

Pohl, J. P., Hellmann, H.-M. and Grossman, G. (1998). "Investigation and Comparison of Two Configurations of a Novel Open-Cycle Absorption Chiller." *International Journal of Refrigeration* 21(2): 142-149.

PolarPower. (2005). "*Solar Refrigerator*."Last Update**:** July 18, 2005, Retrieved: July 18, 2005, from http://www.polarpowerinc.com/.

Pons, M., Guilleminot, J. J., Grenier, P. and Meunier, F. (2001). "*Presentation of Some Adsorption Units Developed for Solar Refrigeration*."Last Update, Retrieved: 19 October 2005, from http://www.limsi.fr/Individu/mpons/solaradsor.htm.

Pridasawas, W. and Lundqvist, P. (2002). Working Fluid Selection for an Ejector Refrigeration Cycle. *Zero Leakage – Minimum Charge*, Stockholm, Sweden**:** C.9, Paris: International Institute of Refrigeration.

Pridasawas, W. and Lundqvist, P. (2003). A Year-Round Simulation of a Solar-Driven Ejector Refrigeration. *Proceedings of the International Conference on Fluid and Thermal Energy Conversion 2003*, Bali, Indonesia.

Pridasawas, W. and Lundqvist, P. (2004a). Butane, as a Refrigerant for a Solar-Driven Ejector Refrigeration System. *The 6th IIR Gustav Lorentzen Natural Working Fluids Conference*, Glasgow, UK.

Pridasawas, W. and Lundqvist, P. (2004b). "An Exergy Analysis of a Solar-Driven Ejector Refrigeration System." *Solar Energy* 76: 369–379.

Pridasawas, W. and Lundqvist, P. (2004c). Optimization of a Small-Scale Solar-Driven Ejector Refrigeration System. *Eurosun2004, 14. In-*

terna. Sonnenforum, Freiburg, Germany, **03 – Solar Cooling:** 2-093-102, PSE GmbH.
Prigmore, D. and Barber, R. (1975). "Cooling with the Sun's Heat. Design Considerations and Test Data for a Rankine Cycle Prototype." *Solar Energy* 17(3): 185-192.
Rabl, A. (1985). *Active Solar Collectors and Their Applications*. USA, Oxford University Press Inc.
Remund, J., Lang, R. and Kunz, S. (2001). *Meteonorm Version 5.0*. Bern, Meteotest.
Riffat, S. B. and Holt, A. (1998). "A Novel Heat Pipe/Ejector Cooler." *Applied Thermal Engineering* 18(3-4): 93-101.
Rogdakis, E. D. and Alexis, G. K. (2000). "Design and Parametric Investigation of an Ejector in an Air-Conditioning System." *Applied Thermal Engineering* 20: 213-226.
Rotartica. (2006). "*Rotartica Absorption*."Last Update, Retrieved: 15 September 2006, from http://www.rotartica.com/.
Rusly, E., Charters, W. W. S., Ooi, A. and Aye, L. (2002). Combined Solar and Electric System for Space Cooling. *the 7th International Energy Agency Heat Pump Conference*, Beijing**:** 301-312, IEA.
Saghiruddin, M. A. S. (2001). "Economic Analysis of Two Stage Dual Fuid Absorption Cycle for Optimizing Generator Temperatures." *Energy Conversion & Management* 42: 407-437.
Said, S. A. M. and Zubair, S. M. (1993). "On Second-Law Efficiency of Solar Collectors." *Journal of Solar Energy Engineering, Transactions of the ASME* 115: 2-4.
Schmidt, R. (2005). "*Solar Cooling*."Last Update**:** 21 September 2005, Retrieved: 24 October 2005, from http://www.zeo-tech.de/e_index.htm.
Schnabel, L., Hindenburg, C. and Geucke, T. (2004). Detailed Monitoring Results of the First Thermally Solar Autonomous Air Conditioning System in Germany. *Eurosun2004, 14. Interna. Sonnenforum*, Freiburg, Germany, **03 – Solar Cooling:** 2-113-122, PSE GmbH, 79072 Freiburg, Germany.
Sofrata, H. (1996). "Heat Rejection Alternatives for Thermoelectric Refrigerators." *Energy Conversion and Management* 37(3): 269-280.
Sokolov, M. and Hershgal, D. (1993). "Optimal Coupling and Feasibility of a Solar-Powered Year-Round Ejector Air Conditioner." *Solar Energy* 50(6): 507-516.
Sør, L. and Lund, S. (1999). Efficiency Improvement of Low Pressure Steam Jet Driven Ejector Cooling Plants. *the 20th International Congress of Refrigeration*, Sydney, IIF/IIR.
Sözen, A. and Özalp, M. (2003). "Performance Improvement of Absorption Refrigeration
System Using Triple-Pressure-Level." *Applied Thermal Engineering* 23: 1577-1593.

Sözen, A. and Özalp, M. (2005). "Solar-Driven Ejector-Absorption Cooling System." *Applied Energy* 80: 97-113.

Sumathy, K. (2004). Performance of a No-Valve Solar Adsorption Ice Maker. *Eurosun2004, 14. Interna. Sonnenforum*, Freiburg, Germany, **03 – Solar Cooling:** 2-123-128, PSE GmbH, 79072 Freiburg, Germany.

Sun, D.-W. (1999). "Comparative Study of the Performance of an Ejector Refrigeration Cycle Operating with Various Refrigerants." *Energy Conversion & Management* 40: 873-884.

Sun, L. M., Feng, Y. and Pons, M. (1997). "Numerical Investigation of Adsorptive Heat Pump Systems with Thermal Wave Heat Regeneration under Uniform-Pressure Conditions." *International Journal of Heat and Mass Transfer* 40(2): 281-293.

Sundanzer. (2005). "*Energy Efficient Refrigeration, Dcr/Dcf Series Battery-Powered Units*."Last Update, Retrieved: July 18, 2005, from http://www.sundanzer.com/.

Tamm, G., Goswami, D. Y., Lu, S. and Hasan, A. A. (2004). "Theoretical and Experimental Investigation of an Ammonia–Water Power and Refrigeration Thermodynamic Cycle." *Solar Energy* 76: 217-228.

Tchernev, D. (2006). "*The Zeopower Company*."Last Update.

Thévenot, R. (1979). *A History of Refrigeration Throughout the World*. Paris, International Institute of Refrigeration.

Torres R, E., Picon Nunez, M. and Cervantes de G, J. (1998). "Exergy Analysis and Optimization of a Solar-Assisted Heat Pump." *Energy* 23(4): 337-344.

Twidell, J. and Weir, T. (1998). *Renewable Energy Resources*. Great Britain, E&FN Spon.

Valizadeh, H. and Ashrafi, N. (1996). "A Continuous Cycle Solar Thermal Refrigeration System." *Renewable Energy* 9(1-4): 632-640.

Velázquez, N. and Best, R. (2002). "Methodology for the Energy Analysis of an Air Cooled Gax Absorption Heat Pump Operated by Natural Gas and Solar Energy." *Applied Thermal Engineering* 22: 1089-1103.

Venkatesh, A. and Mani, A. (1989). "Comparison of Performances of Single Stage and Two Stage Intermittent Ammonia-Water Solar Refrigeration Systems, Technical Note." *Solar & Wind Technology* 6(1): 75-78.

Wali, E. (1980). "Optimum Working Fluids for Solar Powered Rankine Cycle Cooling of Buildings." *Solar Energy* 25(3): 235-241.

Webb, P. A. (2003) "*Introduction to Chemical Adsroption Analytical Techniques and Their Applications to Catalysis*." DOI, http://www.particular.ie/intro_to_chemical_adsorption.pdf#search=%22chemical%20%2B%20adsorption%22

WHO. (1996). "*Solar Energy and Rural Health Care, Fact Sheet N132*."Last Update, Retrieved: March 12, 2001, from http://www.int/inf-fs-en-fact132.html.

WHO. (1999). "*Epi Equipment Test Procedures: E3*." E3: Refrigerators and freezers for storing vaccines and freezing icepacks,Last Update**:** Febuary 18, 1999, Retrieved: July 18, 2005, from http://www.who.int/vaccines-access/vacman/pis/e03.pdf.

WHO. (2005). "*Product Information Sheets (Pis) since 2000 Edition, E3: Refrigerators and Freezers for Storing Vaccines and Freezing Icepacks*." E3: Refrigerators and freezers for storing vaccines and freezing icepacks,Last Update**:** June 17, 2005, Retrieved: July 18, 2005, from http://www.who.int/vaccines-access/vacman/pis/new%20sheets%20intro.htm.

Wiemken, E., Motta, M., Hindenburg, C. and Henning, H.-M. (2004). Design and Planning Support for Solar Assisted Air-Conditioning: Guidelines and Tools. *Eurosun2004, 14. Interna. Sonnenforum*, Freiburg, Germany, **03 – Solar Cooling:** 2-129-139, PSE GmbH.

Wolpert, J. L. and Riffat, S. B. (1999). "*Hybrid Solar/Gas Cooling Ejector Unit for a Hospital in Mexico*."Last Update**:** -, Retrieved: 10 August 2006, from http://www.kenes.com/ises.abstracts/Htm/0171.htm.

Wolpert, J. L., Riffat, S. B. and Redshaw, S. (2003). Prototype for a Novel Solar Powered Ejector Air Conditioning System in Mazunte, Mexico. *ISES Solar World Congress 2003, Solar Energy for a Sustainable Future*, Göteborg, Sweden**:** O5 19.

Xu, F., Goswami, D. Y. and Bhagwat, S. S. (2000). "A Combined Power/Cooling Cycle." *Energy* 25: 233-246.

Zhang, X. J. and Wang, R. Z. (2002a). "Design and Performance Simulation of a New Solar Continuous Solid Adsorption Refrigeration and Heating Hybrid System." *Renewable Energy* 27: 401-415.

Zhang, X. J. and Wang, R. Z. (2002b). "A New Combined Adsorption–Ejector Refrigeration and Heating Hybrid System Powered by Solar Energy." *Applied Thermal Engineering* 22: 1245-1258.

Appendix A: Permission of Using Figures

Dear Wimolsiri Pridasawas

We hereby grant you permission to reproduce the material detailed below at no charge **in your thesis** subject to the following conditions:

1. If any part of the material to be used (for example, figures) has appeared in our publication with credit or acknowledgement to another source, permission must also be sought from that source. If such permission is not obtained then that material may not be included in your publication/copies.

2. Suitable acknowledgment to the source must be made, either as a footnote or in a reference list at the end of your publication, as follows:

> "Reprinted from Publication title, Vol number, Author(s), Title of article, Pages No., Copyright (Year), with permission from Elsevier".

3. Reproduction of this material is confined to the purpose for which permission is hereby given.

4. This permission is granted for non-exclusive world **English** rights only. For other languages please reapply separately for each one required. Permission excludes use in an electronic form. Should you have a specific electronic project in mind please reapply for permission.

5. Should your thesis be published commercially, please reapply for permission.

Yours sincerely

Jennifer Jones
Rights Assistant

Your future requests will be handled more quickly if you complete the online form at www.elsevier.com/permissions

-----Original Message-----
From: wimol@energy.kth.se
[mailto:wimol@energy.kth.se]
Sent: 15 August 2006 14:09
To: permissions@elsevier.com
Subject: Obtain Permission

This Email was sent from the Elsevier Corporate Web Site

and is related to Obtain Permission form:

Product: Customer Support

Component: Obtain Permission

Web server: http://www.elsevier.com

IP address: 10.10.24.149

Client: Mozilla/4.0 (compatible; MSIE 6.0; Windows NT 5.1; SV1; InfoPath.1)

Invoked from: http://www.elsevier.com/wps/find/obtainpermission-form.cws_home?isSubmitted=yes&navigateXmlFileName=/store/prod_webcache_act/framework_support/obtainpermission.xml

Request From:

Request for Pemission Wimolsiri Pridasawas

Royal Institute of Technology, EGI

Brinellvägen 68

10044

Stockholm

Sweden

Contact Details:

Telephone: +46 (0)8 790 7889

Fax: +46 (0)8 203007

Email Address: wimol@energy.kth.se

To use the following material:

ISSN/ISBN:

Title: Renewable Energy

Author(s): Dai, Y. J., Wang, R. Z. and Ni, L.

Volume: 28

Issue: 1

Year: 2003

Pages: 949 - 959

Article title: Experimental Investigation on a Thermoelectric Ref

How much of the requested material is to be used:

Figure 1

Are you the author: Yes

Author at institute: Yes

How/where will the requested material be used: In a thesis or dissertation

Details:

Figure 1 in this article will be used in the literature survey part of my thesis in title 'Solar-Driven Refrigeration System: Focus on an Ejector Refrigeration Cycle" The reference to the authors and journal will be cited clearly.

Additional Info: There are also 27 articles, requested for permission The articles are listed be-

low. All of them will be used in the literature survey part of the thesis in title 'Solar-Driven Refrigeration System: Focus on an Ejector Refrigeration Cycle" The references to the authors and journals will be cited clearly.

Figure 1 from Dai, Wang et al., 2003

Dai, Y. J., Wang, R. Z. and Ni, L. (2003). "Experimental Investigation on a Thermoelectric Refrigerator Driven by Solar Cells." Renewable Energy 28: 949-959.

Figure 1 from Dai, Wang et al., 2002

Dai, Y. J., Wang, R. Z. and Xu, Y. X. (2002). "Study of a Solar Powered Solid Adsorption-Desiccant Cooling System Used for Grain Storage." Renewable Energy 25: 417-430.

Figure 3 from Dorantès, Estrada et al., 1996

Dorantès, R., Estrada, C. A. and Pilatowsky, I. (1996). "Mathematical Simulation of a Solar Ejector-Compression Refrigeration System." Applied Thermal Engineering 16(8/9): 669-675.

Figure 1 from Enibe and Iloeje, 1997

Enibe, S. and Iloeje, C. (1997). "Design Optimization of the Flat Plate Collector for a Solid Absorption Solar Refrigerator." Solar Energy 60(2): 77-87.

Figure 1 from Erhard, Spindler et al., 1998

Erhard, A., Spindler, K. and Hahne, E. (1998). "Test and Simulation of a Solar Powered Solid Sorption Cooling Machine." International Journal of Refrigeration 21(2): 133-141.

Figure 1 from Field, 1980

Field, R. L. (1980). "Photovoltaic/Thermoelectric Refrigerator for Medicine Storage for Developing Countries." Solar Energy 25(5): 445-447.

Figure 1 from Göktun, 2000

Göktun, S. (2000). "Optimization of Irreversible Solar Assisted Ejector-Vapor Compression Cascaded Systems." Energy Conversion & Management 41: 625-631.

Figure 1 from Hara, Azuma et al., 1998

Hara, T., Azuma, H., Shimizu, H., Obora, H. and Sato, S. (1998). "Cooling Performance of Solar Cell Driven, Thermoelectric Cooling Prototype Headgear." Applied Thermal Engineering 18(11): 1159-1169.

Figure 1 from Hu, 1996

Hu, E. J. (1996). "Simulated Results of a Non-Valve, Daily-Cycled, Solar-Powered Carbon/Methanol Refrigerator with a Tubular Solar Collector " Applied Thermal Engineering 16(5): 439-445.

Figure 1 from Huang, Chang et al., 1998

Huang, B. J., Chang, J. M., Petrenko, V. A. and Zhuk, K. B. (1998). "A Solar Ejector Cooling System Using Refrigerant R141b." Solar Energy 64(4-6): 223-226.

Figure 1 from Kane, Larrain et al., 2003

Kane, M., Larrain, D., Favrat, D. and Allani, Y. (2003). "Small Hybrid Solar Power System." Energy 28(14): 1427-1443.

Figure 1 from Kessling, Laevemann et al., 1998

Kessling, W., Laevemann, E. and Kapfhammer, C. (1998). "Energy Storage for Desiccant Cooling Systems Component Development." Solar Energy 64(4-6): 209-221.

Figure 2 from Khalid Ahmed, Gandhidasan et al., 1998

Khalid Ahmed, C. S., Gandhidasan, P., Zubair, S. M. and Al-Farayedhi, A. A. (1998). "Exergy Analysis of a Liquid-Desiccant-Based, Hybrid Air-Conditioning System." Energy 23(1): 51-59.

Figure 1 from Khire, Messac et al., 2005

Khire, R. A., Messac, A. and Van Dessel, S. (2005). "Design of Thermoelectric Heat Pump Unit for Active Building Envelope Systems." International Journal of Heat and Mass Transfer 48(19-20): 4028-4040.

Figure 2 from Kinsara, Elsayed et al., 1996

Kinsara, A. A., Elsayed, M. M. and Al-Rabghi, O. M. (1996). "Proposed Energy-Efficient Air-Conditioning System Using Liquid Desiccant." Applied Thermal Engineering 16(10): 791-806.

Figure 1 from Li, Wang et al., 2002

Li, C. H., Wang, R. Z. and Lu, Y. Z. (2002). "Investigation of a Novel Combined Cycle of Solar Powered Adsorption-Ejection Refrigeration System." Renewable Energy 26: 611-622.

Figure 1 from Lior, 1977

Lior, N. (1977). "Solar Energy and the Steam Rankine Cycle for Driving and Assisting Heat Pumps in Heating and Cooling Modes." Energy Conversion 16(3): 111-123.

Figure 1 from Lu, Wang et al., 2003

Lu, Y. Z., Wang, R. Z., Zhang, M. and Jiangzhou, S. (2003). "Adsorption Cold Storage System with Zeolite-Water Working Pair Used for Locomotive Air Conditioning." Energy Conversion and Management 44: 1733-1743.

Figure 2 from Oertel and Fischer, 1998

Oertel, K. and Fischer, M. (1998). "Adsorption Cooling System for Cold Storage Using Methanol/Silicagel." Applied Thermal Engineering 18: 773-786.

Figure 1 from Oliveira, Afonso et al., 2002

Oliveira, A. C., Afonso, C., Matos, J., Riffat, S., Nguyen, M. and Doherty, P. (2002). "A Combined Heat and Power System for Buildings Driven by Solar Energy and Gas." Applied Thermal Engineering 22(6): 587-593.

Figure 1 from Pohl, Hellmann et al., 1998

Pohl, J. P., Hellmann, H.-M. and Grossman, G. (1998). "Investigation and Comparison of Two Configurations of a Novel Open-Cycle Absorption Chiller." International Journal of Refrigeration 21(2): 142-149.

Figure 3 from Prigmore and Barber, 1975

Prigmore, D. and Barber, R. (1975). "Cooling with the Sun's Heat. Design Considerations and Test Data for a Rankine Cycle Prototype." Solar Energy 17(3): 185-192.

Figure 1 from Sofrata, 1996

Sofrata, H. (1996). "Heat Rejection Alternatives for Thermoelectric Refrigerators." Energy Conversion and Management 37(3): 269-280.

Figure 1 from Sözen and Akcayol, 2004

Sözen, A. and Akcayol, M. A. (2004). "Modelling (Using Artificial Neural-Networks) the Performance Parameters of a Solar-Driven Ejector-Absorption Cycle." Applied Energy 79: 309-325.

Figure 1 from Sun, 1997

Sun, D.-W. (1997). "Solar Powered Combined Ejector-Vapour Compression Cycle for Air Conditioning and Refrigeration." Energy Conversion Management 38(5): 479-491.

Figure 1 from Venkatesh and Mani, 1989

Venkatesh, A. and Mani, A. (1989). "Comparison of Performances of Single Stage and Two Stage Intermittent Ammonia-Water Solar Refrigeration Systems, Technical Note." Solar & Wind Technology 6(1): 75-78.

Figure 1 from Xu, Goswami et al., 2000

Xu, F., Goswami, D. Y. and Bhagwat, S. S. (2000). "A Combined Power/Cooling Cycle." Energy 25: 233-246.

Figure 1 and 2 from Zhang and Wang, 2002

Zhang, X. J. and Wang, R. Z. (2002). "A New Combined Adsorption-Ejector Refrigeration and Heating Hybrid System Powered by Solar Energy." Applied Thermal Engineering 22: 1245-1258.

- end -

For further info regarding this automatic email, please contact:

WEB APPLICATIONS TEAM (esweb.admin@elsevier.co.uk)

Appendix B
Component Models

B-1Building Models

The model is created in TRNBuild, the visual building interface of TRNSYS16 (Klein, Beckman et al., 2004b). The size of the building is 150 m^3 with the area of 50 m^2. There are 2 thermal zones: working space and attic. The walls are made of brick, insulation and plaster with a total area of 0.355 m and a U-value of 0.339 W m^{-2} K^{-1}. The ground is made of a floor layer, stone, silence, concrete and insulation with a total area of 0.425 m and a U-value of 0.313 W m^{-2} K^{-1}. The roof is made of concrete and insulation. Overhang and wing-wall shading is modelled by Type 34. There are 3 m^2 windows area on the north, and 1.5 m^2 on the east, south and west sides. All windows are single glazed; the properties of the window are called from the TRNSYS 16 library, ID 1001. The U-value of the window is 5.68 W m^{-2} K^{-1}, g-value is 0.522. The frame is accounted for 15% of the window's area with a U-value of 2.27 W m^{-2} K^{-1}. Summary of the building parameters are shown in Table B-1.

Table B-1Key Parameter Values for the Building

Parameters	Values
Floor	
Area	50 m^2 (5 x 10 m)
Material	Floor (0.005 m), Stone (0.060 m), Silence (0.040 m), Concrete (0.240 m), Insulation (0.080m)
U-value	0.313 W m^{-2} K^{-1}
Wall/Window	
Wall/Window North Area:	30/3 m^2
Wall/Window East Area:	15/1.5 m^2
Wall/Window South Area:	30/1.5 m^2

Parameters	Values
Wall/Window West Area:	15/1.5 m^2
Walls Material	Brick (0.240 m), Insulation (0.100 m), and Plaster (0.015 m)
Walls U-Value	0.339 $m^{-2} K^{-1}$
Windows	
ID	Window ID 1001 from TRNSYS Library
Windows U-Value	5.68 W $m^{-2} K^{-1}$
g-Value	0.522 %
Tilt	90°
Roof Area:	22.4 m^2
Volume :	150 m^3

Design Conditions

The building is assumed to be an office building, and the cooling supply subsystem operates only during working hours of the weekdays, from 8:00 to 18:00. The building model is a non-geometrical balance model with one air node per zone. Heat gain into the building comes from internal gains, convective heat flow to the air node and radiative heat flow to the walls and windows. Temperature of the building is controlled by the three-stage room thermostat, type 8, at the maximum indoor air temperature at 26°C.

Table B-2 Summary of the Key Values for the Design Conditions in the Building

Parameters	Values
Occupation Times	08:00-18:00 Workdays
Maximum Indoor Air Temperature:	26 °C
Set Temperature (for Cooling)	MAX[(MIN(27, (T_{amb}+49)*0.33)),25]
Infiltration	0.8 h^{-1}
Ventilation	Natural ventilation at ACH=0.8 h^{-1}

Gain	
Internal Gain - Constant	1 kW
Internal Gain – Artificial Light	10 W m^{-2}, Turn on when the total horizontal radiation is less than 120 W m^{-2} Turn off when the total horizontal radiation is more than 140 W m^{-2}
Gain from People	3 persons x (140 W/person) = 420 W

B-2 Solar Collector Model

In this study, solar collector Type 1b and Type 71 for the Flat Plate and Evacuated Tube solar collectors are used respectively. Summary of the main parameters are shown in Table B-3.

Table B-3 Key Parameters for the Solar Collector Models

Parameters	**Flat Plate Single-Glazed (Type 1b)**	**Flat Plate Double-Glazed (Type 1b)**	**Evacuated Tube (Type 71)**
Efficiency Mode	Average Temp.	Average Temp.	Average Temp.
Flow at Test Conditions	40 kg h^{-1} m^{-2}	40 kg h^{-1} m^{-2}	40 kg h^{-1} m^{-2}
Intercept Efficiency (Gross Area)	0.80	0.80	0.80
First Order Loss Coefficient	5 W m^{-2} K^{-1}	3.5 W m^{-2} K^{-1}	1.5 W m^{-2} K^{-1}
Second Order Loss Coefficient	0.014 W m^{-2} K^{-1}	0.014 W m^{-2} K^{-1}	0.008 W m^{-2} K^{-1}

B-3 Storage Tank Model

The stratified storage tank Type 4c with a volume of 2 m^3 is used in this study. There are 7 temperature levels (nodes) with a heat loss coefficient of 0.69 W $h^{-1}m^{-2}K^{-1}$. There is no power for the heating element installed in the tank.

B-4 Auxiliary Heater Model

The electric heater Type 6 is used with a maximum heating rate of 6.5 kW. Overall loss coefficient for heater during operation is assumed to be zero.

B-5 Storage Tank Model

The stratified storage tank Type 4c with a volume of 2 m^3 is used in this study. There are 7 temperature levels (nodes) with a heat loss coefficient of 0.69 W $h^{-1}m^{-2}K^{-1}$. There is no heating element installed in the tank.

B-6 Absorption Chiller

The single effect hot-water fired absorption chiller Type 680 is used with a rated capacity of 1494.44 kW and a rated COP of 0.53. The fraction of design energy input data is provided by the example file in TRNSYS at .\Inputs\Single-Effect\HotWater-Fired\S1.dat
Example of the cooling machine performance data operated at a full rated capacity with the chilled water set point of 10°C is shown in Figure B-1. The required heat from the solar collector subsystem and the COP of the machine can be calculated from,

$$\dot{Q}_{hw} = \frac{Capacity_{Rated}}{COP_{Rated}} f_{DesignEnergyInput} \qquad \text{Eq. B-1}$$

$$COP = \frac{\dot{Q}_{chw}}{\dot{Q}_{aux} + \dot{Q}_{hw}} \qquad \text{Eq. B-2}$$

Where

$Capacity_{rated}$ = Rated cooling capacity of the machine

COP_{rated} =Machine's rated Coefficient of Performance
$\dot{Q}_{aux}$ =Energy draw of parasitics equipments (pumps, controls), kJ h^{-1}
$\dot{Q}_{chw}$ =Energy romoved from the 'chilled water' stream, kJ h^{-1}
$\dot{Q}_{hw}$ =Energy taken from the 'hot water' stream, kJ h^{-1}

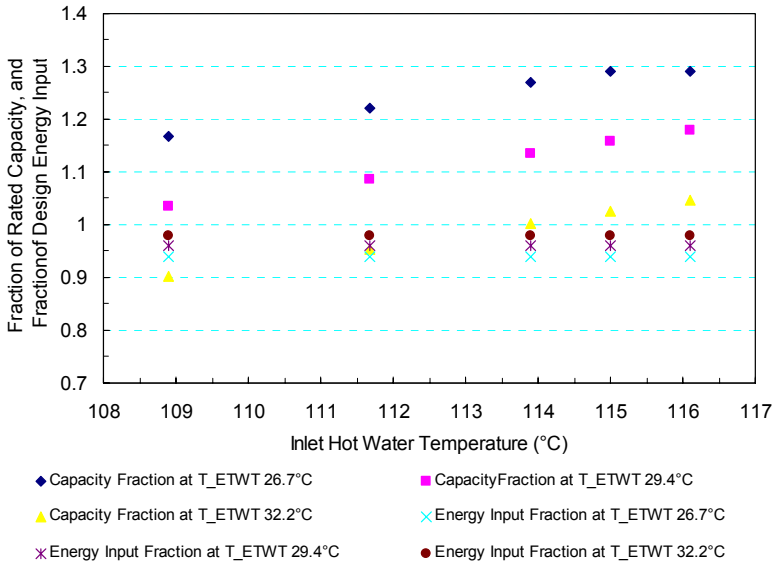

Figure B-1: Fraction of Rated Capacity and Fraction of Design Energy Input at a Full Rated Capacity with the Chilled Water Set Point Temperatuare of 10°C

Further details of the model can be found in TRNSYS Manual –TESS Library Type 680 or Standard TRNSYS 16 Manual Type 107.

B-7 Circulation Pumps

Variable Speed Pump Type 3 is used. This pump model calculates a mass flow rate using a variable control function (0 and 1) and a specified maximum flow capacity.

B-8 Controllers

In the solar collector subsystem, the differential controller Type 2b is used. The three-stage room thermostat Type 8 is used to control the temperature in the building model. In Type 8, the first and second stages (heating mode) are disabled, only the cooling mode is activated.

The holiday calculator, Type 95c calculates the holiday time and the forcing function type 14h calculates the working hours (08:00-18:00). Both models send the signal to the building to switch on/turn off the cooling machine.

B-9 Weather Data Reader and Processors

The weather data is read from the TMY2 format (Marion, 1995) by Type 109. The radiation in different directions is also calculated from the radiation processor Type 109.

The effective sky temperature using in the building model is determined from Type 69a. This effective sky temperatuare is used for calculation of the long-wave radiation exchange between the external surfaces of the building and the sky.

The Psychrometrics parameters are calculated by Psychrometrics utility subroutine Type 33. By supplying the dry bulb temperature and one more property, the others parameter e.g. wet bulb temperature, enthalpy, density of the air-water mixture and humidiy ratio can be calculated.